Diese Dissertation haben begutachtet

Univ.-Prof. Dr. Ulrich Schubert

Prof. Ing. Jaromír Havlica, DrSc.

DISSERTATION

Investigation of CdS Clusters in Solution for their Use as Building Blocks in Hybrid Materials

ausgeführt zum Zwecke der Erlangung des akademischen Grades eines
Doktors der technischen Wissenschaften

unter der Leitung von
Univ.-Prof. Dr. Ulrich Schubert

am
Institut für Materialchemie / E165

eingereicht an der Fakultät für Technische Chemie
der Technischen Universität Wien

von
Ing. Mária Bendová

Matr. Nr. 0627868
Nitrianske Sučany 481, 972 21, Slowakei

Wien, am 15. Juni 2010   Ing. Mária Bendová

Acknowledgements

Kurzfassung

Halbleitende CdS Nanopartikel (NP) befinden sich an der Grenze zwischen "bulk" Materie und Molekülen und besitzen neuartige Eigenschaften, die auf "quantum size effect" beruhen. Dies führt zu einem breiten Feld von Anwendungen im Bereich Optoelektronik. Ein Teil der Forschung beschäftigt sich mit Einbau von NP in eine polymere Matrix, was zu hybriden Materialien mit fotolumineszierenden Eigenschaften führt. Cluster sind eine Subgruppe der NP mit einer genau definierten molekularen Struktur. Der Ziel dieser Arbeit war, hybride Materialien vorzubereiten, die kovalent gebundene CdS Cluster in einer polymeren Matrix beinhalten. Um das zu erreichen, müssen zuerst funktionelle Cluster vorbereitet werden, d.h. Cluster mit einer organischen Gruppe auf der Oberfläche, die polymerisieren kann, dann müssen diese kovalent in eine polymere Matrix eingebettet werden. Während des ganzen Prozesses muss der Cluster eine genau definierte molekulare Struktur haben.

Der Verlauf der Arbeit war aber anders. Im ersten Teil wurde die molekulare Struktur von ausgewählten Clustern in Lösung untersucht, wobei die Reaktionsbedingungen ähnlich zu einer Polymerisation waren. Am Beispiel des gut untersuchten $(NMe_4)_4[Cd_{10}S_4(SPh)_{16}]$ Clusters wurde gezeigt, dass Koordination des Lösungsmittels eine große Rolle für das Erhalten der Clusterstruktur spielt. Wenn ein stark koordinierendes Lösungsmittel (DMSO, DMF) verwendet wird, wird der Cluster in größere Cluster und NP umgewandelt, in schwächer koordinierenden Lösungsmitteln (MeCN) ist der Effekt weniger ausgeprägt, und nur ein Teil des Clusters wächst bei höheren Temperaturen. Gleichzeitig mit dem Enstehen größerer Partikel wird ein Nebenprodukt freigesetzt, das in DMSO als $[Cd(SPh)_x(DMSO)_y]^{(2-x)}$ (x = ca. 3) charakterisiert wurde. Eine andere Verbindung, "$Cd_{10}S_4(SPh)_{12}$", zeigte das gleiche Verhalten in stark koordinierenden Lösungsmitteln, wobei aus derer Lösungen verschiedene Cd54 Cluster auskristallisiert wurden.

Die Verbindung "$Cd_{10}S_4(SPh)_{12}$" wurde noch aus einem zusätzlichen Grund untersucht. Theoretisch sollte sie vier freie Cd Koordinationsstellen haben, welche zur Funktionalisierung geeignet sein sollten. Es hat sich aber gezeigt, dass die Verbindung nicht die postulierte $Cd_{10}S_4(SPh)_{12}$ Struktur hat, sondern aus einer Mischung von Clustern unterschiedlicher Größe zusammengesetzt ist. Deswegen kann sie nicht zur Funktionalisierung verwendet werden.

Der zweite Teil der Arbeit beschäftigt sich mit Charakterisierung von einigen OH- und NH_2-funktionalisierten Clustern im festen Zustand und in Lösung. Es wurde gezeigt, dass der Cluster $[Cd_{10}(SCH_2CH_2OH)_{16}]^{4+}$ durch Wasserstoffbrückenbindungen in Lösung stabilisiert ist. Wenn das Netzwerk aber gebrochen wird (z.B. durch Lösungsmittel, die als starke Wasserstoffbrückenakzeptoren wirken, wie DMSO, oder durch Reaktion der OH Gruppen), wird der Cluster destabilisiert und in Lösung abgebaut. Ausserdem führt die Reaktion mit Acetanhydrid zu S-Acetylierung der Liganden, was im kompletten Abbau des Clusters endet.

Ein neuer, NH_2-funktionalisierter Cluster $\{[Cd_{17}S_4(SPh\text{-}pNH_2)_{24}(DMF)_2]X_2\}_\infty$ wurde durch Modifikation der $[Cd_{10}S_4(SPh)_{16}]^{4-}$-Synthese hergestellt. Im festen Zustand sind die Cluster in einer 1D Kette durch Cd–N Koordination verbunden. Deswegen braucht man stark koordinierende Lösungsmittel, um isolierte Cluster in Lösung zu bekommen. Das führt

wahrscheinlich zum Wachstum des Clusters in DMSO und bedeutet, dass der Cluster nicht zur Herstellung der gewünschten Hybridmaterialien geeignet ist.

Im letzten Teil wurde die Möglichkeit einer radikalischen Polymerisation in der Gegenwart des Modelclusters $[Cd_{10}S_4(SPh)_{16}]^{4-}$ untersucht. Es wurde gezeigt, dass die Ligandhülle teilweise durch die Radikale oxidiert wird und dass dann die nicht ausreichend geschützten Clusterkerne zusammenwachsen und größere Cluster bilden. Andererseits war Radikalpolymerisation möglich und es wurden sogar keine größeren Unterschiede in Monomerkonversion und in Molekulargewicht-Verteilung des Polymers bei der Polymerisation mit und ohne Cluster beobachtet. Ausserdem wurde festgestellt, dass Cluster mit ungesättigten Thiolaten auf der Oberfläche stabil sind.

Diese Beobachtungen führen zur Schlußfolgerung, dass eine kovalente Integration der Cluster in eine polymere Matrix und gleichzeitige Erhaltung deren genau definierter molekularen Struktur keine einfache Aufgabe ist. Zur Auflösung der Cluster werden meistens koordinierende Lösungsmittel gebraucht, die aber zum ungewünschten Clusterwachstum führen.

Abstract

Semiconductor CdS nanoparticles (NPs) represent a system between bulk solids and molecules with novel properties of matter, originating from "quantum size effects". This results in a wide field of semiconductor NP application especially for optoelectronic devices. Part of the research is aiming to prepare polymers doped with CdS NPs, so called hybrid materials, in order to introduce photoluminescent properties. Clusters are a special case of NPs with defined molecular structure. The aim of this work is related: to prepare hybrid materials with CdS clusters covalently bound in a polymeric matrix. To this end, functional CdS clusters had to be prepared first, with organic groups on the surface capable of polymerization; then they had to be covalently incorporated into a polymeric matrix. During the whole procedure, the molecular structure of the cluster has to be precisely defined.

However, the investigations proceeded differently. In the first part, the molecular structure of the chosen model clusters was investigated in solution at conditions similar to polymerization. On the example of the well known $(NMe_4)_4[Cd_{10}S_4(SPh)_{16}]$ cluster it was shown that solvent coordination plays an important role in the maintainance of the cluster structure. When strongly coordinating solvents were used (DMSO, DMF), the cluster rearranged to bigger clusters and NPs, in weakly coordinating solvents (MeCN) the effect was observable only at elevated temperatures and proceeded only to low degrees. Concomitant with the formation of bigger particles, a byproduct was formed which was characterized as $[Cd(SPh)_x(DMSO)_y]^{(2-x)}$ (x = ca. 3) in DMSO. The second investigated compound, "$Cd_{10}S_4(SPh)_{12}$", revealed the same behavior in coordinating solvents which led also to crystallization of diverse Cd54 clusters.

The compound "$Cd_{10}S_4(SPh)_{12}$" was investigated also for different reasons: theoretically, it should have four free Cd coordination sites capable of functionalization. It turned out, that it does not have the postulated structure $Cd_{10}S_4(SPh)_{12}$, but that it is a mixture of differently sized CdS clusters. Thus, it could not be used for controlled functionalization.

The second part deals with the characterization of few OH- and NH_2-functionalized clusters in solid state and solution. It was shown that clusters of $[Cd_{10}(SCH_2CH_2OH)_{16}]^{4+}$ type are stabilized by a hydrogen bond network in solution. When the network is broken (by a strong hydrogen bond acceptor solvent, like DMSO, or by reaction of the OH groups), the cluster is destabilized and disintegrated in solution. Reaction of the cluster with acetic anhydride led to complete cluster degradation due to reaction also with the S-side of the ligands.

A new, NH_2-functionalized cluster $\{[Cd_{17}S_4(SPh\text{-}pNH_2)_{24}(DMF)_2]X_2\}_\infty$ was synthesized by modification of the $[Cd_{10}S_4(SPh)_{16}]^{4-}$ preparation procedure. In solid state, it is a 1D chains of clusters connected by the stabilizing ligands through Cd–N coordination. This resulted in the necessity to use coordinating solvents in order to obtain single clusters in solution, which led very probably to growth of the cluster in DMSO solution. Therefore, the prepared NH_2-substituted cluster is not suitable for preparation of the aimed hybrid materials.

In the last part, the possibility of radical polymerization in the presence of $[Cd_{10}S_4(SPh)_{16}]^{4-}$ was investigated. It was shown that the cluster ligand shell is partially

oxidized by radicals and the insufficiently protected cluster cores aggregate and form bigger clusters. However, radical polymerization is possible and no substantial differences (monomer conversion, polymer chain length distribution) were observed between polymerization with and without the cluster. Beside this, clusters with unsaturated thiolates on the surface were shown to be stable.

Therefore, covalent incorporation of clusters into a polymeric matrix and maintaining their precisely defined structure is not an easy task. It requires cluster dissolution, for which coordinating solvents are usually necessary, which, on the other hand, cause undesired cluster rearrangement.

Parts of this work have been published

M. Bendova, M. Puchberger, S. Pabisch, H. Peterlik, U. Schubert, Studies on the Formation of CdS Nanoparticles from Solutions of $(NMe_4)_4[Cd_{10}S_4(SPh)_{16}]$, *Eur. J. Inorg. Chem.* **2010**, 2266–2275, DOI 10.1002/ejic.201000080.

M. Bendova, M. Puchberger, S. Pabisch, H. Peterlik, U. Schubert, Characterization of "$Cd_{10}S_4(SPh)_{12}$", the Thermal Decomposition Product of $(NMe_4)_4[Cd_{10}S_4(SPh)_{16}]$. Synthesis of a Neutral Cd_{54} Sulfide Cluster and of a Polymeric Chain of Thiolate-bridged Cd_{17} Sulfide Clusters. *Eur. J. Inorg. Chem.*, accepted, DOI 10.1002/ejic.201000454.

Abbreviations

1D	one dimensional
2θ	diffraction angle
2D	two dimensional
3D	three dimensional
AIBN	azobisisobutyronitrile
COSY	correlation spectroscopy
CP	cross polarization
CSD	the Cambridge Structural Database
DLS	dynamic light scattering
DMF	N,N–dimethylformamide
DMPO	5,5-dimethyl-1-pyrroline-N-oxide
DMSO	dimethylsulfoxide
e^-	electron
EXSY	2D exchange spectroscopy
F	structure factor
GOF	goodness of fit
GPC	gel permeation chromatography
h^+	hole
HBA	hydrogen bond acceptor
HDA	hexadecylamine
HMBC	heteronuclear multiple-bond correlation
HSQC	heteronuclear single quantum correlation
I	intensity
λ	wavelength
MAS	magic angle spinning
MeCN	acetonitrile
MMA	methyl methacrylate
MS	mass spectrometry
MV^{2+}	methyl viologen dication
μ	absorption coefficient
Na-VBT	sodium 4-vinylbenzylthiolate
NMR	nuclear magnetic resonance
NP	nanoparticle
PDI	polydispersity index
q	scattering vector

SAXS	small-angle X-ray scattering
SC-XRD	single-crystal X-ray diffraction
$T10$	temperature of 10-h half-life
TEM	transmission electron microscopy
TEMPO	2,2,6,6-tetramethylpiperidine oxide
TGA	thermogravimetric analysis
THF	tetrahydrofuran
TOPO	trioctylphosphine oxide
XRD	X-ray diffraction
Z	number of formula units per unit cell

NMR Abbreviations

δ	chemical shift
s	singlet
d	doublet
t	triplet
q	quartet
p	pentet
m	multiplet
br	broad

Cluster Abbreviations

Cd4a	$[Cd_4(SPh)_{10}]^{2-}$
Cd4b	$[Cd_4(SPh)_8]_\infty$
Cd10a	$(NMe_4)_4[Cd_{10}S_4(SPh)_{16}]$
Cd10b	"$Cd_{10}S_4(SPh)_{12}$"
Cd10c	$[Cd_{10}(SCH_2CH_2OH)_{16}]^{4+}$
Cd17a	$(NMe_4)_2[Cd_{17}S_4(SPh)_{28}]$
Cd17b	$[Cd_{17}S_4(SCH_2CH_2OH)_{26}]_\infty$

Table of Contents

1 Introduction

CdS nanoparticles (NPs), as a subset of semiconductor NPs, have gained a lot of scientific attention since the early 1980s. They constitute a system lying in the transition regime between bulk solids and molecules which gives them novel properties of matter, usually described as "quantum size effect". A very nice demonstration of this size dependent property is the drastic color change of their colloidal solutions with decreasing particle size (Figure 1.1). The effect results in a wide field of semiconductor NP application in optoelectronic devices ranging from solar cells, through light-emitting devices, electrochemical sensors, and photocatalysts, to biological labels.

A part of the semiconductor NP research is aiming to prepare polymers doped with NPs, so called hybrid materials, which combine properties of its both constituents. Thus, a luminescent polymeric material is obtained. NPs can be differently bonded in the polymeric matrix: either by only weak interactions like van der Waals contacts, hydrogen bonds, π-π interactions or electrostatic forces, or by strong chemical bonds like covalent, ionic or Lewis acid-base bonds. In the second case, a cross-linked organic-inorganic network is obtained. It requires NPs which are surface modified with organic groups capable of a polymerization (so called functional NPs).

This is also the aim of this work, to prepare hybrid materials with constituents covalently linked; however, instead of CdS NPs in general, CdS molecular clusters have to be used. Clusters are a subset of NPs which are characteristic by a defined molecular structure and still bear the physical properties typical for NPs. To this end, functional CdS clusters have to be prepared first, with organic groups on the surface, like hydroxy, carboxy, amino or double bonds; then they have to be covalently incorporated into a polymeric matrix. During the whole procedure, the molecular structure of the cluster has to be defined, or precisely known.

In the next chapters, the problems are described which we had to face on the way to such hybrid materials.

Figure 1.1. Size-dependent change of emission of colloidal suspensions of 1.7–5 nm core CdSe/ZnS core-shell NPs. Figure taken from Ref. 1.

2 Literature Review

2.1 CdS Clusters and Nanoparticles

There is not a clearly defined border between clusters and nanoparticles (NPs). One can define semiconductor clusters as large, discrete molecular complexes with up to several tens of heavy metal atoms.[2] The metal atoms are not connected directly by metal-metal bonds as in metal clusters, but contain chalcogen atoms in between as bridges, *i.e.* the cluster core is made up of metal and chalcogen atoms. Clusters have zero size distribution and have been structurally characterized in detail. Thus, clusters are monodisperse and show properties in the "molecular" size regime.

Semiconductor NPs are chemically very similar to clusters. They are bigger in diameter, but still in the nanometer regime. However, their exact molecular structure is not known and they are usually polydisperse in size. NPs are thus characterized by other properties than their molecular structure: average size and polydispersity and/or some physical characteristics like UV/Vis absorption or luminescence for CdS NPs.

Both CdS clusters and NPs have a semiconductor core, from which an essential part are surface metal atoms, and a surface structure of capping ligands. The core is mainly responsible for physical properties, their surface being site for chemical reactions. Clusters and NPs have a lot of in common, but show also differences. In the next chapters, some of them will be discussed.

This concept of clusters and nanoparticles will be used in this thesis.

Sometimes, the term clusters or nanoclusters is used generally for all particles with sizes bigger than a molecule, but too small to bear properties typical for bulk matter.[3,4,5] Particles of the same size orders are also frequently called nanocrystals,[6] or quantum dots[7] (see later).

The field of semiconductor NPs and clusters is very broad due to wide range of possible applications in electronics, optics, and sensors. It is neither possible nor necessary for the purpose of this thesis to cover all of its details. Thus, only substantial effects and their impact on some properties with few applications will be discussed in the following chapter.

2.1.1 Quantum Size Effect in Semiconductor Clusters and Nanoparticles

As the size of a bulk material decreases and a particle is formed, size effects of two types can be observed. First one is related to the increase in surface area with smaller particle size, which becomes prominent at sizes 10–100 nm. Due to this effect, thermodynamic properties are largely changed, like melting temperature, solid–solid phase transitions, surface energetics.[8] Other effects originate from changes in the electronic state as a certain particle size is achieved. This effect is called *quantum size effect* and particles in the responsible size regime *quantum dots* (QDs) or Q-particles.[9,7] This leads to changes in optical and electrical properties of NPs. Meanwhile this became a prominent feature of metal and semiconductor

NPs leading to a number of promising uses. Quantum size effect in semiconductor NPs arises at much larger particle sizes compared with metals and insulators.[8]

The band gap of a direct semiconductor is defined as energy necessary to create an electron (e^-) and a hole (h^+) pair. This happens when a photon is absorbed by an e^- in a semiconductor material. It leaves a h^+ in the valence band and is excited into the conduction band. The band gap energy differs for diverse semiconductor materials: *e. g.* 3.91 (hexagonal ZnS), 3.54 (cubic ZnS), 2.42 (CdS), and 1.73 eV (CdSe). If the e^- and h^+ approach each other they may form a bound state (Mott–Wannier exciton). The lowest exciton in CdS has a Bohr diameter of ca. 6 nm,[4] which is given by

$$r_{\mathrm{B}} = \frac{\hbar^2 \varepsilon}{e^2} \left(\frac{1}{m_{\mathrm{e}}} + \frac{1}{m_{\mathrm{h}}} \right) \tag{2.1}$$

where ε is the dielectric constant and m_{e} and m_{h} are effective masses of e^- and h^+. As the size of a NP approaches the exciton size, the exciton is confined by the size of the NP and its energy has to be quantized into a state with higher kinetic energy. Thus, the valence and conduction bands of a semiconductor NP have to be quantized with NP size smaller than the critical size being ca. 6 nm for CdS.[9,10] The situation is depicted schematically in Figure 2.1. Thus, the lowest excited electronic state (or band gap) of semiconductor NPs is size dependent.
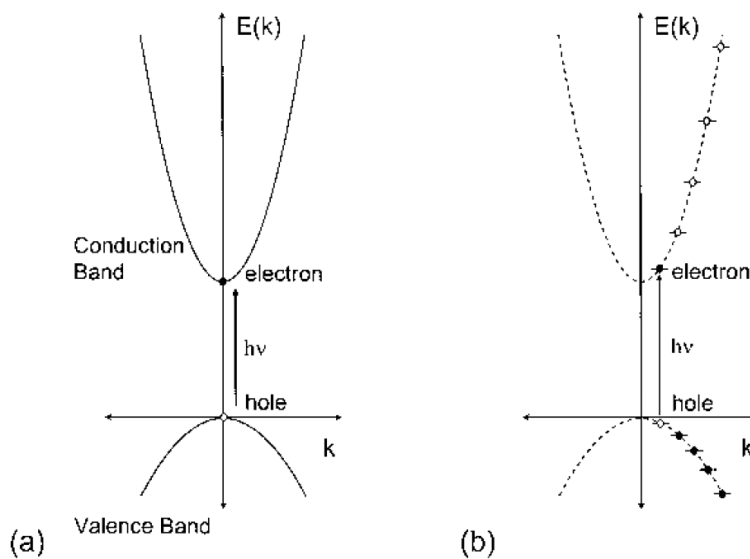
Figure 2.1. (a) Band diagram for a simple two-band model for direct-gap semiconductors. (b) Schematic electron transitions in small-size semiconductor NPs. Figure after Ref. 11.

Quantum size effects result in changes of absorption and emission energies. Thus, in the absorption spectra of molecular clusters and nearly monodisperse NPs, a sharp maximum is observed which is blue shifted from the absorption onset of bulk CdS. This maximum is assigned to excitonic transition and is a measure for the size of the band gap of the cluster/NPs.[3,10] The size of the band gap increases with decreasing particle size, leading to

a shift of the absorption maximum to higher energy.[3] Therefore, instead of orange bulk CdS, yellow or even colorless CdS NPs can be produced.[3]

Qualitatively, changes in exciton energy of QDs can be understood quantum mechanically as a "particle in a box" problem, where energy levels increase as the dimensions of the box decrease. Quantitatively, more elaborate approaches have to be used. The dependence of band gap energy on NP size can be predicted using three mostly employed theoretical methods. *Effective mass approximation*,[10,3] the simplest three dimensional (3D) confinement model, is based on Coulombic interaction between the e^- and h^+ where the valence and conduction bands are assumed to be parabolic near the band gap. This model does not fit very well with experimental results (Figure 2.2). Another method, *tight-binding calculation*,[12] offers a better match between calculated and experimental band gap energies (Figure 2.2). It is a more molecular approach based on linear combination of atomic orbitals. The *empirical pseudopotential method*[13] allows treatment of the atomistic character of a QD as well as the surface effects. Good agreement with experiment has been obtained,[14] but the band gap energy cannot be calculated for large QDs due to the big size of the Hamiltonian.[15]

However, the comparison of theoretical calculation with experimental results has some limitations. Experimentally, the size of NPs can be determined by different methods which can lead to different sizes, depending whether only the core or also the outer shell bearing the ligands is observed. Simultaneously, the determination of band gap energy from absorption spectra is not always explicit. Thus, NP sizes determined by powder X-ray diffraction (powder XRD) differ from those obtained by transmission electron microscopy (TEM), although both should result in NP core sizes (Figure 2.2).
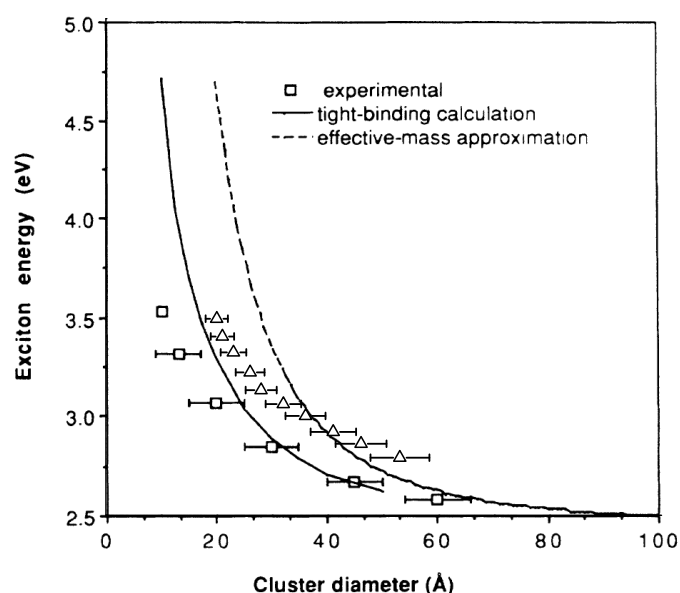
Figure 2.2. The exciton transition energy as a function of CdS NP diameter. Effective mass approximation results are given by the dashed curve, tight-binding model gives the solid curve. Figure after Ref. 3, tight-binding calculation taken from Ref. 12. Experimental data: (□) Ref. 16, NPs stabilized by PhSH, sizes determined from powder XRD using Scherrer's equation; (△) Ref. 17, NPs stabilized by oleic acid, sizes obtained by TEM.

After light absorption and e^- excitation, several processes can take place in a QD (Figure 2.3). The "hot" exciton,[18] which is initially formed, is relaxed by an electron-phonon relaxation or thermalization mechanism until it reaches its band gap energy (Figure 2.3, process 2).[18] Afterwards, the following processes are probable (Figure 2.3): (i) non-radiative relaxation to the ground state (process 6), (ii) capture of the charge carriers by surface traps (process 7 and 8), (iii) radiative recombination, *i. e. photoluminescence* (process 9 and 10, see also Figure 1.1), (iv) charge transfer onto adsorbed species (process 11 and 12). The probability of these processes is influenced very much by the size of the QD and character of its surface. Since QDs are very small, charge carriers are delocalized near the surface. This simplifies their trapping by surface states and prevents their direct radiative recombination, photoluminescence.[7] QD surfaces are usually imperfect and provide various sites for e^- and/or h^+ trapping.[4] *Trapping of charge carriers* can have the following consequences. It can lead to absorption bleaching due to saturation of the excitonic transition, since the charge carriers trapped at the surface interact with the possible newly formed exciton.[19] One trapped e^-–h^+ pair can bleach the excitonic transition of the whole QD.[20] The recovery time for the excitonic transition is then based on the trapped-carrier relaxation time and mechanism, which is dependent on the surface chemistry.[19] This phenomenon changes optical properties of QDs and causes nonlinear optical effect.[4] Further consequences result from trapped-carrier relaxation mechanism. Either they are recombined radiatively (photoluminescence, process 10 in Figure 2.3) or they lead to oxidation or reduction of species on the QD surface (processes 11 and 12). This effect can be desired for *photochemical reactions*[4] or can be harmful due to *photodecomposition* of QDs.[8] Photodegradation of QDs depends on the presence of oxygen, on the character of solvent,[21] and on the character of the ligand shell.[2,22] In aqueous solutions, CdS QDs are decomposed only in the presence of O_2,[23,22] but, depending on the ligand shell, the particles either decrease or increase in size.[22] In THF, photodegradation is observed in the presence of O_2, and formation of bigger NPs in the absence of O_2 due to destabilization of the NPs by destruction of the ligand shell.[21] In *N,N*–dimethylformamide (DMF), photodecomposition in the absence of O_2 leads also to formation of bigger aggregates due to loss of stabilizing ligands.[24] In these processes, h^+ often acts as oxidizing agent and leads to formation of surface $S^{\cdot-}$ [25,7] or $RS^{\cdot}$ [21] radicals, leading to formation of sulfites, sulfates, disulfides or free thiolates,[8,21] depending on the presence of oxygen.[21] On the other hand, e^- reducing agents can reduce Cd^{2+} to Cd^0 or O_2 to O_2^-.[21] In this way, CdS QDs can be degraded and destroyed within few days of illumination[8] or can increase in size in the absence of O_2.[21]

1. $SC + hv_{ex} \rightarrow (e^- ... h^+)^*$
2. $(e^- ... h^+)^* \rightarrow e^-_{CB} .. h^+_{VB}$
3. $e^-_{CB} .. h^+_{VB} \rightarrow e^-_{CB} + h^+_{VB}$
4. $2(e^-_{CB} .. h^+_{VB}) \rightarrow (e^-)^* + h^+_{VB}$
5. $2(e^-_{CB} .. h^+_{VB}) \rightarrow e^-_{solv} + h^+_{VB}$
6. $e^-_{CB} + h^+_{VB} \rightarrow n(ph)$
7. $e^-_{CB} \rightarrow e^-_{tr}$
8. $h^+_{VB} \rightarrow h^+_{tr}$
9. $e^-_{CB} + h^+_{VB} \rightarrow hv_{lum}$
10. $e^-_{tr} + h^+_{VB} \rightarrow hv'_{lum}$
11. $e^-_{tr} + A_{ads} \rightarrow A^{\bullet-}_{ads}$
12. $h^+_{tr} + D_{ads} \rightarrow D^{\bullet+}_{ads}$
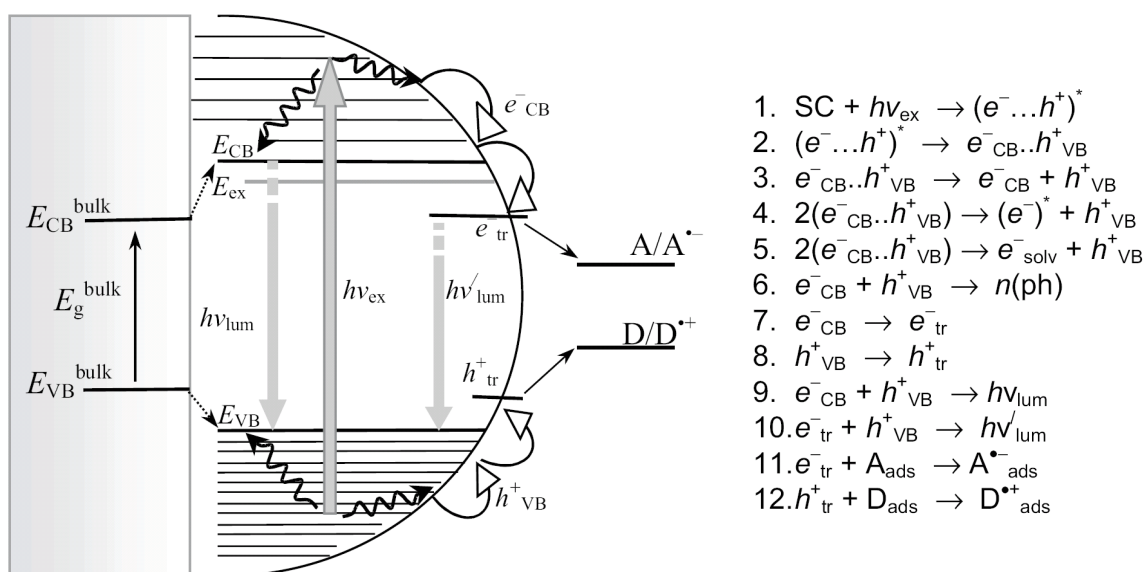
Figure 2.3. Scheme of diverse electron transitions in a semiconductor NP. SC: semiconductor; $(e^- ... h^+)^*$: "hot" exciton; hv_{ex}, hv_{lum}, hv': quanta of exciting light, exciton and "defect" luminescence; ph: phonon; e^-_{solv}: solvated e^-; e^-_{tr} and h^+_{tr}: e^- and h^+ captured by surface traps; A_{ads}, D_{ads}: adsorbed e^- acceptor and donor. Figure after Ref. 18.

It therefore appears that the desired property of QDs, photoluminescence, competes with their photodegradation. Few approaches have been developed to suppress photodecomposition. They are based on the modification of the NP surface and elimination of surface traps for excitonic charge carriers. One example is exchange of organic ligands on the QD surface by other ligands like amines, phosphines, or phosphonic acids.[26] This leads to elimination of surface traps compared with thiolates and increase of photoluminescence and photostability. Another possibility is surface modification by an inorganic shell, leading to composite QDs (Figure 2.4, type I). Its shell is formed by a large band gap semiconductor and the band edges of the core QD lie in between.[7] Investigated systems include CdS–Cd(OH)$_2$,[27] CdSe–ZnS,[28,29] and CdSe–ZnSe[30] core–shell NPs. In all these cases, strong excitonic fluorescence was observed. Beside this, the CdS–Cd(OH)$_2$ system showed strong improvement of photostability, but no complete removal of surface trapping was achieved.[27] Another possibility (type II) is to connect materials, of which one has conduction and valence bands below those of the other material. Thus, core–shell or sandwich (Figure 2.4, right) NPs can be prepared. Such core–shell NPs are characterized by effective charge carrier separation, enhanced luminescence and photostability. For example, CdSe–CdS[31] or CdTe–CdS[32] core–shell QDs have been investigated. Photostability of this type QDs originates from the h^+ confinement in the core, whereas e^- are accessible for further processes. This makes them also suitable for optoelectronic devices.[31] If a biocompatible shell is added (ZnS), multiple core–shell QDs can be synthesized which are suitable for biological application.[33] Moreover, the valence and conduction band relations can be tuned in such a way that effective band gap of a composite QD would be smaller than those of only core or shell. Thus, CdTe–CdSe core–shell QDs can emit infrared radiation.[34]
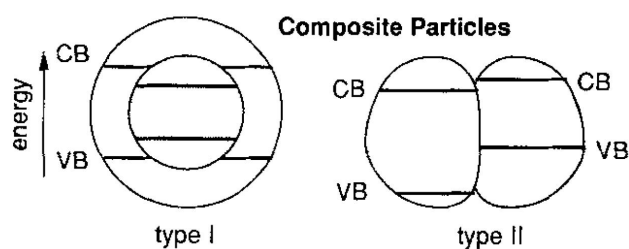
Figure 2.4. Schematic representation of composite NPs. VB is valence band edge, CB conduction band edge. Figure after Ref. 7.

It should be apparent by now that optical properties of NPs can be tuned easily and in more ways than those of clusters which have an exact molecular structure. Variable parameters are core size, chemical composition of the core, surface modification, diverse core–shell combinations.[35] Chemical modification of the core, besides influencing the optical properties, can introduce additional physical properties to the NPs. Thus, doping with Mn^{2+} [36] or Co^{2+} [37] leads to additional magnetic properties of QDs. Doping is also possible for clusters, but is much more complicated. For example, small clusters with mixed Cd/Zn core have been synthesized,[38] however, addition of Zn does not introduce new physical properties to the cluster and "only" tunes already present optical properties.

Semiconductor QDs and their variations offer a wide range of applications. As already mentioned, charge carriers arisen from light absorption can be utilized for diverse optoelectronic devices.[31] Here, two main arrangements are possible (Figure 2.5): either the h^+ oxidizes an electron donor adsorbed on the QD and the excited e^- is transferred to the electrode (anodic photocurrent), or the excited e^- reduces an electron acceptor and the h^+ is recombined with an e^- taken from the electrode (cathodic photocurrent).[39] Thus, semiconductor QDs offer new possibilities in different application fields: hybrid solar cells,[40] dye-sensitized solar cells,[41] light-emitting devices,[1] electrochemical sensors,[42] photocatalysis,[43,44] biological labeling,[39] *etc*.
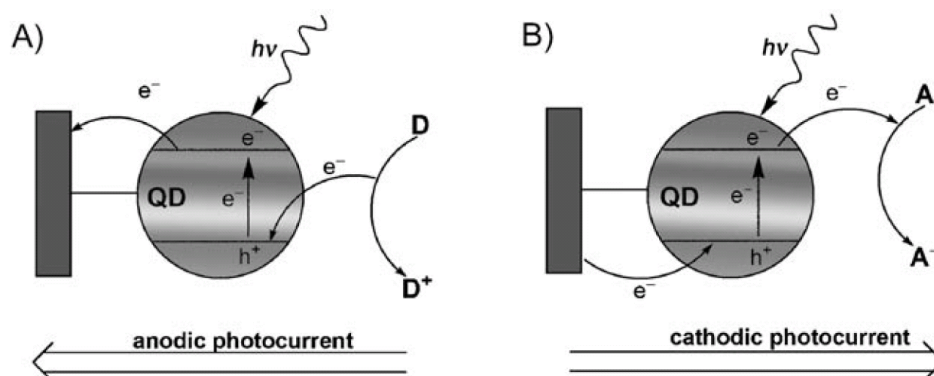
Figure 2.5. Photocurrents generated by semiconductor QDs after light absorption: A) anodic photocurrent, B) cathodic photocurrent. Figure after Ref. 39.

7

2.1.2 CdS Clusters and Their Characterization

CdS clusters with different core sizes and stabilizing ligands have been synthesized by now. The most important are summarized in Table 2.2, together with schematic syntheses and UV/Vis characteristics. Cores of all of them are tetrahedrally shaped and are built of adamantane and/or barrelene cages. Adamantane cages are building blocks of the cubic zinc blende structure, while barrelene cages are those of the hexagonal wurtzite type. The most typical CdS clusters are those with following cores: Cd10, Cd17, Cd32, and Cd54 (Figure 2.6). Their ideal compositions are summarized in Table 2.1.[65] They are capped by different thiolate ligands, usually by PhS⁻, but also clusters with $HOCH_2CH_2S^-$ and other thiolates are known.

Cd10a   **Cd17a**   Cd32   Cd54
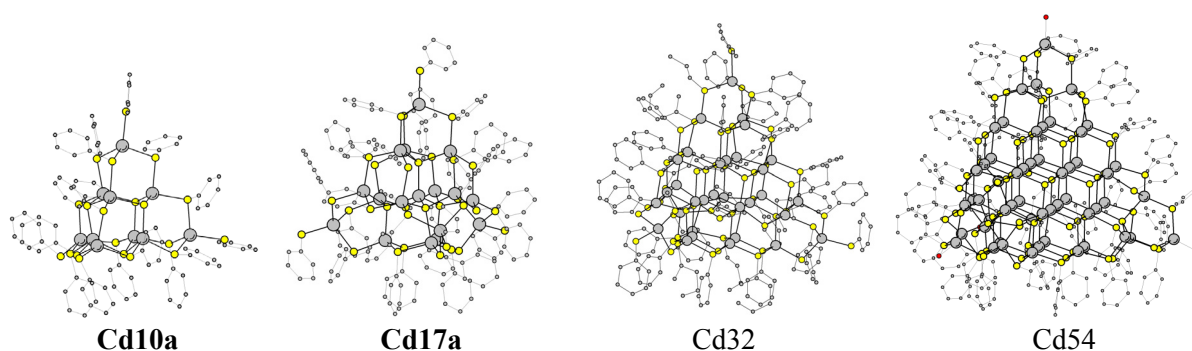
*Figure 2.6. Drawings of **Cd10a**, **Cd17a**, Cd32, and Cd54 thiophenolate-capped CdS clusters: $[Cd_{10}S_4(SPh)_{16}]^{4-}$, $[Cd_{17}S_4(SPh)_{28}]^{2-}$, $[Cd_{32}S_{14}(SPh)_{40}]^{4-}$, and $[Cd_{54}S_{32}(SPh)_{48}L_4]^{4-}$. Figures are according to crystal structures in Ref. 47, 58, and 59.*

*Table 2.1. Chemical composition of idealized CdS clusters in the system Cd^{2+}–S^{2-}–PhS^-.[47,65] Note the increasing negative charge with increasing cluster size. The **Cd10a** cluster belongs to the first series of tetrahedral clusters called supertetrahedral Tn clusters,[45] being the T3 cluster, all the others belong to the third series called capped supertetrahedral Cn clusters.[45]*

Core size	Idealized composition	Nr. of μ_4– S^{2-} sites	Nr. of μ_3– S^{2-} sites	Nr. of μ_2– PhS^- sites	Nr. of terminal PhS^- sites
Cd8	$[Cd_8S(SPh)_{16}]^{2-}$	1	0	12	4
Cd10	$[Cd_{10}S_4(SPh)_{16}]^{4-}$	0	4	12	4
Cd17	$[Cd_{17}S_4(SPh)_{28}]^{2-}$	4	0	24	4
Cd32	$[Cd_{32}S_{14}(SPh)_{40}]^{4-}$	10	4	36	4
Cd54	$[Cd_{54}S_{32}(SPh)_{52}]^{8-}$	20	12	48	4
Cd84	$[Cd_{84}S_{59}(SPh)_{64}]^{14-}$	35	24	60	4
Cd123	$[Cd_{123}S_{96}(SPh)_{76}]^{22-}$	56	40	72	4
Cd172	$[Cd_{172}S_{144}(SPh)_{88}]^{32-}$	84	60	84	4

Table 2.2. Brief summary of diverse CdS clusters. MV^{2+} = methyl viologen dication.

Core size	Composition, counter-ions (crystal structure)	Synthesis	UV/Vis absorption		Label	Ref.
			Max. (nm)	Solvent		
Cd4 [a]	$[Cd_4(SPh)_{10}]^{2-}$; NEt_4^+, $NHEt_3^+$, NMe_4^+	Cd^{2+} + PhSH + NEt_3 + NMe_4^+ in MeOH	275[67]	MeCN	**Cd4a**	46, 47, 48
	$[Cd_4(SPh)_8]_\infty$	Cd^{2+} + PhSH + NEt_3 in DMF/*e. g.* EtOH	–		**Cd4b**	49, 50
Cd8	$[Cd_8S(SPh)_{16}]^{2-}$; MV^{2+}, NEt_4^+	(1) $[Cd_x(SPh)_y]$ + CS_2 in org. solvents (2) Cd^{2+} + PhS^- + S^{2-} + NEt_4^+ in EtOH/MeCN	–			51, 52
Cd10	$[Cd_{10}S_4(SPh)_{16}]^{4-}$; NMe_4^+, $NHEt_3^+$	(1) $[Cd_4(SPh)_{10}]^{2-}$ + S in MeCN or DMF (2) Cd^{2+} + PhS^- + S^{2-} + NMe_4^+ in MeCN	292[67]	MeCN	**Cd10a**	47, 53
	"$Cd_{10}S_4(SPh)_{12}$"	$[Cd_{10}S_4(SPh)_{16}]^{4-}$ heating *in vacuo*	ca. 346[54] c	pyridine	**Cd10b** [b]	54
	$[Cd_{10}(SCH_2CH_2OH)_{16}]^{4+}$; SO_4^{2-}, NO_3^-, ClO_4^-	Cd^{2+} + $HSCH_2CH_2OH$ + X^- in H_2O	254[68]	H_2O	**Cd10c** [a]	55, 56, 57
Cd17	$[Cd_{17}S_4(SPh)_{28}]^{2-}$; NMe_4^+	Cd^{2+} + PhSH + NEt_3 + S^{2-} + NMe_4^+ in MeCN/MeOH	–		**Cd17a**	58
	$[Cd_{17}S_4(SPh)_{26}L_x]_{1\ or\ \infty}$, $x = 0–2$	$[Cd_x(SPh)_y]$ + thiourea in MeCN (solvothermal)	291[59] 305[60]	THF solid		59, 60, 61, 62
	$[Cd_{17}S_4(SCH_2CH_2OH)_{26}]_\infty$	Cd^{2+} + $HSCH_2CH_2OH$ + H_2S in H_2O (dialysis)	ca. 290[63] ca. 305[69]	different solid	**Cd17b**	63
Cd32	$Cd_{32}S_{14}(SPh)_{36}L_4$	"$Cd_{10}S_4(SPh)_{12}$" in pyridine/DMF	358[64] c	THF		64
	$[Cd_{32}S_{14}(SPh)_{40}]^{4-}$; PPh_4^+	$[Cd_4(SPh)_8]_\infty$ + thiourea in MeCN (solvothermal)	327[59]	DMF		59
	$[Cd_{32}S_{14}(SPh)_{36}L_x]_\infty$, $x = 2, 4$	$[Cd_x(SPh)_y]$ + thiourea in MeCN (solvothermal)	335[60]	solid		60, 65
	$Cd_{32}S_{14}(SCH_2CH(OH)CH_3)_{36}(H_2O)_4$	Cd^{2+} + $HSCH_2CH(OH)CH_3$ + H_2S in H_2O, dialysis	ca. 325[66]	DMF, solid		66
Cd54	$[Cd_{54}S_{32}(SPh)_{48}(H_2O)_4]^{4-}$; NMe_4^+, PPh_4^+	$[Cd_4(SPh)_8]_\infty$ + thiourea in MeCN (solvothermal)	353[59]	DMF		59

a This is not a CdS cluster, but a polynuclear Cd thiolate complex.
b Crystal structure was not obtained.
c Absorption maximum does not match with cluster size.

Coordination modes of sulfide (S^{2-}) and thiolate (RS^-) ligands in CdS clusters are manifold. S^{2-} can adopt either μ_3- or μ_4- coordination, depending on its position in the cluster (surface or core). RS^- ligands are present on the cluster surface and can be either double-bridging (μ_2) or terminal (μ_1). This high flexibility of sulfide and thiolate ligands offers more possibilities for ligand shell arrangement and thus easier formation of cluster surface. By the presence of ligand shell, clusters are kinetically stabilized and protected from agglomeration and formation of bigger CdS NPs.[2] Other chalcogenide ligands (Se, Te) prefer higher coordination modes, compared with S ligands, which is a consequence of larger ionic radii and larger polarizability. Thus, selenolate and tellurolate ligands act usually as doubly and also as higher bridging ligands.[2]

Another trend can be observed in Table 2.2: with increasing size of SPh-capped clusters, terminal PhS^- ligands are replaced by zero-charged ligands L. L stands for monodentate coordinating ligands like solvent molecules (DMF),[64] bidentate pyridyl ligands,[60,65] or even quadridentate pyridyl ligands,[62] which possibly allow synthesizing MOF-like structures (*i.e.* metal organic frameworks).

Synthetic routes leading to semiconductor clusters have been reviewed in detail previously.[70] A frequently used method for the synthesis of CdS clusters and NPs is from the ions in the presence of a stabilizing ligand:

$$Cd^{2+} + S^{2-} \text{ (or } HS^- \text{ or } H_2S) + RS^- \rightarrow [Cd_xS_y(SR)_z]^w \qquad (2.2)$$
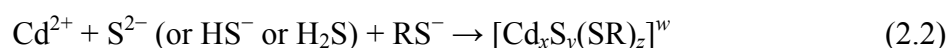
The growth of clusters into bigger NPs would be thermodynamically preferred (Ostwald ripening) but is kinetically hindered by the presence of stabilizing ligand. A careful adjustment of reactant ratios is necessary in order to obtain one cluster type.[71] The use of either protic or aprotic solvents has also an influence. Aprotic solvents like acetonitrile (MeCN) or *N,N*–dimethylformamid (DMF) are usually used for the synthesis of PhS-capped CdS clusters,[52,58] formation of CdS clusters with more polar surfaces is carried out in aqueous solutions.[63,66]

Another method, which is commonly used for the synthesis of $[Cd_{10}S_4(SPh)_{16}]^{4-}$ (**Cd10a**), is reduction of sulfur by PhS^- using a Cd-thiolate precursor:[47]

$$5 [Cd_4(SPh)_{10}]^{2-} + 8 S \rightarrow 2 [Cd_{10}S_4(SPh)_{16}]^{4-} + 8 PhSSPh + 2 PhS^- \qquad (2.3)$$
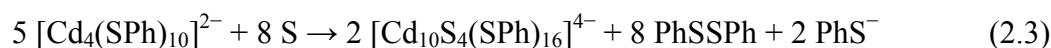
The same result can be achieved starting from Cd^{2+} ions followed by reduction with elemental sulfur:[70]

$$10 Cd^{2+} + 24 PhS^- + 4 S \rightarrow [Cd_{10}S_4(SPh)_{16}]^{4-} + 4 PhSSPh \qquad (2.4)$$

The third commonly used method for the synthesis of CdS clusters is solvothermal reaction of diverse Cd-thiophenolate precursor complexes with thiourea as sulfur source and suitable counter-ions (NMe_4^+, PPh_4^+) or with neutral pyridyl ligands in MeCN. This synthetic procedure led to crystallization of the biggest CdS and CdSe clusters obtained by now, *i.e.* Cd54 clusters. However, it is very probable that a bigger member of this cluster series,

a Cd123 cluster (Table 2.1), has been synthesized recently, but was not crystallographically characterized.[59]

Syntheses of Cd chalcogenide NPs are possible also by other methods than association of ions and solvothermal synthesis.[1,72,73] A very common procedure is pyrolysis of organometallic reagents like $CdMe_2$ with trioctylphosphine selenide (TOPSe) in hot coordinating solvents which act also as stabilizing ligands. It is characterized by separation of nucleation and growth which can optimally lead to homogeneously sized NPs. Instead of toxic $CdMe_2$, other Cd sources have been examined and utilized, e.g. $Cd(acetate)_2$ or CdO. Other methods involve growth in confined spaces like inverse micellar solutions or a structured medium (zeolite).

The organometallic procedure is usually not used for the synthesis of CdS/CdSe clusters. However, it was observed, that at specific conditions it results in the formation of specifically sized NPs called magic sized clusters (MSCs). They can be considered as NPs which are thermodynamically more stable than somewhat smaller or bigger ones.[74] Thus, they have discrete sizes which are characteristic by a sharp maximum in the absorption spectra. However, their precise molecular structure was not confirmed by other methods, like single-crystal X-ray diffraction (SC-XRD), since their crystallization is difficult due to the presence of long-chain stabilizing ligands on their surface. It might be speculated that the core structures of the MSCs could be similar to those of the known cluster series (Cd17, Cd32, Cd54, etc. see Table 2.1). Indeed, absorption maxima of some series of MSCs can be correlated with maxima of Cd-thiophenolate clusters.[75,59,76] On the other hand, the variability of surfactants used in their synthesis (long-chain acids,[75] phosphonic acids,[74] phosphines,[74] amines,[75] and their combinations), which bind in different modes to the NP surface, indicates formation of MSCs with sizes different from the known cluster series or with different optical properties.

As already indicated, CdS/CdSe clusters reveal optical properties characteristic for monodisperse NPs. It can be seen from Table 2.2 that their absorption maxima are indeed size dependent, at ca. 290, 325, and 350 nm for Cd17, Cd32, and Cd54 thiolate-capped CdS clusters in solution. However, smaller CdS clusters or complexes ($[Cd(SPh)_4]^{2-}$ and $[Cd_4(SPh)_{10}]^{2-}$) show an opposite effect: a blue shift with increasing size.[67,77] This originates from a combination of ligand-to-metal charge transfer (LMCT) (which can be formally assigned also to the origin of the band-gap transition in semiconductors[67]) and intraligand transitions[67] and from the fact that the energy levels of terminal thiophenolate levels lie higher in energy than the bridging ones.[77] An interesting effect has been observed for absorption measurements in solid state and in 3D cluster networks where particle-particle interactions play an important role.[78,69] Small, almost monodisperse 1-thioglycerol-stabilized CdS NPs had absorption maxima red-shifted from 260 nm in solution to 270 nm when closely packed in thin-film layers.[78] The shift was most pronounced for smallest NPs of approximately ten Cd atoms. This effect was explained by collective electronic modes similar to the energy bands of conventional bulk semiconductors.[78] Similarly, Döllefeld et al.[69] investigated the absorption of solid 3D networks of Cd17 clusters stabilized by 2-mercaptoethanol and observed a red shift of absorption in solution compared with solid state

from 290 to 305 nm. This shift was explained by calculations involving electronic and dipole-dipole interactions. It was found that the shift was higher for smaller NPs with smaller mutual distances.[69]

Another property related to the absorption behavior of clusters is their photostability. Similar processes take place, as described for CdS NPs in Chapter 2.1.1, which can lead to cluster decomposition or growth and formation of byproducts like sulfites, sulfates, disulfides or free thiolates, depending on the presence of oxygen and on solvent. Small CdS clusters and complexes ($[Cd(SPh)_4]^{2-}$, $[Cd_4(SPh)_{10}]^{2-}$, and $[Cd_{10}S_4(SPh)_{16}]^{4-}$ (**Cd10a**)) in MeCN are decomposed after UV irradiation to other decomposition products than disulfides: thianthrene, dibenzothiophene, and thiophenol (Scheme 2.1).[67] Interestingly, decomposition rates were not dependent on the presence of oxygen. Their formation starts probably from trapping of a h^+ by PhS^- ligands leading to $PhS^{\cdot}$ radicals. The following overall reactions have been proposed:

$$Cd(SPh)_2 \rightarrow Cd + H_2 + \text{thianthrene} \tag{2.5}$$

$$Cd(SPh)_2 \rightarrow Cd + H_2S + \text{dibenzothiophene} \tag{2.6}$$
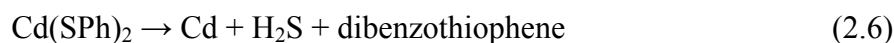
Beside this, it was suggested that excitonic e^- leads to reduction of Cd^{2+} and formation of Cd^0. Decomposition rates decreased with increasing cluster size.[67]

thianthrene   dibenzothiophene
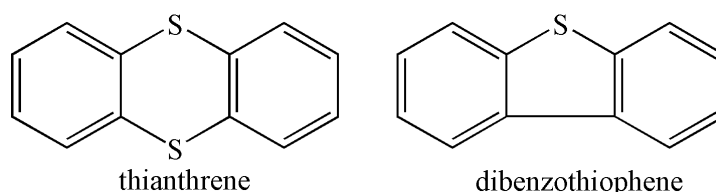
Scheme 2.1. Structures of thianthrene and dibenzothiophene molecules.

Molecular structures of CdS/CdSe clusters are usually determined in solid state and in solution. It might differ in these states due to thermodynamic stability/instability of the cluster in solution, thus other cluster(s) could be present in solution than in solid state. This knowledge is crucial for further cluster utilization, since most of the procedures are performed in solution.

Characterization in the solid state is based on crystallization of clusters from a solution, followed by structural investigation by means of SC-XRD. However, crystallization of clusters often starts when the reaction mixture is not in thermodynamic equilibrium. If it is in equilibrium, the preferred crystallization of one cluster type from the reaction solution can move the equilibrium to the side of the better crystallizing cluster. Thus, it is possible that the compound which crystallizes in high yields is not present in such high proportions in the reaction solution. This situation can occur mainly if a cluster in its crystal structure is stabilized by pronounced lattice energy due to nonbonding attractive interactions between the clusters, like hydrogen bonds or π–π interactions. For example, if one cluster type is known

only with PPh_3 or PPh_4^+ and not also with alkylphosphine ligands or cations, the probability is high that it is stable only in crystalline state. Thus, capability of crystallization is a measure for crystal stability, and not necessarily for molecular stability.[70]

Molecular stability of clusters and the identity of the structure in crystalline state have to be verified in solution. One of the best methods for CdS or CdSe clusters for this purpose is nuclear magnetic resonance (NMR), mainly ^1H, ^{13}C, and ^{113}Cd NMR, and for CdSe clusters also ^{77}Se NMR in solution, and their combinations. In this way, the molecular symmetry of the cluster in solution can be established through the number of equivalent ligands and Cd sites and ^1H–^{113}Cd correlations through more bonds (heteronuclear multiple-bond correlation, HMBC). This should be in agreement with the crystal structure. A well investigated structure is $[Cd_{10}S_4(SPh)_{16}]^{4-}$ (**Cd10a**, Figure 2.6) in DMF which shows two distinct ^{113}Cd signals and two sets of PhS$^-$ ligands in agreement with its crystal structure (but see also Chapter 4.1).[79]

However, when a cluster shows molecular stability in solution, it does not mean that all of its constituents are rigid. In the **Cd10a** cluster, the PhS$^-$ ligands can adopt positions different to those in the solid state. The terminal groups can rotate freely around the Cd–S bond and bridging ones can be situated in two different positions. Additionally, the two ligands can exchange intramolecularly (Scheme 2.2) and intermolecularly between each other, thus only one set of PhS$^-$ signals is observed at higher temperatures.[79] Other positions in the cluster are also not fixed. The two Cd and one S sites can exchange intermolecularly with different rates.[80] Mechanisms for these exchange types are probably much more complicated than for intramolecular ligand exchange (Scheme 2.2) and have to involve disruption and reformation of many bonds.[80] Thus, it is to be considered that clusters behave dynamically in solution. Exchange rates can be slowed down by decreasing measurement temperature, which favors use of low-melting solvents, like DMF ($t_m = -60.5$ °C), but decreases cluster solubility.

Molecular structures of CdS clusters in solution can be investigated also by means of electrospray mass spectrometry.[81,82] It could reveal which species are present in solution. However, the result is much dependent on ionization parameters, like the cone voltage. It was shown using this method that charged clusters have the tendency to lower their overall charge by losing some small charged species.[81,82] This effect should be more pronounced in the case of bigger clusters, as they possess a higher overall charge (Table 2.1).
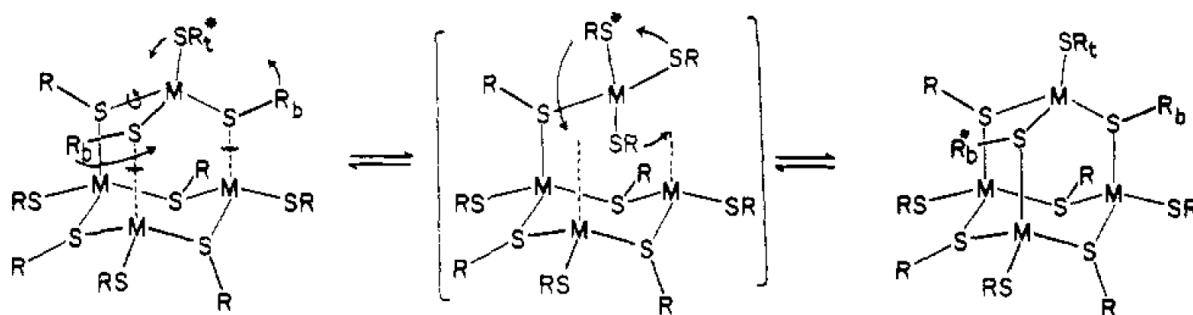
Scheme 2.2. Scheme of the intramolecular exchange between terminal and bridging PhS$^-$ ligands in $[Cd_4(SPh)_{10}]^{4-}$. Figure after Ref. 48.

2.2 Functional CdS Clusters and Nanoparticles

In general, functional clusters and NPs are species which have been somehow modified or adjusted to bear some specific physical, optical, electronic, magnetic, chemical or biomedical property. However, CdS clusters and NPs are supposed to have special physical properties by nature, as summarized in Chapter 2.1.1. Thus, functional CdS cluster, in the context of this thesis, will mean a surface modified cluster with ligands bearing a functional group which is capable of a polymerization reaction.

Synthesis of functional CdS clusters can be performed in following ways (Scheme 2.3):

i. by preparing the cluster in the presence of the functional ligand instead of the non-functional one ("in-situ functionalization"),

ii. by exchanging non-functional ligands against functional ligands ("post-synthesis modification"),

iii. by functionalizing existing ligands ("ligand functionalization").
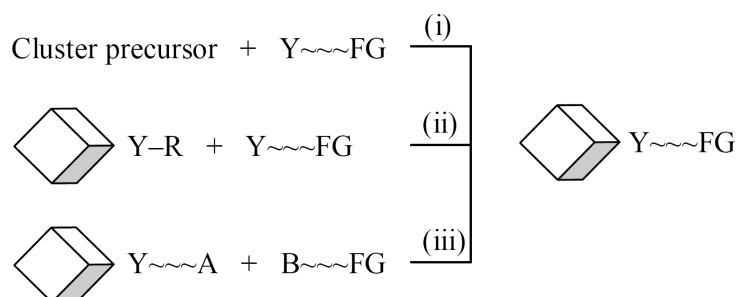
Scheme 2.3. Synthetic routes for preparation of functional clusters. Y = binding group to cluster surface, FG = functional group, A, B = coupling sites.

Such functional clusters and NPs can be utilized for covalent incorporation into a polymeric matrix. This should result in advantages to the properties of both components, additionally, properties arising from synergistic effects may be obtained, and the compatibility between NP surface and the matrix should be effectively enhanced. The clusters would act as cross-linking units, which would convert a linear polymer into a 3D network, and would change the properties of the hybrid polymer also by a nanofiller effect. Thus, temperature and mechanical stability should be improved. Simultaneously, luminescence properties of the CdS clusters could be enhanced by the polymeric matrix or by covalent bonding of surface ligands to the matrix. This could concurrently prevent cluster from photodegradation.

Functional groups (suitable for polymerization) can be of different kind: *e. g.* double bonds for chain radical polymerizations, or –OH, –NH$_2$, –COOH groups for step polymerizations. In following, the suitability of different functional groups in combination with CdS clusters and NPs will be discussed.

2.2.1 Radical Polymerization of CdS Clusters and Nanoparticles

Organic functionalization of clusters is focused mainly on modification with ligands bearing double bonds, aiming to radical polymerizations,[83] but other reaction types have been also investigated.[83,84] A great potential is present thanks to a wide number of metal oxo clusters (Si, W, Mo, Mn, Zr, Ti, Sn, Ta, Nb,…)[83] and metal chalcogenide clusters (Cu, Ag, Au, Cd, Zn, Fe, Mo, W, Ni, Co,…).[70,85] Diverse modification procedures led to formation of functionalized clusters: post-synthesis modification by exchange of surface groups or by ionic interaction, ligand functionalization with silane coupling agents, and also in-situ functionalization.[83] For example, Ti, Zr, and Mn oxo clusters have been functionalized with methacrylic and other functional acids, which enabled covalent incorporation of the clusters into a polymeric matrix by radical polymerization, leading to formation of inorganic-organic hybrid materials.[84] Thus, the possibility of functionalization of CdS clusters with ligands bearing double bonds and possible diverse effects of radicals on CdS clusters have to be examined in detail.

It is known that thiols (which are one of the most efficient capping ligands for CdS clusters and NPs) containing double bond unfortunately are unstable and undergo thiol-ene polymerization, addition of thiols to alkenes.[86] This reaction can be photochemically or thermally induced. It is known to proceed by a radical mechanism and to give an anti-Markovnikov-type polythioether (Scheme 2.4).[87] As side reaction, thiyl radical coupling is possible, which leads to formation of disulfides. Thus, stable thiols containing double bonds cannot be purchased. On the other hand, synthesis of 4-mercaptomethylstyrene has been well established.[e.g. 88] It has been used e. g. for monolayer self-assembly on Ag-substrates followed by polymerization,[89] stabilization of Ag NPs followed by polymerization in micelles,[90] stabilization of ZnS NPs followed by co-polymerization with urethane-methacrylate macromere.[88] However, polymerization reaction of pure 4-mercaptomethylstyrene with azobisisobutyronitrile (AIBN) as initiator at 70 °C yielded an almost linear thioether polymer due to thiol-ene reaction (Scheme 2.4).[91] Radical polymerization reaction of the vinyl groups was suppressed and was responsible for only few branching chains.[91]
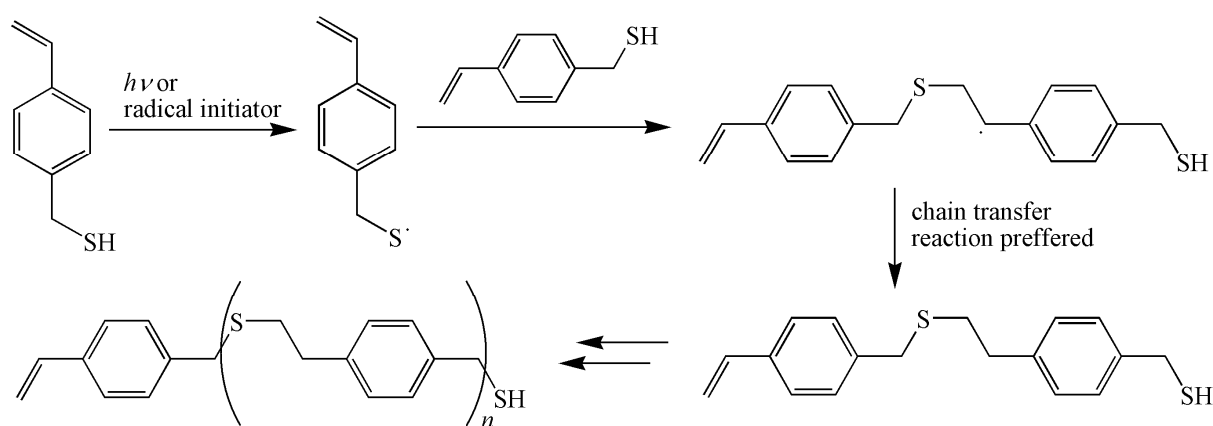
Scheme 2.4. Schematic illustration for thiol-ene polymerization of 4-mercaptomethylstyrene.

A possible solution for this problem could be use of thiolates instead of thiols in the cluster synthesis (as it is possible in the synthesis of **Cd10a**), or the use of coupling reactions (approach iii in Scheme 2.3). CdS clusters functionalized by double bonds could thus be obtained.

Another important issue is the stability of CdS clusters and NPs in the presence of free radicals. Additionally, if functionalized clusters or thiolate-capped CdS clusters/NPs in general would act as radical quenchers or scavengers, they could not be used for radical polymerizations. It is to expect that the character of the ligand shell has influence on the stability as well as on radical quenching. Literature dealing with these topics is unfortunately not extensive. It was shown that CdS NPs stabilized by polyphosphates in aqueous solution are not stable in the presence of $OH^.$ radicals and undergo anodic dissolution.[92] An $OH^.$ radical takes an e^- and leaves a h^+ in the NP. This leads to formation of solvated Cd^{2+}, sulfite, sulfate, and fluorescence quenching.[92] The radical scavenging effect in $[Cd_4(SAr)_{10}]^{2-}$ was also investigated.[93] It was shown that it has a higher scavenging effect on DMPO-$OH^.$ than TEMP$^.$ (DMPO = 5,5-dimethyl-1-pyrroline-N-oxide, TEMP = 2,2,6,6-tetramethyl-4-hydroxyl-1-piperidine-N-oxide), which was attributed to higher stability of TEMP$^.$ compared with DMPO-$OH^.$.[93] No information was given on the quenching mechanism, stability of the Cd4 complex in the presence of the radicals or possible reaction products. Another effect of free radicals on CdS/CdSe QDs consists in luminescence quenching. It has been shown on TOPO-capped CdSe QDs that nitroxide-free radicals like TEMPO quench their fluorescence (TOPO = trioctylphosphine oxide, TEMPO = 2,2,6,6-tetramethylpiperidine oxide).[94] If 4-NH_2-TEMPO was used, fluorescence quenching was by at least 3 orders of magnitude more efficient due to the binding to the QD surface.[95,96] Additionally, it was found that a protective ZnS layer on a CdSe core protects the core from quenching by TEMPO and 4-NH_2-TEMPO.[97] However, it is not clear whether the QDs are stable in the presence of free radicals.

Another very similar area is the influence of photogenerated radicals on the stability of CdS/CdSe QDs which was discussed briefly in Chapter 2.1.1. Photogenerated e^-–h^+ pairs can be trapped by surface states which can lead to formation of radicals on the NP surface followed by NP aggregation or degradation. NPs capped by thiols and thiolates are very susceptible compared with other ligands.[26] However, photodegradation of NPs can be utilized for synthesis of smaller NPs from bigger ones by the photoetching technique, which is based on irradiation with radiation of defined wavelength. It is applied usually on CdS/CdSe QDs in aqueous media saturated with oxygen.[98] Another way how photogenerated e^-–h^+ pairs can be employed is for photocatalytic processes.[43,44] Additionally, radical polymerizations can be induced by photogenerated e^-–h^+ pairs in CdS NPs.[99,100,101] The initiation mechanisms vary. Either vinylic or methacrylate monomers are reduced by excited e^- and h^+ are scavenged by solvent molecules,[99,101] or methyl methacrylate (MMA) is oxidized by the h^+, whereas polymeric chains are terminated by remaining reduced CdS NPs.[100] A thorough discussion of radical polymerizations in aqueous solution photoinitiated by polyphosphate-stabilized CdS QDs and its possible mechanisms has been performed by Stroyuk *et al.*[102] They showed that the monomer (acrylic acid and

acrylamide) can be reduced by e^- (as in Ref. 101) and also oxidized by h^+ (as in Ref. 100) leading to the formation of ion radicals. These mechanisms can be separated by addition of agents capable of selective scavenging of one kind of charge carriers: *e. g.* methyl viologen dication (MV^{2+}) for e^- or sulfite for h^+ scavenging.[102] This led to the conclusion that monomer reduction by e^- is strongly preferred to its oxidation by h^+, by a factor of around 4. Additionally, a complementary initiation mechanism was confirmed, namely photocatalytic production of H˙ from water by e^- reduction. On the other hand, photocorrosion of QDs took place in the presence of both monomers. Another study dealing with bulk polymerization of MMA photoinitiated by oleic acid-capped CdS QDs showed that the presence of amines serves for h^+ scavenging,[103] similarly as alcohol solvent molecules.[101] Beside this it was shown that oxidation of MMA by h^+ is unlikely and reduction by e^- thermodynamically favorable due to the redox potentials of MMA and CdS QDs valence and conduction bands.[103] Thus, the most probable initiation mechanism is as in Scheme 2.5. Additionally, if photogenerated e^- and h^+ are both involved in fast defined processes, photodegradation of the NPs could be suppressed. These results have to be taken into account as a possibility for the preparation of hybrid materials containing CdS clusters by radical polymerization.
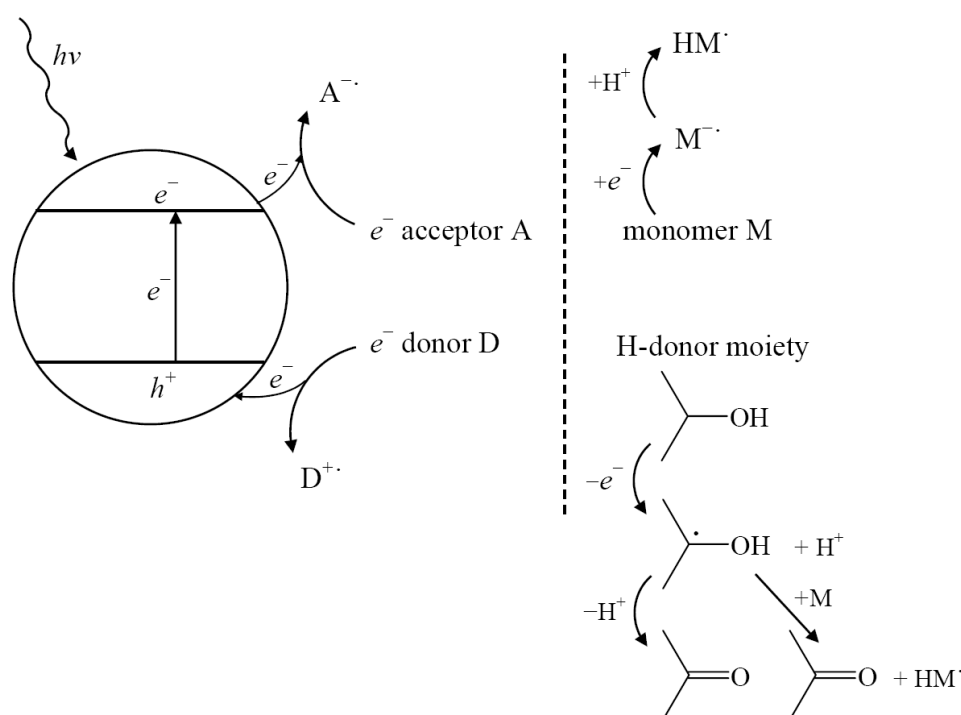
Scheme 2.5. Scheme of the most probable initiation mechanism of photopolymerization by CdS QDs according to Ref. 101, 102, and 103.

Few investigations dealing with radical polymerizations in the presence of CdS QDs can be found in the literature. Sometimes authors observe that conventional radical polymerizations are not compatible with Cd chalcogenide NPs. It was shown that TOPO-capped CdSe NPs are degraded by free radicals produced from AIBN or benzoyl peroxide as evidenced by color change of NP solutions and blue shift of fluorescence spectra.[104] On the

other hand, few reports were published showing that CdS/CdSe NPs are not changed in the course of radical polymerization. Organically capped CdS/CdSe NPs were polymerized with styrene and butyl acrylate and the optical properties confirmed their integrity after polymerization.[105] Few reports deal with polymerization of NPs functionalized by ligands with double bonds. ZnS NPs, stabilized by a mixture of PhSH and 4-mercaptomethylstyrene, were radically polymerized with urethane methacrylate macromer with AIBN as initiators.[88] NPs were uniformly dispersed in the polymeric matrix and retained their original size.[88] However, use of thiolates as capping ligands is known to quench the band edge fluorescence of the NPs (see Chapter 2.1.1). Thus, CdTe NPs stabilized by octadecyl-4-vinylbenzyldimethylammonium chloride were prepared and bulk polymerized with styrene and MMA using AIBN as initiator.[106] NPs were homogeneously dispersed in the polymeric matrix and showed band edge photoluminescence with positions almost identical with original NPs, meaning that the NPs were not degraded during the polymerization.[106] In another report, 2-mercaptoethanol-capped CdS NPs were functionalized with methacryloxypropyltrimethoxysilane $[(CH_3O)_3Si-(CH_2)_3-O-CO-C(CH_3)=CH_2]$ and were polymerized with MMA using AIBN as initiator in DMF.[107] The UV/Vis and luminescence behavior of the NPs before and after polymerization was almost identical, confirming the preservation of NPs during polymerization. However, the fluorescence spectra showed a great fraction of trapped luminescence.[107]

Data on the possibility of radical polymerizations with CdS QDs and on their stability in the presence of radicals are quite ambiguous. Thus, this topic should be investigated in more detail. In following, other functionalities compatible with CdS clusters and NPs will be discussed.

2.2.2 CdS Functionalities Suitable for Step Polymerization

Another possibility how to obtain inorganic-organic hybrid materials with covalent bonding between inorganic particles and organic matrix is functionalization of the CdS clusters with functional groups suitable for step polymerization reactions, like $-OH$, $-NH_2$, and $-COOH$ groups. More examples on NP than on cluster functionalization of this kind can be found in the literature.

Functionalization of CdS NPs with $-OH$ groups has been studied most extensively, since it renders the particles compatible with polar protic solvents like water. Diverse thiols containing $-OH$ group were used as stabilizing agents: *e. g.* 2-mercaptoethanol,[108,109,107] 1-thioglycerol,[78,109] or 4-hydroxythiophenol.[110] The presence of hydroxy groups could be utilized either directly for step polymerizations with acyl halides or anhydrides, or for further functionalization with acyl halides, anhydrides, chlorosilanes,[83] alkyltrimethoxysilanes,[107] or *N*-acylimidazoles[110] bearing double bonds or epoxy groups.

Few investigations have been performed on CdS NPs bearing $-NH_2$ groups, namely L-cysteine[108] and 4-aminothiophenol.[111,112] It was shown that an amino group in *para* position negatively influences photoluminescence and photostability of the NPs.[24,112] Subsequent

acylation with acyl halides or anhydrides should be possible in order to obtain polyamides. Other reactions of the amino group have been also investigated.[111]

CdS NPs bearing –COOH groups have been also synthesized. Various stabilizing ligands were used: 3-mercaptopropionic acid,[108] thioglycolic acid,[109] thiolactic acid,[109] L-cysteine,[108] and 4-carboxythiophenol.[24] However, it was shown that the carboxy groups have a tendency to coordinate to Cd atoms.[113] Therefore, ligands containing both thio and carboxy groups act as bidentate ligands and can bind either to the same or to neighboring clusters, which could lead to cluster aggregation. On the other hand, such behavior was not mentioned when 4-carboxythiophenol as capping ligand was used.[24]

CdS clusters bearing some functionality are not so common and only clusters with hydroxy groups are currently known. They are summarized together with non-functional CdS clusters in Table 2.2. The $[Cd_{10}(SCH_2CH_2OH)_{16}]^{4+}$ (**Cd10c**) cluster has been prepared and structurally characterized with sulfate [55] and perchlorate.[68,114,57] as counter-anions. Solution and solid state NMR investigation has been performed in order to confirm the integrity of the cluster in solution.[68,114,57] A bigger cluster, $[Cd_{17}S_4(SCH_2CH_2OH)_{26}]_\infty$ (**Cd17b**), was synthesized as a 3D network of Cd17 clusters connected via μ_2-SCH$_2$CH$_2$OH bridges.[63] It was structurally characterized in the solid state (SC-XRD,[63] UV/Vis absorption[69]) and in solution (UV/Vis absorption and NMR),[63] which showed that the cluster core remains intact after dissolution. By now, the biggest cluster with –OH groups on the surface is a Cd32 cluster with 1-mercapto-2-propanol as stabilizing ligand ($Cd_{32}S_{14}L_{36}(H_2O)_4$).[66] Beside SC-XRD, it was characterized only by UV/Vis absorption in the solid state and solution,[66] which supports the presence of the Cd32 core also in solution (see Table 2.2).

Other functionalities have been incorporated into CdS clusters only using exchange reactions. An extensive mass spectrometry study on ligand exchange of the $[Cd_{17}S_4(SPh)_{28}]^{2-}$ (**Cd17a**) cluster has been performed with thiol alcohols (2-mercaptoethanol, 4-hydroxythiophenol), thiol acids (2-mercaptopropionic, 2-mercaptobenzoic acid), cysteine, and other ligands.[113] Interestingly, exchange with thiol acids led to bis-deprotonation of the acids and replacement of two thiophenolate ligands by one acid dianion.[113] This showed that acid dianion ligands are chelating and connect two neighboring Cd atoms by coordination of the thiolate S atom and one of the O atoms of the carboxylic group.[113] Thus, it has to be expected that CdS clusters with free –COOH groups on the surface are not easy to prepare.

Only one study was found, which uses the mentioned functional clusters for further reactions. The **Cd10c** cluster was covalently incorporated into a polyphosphazene film containing hydroxy groups by cross-linking with diisocyanate moieties.[115] Then the cluster was used as precursor for in-situ generation of CdS NPs in the polymeric film by reaction with Na$_2$S.[115] However, the integrity of the **Cd10c** cluster upon incorporation into the film was not verified.[115] Thus, the possibility of further reactions of CdS clusters functionalized with –OH groups and retention of their molecular structure have to be investigated in more detail.

3   Research Goals and Scope of Work

The aim of this work is to prepare hybrid materials with special physical properties, like photoluminescence, by covalent incorporation of functional CdS clusters into a polymeric matrix. To this end, two goals had to be accomplished:

i.   synthesis and characterization of functional CdS clusters with defined structural and chemical properties,

ii. synthesis and characterization of hybrid materials prepared from them by polymerization in the presence of an organic monomer.

A synergistic effect could arise from protecting role of the polymeric matrix which could lead to enhancement of luminescence properties and of photodegradation stability of the clusters compared with unprotected ones. Covalent incorporation of clusters and their role as cross-linking units should also influence the mechanical and thermomechanical behavior of the materials.[116]

Why use molecular clusters and not NPs? There are a few advantages: (i) clusters are uniform and perfectly defined which facilitates the study of surface modification and of structure–property correlations, and allows higher degree of control of the material properties, (ii) cluster properties are in the "molecular" size regime, (iii) most of the metal atoms are surface atoms leading to high interface area between the particles and the matrix.

On the other hand, physical properties of clusters cannot be tuned in such a wide range as that of NPs. For a cluster, they are given by its molecular structure, while for NPs, they can be tuned by the size of the particle, the character of the stabilizing ligand shell, the particle shape, core composition and crystal modification. Further, additional physical properties can be added by variation of the chemical composition of the NP core. Such modifications are possible for clusters in a very restricted extent.

Therefore, results obtained for functionalization of CdS clusters and their incorporation into a polymeric matrix should be applicable also for CdS NPs, but not necessarily the other way round.

In order to make the task feasible, it is necessary to ensure that the molecular structure of used clusters does not change, or only changes in a precisely defined way during functionalization and incorporation into the polymeric matrix. This is the topic of the first part of the thesis which investigates changes of non-functional clusters in solutions at conditions similar to polymerization reactions.

The second part deals with synthesis, characterization and reactivity of functional clusters modified with hydroxy and amino groups suitable for step polymerization, and with radical polymerization in the presence of non-functional clusters and its influence on the cluster structure.

4   Part I: Behavior of CdS Clusters in Solution

In the first part of the thesis, the behavior of $(NMe_4)_4[Cd_{10}S_4(SPh)_{16}]$ (**Cd10a**) and "$Cd_{10}S_4(SPh)_{12}$" (**Cd10b**) as model CdS clusters was investigated in the solid state and in solution. They have been chosen for simple reasons:

Cd10a

– easy to synthesize,[47]

– well investigated in solid state[47,53,117] and in different solvents,[79,80,71,82]

– its possible structural changes in solution can be easily followed by ^{113}Cd NMR and UV/Vis spectroscopy,

– on the other hand, its luminescence properties are not ideal for desired hybrid materials, because it shows mainly trapped emission, which is a general feature for CdS clusters/NPs stabilized by thiolates.[96]

Cd10b

– easy to synthesize,[54]

– well investigated in solid state and in different solvents,[54,64]

– it should have four free coordination sites suitable for further cluster functionalization.[54,118,119,120]

4.1   Rearrangement of $[Cd_{10}S_4(SPh)_{16}]^{4-}$ in Coordinating Solvents

The clusters, which will be incorporated into a polymeric matrix, have to be used in some polymerization reactions, radical or step polymerizations. Both take place usually at elevated temperatures. Therefore it is necessary to prove that the clusters are stable at prolonged heating at higher temperatures and that their molecular structure does not change at the chosen reaction conditions. To this end, the cluster $(NMe_4)_4[Cd_{10}S_4(SPh)_{16}]$ (**Cd10a**) was chosen as model cluster (from reasons already mentioned), which is soluble in coordinating solvents: MeCN, dimethylsulfoxide (DMSO), and *N,N*–dimethylformamide (DMF). Thus, its solutions in these solvents were investigated.

A number of investigation has been performed previously on **Cd10a** (Figure 4.1) concerning its solid state structure[47,53,117] and whether its molecular structure is unchanged after dissolution.[79,80,71,82] According to the crystal structure[47] and theoretical T_d symmetry in solution, it should consist of two chemically inequivalent Cd sites in solution, the outer (apical) and inner Cd site (Cd^o and Cd^i in ratio 4:6), one inequivalent bridging μ_3–S and two inequivalent –SPh ligands, bridging and terminal (ratio 12:4). And indeed, two ^{113}Cd NMR resonances and two thiolate ligands were observed in d$_7$-DMF solution with corresponding intensity ratios.[79,80]
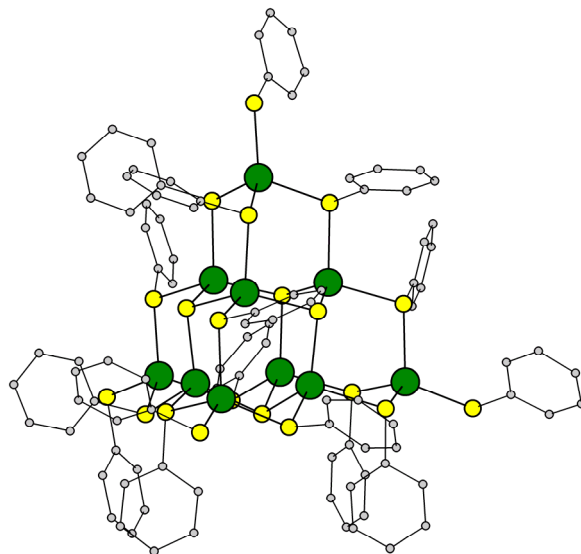
*Figure 4.1. Molecular structure of **Cd10a** according to its crystal structure (**Cd10a-3**).*

As already mentioned in Chapter 2.1.2, the clusters behave dynamically in solution. Thus, different cluster constituents undergo intra- and intermolecular exchange. An example of intramolecular exchange of the thiolate ligands was shown in Scheme 2.2. Previously, it was shown that with increasing CdS cluster size (*e.g.* from Cd4 to Cd10) the exchange reactions become substantially slower at room temperature.[80] Mixing of $[Cd_{10}S_4(SPh)_{16}]^{4-}$ and $[Zn_{10}S_4(SPh)_{16}]^{4-}$ in DMF showed that exchange of the outer metal atoms (M^o) is complete within minutes and that M^o prefer a core of the same metal. Exchange of the inner metal atoms (M^i) takes hours at room temperature, resulting in scrambling of M^i. Mixing of $[Cd_{10}S_4(SPh)_{16}]^{4-}$ and $[Cd_{10}Se_4(SPh)_{16}]^{4-}$ in DMF led to 50 % exchange of the μ_3–S atoms in about 4 days at room temperature. Thus, exchange rates were inversely related to the distance from the surface of the molecule.[80]

Additionally, it was shown that **Cd10a** is in equilibrium with other cluster types in DMF solution: with Cd8 (*e.g.* $[Cd_8S(SPh)_{16}]^{2-}$) and **Cd17a** ($[Cd_{17}S_4(SPh)_{28}]^{2-}$) clusters, during its synthesis from $Cd^{2+}/S^{2-}/SPh^-$ reaction solutions.[71] The equilibrium depends on the concentration and composition of the reaction solution. It was concluded that the thermodynamic stability of the clusters decreases in the order Cd8 > **Cd10a** > **Cd17a**, and solubility of their NMe_4^+ salts increases in the order **Cd10a** < **Cd17a** < Cd8. As a consequence, Cd8 clusters are formed in DMF solutions of **Cd10a** or **Cd17a** clusters at room temperature (high stability of Cd8 cluster). If the solution contains only Cd8 and **Cd17a** clusters, addition of NMe₄Cl causes their conversion to the **Cd10a** cluster which crystallizes from this solution since NMe_4^+ salt of **Cd10a** is the least soluble species.[71]

Therefore, it has to be taken care in making conclusions about the identity of the molecular structure of **Cd10a** in solution compared with the solid state structure. It seems that the structure is the same, but the highly dynamic behavior cannot be underestimated.

Two different crystal structures of **Cd10a** were previously obtained. The first (**Cd10a-1**), space group *I−4*, was crystallized by adding water to a hot DMF solution of **Cd10a** and the

second (**Cd10a-2**), space group *I−42m* or *P−42₁c* by cooling a hot saturated MeCN solution of **Cd10a**.[47] During the course of this work, a third modification (**Cd10a-3**) was obtained which crystallized in space group *Aba*2, Figure 4.1, by adding toluene to a DMSO solution of **Cd10a**. The structures are principally the same; they differ only slightly in the orientation of the thiolate ligands.

In contrast to the previous conclusions, that the molecular structure of **Cd10a** is principally identical with its crystal structure,[79,80] were UV/Vis, dynamic light scattering (DLS), and NMR investigations in MeCN, DMF, and DMSO, described in the following.

The UV/Vis spectra of MeCN, DMSO and DMF solutions of **Cd10a** as well as DLS measurements (Figure 4.2) showed substantial differences between the solvents. In MeCN, the absorption maxima were at 290, 256 and 207 nm, which is in good agreement with previous reports.[67] The hydrodynamic radius was <1.5 nm with a maximum at 0.5 nm. Similar data were obtained for DMF solution, *viz.* a shoulder at ca. 310 nm and a hydrodynamic radius <2 nm with a maximum at 0.5 nm. A diameter of ca. 2.0 nm was expected from SC-XRD analysis (cluster core together with the ligand shell) which is substantially higher than the one obtained by DLS; this could not be explained. In contrast, the absorption maximum in DMSO was at 336 nm, which is red shifted compared with the other solutions, meaning that bigger particles should be present. The hydrodynamic radius was <3 nm with a maximum at 0.8 nm which is also an indication of presence of bigger particles. These observations were first indications that **Cd10a** behaves differently in DMSO compared with DMF and MeCN solutions, and that it probably grows or agglomerates/aggregates in DMSO solution.
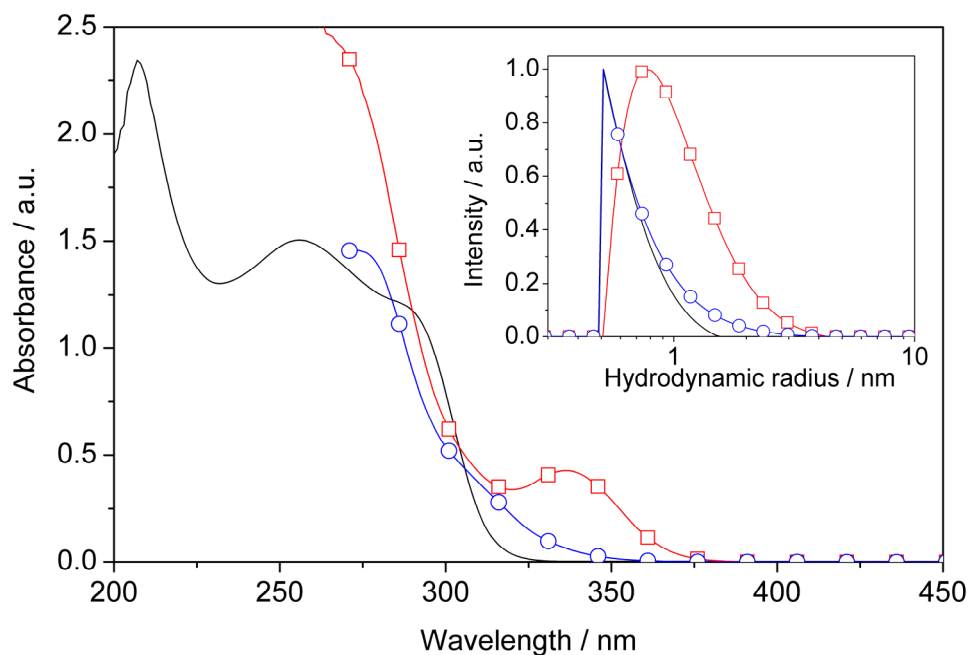
*Figure 4.2. UV/Vis spectra of **Cd10a** in different solvents (0.02 mg/ml in MeCN (–), 0.08 mg/ml in DMSO (□), 0.025 mg/ml in DMF (○)). Insert: Corresponding DLS hydrodynamic radii distribution functions of **Cd10a** (concentration ca. 10 mg/ml).*

NMR measurements of **Cd10a** in d_3-MeCN, d_6-DMSO, and d_7-DMF showed also substantial differences (for example ^{1}H NMR spectra see Figure 4.3). Two PhS groups with an intensity ratio of 3:1 were observed in the ^{1}H NMR spectrum in d_3-MeCN solution. The two sets of resonances were assigned to bridging and terminal groups (Table 4.1). The terminal group showed ^{1}H-^{113}Cd correlation to one Cd signal (Cd^o, at 602 ppm), the bridging group to both Cd signals (Cd^o and Cd^i, at 687 ppm) (Figure 4.4). The NMR data are thus in agreement with the solid-state structure of **Cd10a**.[47]
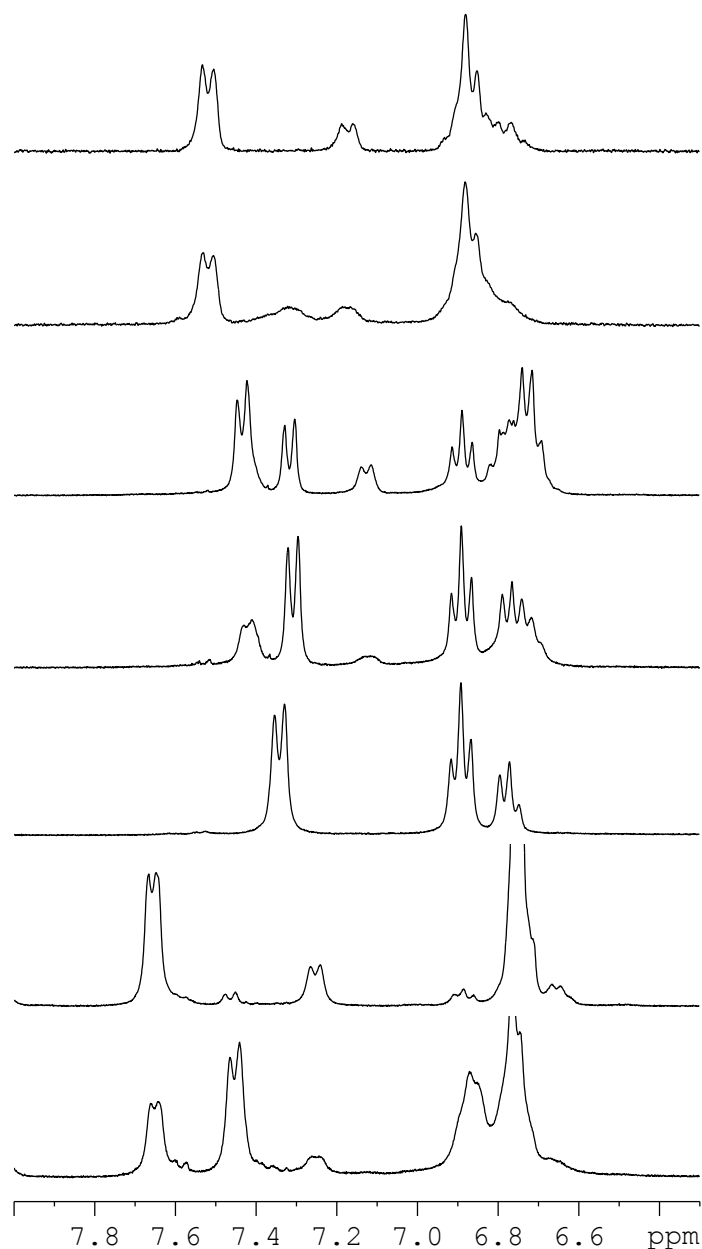
Figure 4.3. ^{1}H NMR spectra of **Cd10a** in d_3-MeCN, d_6-DMSO, and d_7-DMF (10 mg/ml). From above: **Cd10a** in d_3-MeCN after dissolution (1), after 21 h at 75 °C (2), **Cd10a** in d_6-DMSO after dissolution (3), after 5 days at room temperature (4), after 90 min at 80 °C (5), **Cd10a** in d_7-DMF after dissolution (6) and after 27 days at room temperature (7). All spectra were measured at room temperature, only (5) at 80 °C.
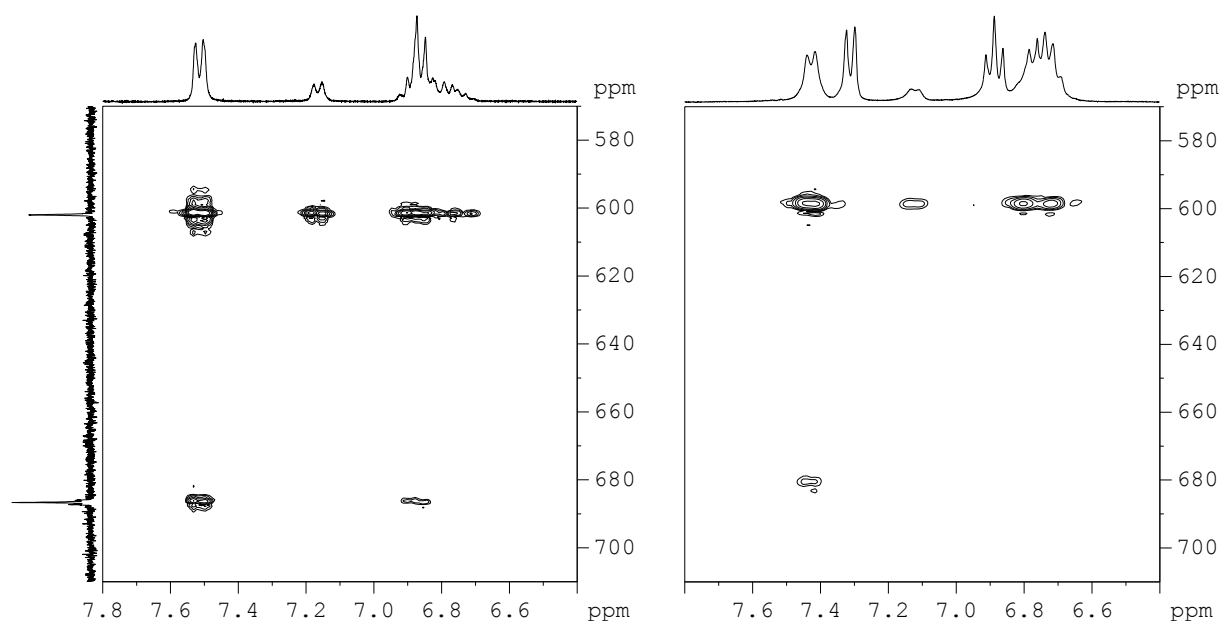
*Figure 4.4. ^{1}H-^{113}Cd HMBC correlation spectra of **Cd10a** in d_3-MeCN (left) and in d_6-DMSO (right) (10 mg/ml).*

*Table 4.1. Comprehensive summary of NMR characterization of **Cd10a** in d_3-MeCN, d_6-DMSO and d_7-DMF (concentration 10 mg/ml, δ in ppm). PhS groups: bridging (b), terminal (t), and "unknown" (u) with ratio 3:1:x.*

Solvent		d_3-MeCN		d_6-DMSO			d_7-DMF		
x		−		1.5, 3.0[a]			0.3, 2.2[b]		
		b	t	b	t	u	b	t	u
	ipso	139.6	146.6	138.7	145.4	145.8	?	?	?
	ortho	7.54	7.19	7.43	7.13	7.32	7.67	7.26	7.48
		135.0	134.0	133.6	132.5	132.5	134.1	132.8	132.7
SPh – ^{1}H, ^{13}C	*meta*	6.87	6.81	6.72	~6.75	6.89	6.75–6.77		6.90
		128.4	128.2	127.1	127.1	127.2	127.2		127.2
	para	6.89	6.77	6.80	~6.70	~6.76	6.76	6.66	6.77
		124.3	121.9	122.9	120.6	120.9	122.7	120.6	122.7
^{113}Cd NMR		602.0 (Cd^o), 687 (Cd^i)		598.5 (Cd^o), 680 (Cd^i)			598; 682.5		

[a] after 3 days at room temperature; [b] after 7 days at room temperature

In contrast, *three* sets of PhS NMR signals were observed in d_6-DMSO solutions. Two of them correlated to Cd signals (598.5, 680 ppm) in the ^{1}H-^{113}Cd HMBC spectra similar to the MeCN solution (Figure 4.4). They were therefore assigned to bridging and terminal groups (Table 4.1). The third group did not show a correlation to Cd and was thus assigned to an "unknown" PhS group. The chemical species giving rise to this signal is one of the main issues in the remainder of this chapter. Interestingly, the ratio of the PhS peak intensities changed with time; the proportion of the "unknown" PhS group increased and that of bridging and terminal decreased, but the ratio between bridging and terminal remained 3:1 (Table 4.1).

Furthermore, a second d_6-DMSO solvent signal (2.53 ppm) was observed, probably due to coordinated solvent.

Similar, but less pronounced, behavior was observed in a d_7-DMF solution of **Cd10a**. Three PhS groups in the ^{1}H NMR spectrum were again assigned to bridging, terminal, and "unknown" PhS groups (Table 4.1). The ratio of the bridging and terminal PhS groups was around 3:1 and remained approximately constant with time. The intensity of the "unknown" PhS group increased with time, but slower than in d_6-DMSO solution (Table 4.1). In the ^{113}Cd NMR spectrum, two signals were obtained (598 and 682.5 ppm) which were shifted similarly to those in d_3-MeCN and d_6-DMSO solutions.

As already mentioned, the NMR investigation of **Cd10a** in d_7-DMF performed by Dance et al.[79] was in good agreement with the crystal structure and only two sets of ligand signals were observed. Beside this the two sets of ligand resonances coalesced at ca. 340 K due to intramolecular exchange as proposed by Hagen et al. for $[Cd_4(SPh)_{10}]^{2-}$ (Scheme 2.2).[48] No other PhS groups were mentioned. However, this is in contrast with currently performed measurements. Lee et al.[58] recorded time and temperature dependent ^{113}Cd NMR spectra of DMF solutions of $[Cd_{17}S_4(SPh)_{28}]^{2-}$ (**Cd17a**) and postulated fast and slow rearrangement processes. This could be eventually similar with the observed NMR behavior of **Cd10a** in DMF and DMSO solutions. However, it cannot explain the growth of the cluster core of **Cd10a** in DMSO, which was indicated by UV/Vis and DLS measurements.

The former assumption that DMSO and/or DMF could cause cluster agglomeration or aggregation is not very likely because this kind of behavior is not typical for strongly coordinating solvents. In spite of that, agglomeration/aggregation, or particle-particle interactions, should influence the cluster electronic properties in following way. Vossmeyer et al.[78] observed that the absorption maxima of small, almost monodisperse 1-thioglycerol-stabilized CdS NPs shifted to higher wavelengths (from 260 to 270 nm) when closely packed in layers. The shift was most pronounced for the smallest NPs with 0.64 nm radius, which corresponds to clusters of approximately ten Cd atoms. This effect was explained by collective electronic modes similar to the energy bands of conventional bulk semiconductors. Döllefeld et al.[69] investigated the absorption of solid nanocrystal assemblies of defined Cd17 clusters stabilized by 2-mercaptoethanol and observed a shift of absorption in solution and in solid state from 290 to 305 nm. They explained this observation by calculations involving electronic and dipole-dipole interactions and found that the shift was higher for smaller NPs with smaller mutual distances. In both cases[69,78] a red shift of about 10–15 nm was reported for CdS NP arrays compared with separated NPs. In DMSO solution of **Cd10a**, a red shift of ca. 50 nm was observed compared with MeCN solution. This shift is too high to be explained by only cluster agglomeration/aggregation.

4.1.1 Growth of $[Cd_{10}S_4(SPh)_{16}]^{4-}$ in Coordinating Solvents

To find evidence for the possible growth of **Cd10a** in DMSO observed by UV/Vis, DLS, and NMR, DMSO solutions were investigated in two series of experiments, viz. time-dependence at room temperature (series A) and at 80 °C (series B).

Series A. A 10 mg/ml solution of **Cd10a** in DMSO was stored at room temperature. DLS data (Figure 4.5, insert) indicated continuous growth of the cluster within 2 months. However, the UV/Vis absorption spectra (Figure 4.5) were not typical for continuously growing NPs. After about one week, two distinct maxima at ca. 348 and ca. 325 nm were dominant (their positions did not change substantially with time). The ratio between the maximum at 348 and at 325 nm was slightly increasing with time. According to the knowledge of quantum size effect for CdS clusters and NPs (see Table 2.1 and Table 4.6), these spectroscopic features were tentatively assigned to two clusters with core sizes of Cd54 and Cd32, with probable compositions of $[Cd_{54}S_{32}(SPh)_{48}(DMSO)_4]^{4-}$ and $Cd_{32}S_{14}(SPh)_{36}(DMSO)_4$ (similar to other Cd54 and Cd32 clusters with neutral ligands, see Table 2.1). Thus, the Cd54:Cd32 cluster ratio was increasing with time.
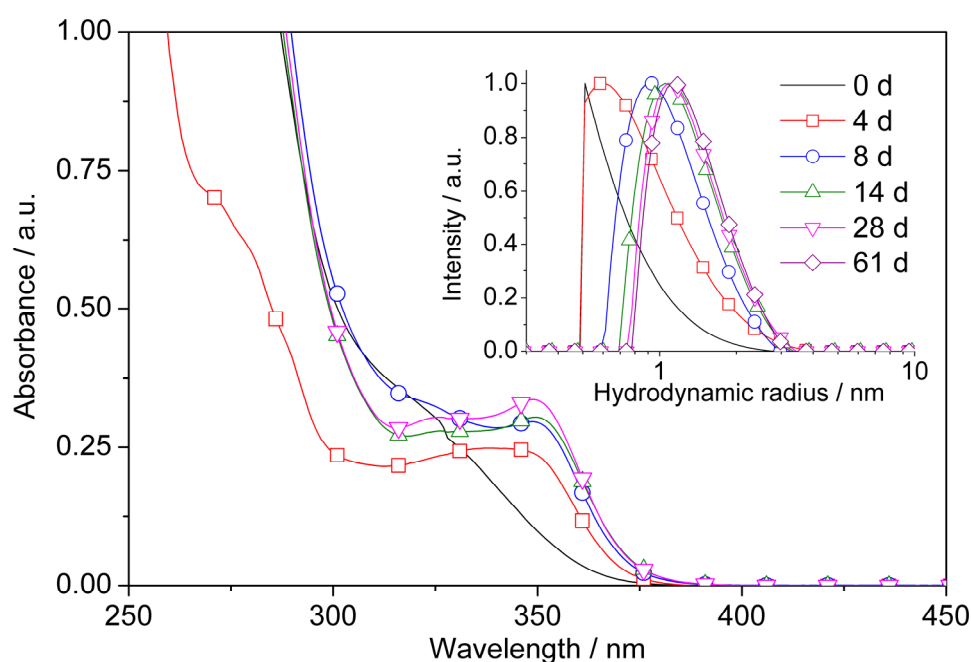
*Figure 4.5. UV/Vis spectra of **Cd10a** in DMSO after different time periods (up to 61 days) at room temperature. Solutions were diluted to concentration 0.07 mg/ml for measurements. Insert: Corresponding DLS hydrodynamic radii distribution functions, measured at 10 mg/ml.*

The "unknown" PhS group was again observed in ¹H NMR spectra (10 mg/ml in d₆-DMSO, see also Figure 4.3), and its intensity increased with time as described above. After 19 days, only the "unknown" PhS group was present, together with ca. 5 % of diphenyl disulfide [7.53 (d, 2H), 7.38 (t, 2H), 7.28 (t, 1H) ppm]. Chemical shifts of the "unknown" PhS group changed slightly with time. A similar NMR experiment was also performed with a d₇-DMF solution of **Cd10a** (10 mg/ml). After 27 days at room temperature, ca. 45 % of all PhS groups belonged to **Cd10a**, the rest to the "unknown" group (Figure 4.3). The transformation was thus much slower in DMF compared with DMSO solution.

Series B. Solutions of **Cd10a** in DMSO with different cluster concentrations (10 or 40 mg/ml) were heated at 80 °C for 16 or 72 h (samples B1–B4, see Table 4.2). DLS

hydrodynamic radii distributions were similar for all samples, but differed to that of the experiments in Series A. While the radius was between 0.8 and 3.5 nm for the sample in Series A after 61 d (Figure 4.5) the radii in Series B were bigger (1–5 nm). The UV/Vis data are summarized in Table 4.2. In addition to the absorption maxima, also the first derivatives of the absorption curves were used for the evaluation of the spectra, which facilitated distinction of CdS clusters or NPs of different sizes (Figure 4.6). In this thesis, an absorption edge is defined as an inflection point of the absorption curve, *i.e.* a minimum of the first derivative curve.[121] Table 4.2 contains two different values for absorption edge/maxima, those of the more pronounced excitonic transition of smaller NPs and, in parentheses, that of the less pronounced excitonic transition of bigger NPs, which is expressed by a shoulder (samples B1, B2) or a smaller maximum (samples B3, B4). Samples B1 and B2 showed an additional small shoulder at ca. 325 nm (not listed in Table 1).
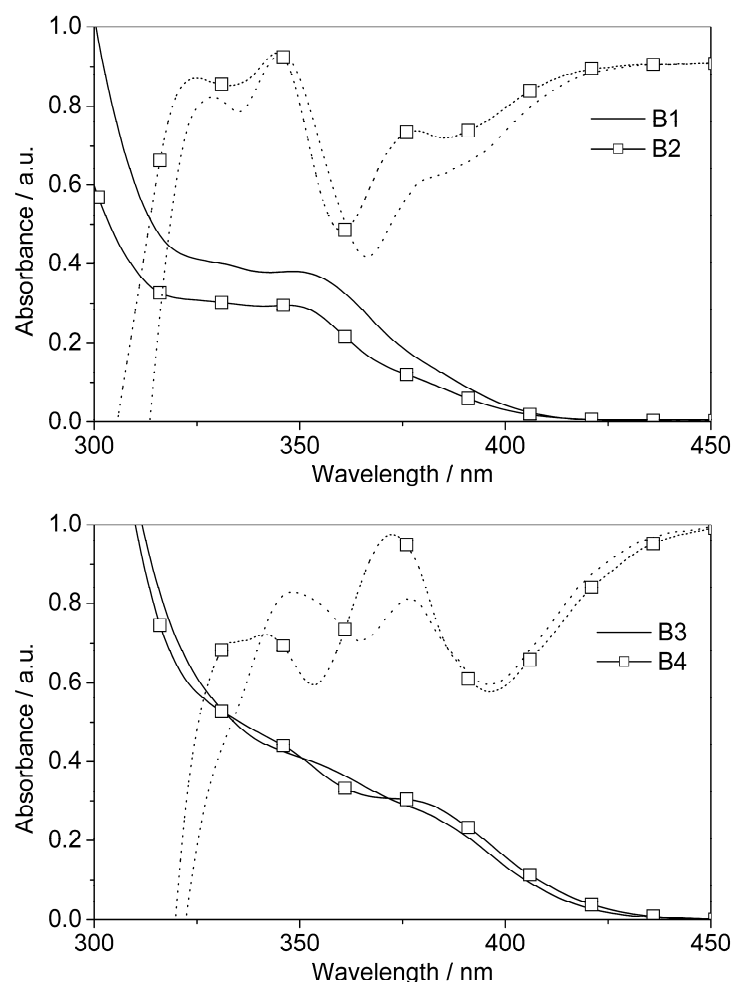
*Figure 4.6. UV/Vis spectra for samples B1–B4 (**Cd10a** in DMSO after heating at 80 °C), measurement concentrations were 0.11–0.15 mg/ml. Solid lines represent UV/Vis absorptions, dashed lines are their 1st derivatives.*

*Table 4.2. Summary of UV/Vis data for **Cd10a** in DMSO after heating at 80 °C.*

Sample	Sample concentration / mg/ml	Heating time / h	Absorption edge/maximum / nm	
B1	10	16	(ca. 380/?)	366/348
B2	40	16	(386/ca. 380)	361/346
B3	10	72	(396/ca. 376)	365/ca. 348
B4	40	72	(396/ca. 375)	354/ca. 340

In summary, samples heated for 16 h (B1 and B2) contained Cd32, Cd54 and bigger clusters with an absorption edge at 380–385 nm. Samples heated for 72 h (B3 and B4) contained Cd54 (B4 only probably) and bigger clusters with an absorption edge at 396 nm and maximum at ca. 375 nm.

Additionally, the 10 and 40 mg/ml solutions of **Cd10a** in DMSO were investigated continuously by UV/Vis absorption (Figure 4.7). The 10 mg/ml solution revealed that formation of Cd54 clusters was the main feature during the first 4 h of heat treatment. Then, the formation of bigger NPs was noticed with absorption edges starting at ca. 380 and ending at ca. 410 nm after 330 h. This corresponds to NP diameters of about 2.1 and 3.0 nm, respectively, as estimated by TEM.[122] The band characteristics for the Cd54 cluster disappeared concomitantly and new features appeared. The UV/Vis spectra indicated that the size distribution of the biggest NPs was broader with increasing heating periods. The results were similar for a cluster concentration of 40 mg/ml, but NPs bigger than Cd54 were formed earlier than in the 10 mg/ml sample (Figure 4.7).
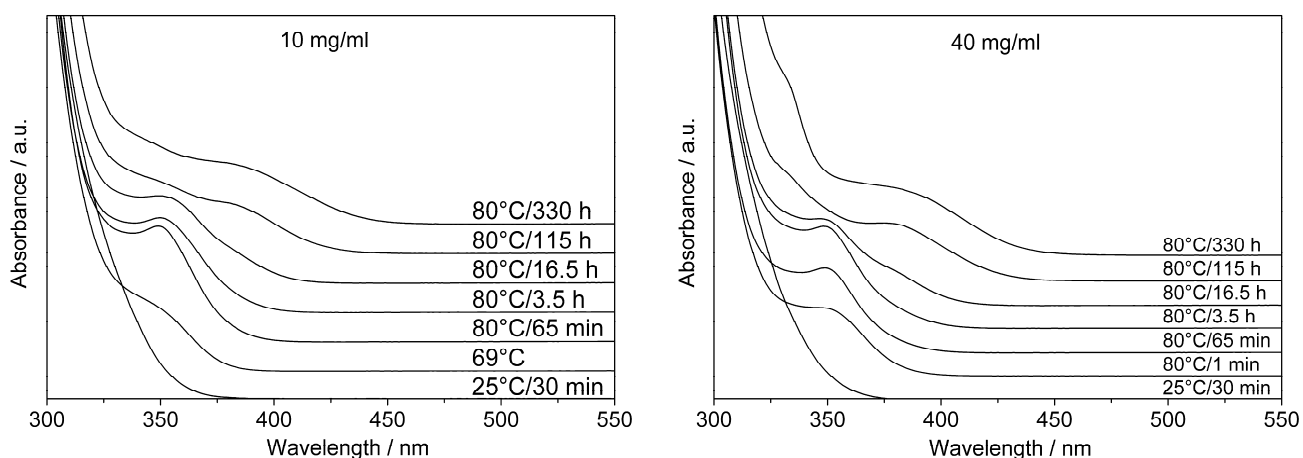
*Figure 4.7. UV/Vis absorption spectra of **Cd10a** in DMSO (10 and 40 mg/ml, top and bottom) after different heating periods.*

^{1}H NMR spectra of a 10 mg/ml sample showed the same behavior as in Series A. Signals for **Cd10a** disappeared faster, and after 90 min at 80 °C only the "unknown" SPh group was present. The spectra did not change during 4 days of heating at 80 °C. Formation of ca. 5 % of

diphenyl disulfide was again observed. The [113]Cd NMR spectrum revealed no signals, probably due to relatively low sample concentration connected with undefined species. ^{1}H NMR spectra of the B2 sample (40 mg/ml, 80 °C/16 h) revealed the presence of the same "unknown" PhS group. The chemical shifts for the aromatic *meta* and *para* protons differed slightly (± 0.2 ppm), but the ^{13}C chemical shifts were almost identical. Three broad, weak signals were obtained by [113]Cd NMR at 593, 517 and 67 ppm (see later Figure 4.12, top), which will be discussed later.

DMF and MeCN solutions of **Cd10a** (10 mg/ml, 16 or 21 h) were also heated to 80 or 75 °C, respectively. Changes were monitored by NMR and UV/Vis absorption and were similar to the DMSO solution. Absorption maxima of the biggest NPs were at 369 and 353 nm in DMF and MeCN. However, according to NMR (Figure 4.3) and absorption spectra (Figure 4.8), the MeCN solution still contained an appreciable proportion of **Cd10a** (ca. 75 %) after 21 h of heating.
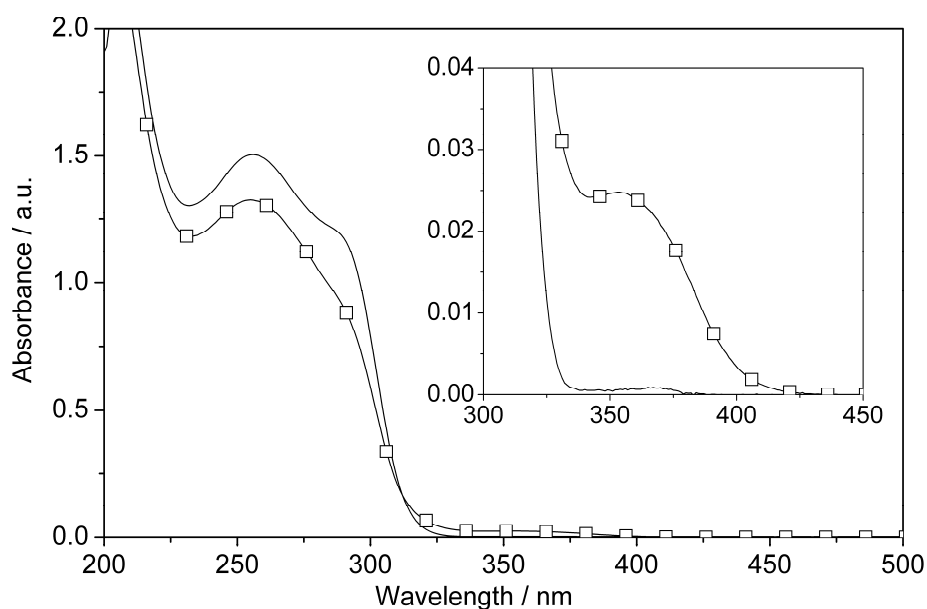
*Figure 4.8. UV/Vis spectra of **Cd10a** before (–) and after (□) heating in MeCN (10 mg/ml, 75 °C, 21 h). Measurement concentration of 0.019 mg/ml.*

Thus, it should be clear that **Cd10a** is indeed growing in DMSO at room temperature and at 80 °C. Beside this, it was shown that its size increases also in DMF and MeCN solutions. The transformation rate increases in the order MeCN < DMF < DMSO.

The CdS NPs prepared in samples B1–B4 (DMSO solutions) were precipitated from the reaction solutions by addition of a >3-fold excess of toluene. The precipitate was separated by sedimentation or centrifugation, washed with toluene and dried in vacuum. The solid yield was ca. 45 wt% for samples B1 and B2, and ca. 25 wt% for B3 and B4 samples, relative to **Cd10a**. Powder XRD measurements of the precipitates confirmed the presence of very small CdS NPs (Figure 4.9). The modification (wurtzite or sphalerite) could not be identified precisely because of the small particle size. Since the size of very small NPs cannot be

calculated with sufficient accuracy from Scherrer's equation, small-angle X-ray scattering (SAXS) investigation was also performed. Scattering curves for samples B1–B4 are shown in Figure 4.10.
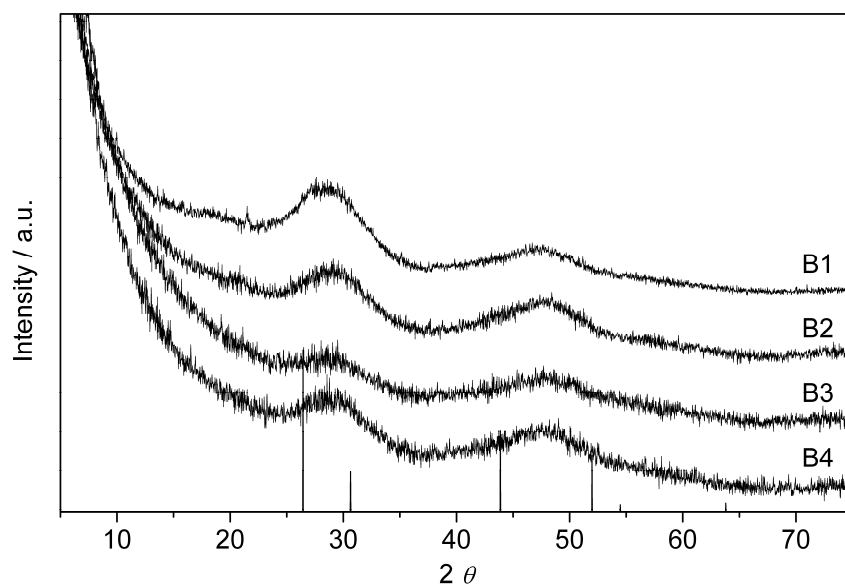
Figure 4.9. X-ray powder diffractogram of CdS NPs isolated from samples B1–B4 by addition of toluene. Bars represent sphalerite CdS.
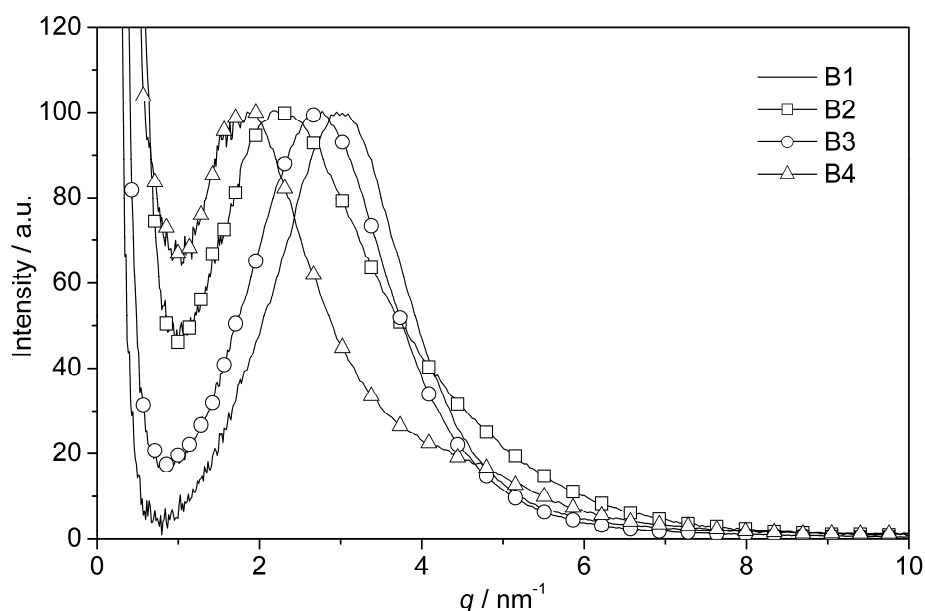
Figure 4.10. SAXS scattering curves of CdS NPs isolated from samples B1–B4 by addition of toluene. The curves were normalized for the same height of the scattering peak.

The scattering intensities $I(q)$ were fitted with asymmetric Gaussian and Lorentzian functions for the samples from lower and higher concentration, respectively (see Figure 6.1 in

31

the Experimental Part). The peak maxima and half-widths were converted to distances and distribution widths in real space. They are attributed to a short range order of NPs, which gives the size of the NPs in the case of hard spheres arranged close to each other. The data are summarized in Table 4.3. There is an obvious asymmetry towards smaller sizes in real space (*i.e.* towards larger q-values in reciprocal space as seen in Figure 4.10). This supports the notion that the average size of the particles increases continuously. The growth is controlled by the sample concentration as well as by time: The particle distance, and therefore the size as well, grows from 2.13 nm and 2.86 nm after 16 h (B1 and B2) to 2.37 nm and 3.51 nm after 72 h (B3 and B4). The distance distribution is significantly more asymmetric in the case of the higher concentrations (B2 and B4) as in the lower ones (B1 and B3). This leads to the conclusion that there is a more uniform growth in the latter case. In sample B4, a very weak peak at about $q = 4.7 \, nm^{-1}$ is observed, which corresponds to a distance of 1.3 nm in real space. A cluster-cluster aggregation, however, is quite improbable, as there is no significant scattering intensity towards high q-values.

Table 4.3. NP-NP distance and half-width from the asymmetric fits for the CdS NPs isolated from samples B1–B4 by addition of toluene.

Sample	NP distance (nm)	Asymmetric half-widths (nm)
B1	2.13	+0.5 / −0.8
B2	2.86	+1.2 / −2.4
B3	2.37	+0.6 / −1.0
B4	3.51	+1.4 / −2.8

CdS NPs obtained from sample B2 by precipitation with toluene were further characterized by solid-state ^{13}C and ^{113}Cd NMR. ^{13}C NMR spectra showed the presence of PhS^- and Me_4N^+ groups. ^{113}Cd NMR revealed only very weakly resolved broad signals at ca. 600, 680 and 730 ppm. Since the formation of PhS-capped CdS NPs in the DMSO solutions is assumed, these NMR results can be compared with solid-state ^{113}Cd NMR spectra of sphalerite PhS-capped CdS NPs of various sizes measured by Herron *et al.*[16] Sharp resonances at 586 ppm were assigned to Cd only coordinated by PhS (similarly as it was observed for $[Cd(SPh)_4]^{2-}$, $[Cd_4(SPh)_{10}]^{2-}$ and Cd^o in **Cd10a**)[16] and that at ca. 725 ppm for Cd only coordinated by S^{2-} (for comparison: 706 ppm in wurtzite).[16] Another, extremely broad resonance at ca. 480–880 ppm was probably due to mixed $CdS_x(SPh)_y$ environments.[16] The peaks which were observed for B2 CdS NPs can therefore be assigned as follows: ca. 600 ppm for $Cd(SPh)_4$, ca. 680 ppm for $CdS_2(SPh)_2$ (as Cd^i in **Cd10a**) and ca. 730 ppm for CdS_4 environments, which is in good agreement with proposed formation of CdS NPs.

Contrary to the solid-state ^{113}Cd NMR spectrum of the B2 sample, its reaction solution spectrum (Figure 4.12, top) showed only the byproduct signals (593, 517, and 67 ppm), but no signal which could be assigned to the NPs. This was caused probably by longer relaxation times of Cd atoms in NPs. Only the "unknown" PhS group was observed in the ^1H NMR

spectra of all reaction solutions. However, when the NPs from sample B2 were separated by precipitation with toluene and re-dispersed in d_6-DMSO, some unresolved broad, downfield-shifted signals for PhS groups were observed besides the "unknown" PhS group (Figure 4.11). The broad signals belong probably to PhS groups on the surface of the NPs. They were present only in samples of NPs separated by precipitation.
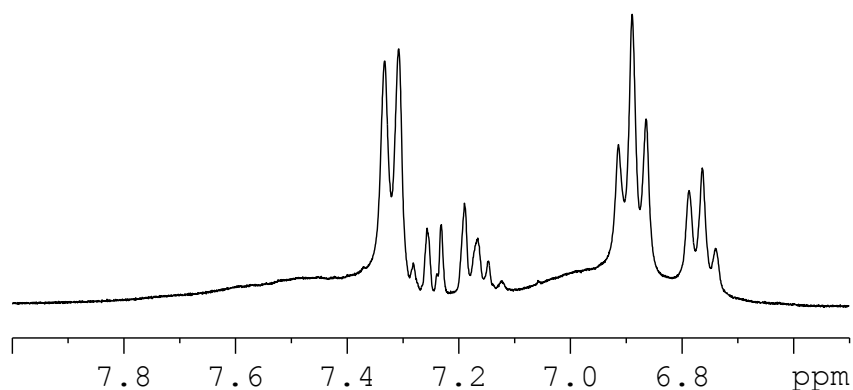
Figure 4.11. ^{1}*H NMR spectrum of CdS NPs prepared by precipitation with toluene from sample B2 and re-dispersed in d_6-DMSO. Signals between 7.12–7.28 ppm originate from toluene.*

In summary, it was shown in the experiments of series A and B that **Cd10a** is growing in DMSO solutions. At room temperature (series A), a mixture of Cd32 and Cd54 clusters was formed and no bigger NPs were observed by UV/Vis absorption even after 2 months. At 80 °C (series B) **Cd10a** transformed rapidly into a mixture of bigger clusters and NPs. Depending on the heating period and concentration, Cd32 and Cd54 were identified by analyzing the UV/Vis spectra. The presence of bigger NPs than Cd54 cluster was proven for heating times >4 h; the absorption edge increased to ca. 410 nm after 14 days of heating. The formed CdS NPs were separated from the reaction solutions by precipitation with toluene and characterized by powder XRD and SAXS. The growth was observed also in MeCN and DMF, whereas the rate of transformation increased in the order MeCN < DMF < DMSO.

During the transformation of **Cd10a** in DMSO into bigger CdS NPs, formation of a new PhS group in the ^{1}H and ^{13}C NMR spectra was observed, characterized by doublet at 7.31–7.32 ppm for the *ortho* protons of the PhS group. The shifts of *meta* and *para* triplets varied slightly (6.88–6.90, 6.76–6.80 ppm) (see also Figure 4.3). In d_7-DMF solution, a new PhS group was also formed, whereas in d_3-MeCN, new broad unresolved resonances were present. In the following part, the origin of this "unknown" PhS group will be examined in DMSO, thus the byproducts will be characterized which are formed during the cluster growth. The mechanism of the transformation will be elucidated in this way.

4.1.2 Mechanism of Cluster Growth

Rearrangement of smaller CdS/CdSe clusters in strongly coordinating solvents and formation of bigger CdS/CdSe NPs was observed previously. Herron *et al.*[64] obtained a Cd32 cluster from a pyridine solution of $Cd_{10}S_4(SPh)_{12}$ (**Cd10b**) after addition of DMF. They proposed that pyridine causes rapid fracture of the cluster core into a mixture of species with lower nuclearities which assemble and form bigger species. The latter are in fast exchange with smaller species. The Cd32 cluster crystallized then from the system as the least soluble species.[64] Cumberland *et al.*[123] investigated the formation of semiconductor NPs from M10 (CdS/CdSe/ZnS/ZnSe) clusters, being similar to **Cd10a**, in hexadecylamine (HDA). Formation of 2–9 nm HDA-stabilized CdSe NPs was observed when $Li_4[Cd_{10}Se_4(SPh)_{16}]$ in HDA was slowly heated to 220–240 °C.[123] It was proposed that the mechanism of NP formation is a combination of ligand exchange reaction and fragmentation related to the loss of apical $[Cd(SPh)_3]^-$ species from the precursor cluster followed by aggregation of remaining Cd_xSe_y species (Scheme 4.1).[123] However, the authors did not characterize any byproducts that would have supported their mechanistic proposal.
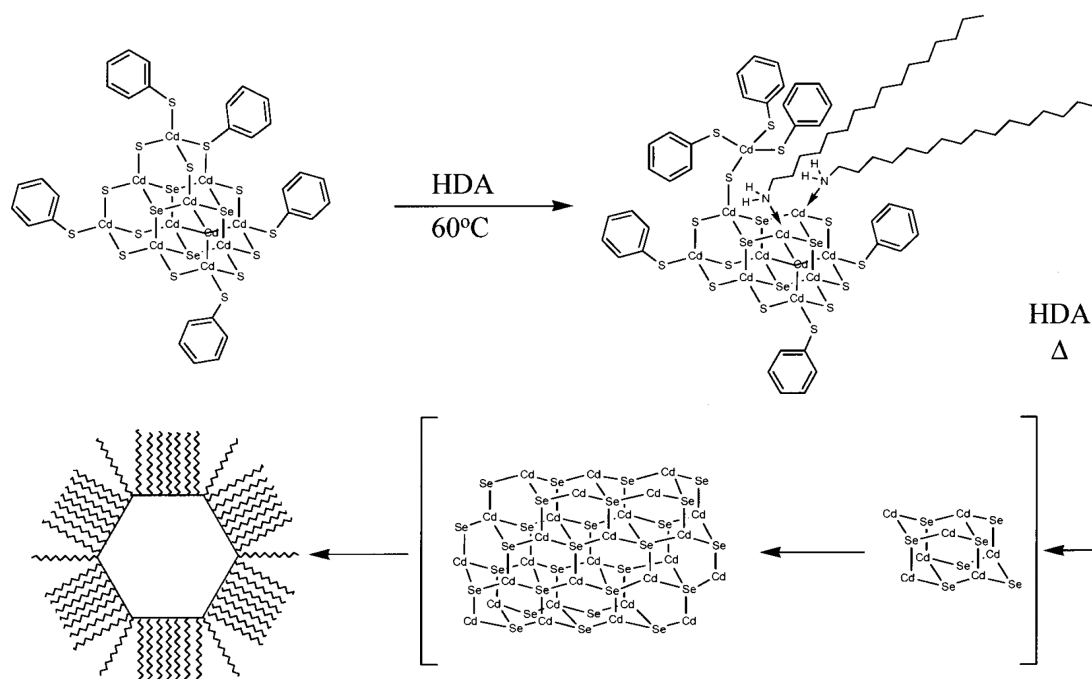
Scheme 4.1. Scheme of the rearrangement reaction of a $[Cd_{10}Se_4(SPh)_{16}]^{4-}$ cluster in HDA as proposed by Cumberland et al.[123]

Further investigations on transformations of clusters similar to **Cd10a** in HDA at elevated temperatures were subsequently carried out.[124,125,126,127,128] DeGroot *et al.*[125] reacted the mixed-metal cluster $M_{10}Se_4(SePh)_{12}(PPr_3)_4$ (M = Cd+Zn) in HDA at 120–240 °C. Zn atoms preferably occupy apex M° positions in these M10 clusters, according to NMR studies in CD_2Cl_2 and crystal structure analyses,[38] which should be released first during the transformation. However, the formed NPs revealed the same Cd:Zn ratio as the precursor

which implies that release of the M^o positions is not preferred. This conclusion should be applicable also to the mono-metallic **Cd10a** cluster, but is in disagreement with the mechanism proposed by Cumberland *et al.*[123] However, the molecular structures and exchange dynamics of M10 clusters used in the study of DeGroot *et al.*[125] could be different in HDA reaction solutions[125] than in CD_2Cl_2 solutions,[38] and, also, charge differences between the neutral[125] and negatively charged Cd10 clusters used by Cumberland *et al.*[123] can have an influence. Furthermore, the formation of diphenyldiselenide Ph_2Se_2 at 120–160 °C was confirmed by GC/MS analyses.[125] Its proportion decreased with increasing reaction temperature, concurrent with the appearance of diphenylselenide Ph_2Se. The authors considered the presence of Ph_2Se_2 in the GC/MS spectra as an indication of the presence of $[M(SePh)_2]$ or $[M(SePh)_3]^-$ species,[125] which is in contrast to their previous statement that the apical sites are not preferentially released.

Finally, Lovingood *et al.*[126] proved the formation of CdSSe NPs instead of CdSe NPs[123] from $Li_4[Cd_{10}Se_4(SPh)_{16}]$ in HDA. NPs prepared at higher temperatures (230 °C) had a higher S^{2-} proportion compared to those prepared at 120 °C. S^{2-} originated from the decomposition of PhS^- at higher temperatures to give Ph_2S and S^{2-}. The overall decomposition reaction at higher temperatures can be then formally written as

$$Li_4[Cd_{10}Se_4(SPh)_{16}] \longrightarrow (Cd_{10}Se_4S_6) + 6\ Ph_2S + 4\ LiSPh \qquad (4.1)$$

Thus, the mechanism of transformation of M10 clusters in HDA into bigger NPs was not elucidated satisfactorily until now. In this chapter, the possibility of formation of some $[Cd(SPh)_x(DMSO)_y]^{(2-x)}$ species will be investigated, based on the proposal of Cumberland *et al.*[123] It will be aimed to prove that the "unknown" PhS group, which was observed by NMR, belongs to the proposed $[Cd(SPh)_x(DMSO)_y]^{(2-x)}$ species.

There are substantial compositional differences between **Cd10a** and larger clusters or thiolate-capped CdS NPs (Table 4.4). The S:Cd ratio increases and PhS:Cd ratio decreases with increasing size. Therefore, one or more byproducts must be formed which balance the sulfide and thiolate inventory, *e.g.* a compound containing mainly Cd and thiolate. Thus, suggested $[Cd(SPh)_x(DMSO)_y]^{(2-x)}$ species, according to Cumberland *et al.*,[123] are suitable candidates.

Table 4.4. Summary of few CdS clusters and NPs according to their size and composition. The diameter of the NPs was estimated by powder XRD[16] which gives the NP core size.

Cluster/NP size	Composition
$[Cd_{10}S_4(SPh)_{16}]^{4-}$ (**Cd10a**)	$CdS_{0.40}(SPh)_{1.60}$
$[Cd_{32}S_{14}(SPh)_{40}]^{4-}$	$CdS_{0.44}(SPh)_{1.25}$
CdS NPs ($\varnothing$ = 2 nm)	$CdS_{0.54}(SPh)_{0.96}$[16]
$[Cd_{54}S_{32}(SPh)_{48}L_4]^{4-}$	$CdS_{0.59}(SPh)_{0.89}$
CdS NPs ($\varnothing$ = 2.5 nm)	$CdS_{0.78}(SPh)_{0.48}$[16]
CdS NPs ($\varnothing$ = 3 nm)	$CdS_{0.84}(SPh)_{0.39}$[16]
CdS NPs ($\varnothing$ = 3.5 nm)	$CdS_{0.92}(SPh)_{0.25}$[16]

The proof can be divided into four parts.

(1) The ^{13}C NMR chemical shifts of the "unknown" PhS group were compared with terminal and bridging PhS groups of **Cd10a**, $(Me_4N)_2[Cd(SPh)_4]$ (**Cd1**),[47] and $[Cd_4(SPh)_8]_\infty$ (**Cd4b**)[49] in d_6-DMSO (Table 4.5). For bridging PhS groups, the chemical shift of the *ipso* carbon atoms is ca. 140 ppm, and for terminal groups ca. 146/150 ppm. An opposite trend was observed for the *para* carbon atoms. In terminal groups they are shifted upfield by ca. 2 ppm compared to bridging groups. The same trend for *ipso* and *para* carbon atoms was present also in d_3-MeCN (*ipso*: 140 and 147/150 ppm, *para*: 124 and 121/122 ppm for bridging and terminal PhS groups, respectively). On this basis the "unknown" PhS group in DMSO can be assigned to a terminal PhS group, assuming that it originates from a Cd-SPh species. A terminal PhS group can originate only from mononuclear Cd complex, since a complex with more Cd atoms would require also bridging PhS groups.

*Table 4.5. Summary of the ^{13}C NMR data of terminal and bridging PhS groups of **Cd10a**, $(Me_4N)_2[Cd(SPh)_4]$ (**Cd1**) and $[Cd_4(SPh)_8]_\infty$ (**Cd4b**), measured in d_6-DMSO at room temperature.*

PhS group	Compound	[13]C shifts / ppm			
		ipso	*ortho*	*meta*	*para*
"unknown"		145.8	131.7–132.5	127.2–127.3	120.9
terminal	**Cd10a**	145.4	132.5	127.1	120.6
	Cd1	149.3	132.7	126.7	119.4
bridging	**Cd10a**	138.7	133.6	127.1	122.9
	Cd4b	140.0	132.9	127.7	122.9

(2) As already mentioned, the B2 sample (40 mg/ml, 80 °C/16 h) showed the presence of the "unknown" PhS group in the ^{1}H NMR spectrum and broad, weak signals in the [113]Cd NMR spectrum at 593, 517, and 67 ppm (Figure 4.12, top). The resonance at 593 ppm can be assigned to a $Cd(SPh)_4$ environment. The resonances at 517 and 67 ppm could indicate partial coordination of DMSO to Cd,[50,68] *viz.* $[Cd(SPh)_3(DMSO)_y]^-$ (resonance at 517 ppm) and mononuclear Cd complexes with a higher proportion of DMSO (resonance at 67 ppm).

In order to gain further insight, $(NMe_4)_2[Cd(SPh)_4]$ (**Cd1**) was added in a 1:1 molar ratio to the B2 sample. Shifts in the [113]Cd NMR spectra changed drastically. Only one broad signal at 535 ppm (Figure 4.12, bottom) was obtained after addition of **Cd1** (δ [113]Cd of **Cd1** was measured at 602 ppm in d_6-DMSO). Furthermore, only one PhS group was observed in the NMR spectra after addition of **Cd1**, the *meta* and *para* protons of which shifted slightly in ^{1}H NMR (Figure 4.13) and which had the character of a terminal group (^{13}C shifts). The presence of one set of PhS resonances is probably due to fast PhS exchange between the byproduct and **Cd1**, which is in line with expectation that the byproduct has similar nature as **Cd1**.
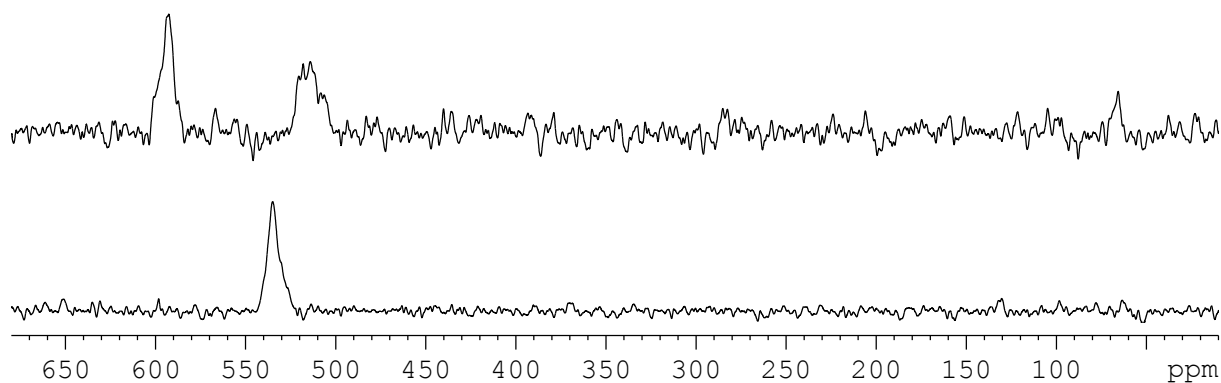
*Figure 4.12. ^{113}Cd NMR spectrum of B2 sample in d_6-DMSO (40 mg/ml, 80 °C/16 h) before (top) and after (bottom) 1:1 molar addition of $(NMe_4)_2[Cd(SPh)_4]$ (**Cd1**).*
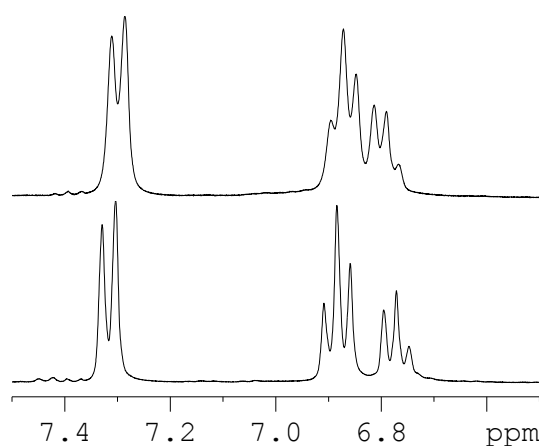
*Figure 4.13. ^1H NMR spectrum of B2 sample in d_6-DMSO (40 mg/ml, 80 °C/16 h) before (top) and after (bottom) 1:1 molar addition of $(NMe_4)_2[Cd(SPh)_4]$ (**Cd1**).*

(3) In an attempt to crystallize some $[Cd(SPh)_x(DMSO)_y]^{(2-x)}$ species from the DMSO reaction solutions of **Cd10a** by addition of other solvents (see Experimental Section), crystals of the known compound $[Cd_4(SPh)_8]_\infty$ (**Cd4b**)[49] and of $(NMe_4)_2[Cd_8S(SPh)_{16}]$ (**Cd8**) were obtained. A SC-XRD analysis showed that the cluster anion of **Cd8** has essentially the same structure as that in $(MV)[Cd_8S(SPh)_{16}]$[51] (MV = methyl viologen dication), $(NEt_4)_2[Cd_8S(SePh)_{16}]$[52] and $[Cd_8S(SePh)_{12}Cl_4]^{2-}$.[129]

In order to examine whether **Cd4b** and **Cd8** were present in the reaction solutions directly after the heat treatment, the NMR spectra of **Cd4b** and **Cd8** were compared with those of reaction solutions. Cluster **Cd8** was characterized previously in d_7-DMF solution by ^{113}Cd NMR,[52] whereas its integrity was confirmed in solution. The Cd^i and Cd^o resonances of **Cd8** were at 625 and 584 ppm, respectively.[52] The Cd^i value is distinctly upfield shifted compared to the Cd^i resonance of **Cd10a** (682.5 ppm, for Cd^o 598 ppm). However, the coordination sphere of Cd^i in **Cd8** is different to that in **Cd10a**: $CdS(SPh)_3$ vs. $CdS_2(SPh)_2$, and, in this way, the upfield shift of Cd^i resonance in **Cd8** can be reasonably explained. Anyway, the shifts of **Cd8** are different to those obtained for the B2 sample (593, 517 and 67 ppm), which suggests that **Cd8** is not present in DMSO reaction solutions after the thermal treatment.

However, as pointed out at the beginning of this chapter, clusters of different sizes are in equilibrium in solution, and **Cd8** may be formed as the least soluble species after the change of solvent conditions.

Similar arguments apply for **Cd4b**. It was previously proposed that the 3D network of Cd4 clusters present in crystalline **Cd4b** is broken in DMF solution and aggregates of Cd4 clusters are formed.[50] The aggregates are bigger at lower temperature and disintegrate due to solvent coordination with increasing temperature.[50] A similar behavior was now observed in d_6-DMSO solution of **Cd4b**, but the temperature dependence was different. At room temperature, there was one ^{113}Cd NMR resonance at 591 ppm, which was assigned to an average Cd(SPh)$_4$ environment. It was similar to the resonance of **Cd4b** in d_7-DMF at ca. 250 K (based on similar FWHM and δ ca. 602 ppm).[50] The ^{13}C NMR spectrum revealed one bridging PhS group. No sharp signals were observed in the ^{113}Cd NMR spectrum at 353 K (corresponds to room temperature in d_7-DMF)[50]. Thus, it can be concluded, that aggregates of Cd4 clusters are present in the DMSO solution of **Cd4b** at room temperature, similarly to DMF solution at lower temperatures.[50] This actually would mean that DMF breaks Cd4 aggregates more easily than DMSO and thus coordinates stronger to Cd, which is in disagreement with the by now obtained sequence of increasing coordination strength: MeCN < DMF < DMSO. On the other hand, the two investigations (in d_7-DMF[50] and d_6-DMSO) were performed with different concentrations of **Cd4b** (0.3[50] and 0.1 mg/ml), which could also lead to the observed differences. In any case, this shows that such aggregates of Cd4 clusters are not present directly in the DMSO solutions of **Cd10a**. They are formed only upon addition of other solvents.

(4) The UV/Vis spectra of CdS NPs precipitated by addition of toluene to samples B1–B4 showed a substantial decrease of absorption in the area <325 nm compared with the reaction solutions (for sample B1 see Figure 4.14). This can be explained by byproduct(s) with absorption <325 nm which are not or only partially precipitated from the reaction solutions. The UV/Vis spectra of DMSO solutions of (NMe$_4$)$_2$[Cd(SPh)$_4$] (**Cd1**) and [Cd$_4$(SPh)$_8$]$_\infty$ (**Cd4b**) (Figure 4.14) are similar to each other, with absorption maxima at 279 and 272 nm, respectively, which could fit well with the absorption of byproduct(s). In order to find evidence whether **Cd1,** possibly **Cd4b**, or related species are present in the DMSO reaction solution, the spectrum of the solution B1 was calculated by superposition of the spectra of re-dispersed NPs precipitated from the solution B1 and **Cd1** in DMSO (calculation 1 in Figure 4.15) or both **Cd1** and **Cd4b** in DMSO (calculation 2 in Figure 4.15). The value $\Sigma |(A_c - A_o) / (A_c + A_o)|$ was minimized in the range 265–400 nm in the calculations. Calculation 2 led to a better fit with the following composition for the $3.3 \cdot 10^{-6}$ M B1 reaction solution: $5.6 \cdot 10^{-6}$ M of **Cd1**, $5.3 \cdot 10^{-6}$ M of **Cd4b** and 0.0048 mg/ml of B1 NPs. Calculation 1 led to following composition: $1.2 \cdot 10^{-5}$ M of **Cd1** and 0.0046 mg/ml of B1 NPs. The calculated NPs yield was in good agreement with the yield determined in the previous section.
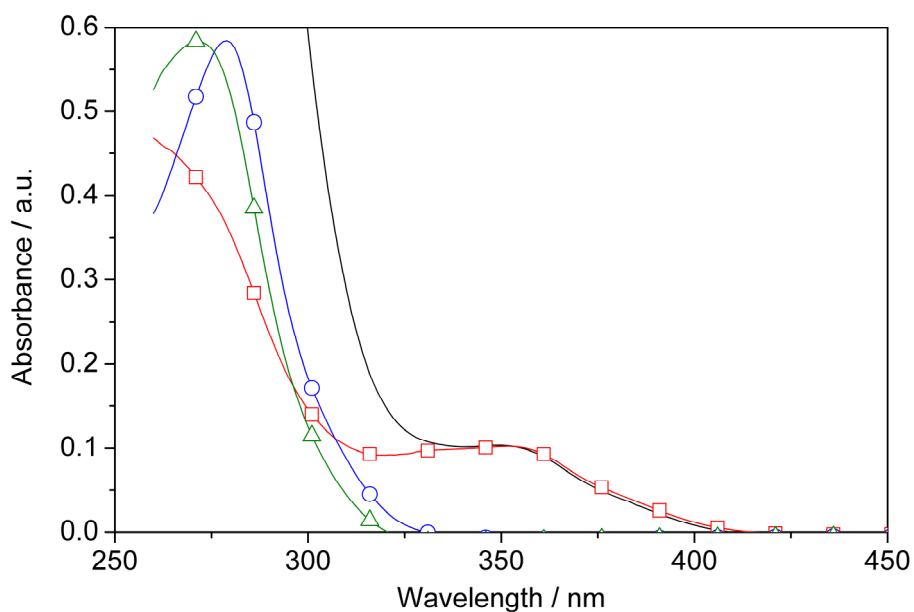
Figure 4.14. UV/Vis spectra of B1 reaction solution (0.028 mg/ml, –), re-dispersed NPs precipitated from B1 (0.013 mg/ml, □), (NMe₄)₂[Cd(SPh)₄] **(Cd1)** *(0.009 mg/ml, ○), and [Cd₄(SPh)₈]∞* **(Cd4b)** *(0.013 mg/ml, △) in DMSO.*
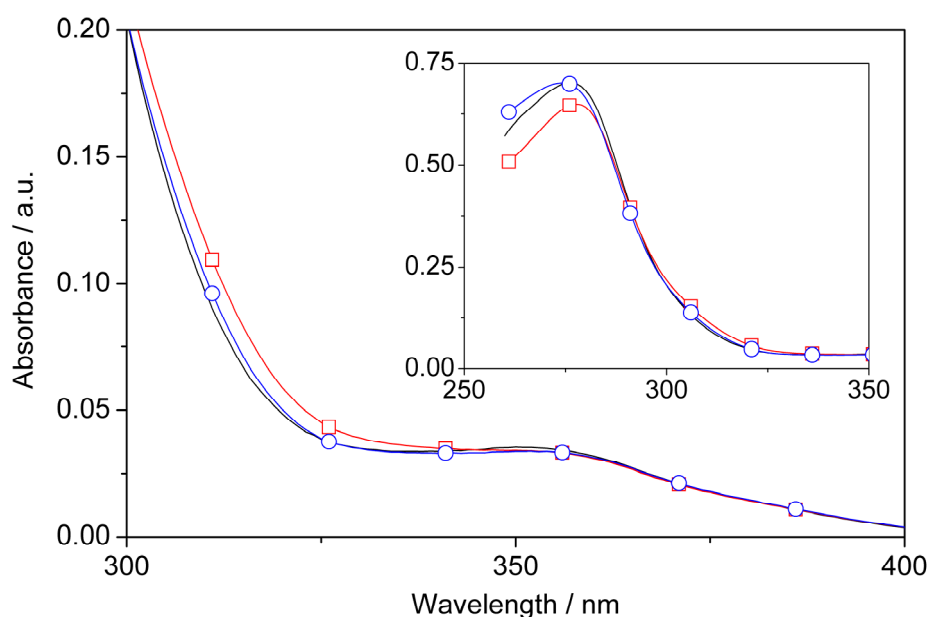
*Figure 4.15. Calculation of the UV/Vis spectrum of the B1 reaction solution (0.011 mg/ml, –) using spectra of re-dispersed NPs precipitated from the B1 solution and **Cd1** in DMSO (calculation 1, □) and both **Cd1** and **Cd4b** in DMSO (calculation 2, ○).*

In order to draw conclusions about the nature of the byproduct and its UV/Vis similarity with **Cd1** and **Cd4b** in DMSO solutions, the following has to be considered. First, solutions for UV/Vis spectroscopy are much diluted compared to solutions investigated by NMR. This

can lead to formation of other species, especially with lower nuclearities in the case of **Cd4b** where aggregates of Cd4 clusters were present at room temperature and higher concentration (NMR). Second, the UV/Vis behavior of very small Cd thiolate complexes is opposite to CdS NPs and exhibits blue shift with increasing complex size.[77] This explains the blue shift of **Cd4b** relative to **Cd1** in DMSO. It also means that **Cd4b** is present in the form of Cd4 clusters in its much diluted DMSO solutions, at least partially. Since calculation 2 led to better fit, it can be assumed that not only mononuclear Cd species are present in the reaction solutions, but also bigger Cd4 clusters. On the other hand, the absorption of mononuclear Cd species can be influenced by solvent coordination; thus, the absorption maxima of $[Cd(SPh)_x(DMSO)_y]^{(2-x)}$ species can be shifted compared with **Cd1**. Therefore, the precise composition of species present in diluted DMSO reaction solutions cannot be elucidated from these data. Nevertheless, the relatively good fit of the spectrum of the B1 reaction solution by calculation 1 allows the conclusion that the byproduct consists of some mononuclear species similar to **Cd1**.

It was proven in this chapter that the byproduct of the formation of CdS NPs from **Cd10a** in DMSO solutions is a mononuclear compound with a likely composition of $[Cd(SPh)_x(DMSO)_y]^{(2-x)}$ (x = ca. 3). This supports the prediction of Cumberland *et al.* about the fragmentation of cluster similar to **Cd10a** which was supposed to start by cleavage of its apical Cd^o positions and formation of $[Cd^o(SPh)_3]^-$ species.[123] The main evidence leading to this conclusion can be summarized as follows:

1. The "unknown" PhS group observed in NMR spectra of reaction solutions is terminal, *i.e.* is bonded to only one Cd atom.

2. Addition of $(NMe_4)_2[Cd(SPh)_4]$ (**Cd1**) to a reaction solution leads to only one PhS group with terminal character, which is similar to the byproduct and **Cd1**. The ^{113}Cd spectrum of a reaction solution changed substantially after addition of **Cd1**. The shift in ^{113}Cd NMR can be attributed to partial coordination of DMSO to Cd before and after addition of **Cd1**.

3. Small clusters, *viz.* $[Cd_4(SPh)_8]_\infty$ (**Cd4b**) and $[Cd_8S(SPh)_{16}]^{2-}$ (**Cd8**), were crystallized from a reaction solution, although they were not present in the reaction solutions as such.

4. Differences in the UV/Vis spectra of reaction solutions and the NPs precipitated from these solutions revealed that the byproduct has UV/Vis characteristics similar to that of **Cd1**.

4.1.3 Conclusions

It was shown in this chapter that $[Cd_{10}S_4(SPh)_{16}]^{4-}$ (**Cd10a**) grows in coordinating solvents. In DMSO, growth is very fast at 80 °C and after 90 min no signals of the original **Cd10a** are present in the solution. At room temperature, a mixture of Cd32 and Cd54 clusters is formed within few days, while bigger clusters and/or NPs are also present after heating at 80 °C. The formed NPs could be precipitated by addition of toluene, MeOH, EtOH or acetone to the reaction solutions. Solid-state NMR confirmed the presence of PhS^- and Me_4N^+ on

their surface and a CdS core. Powder XRD and SAXS were also in good agreement with formation of CdS NPs. NMR spectroscopy of reaction solutions revealed formation of a new, "unknown" PhS group. Growth of **Cd10a** was observed also in DMF and MeCN, in MeCN being relatively slow (after 21 h at 75 °C, ca. 75 % of **Cd10a** remained unchanged). Therefore, the rearrangement rate increases in the order MeCN < DMF < DMSO.

The notion of a possible growth mechanism was obtained from the mechanism proposed by Cumberland *et al.*[123] for the growth of $Li_4[Cd_{10}Se_4(SPh)_{16}]$ heated in hexadecylamine (HDA). They suggested a mechanism which started with the fragmentation of the Cd10 cluster and loss of apical $[Cd(SPh)_3]^-$ species upon which the residual smaller Cd_xSe_y species aggregated and formed bigger clusters or NPs (Scheme 4.1). In disagreement to this mechanism were conclusions of DeGroot *et al.*[125] The current proof that the cluster rearrangement mechanism involves formation of apical $[Cd(SPh)_3]^-$ species was based on the characterization of the byproduct which formed during the transformation. Strong evidence was found that it is a mononuclear species with a composition $[Cd(SPh)_x(DMSO)_y]^{(2-x)}$ (x = ca. 3).

It is very probable that the rearrangement of **Cd10a** in DMF processes by the same mechanism. However, the mechanism can be different in MeCN since no byproduct with sharp resonances in NMR was formed as it was the case in DMSO and DMF. However, the rearrangement is very probably related to the coordination strength of the solvent, which then increases in the sequence MeCN < DMF < DMSO.

A driving force for the rearrangement can be the decrease of the overall cluster charge, when negatively charged species are released from the apical cluster positions. Therefore, clusters with low negative charge density or neutral clusters might be more stable against the solvent coordination effect.

The fundamental question, whether the molecular structure of clusters, **Cd10a** as a model, in solution at prolonged heating is identical with the structure obtained by SC-XRD, was answered. It was important in order to ensure that the cluster and chosen reaction conditions can be used for a polymerization reaction. However, it was shown, that such reactions are not possible in DMF and DMSO, because the cluster is completely rearranged to bigger clusters/NPs. Almost the same applies for MeCN solution, but a substantial part of the cluster is maintained here also at relatively harsh conditions. Therefore, the conditions for further reactions on clusters have to be chosen carefully, in order to minimize the solvent coordination effect and to avoid the cluster rearrangement and growth.

A possible solution for the problem could be use of non-coordinating solvents like toluene, CH_2Cl_2, or $CHCl_3$. However, they are not polar enough for **Cd10a** and most of the charged clusters which are soluble only in polar coordinating solvents. A possibility how to adjust the cluster solubility could be preparation of clusters stabilized by phosphines at the terminal ligand positions, like in the case of few CdSe and CdTe clusters,[130,131,38] or use of more bulky counter-cations, *e. g.* $(NnBu_4)_4[Cd_{10}S_4(SPh)_{16}]$, if it is possible to synthesize such cluster.

4.2   Characterization of "$Cd_{10}S_4(SPh)_{12}$" in Solid State and Solution

The cluster "$Cd_{10}S_4(SPh)_{12}$" (**Cd10b**, Figure 4.16) is prepared by the first step of thermal decomposition of $(NMe_4)_4[Cd_{10}S_4(SPh)_{16}]$ (**Cd10a**, Figure 4.1)[47] upon heating in vacuum (Equation 4.2).[54] The reaction proceeds by a nucleophilic attack of the terminal thiolate groups on a methyl group of the proximal NMe_4^+ cations leading to loss of four NMe_3 and MeSPh equivalents (Equation 4.2) and formation of a cluster with the postulated structure of **Cd10b** (Figure 4.16).[54] This mechanism was supported by thermogravimetric analysis (TGA) coupled with mass spectrometry (MS) which was in good agreement with the theoretical mass loss and identified presence of NMe_3 and MeSPh products in the gas phase.[54] The mechanism was confirmed also by investigation of thermal treatment of $(NEt_4)_4[Cd_{10}S_4(SPh)_{16}]$ and $(NMe_4)_4[Zn_{10}S_4(SPh)_{16}]$ clusters which led to equivalent products. The first step of the thermal treatment took place at ca. 200–250 °C at a heating rate of 10 K/min. The second step (350–450 °C) was related to the loss of residual phenyl groups from the cluster surface in the form of SPh_2, leading to formation of pure CdS with hexagonal wurtzite phase.[54]

$$(NMe_4)_4[Cd_{10}S_4(SPh)_{16}] \text{ (\textbf{Cd10a})} \longrightarrow \text{``}Cd_{10}S_4(SPh)_{12}\text{''} \text{ (\textbf{Cd10b})} + 4\ NMe_3 + 4\ MeSPh$$

$$(4.2)$$
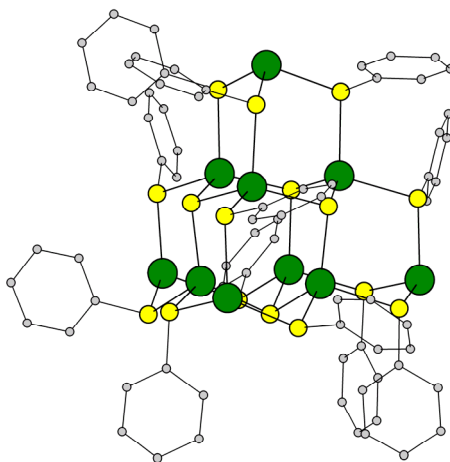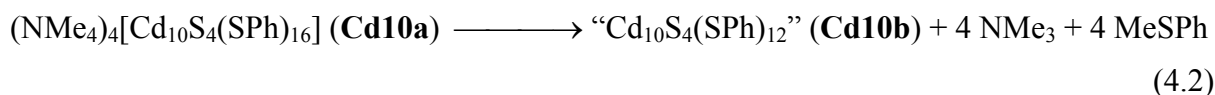
*Figure 4.16. Schematic drawing of the postulated structure of **Cd10b**, derived from the crystal structure of **Cd10a-3** by removal of four terminal SPh ligands.*

The compound **Cd10b** itself was characterized by Farneth *et al.*[54] who concluded from various characterization methods (TGA, powder XRD, UV/Vis absorption, NMR) that **Cd10b** is a neutral $Cd_{10}S_4(SPh)_{12}$ cluster that tends to aggregate to different degrees in the solid state and in solution. Herron *et al.*[64] showed that **Cd10b** changes its structure in pyridine and that a bigger cluster, $Cd_{32}S_{14}(SPh)_{36}(DMF)_4$, crystallizes after addition of DMF. This was attributed to rearrangement processes caused by fracture of cluster cores which led to a dynamic mixture of species with lower nuclearities. The Cd32 cluster apparently assembled from these smaller species and was probably the least soluble one in the system which

resulted in its preferred crystallization.[64] In other studies, the thiophenolate ligands of **Cd10b** were exchanged by $HSC_6H_5(OCH_2CH_2)_nOMe$[119] or dendritic thiols,[120] and it was claimed that a Cd10 cluster capped by these thiolate ligands was formed. A few experiments indicate the possibility that neutral or anionic ligands can be coordinated to the empty coordination sites of **Cd10b** generated by loss of the four SPh⁻ ligands. It was thus postulated that $[Cd_{10}Br_4S_4(SPh)_{12}]^{4-}$ was formed when **Cd10b** was reacted with tetraalkyl ammonium bromides.[118,132]

In this chapter, the results on structural characterization of **Cd10b** are summarized. The motivation leading to the investigation of its structure was based on the possibility to use the four free Cd coordination sites of **Cd10b** for cluster functionalization, similarly to the coordination of Br⁻ from tetraalkyl ammonium bromides.[118,132] Such a reaction would, however, require a precisely defined molecular structure of **Cd10b** which was not unequivocally proven yet.[54] Beside this, some uncertainty resulted from investigations of similar Cd clusters, like $Cd_{10}Se_4(SePh)_{12}(PR_3)_4$, performed by Eichhöfer *et al.*[133] who concluded that this cluster grows upon thermal treatment in the solid state and forms larger clusters. This growth was not totally specific. Similarly, DeGroot *et al.*[38] investigated solid-state thermolysis of mixed metal clusters $M_{10}E_4(EPh)_{12}(PnPr_3)_4$ (M = Zn+Cd; E = Se, Te) and also showed that the M10 clusters grow during the treatment. Therefore, the thermal treatment of **Cd10a** does not necessarily lead to the formation of a cluster with the $Cd_{10}S_4(SPh)_{12}$ composition. On the other hand, the behavior of clusters investigated by Eichhöfer *et al.*[133] and DeGroot *et al.*[38] could be different due to their neutrality compared with the anionic **Cd10a** cluster. Therefore, a thorough investigation of the molecular structure of **Cd10b** was necessary.

It was supposed that **Cd10b** will change its structure after dissolution in strongly coordinating solvents like DMF, DMSO, or pyridine, as it was shown for **Cd10a** in previous chapter (it could also explained the formation of Cd32 cluster in pyridine/DMF solution of **Cd10b** in Ref. 54). Therefore, the structural investigation of **Cd10b** can be divided into two parts: (i) in solid state and solutions of weakly coordinating solvents (like MeCN, tetrahydrofuran (THF)), and (ii) in solutions of strongly coordinating solvents (DMF, DMSO, pyridine). The first part shows that the cluster core of **Cd10a** grows already during the preparation of **Cd10b** (heat treatment). The rearrangement in weakly coordinating solvents is slow and the clusters possess the same molecular structure in them as in solid state which allows reliable characterization. The second part contributes to the already observed rearrangement of CdS clusters in coordinating solvents and leads to crystallization of diverse Cd54 clusters.

4.2.1 Growth of $[Cd_{10}S_4(SPh)_{16}]^{4-}$ during the Heat Treatment in Vacuum

A slightly different synthesis protocol for **Cd10b** was used compared with the procedure of Farneth *et al.*[54] namely heating of **Cd10a** in vacuum at 180 °C for 6 h,[118] by which a yellow solid was obtained. The identity of chemical composition of **Cd10b** prepared by this

method and by Farneth's method[54] was verified by TGA and elemental analysis (see Experimental Part). First, **Cd10b** was characterized in solid state.

The UV/Vis absorption spectrum of solid **Cd10b** in mineral oil (Figure 4.17) revealed a shift of the absorption edge from 323 nm in solid **Cd10a** to ca. 390 nm. The absorption edges allow more accurate comparison of the two absorption spectra since there is no clear maximum in the spectrum of **Cd10b**. The shift to higher wavelength in the case of **Cd10b** means that bigger CdS clusters/NPs are present compared with **Cd10a**. The shift of the absorption edge is due to the quantum size effect (see Chapter 2.1.1). Thus, the UV/Vis spectra clearly indicate that **Cd10b** also contains CdS clusters or NPs which are bigger than the core of **Cd10a**.
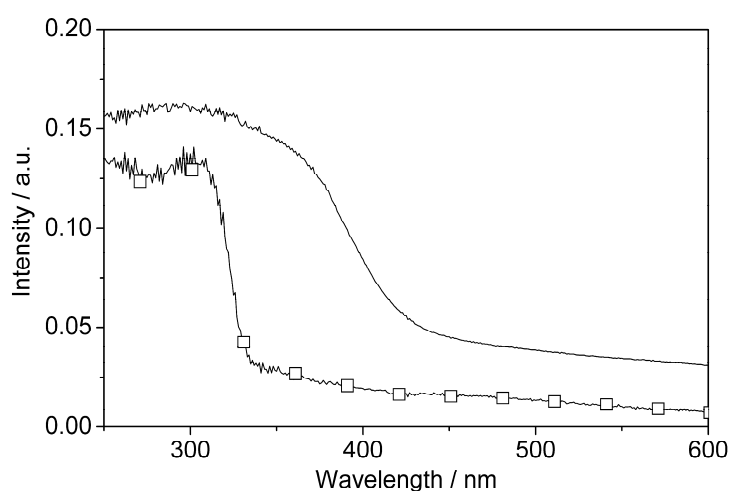
*Figure 4.17. UV/Vis absorption spectra of **Cd10b** (–) and **Cd10a** (□) as a suspension in mineral oil.*

Powder XRD of **Cd10b** (Figure 4.18) revealed a pattern very similar to that reported in Ref. 54. The fact that a (weak) diffraction pattern is obtained is evidence for the presence of CdS NPs in addition to possible other, non-crystalline Cd/S species formed upon thermolysis of **Cd10a**. Because of the small size of the NPs, a distinction between wurtzite or sphalerite is not unequivocally possible. However, compared with the CdS NPs prepared in Chapter 4.1, the shift of the reflection from ca. 28.5° to ca. 26° in the 2θ range 25–30° is an indication that **Cd10b** is present mainly in the wurtzite modification. This is in good agreement with the formation of wurtzite CdS after the thermal treatment of **Cd10a** at higher temperatures (step 2 in Ref. 54) and the known stability of wurtzite and sphalerite phases: under kinetically controlled conditions, sphalerite CdS NPs are formed, whereas wurtzite CdS NPs are obtained under thermodynamically controlled conditions.[78] That means that if higher temperature is applied during NP synthesis, the thermodynamically preferred phase is obtained.[78] This is observed also for NPs prepared by the pyrolysis of organometallic Cd compounds in hot coordinating solvents.[72,73]

The size of crystalline cores of CdS clusters/NPs in **Cd10b** cannot be obtained accurately by powder XRD analysis. Therefore, **Cd10b** was characterized also by means of SAXS which revealed mean core diameter of all particles present in **Cd10b** of 1.39(7) nm, whereas the core

diameter of **Cd10a** is 0.7 nm (this is the distance from the Cd atom at one vertex to the opposite tetrahedral face). This confirms again the growth of cluster core of **Cd10b**.
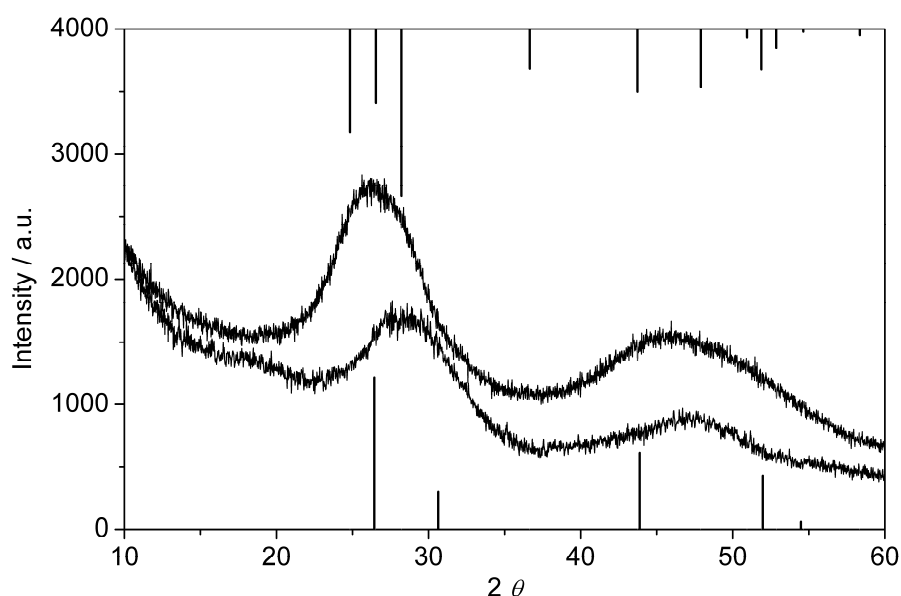
*Figure 4.18. X-ray powder patterns of **Cd10b** (top) and probably sphalerite CdS NPs from Chapter 4.1 (bottom). The peak patterns of wurtzite (top) and sphalerite (bottom) CdS are also shown.*

The solid-state ^{113}Cd NMR spectrum of **Cd10b** (Figure 4.19) showed four broad, overlapping resonances at 494, 589, 660 and 736 ppm. For comparison, crystalline **Cd10a** shows sharp resonances at 598, 668 and 705 ppm in agreement with values from the literature.[53] In a non-crystalline sample such as **Cd10b**, the Cd surrounding is not uniform and therefore no sharp signals can be expected which is indeed the case. However, the broad signals of **Cd10b** also indicate that it does not consist of a single compound.
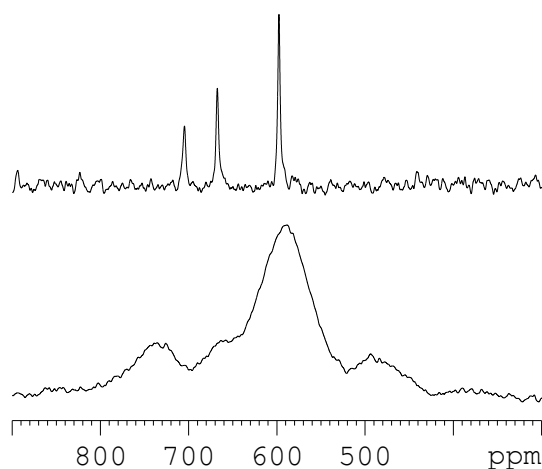
*Figure 4.19. ^{113}Cd-CP MAS spectrum of **Cd10a-1** (crystallized in space group I−4) at 15 kHz (top) and of **Cd10b** at 6 kHz (bottom).*

45

It can be concluded from the investigation of **Cd10b** in the solid state that the core of **Cd10a** grows during the heat treatment (UV/Vis, SAXS) and that a non-uniform product is formed ([113]Cd NMR). The following characterization is based on solutions/suspensions of **Cd10b** in weakly coordinating solvents like THF and MeCN, because the structure of **Cd10b** should not be influenced by them.

Cd10b is not soluble in MeCN but sparingly soluble in THF (ca. 1 mg/ml). UV/Vis measurement was performed in THF after filtration of the suspension through a 0.2 µm Nylon syringe filter. The spectrum revealed absorption edges at ca. 370 and 327 nm (Figure 4.20), confirming the presence of CdS NPs bigger than the Cd10 core. The absorption edge of ca. 370 nm corresponds to a Cd54 cluster (Table 4.6). For comparison, cluster **Cd10a** has an absorption edge at 302 nm in MeCN (Figure 4.2). DLS measurements also confirmed the presence of bigger particles in THF solution of **Cd10b** (see Experimental Part, Figure 6.2) compared with **Cd10a** in MeCN (particle radii were 0.55–3.5 and 0.5–1.5 nm respectively).
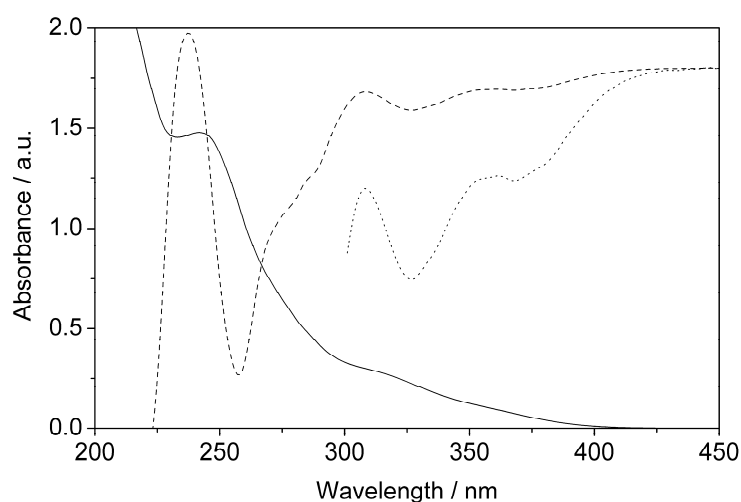
*Figure 4.20. UV/Vis spectrum of **Cd10b** in THF (<0.05 mg/ml). Solid line represents the UV/Vis absorption curve, dashed line is its 1st derivative (dotted line is 5x 1st derivative).*

Additional evidence that **Cd10a** grows during the heat treatment was gained when solutions or suspensions of **Cd10b** were reacted with various thiolates. If **Cd10b** would have the postulated composition $Cd_{10}S_4(SPh)_{12}$, and the structure would be as shown in Figure 4.16, the starting cluster **Cd10a** or its derivatives should be re-formed upon addition of the thiolate anions to the vacant coordination sites. To verify this, NMR measurements were performed which were based on addition of four equivalents of $PhSH/NEt_3$, $NaSPh/(NMe_4)Cl$ or $(NMe_4)SPh$ to the suspension of **Cd10b** in d_3-MeCN. However, the NMR spectra were not identical with the spectrum of **Cd10a**. The most similar ^{1}H NMR spectrum was obtained for the reaction of **Cd10b** with NaSPh in d_3-MeCN (Figure 4.21), although there was a noticeable lowfield shift of one PhS group and a high, unresolved background. Interestingly, when four molar equivalents of PhSH and NEt_3 were added to the suspension of **Cd10b** in d_3-MeCN at high concentration of **Cd10b** (40 mg/ml), crystals of the known derivative $(NHEt_3)_4[Cd_{10}S_4(SPh)_{16}]$[53] formed at room temperature (verified by SC-XRD). However, no

resonances of the Cd10 cluster were observed in the solution NMR spectrum, probably because most of it crystallized and the concentration in solution was too low $((NHEt_3)_4[Cd_{10}S_4(SPh)_{16}]$ has a ca. 10-times lower solubility in MeCN than **Cd10a**). The ^{1}H-^{113}Cd HMBC correlation pattern with the most intense ^{113}Cd signals at 581, 601 and 655 ppm (Figure 4.22), as well as HSQC and HMBC spectra can be assigned to a bigger cluster, probably Cd32 (similarly to a Cd54 cluster formed in d_6-DMSO solution of **Cd10b**, see page 51). This was confirmed by the UV/Vis spectrum of the corresponding reaction solution (which formed at concentration of **Cd10b** < 4.6 mg/ml). A shoulder at 325 nm was observed, which was previously assigned to a Cd32 cluster (Table 2.2). Beside this, features below 300 nm also confirm the presence of $(NHEt_3)_4[Cd_{10}S_4(SPh)_{16}]$ (Figure 4.23). This experiment confirms that **Cd10a** grows during the heat treatment, but also that part of it reacts to real $Cd_{10}S_4(SPh)_{12}$ clusters which can be converted to $(NHEt_3)_4[Cd_{10}S_4(SPh)_{16}]$ by addition of PhSH and NEt$_3$ in MeCN.
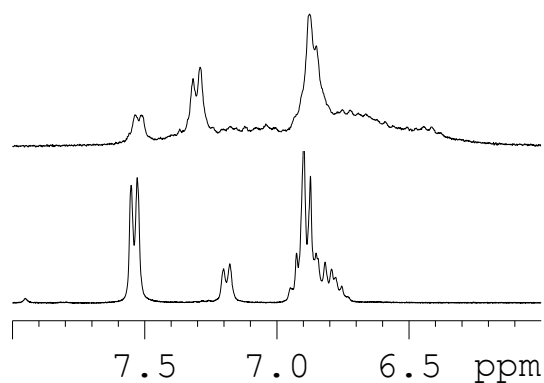
*Figure 4.21. ^{1}H NMR spectra of the reaction of **Cd10b** with NaSPh (top) and of the starting cluster **Cd10a** (bottom) in d_3-MeCN.*
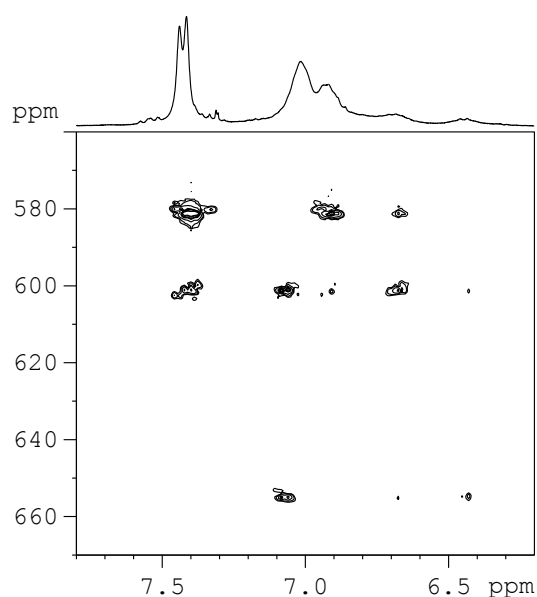
*Figure 4.22. ^{1}H-^{113}Cd NMR correlation spectrum of **Cd10b** in d_3-MeCN (40 mg/ml) after addition of four molar equivalents of PhSH and NEt$_3$ at room temperature.*
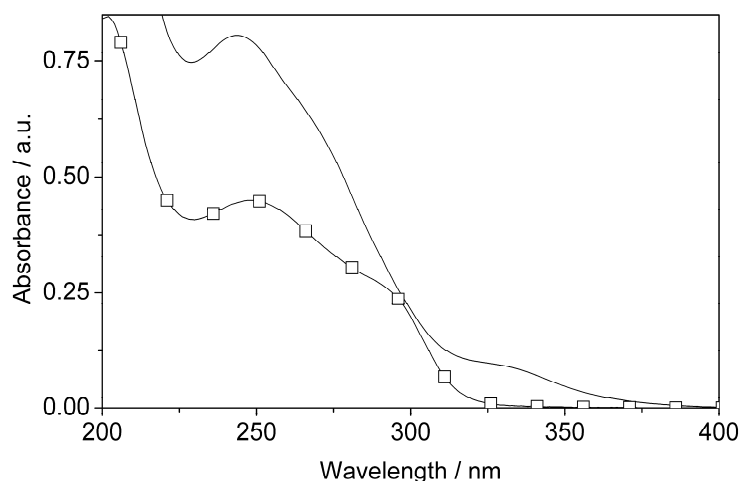
*Figure 4.23. UV-vis spectra of **Cd10b** (0.01 mg/ml) after addition of four equivalents of PhSH/NEt$_3$ (–) and of (NHEt$_3$)$_4$[Cd$_{10}$S$_4$(SPh)$_{16}$] (0.005 mg/ml, □) in MeCN.*

In summary, characterization of **Cd10b** in the solid state and in solutions of weakly coordinating solvents indicate that the solid obtained upon thermolysis of **Cd10a** is not pure Cd$_{10}$S$_4$(SPh)$_{12}$ (as in Equation 4.2). Bigger CdS clusters and/or NPs are also formed. However, presence of bigger clusters should result in a chemical composition different to the proposed Cd$_{10}$S$_4$(SPh)$_{12}$. On the other hand, the composition of a Cd32 cluster fits surprisingly well with Cd$_{10}$S$_4$(SPh)$_{12}$: Cd$_{32}$S$_{14}$(SPh)$_{36}$ = Cd$_{10}$S$_{4.375}$(SPh)$_{11.25}$. Therefore, a mixture of differently sized clusters and/or NPs can be present in **Cd10b** and would be in agreement with the proposed chemical composition of Cd$_{10}$S$_4$(SPh)$_{12}$.

The present conclusion is in contrast to the conclusion of Farneth *et al.*[54] The differences originate most probably from different data interpretation and additional investigation techniques.

To gain more insight into the transformation of the cluster(s), solutions of **Cd10b** in solvents with different coordination capability were investigated.

4.2.2 Characterization of "Cd$_{10}$S$_4$(SPh)$_{12}$" in Strongly Coordinating Solvents

In the following, **Cd10b** was investigated in strongly coordinating solvents like pyridine, DMSO, and DMF with solubility varying from up to 100 mg/ml, through 40 mg/ml to at least 3 mg/ml, respectively. It has to be expected that the structure of **Cd10b** will change after dissolution in these solvents.

Pyridine solutions. UV/Vis and DLS measurements showed that bigger particles than **Cd10a** were present in pyridine solution of **Cd10b**. According to DLS, particle radii were mainly between 0.55 and 4 nm (see Experimental Part, Figure 6.2, 100 mg/ml). In the UV/Vis spectra, only an indistinctive absorption edge at ca. 370 nm was observed (Figure 4.24). NMR investigation in d$_5$-pyridine revealed the presence of one PhS group [7.95 (d, 2H), 7.06 (t, 2H), 6.95 (t, 1H) ppm] which would be in good agreement with the supposed structure of

Cd10b ("$Cd_{10}S_4(SPh)_{12}$") having only one kind of bridging PhS ligands. A similar ^{1}H NMR spectrum had been obtained previously.[54] However, the [113]Cd resonances differed to the reported values. In this work, only one sharp signal at 443 ppm was obtained, whereas two signals at 647 and 440 ppm had been reported,[54] the second being very broad. Since the concentration of the sample was not reported, a comparison is not possible. The resonance at 443 ppm is much upfield shifted compared with ca. 600 and ca. 680 ppm of **Cd10a** (see Chapter 4.1 and Ref. 79) due to coordination of pyridine to Cd.[68] The reason for only one [113]Cd signal instead of two could be fast intramolecular exchange of the PhS ligands.
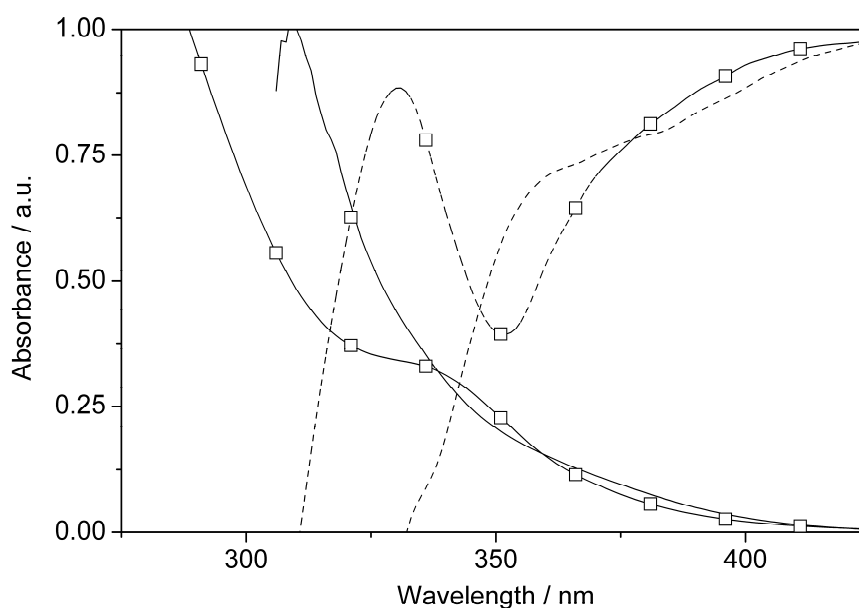
*Figure 4.24. Analysis of UV/Vis data of **Cd10b** in pyridine (0.1 mg/ml, –) and of Py-adduct of **Cd10b** in CH$_2$Cl$_2$ (0.01 mg/ml, □). Solid lines represent UV/Vis absorption curves, dashed lines are their 1st derivatives.*

In order to suppress the exchange in pyridine solution of **Cd10b**, the non-coordinated pyridine was evaporated from the solution and the residue ("Py-adduct of **Cd10b**", Py = pyridine) was dissolved in CH$_2$Cl$_2$. The UV/Vis spectrum directly after the preparation of the solution had an absorption edge at 351 nm and a shoulder at 331 nm (Figure 4.24). This can be due to the presence of Cd32 clusters (see above). Two sets of PhS groups and one [113]Cd signal at 615 ppm were observed in the NMR spectra in CD$_2$Cl$_2$. After two weeks at room temperature, one PhS group disappeared and many small crystals were formed, which were bright in polarized light. Two weeks later, cubic crystals were also present in the sample, which were dark in polarized light. None of them was suitable for SC-XRD probably due to solvent evaporation from their void spaces. After about one month, many bigger crystals, bright in polarized light, were obtained. A SC-XRD determination revealed that the crystals had the composition $[Cd_{17}S_4(SPh)_{26}Py]_\infty$ (**Cd17-Py**) where $Cd_{17}S_4(SPh)_{25}Py$ units are connected by bridging SPh groups. This crystallization sequence was repeated with concentrations 20–50 mg/ml of **Cd10b** in CH$_2$Cl$_2$ several times, but the first two crystalline

compounds could not be characterized by SC-XRD. Other crystalline clusters, $Cd_{54}S_{28}(SPh)_{52}(Py)_{7.5}$ (**Cd54-Py**) and $Cd_{54}S_{28}(SPh)_{52}(L)_x$ (L = DMF or Py, **Cd54-L**), were obtained directly from the pyridine solution of **Cd10b** by addition of toluene or DMF, respectively. Similarly, Herron *et al.*[64] obtained crystalline $Cd_{32}S_{14}(SPh)_{36}(DMF)_4$ by addition of DMF to the pyridine solution of **Cd10b**. However, none of the synthetic ways of cluster preparation from pyridine solutions is suitable for high yield and clean synthesis of CdS clusters (see Experimental Part). The crystal structures of **Cd17-Py**, **Cd54-Py**, and **Cd54-L** will be discussed later.

DMF and DMSO solutions. The UV/Vis spectra of **Cd10b** in DMF and DMSO showed that clusters bigger than **Cd10a** were present (Figure 4.25). Additionally, the spectra changed upon heating at 80 °C for 14 h. A pronounced maximum developed at 325 nm in DMF, and at 350 nm in DMSO. Beside this, the 1st derivative curves showed that more than one species was present in the solutions after heating. The DMF solution could contain Cd32 and Cd54 clusters, whereas the DMSO solution a Cd54 cluster and bigger NPs.
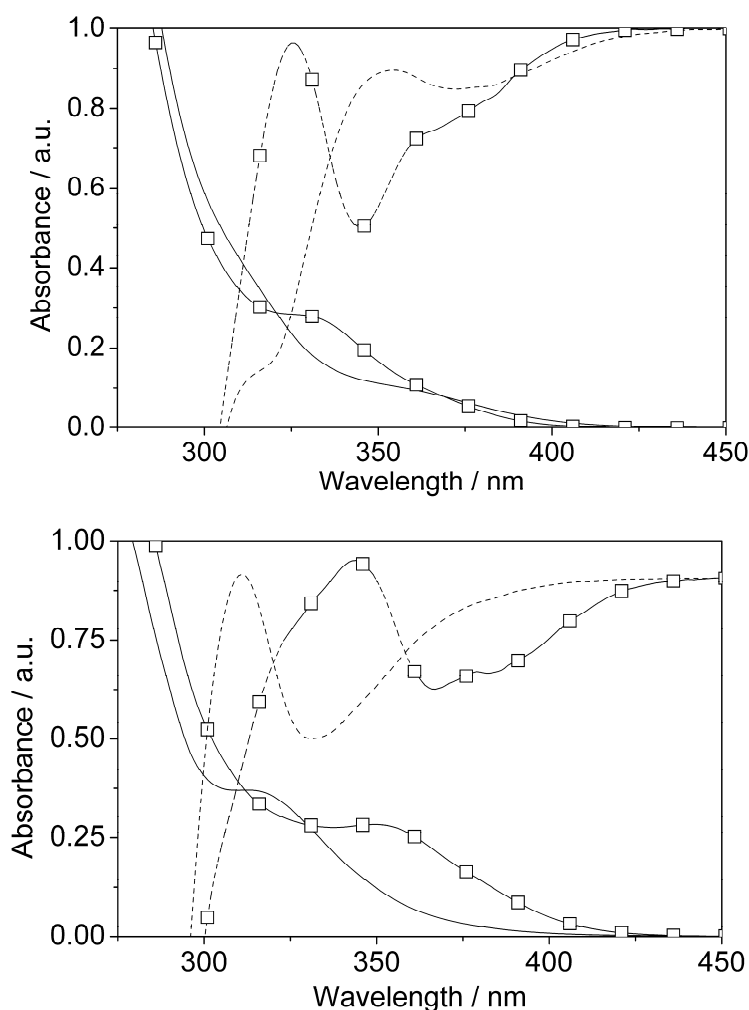
*Figure 4.25. UV/Vis spectra of **Cd10b** in DMF (up) and DMSO (down) before (–) and after (□) heating to 80 °C for 14 h (DMF: 0.04 and 0.03 mg/ml, DMSO: 0.07 and 0.1 mg/ml). Solid lines represent UV/Vis absorption curves, dashed lines are their 1st derivatives.*

NMR spectra of **Cd10b** in d_6-DMSO directly after dissolution were complex. In the ^{1}H-^{113}Cd HMBC correlation spectrum, intense ^{113}Cd resonances were found at 578, 589, 591 and 651 ppm and less intense at 576, 584, 586, 595, 599 and 602 ppm. After heating the solution to 80 °C for 4 h, the spectra simplified substantially as only three intense ^{113}Cd signals at 579, 599.5 and 652 ppm, one less intense at 621.5 ppm, and only four different PhS groups were observed. In the ^{1}H-^{113}Cd HMBC correlation (Figure 4.26), the first PhS group (T^{1}) [7.36 (d, 2H), 6.61 (t, 2H), 6.87 (m, 1H) ppm] correlated to the ^{113}Cd resonances at 579 and 599.5 ppm, the second (T^2) [6.97 (d, 2H), 6.30 (t, 2H), 6.61 (t, 1H) ppm] to those at 599.5 and 652 ppm and the third (T^3) [6.94 (d, 2H)] to that at 621.5 ppm. The fourth group (T^4) [7.25 (m, 2H), 6.90 (m, 2H), 6.83 (m, 1H) ppm] did not show any correlation. Detailed analysis of molecular symmetry and possible solution NMR behavior of a neutral Cd54 cluster (like **Cd54-Py**, **Cd54-L**, or **Cd54-DMF**)[a] indicated that T^1, T^2, and T^3 could originate from a Cd54 cluster formed during heating, which would be in line with the UV/Vis spectra. The observed ^{1}H-^{113}Cd correlations and intensities of ^{1}H and ^{113}Cd signals were also in good agreement with those supposed for a Cd54 cluster. The ^{113}Cd resonance at 579 ppm would then belong to a Cd site with a [Cd(SPh)$_3$L$_x$] environment, those at 599.5 and 621.5 ppm to a [CdS$_1$(SPh)$_3$] and that one at 652 ppm to a [CdS$_2$(SPh)$_2$] coordination. These resonances are slightly upfield shifted compared to ca. 600 ppm for a [Cd(SPh)$_4$] environment in **Cd10a** or [Cd(SPh)$_4$]$^{2-}$, ca. 680 ppm for [CdS$_2$(SPh)$_2$] in **Cd10a**, and ca. 725 ppm for a [CdS$_4$] environment (see Chapter 4.1 and Ref. 79, 16). The fourth observed PhS group (T^4), which did not show a ^{1}H-^{113}Cd HMBC correlation, could originate from byproducts formed during the heat treatment, similar to the byproducts formed in DMSO solutions of **Cd10a** (Chapter 4.1).

From solutions of **Cd10b** in DMF or DMSO, which were heated to 80 °C for 14 h, Cd$_{54}$S$_{28}$(SPh)$_{52}$(DMF)$_4$ (**Cd54-DMF**) and possibly Cd$_{54}$S$_{28}$(SPh)$_{52}$(DMSO)$_4$ (**Cd54-DMSO**) crystallized after addition of acetone or toluene, respectively. Crystals were only obtained when the solutions were heated. The structure of **Cd54-DMF** was determined by SC-XRD (see later), but crystals **Cd54-DMSO** were too small and were characterized only by UV/Vis absorption. Their absorption maximum in THF was at 359 nm (Figure 4.27), which is similar but slightly red-shifted compared to the maxima of other Cd54 clusters (Table 4.6). It suggests that **Cd54-DMSO** had also a Cd54 core although a bigger core cannot be excluded. The crystallization of these Cd54 clusters is in good agreement with the changes observed in

---

[a] For a neutral Cd$_{54}$S$_{28}$(SPh)$_{52}$L$_x$ cluster (**Cd54-Py, Cd54-L, or Cd54-DMF**) with an approximate T_d symmetry in solution, one would expect following NMR pattern. The cluster contains 7 nonequivalent Cd sites with coordination 2 x [CdS$_4$], 1 x [CdS$_3$(SPh)$_1$], 1 x [CdS$_2$(SPh)$_2$], 2 x [CdS$_1$(SPh)$_3$], and 1 x [Cd(SPh)$_3$L$_x$] in a 6:4:4:16:12:8:4 ratio. Only those would be visible in ^{1}H-^{113}Cd HMBC correlation, which are directly bonded to a PhS group and which have enough intensity depending on the number of Cd atoms and PhS ligands. Thus, at least the last four Cd sites should be observable, possibly also the [CdS$_3$(SPh)$_1$] site. Similarly, there are 4 chemically nonequivalent PhS groups: 3 x μ_2-PhS and 1 x μ_3-PhS in a 12:12:24:4 ratio. One μ_2-PhS (T^1) is bonded to the apical Cd atom, two others (T^2) are located on the edges between the tetrahedral corners and are probably chemically very similar and different to T^1.[79,80] T^1 would show ^{1}H-^{113}Cd HMBC correlation to [Cd(SPh)$_3$(DMSO)$_1$] and [CdS$_1$(SPh)$_3$], T^2 to [CdS$_1$(SPh)$_3$] and [CdS$_2$(SPh)$_2$] and μ_3-PhS (T^3) to [CdS$_1$(SPh)$_3$] and [CdS$_3$(SPh)$_1$]. The observed correlations are in good agreement, except the last one related to T^3, which is not observed probably due to low proportion of [CdS$_3$(SPh)$_1$] sites.

the UV/Vis and NMR spectra connected with heating the solutions. Thus, **Cd10b** grows in DMF and DMSO solutions, similarly as **Cd10a** (Chapter 4.1).
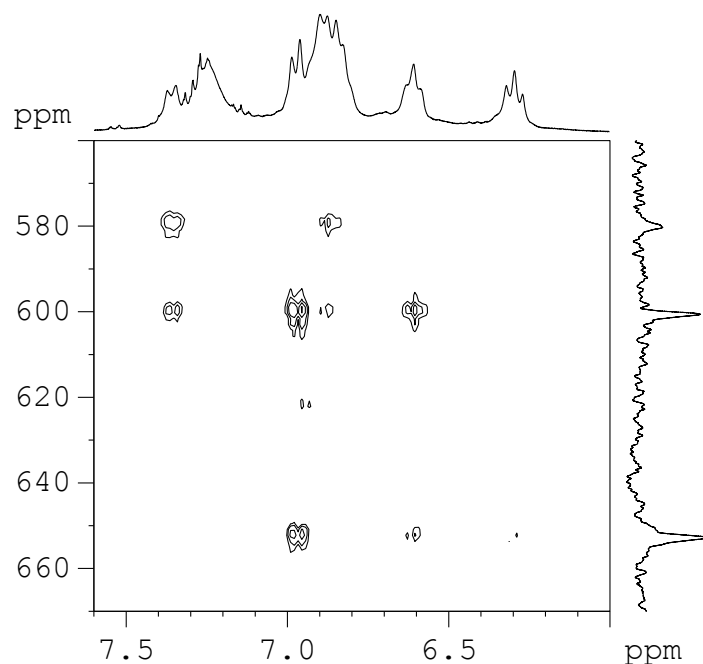
*Figure 4.26. ^1H-^{113}Cd HMBC correlation of **Cd10b** in d_6-DMSO after heating at 80 °C for 4 h.*

The synthesized $Cd_{54}S_{28}(SPh)_{52}L_x$ clusters **Cd54-Py**, **Cd54-L**, **Cd54-DMF**, and **Cd54-DMSO** were characterized in THF, DMF, or DMSO solution by UV/Vis absorption (Figure 4.27, Table 4.6). Their absorption maxima and edges were in the range 339–359 and 354–371 nm, respectively. The range of the absorption maxima is rather broad; this may be due to the different solvents. For example, the absorption maxima of molecular CdSe clusters with a Cd32 core also vary in the range 360–375 nm.[75,76,133,134] Thus, comparing the absorption maxima of the synthesized Cd54 clusters with CdS clusters of the same and smaller sizes (Table 4.6), their dependence on the cluster size is obvious. The fact that the spectra of **Cd54-Py** and **Cd54-DMF** are similar in weakly and strongly coordinating solvents (THF and DMF, DMSO) leads to the conclusion that its core structure determined in solid-state is temporarily preserved in the solutions. However, exchange of ligands by excess solvent molecules is very probable.

Table 4.6. Summary of UV/Vis absorption maxima and edges of single-sized CdS clusters.

Cluster size	Composition	Solvent	Abs. max. /edge / nm	Ref.
Cd17	$Cd_{17}S_4(SPh)_{26}(H_2NCSNH_2)_2$	THF	291	59
	$Cd_{17}S_4(SCH_2CH_2OH)_{26}$	H_2O, DMF, DMSO	ca. 290	63
Cd20	$[Cd_{20}S_{13}(SPh)_{22}]^{8-}$ *	DMF	351	135**
Cd32	$(PPh_4)_4[Cd_{32}S_{14}(SPh)_{40}]$	DMF	327	59
	$Cd_{32}S_{14}(SCH_2CH(OH)CH_3)_{36}(H_2O)_4$	DMF	ca. 325	66
	$Cd_{32}S_{14}(SPh)_{36}(DMF)_4$	THF	358	64**
Cd54	$(PPh_4)_4[Cd_{54}S_{32}(SPh)_{48}(H_2O)_4]$	DMF	353	59
	$Cd_{54}S_{28}(SPh)_{52}Py_{7.5}$	THF	351/371	**Cd54-Py**
		DMF	353/368	
		DMSO	346/361	
	$Cd_{54}S_{28}(SPh)_{52}L_x$	DMSO	ca. 350/370	**Cd54-L**
	$Cd_{54}S_{28}(SPh)_{52}DMF_4$	THF	345/366	**Cd54-DMF**
		DMF	339/354	
	$Cd_{54}S_{28}(SPh)_{52}DMSO_4$ *	THF	359/371	**Cd54-DMSO**

*   No crystal structure.

**   Does not match with size. It can be assumed that other clusters were responsible for UV/Vis absorption in both cases. For example, similar conditions as Herron *et al.*[64] used for crystallization of a Cd32 were used now for crystallization of a Cd54 cluster (**Cd54-L**).
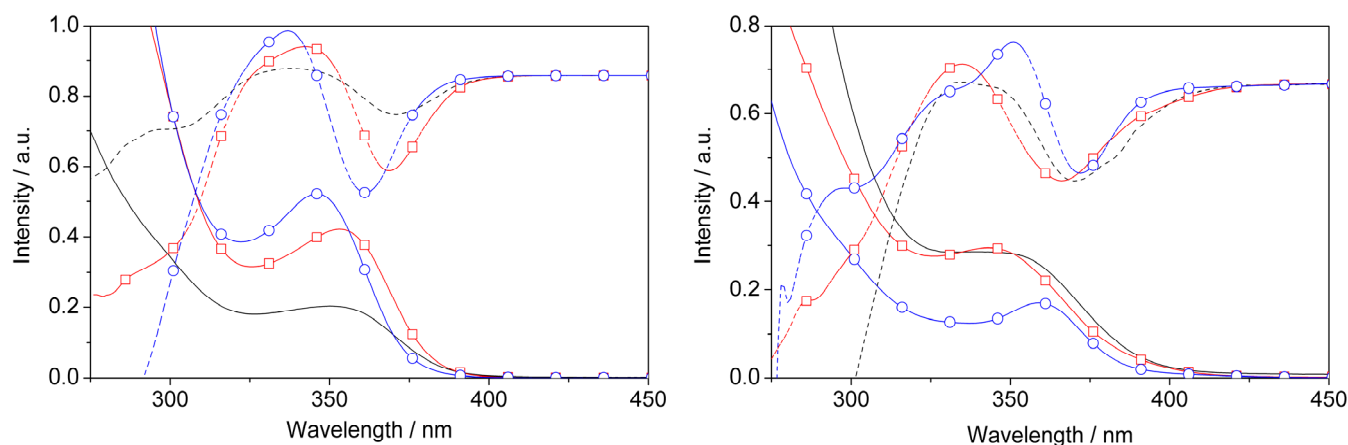
*Figure 4.27. UV/Vis spectra of **Cd54-Py** in THF, DMF and DMSO (0.03 (–), 0.05 (□) and 0.06 (○) mg/ml) (up) and of **Cd54-L** in DMSO (0.03 mg/ml (–)) and of **Cd54-DMF** and **Cd54-DMSO** in THF (0.03 (□) and 0.02 (○) mg/ml) (down). Solid lines represent UV/Vis spectra, dashed lines are their 1st derivatives.*

In conclusion, it was observed that the structure of **Cd10b** changes upon dissolution and/or heating in strongly coordinating solvents. In pyridine, Cd17 (**Cd17-Py**), Cd32[64] and Cd54 (**Cd54-Py**, **Cd54-L**) clusters can be obtained at room temperature after addition of different solvents. In DMF and DMSO, heating to 80 °C caused changes in the UV/Vis and

NMR spectra and allowed crystallization of Cd54 (**Cd54-DMF**, **Cd54-DMSO**) clusters by addition of other solvents. These observations allow the conclusion that the structure of **Cd10b** is changed in strongly coordinating solvents due to rearrangement processes, which had been investigated previously (Chapter 4.1).

4.2.3 Syntheses and Crystal Structures of Cd17 and Cd54 Clusters

The conditions by which the different molecular CdS clusters were obtained from **Cd10b** in this and other works are summarized in Table 4.7. The cluster $[Cd_{17}S_4(SPh)_{26}Py_1]_\infty$ (**Cd17-Py**) was prepared by dissolution of the Py-adduct of **Cd10b** in CH_2Cl_2 as the only one, of at least three different crystalline species, which could be characterized by SC-XRD. Addition of toluene to a concentrated pyridine solution of **Cd10b** resulted in cubic crystals of $Cd_{54}S_{28}(SPh)_{52}Py_{7.5}$ (**Cd54-Py**) which were formed within one month at room temperature. Similarly to the procedure of Herron *et al.*[64] for the synthesis of $Cd_{32}S_{14}(SPh)_{36}DMF_4$, crystals of $Cd_{54}S_{28}(SPh)_{52}L_x$ (L = pyridine/DMF, **Cd54-L**) were obtained from a concentrated pyridine solution of **Cd10b** after addition of DMF. Cubic crystals of other neutral Cd54 clusters crystallized from solutions of **Cd10b** in DMF or DMSO heated to 80 °C after addition of acetone (**Cd54-DMF**) or toluene (**Cd54-DMSO**). They were both the only solid species present. Crystals $Cd_{54}S_{28}(SPh)_{52}DMF_4$ (**Cd54-DMF**) were characterized by SC-XRD. However, the crystals of **Cd54-DMSO** were too small for SC-XRD analysis. According to UV/Vis measurements (Table 4.6) it is assumed that they had the same Cd54 core structure.

*Table 4.7. Summary of crystallization procedures starting from **Cd10b**.*

Preparation	Conc. mg/ml	Cluster	Ref.
Cd10b + 1:4 PhSH/Et$_3$N in MeCN	40	$(Et_3NH)_4[Cd_{10}S_4(SPh)_{16}]$	this work
Cd10b in pyridine, evaporation, dissolution in CH_2Cl_2	25	$[Cd_{17}S_4(SPh)_{26}Py]_\infty$	**Cd17-Py**
Cd10b in pyridine, add. of DMF	?	$Cd_{32}S_{14}(SPh)_{36}DMF_4$	64
Cd10b in pyridine, add. of DMF	100	$Cd_{54}S_{28}(SPh)_{52}L_x$	**Cd54-L**
Cd10b in pyridine, add. of toluene	100	$Cd_{54}S_{28}(SPh)_{52}Py_{7.5}$	**Cd54-Py**
Cd10b in DMF, heating to 80 °C, filtration, add. of acetone	6	$Cd_{54}S_{28}(SPh)_{52}DMF_4$	**Cd54-DMF**
Cd10b in DMSO, heating to 80 °C, add. of toluene	6	probably $Cd_{54}S_{28}(SPh)_{52}DMSO_4$	**Cd54-DMSO**

The cluster core of $[Cd_{17}S_4(SPh)_{26}(Py)]_\infty$ (**Cd17-Py**) (Figure 4.28) is the same as that of the anionic cluster $(NMe_4)_2[Cd_{17}S_4(SPh)_{28}]$ (**Cd17a**).[58] In the latter cluster, each corner of the Cd17 capped "super-tetrahedron"[45] is coordinated by terminal SPh groups which renders the cluster negatively charged. In the related neutral cluster $[Cd_{17}S_4(SCH_2CH_2OH)_{26}]_\infty$ (**Cd17b**), with two anionic SR ligands less, the same tetrahedral coordination of the corner Cd atoms is achieved by SR bridging.[63] In **Cd17b**, a 3D network is thus formed where each

Cd17 tetrahedron shares corners with four neighboring Cd17 tetrahedra through μ_2-SCH$_2$CH$_2$OH bridges. Similar 3D arrangements of clusters owing to bridging SPh groups was also found for other Cd17[61] and Cd32[136] clusters. The structure of **Cd17-Py** is in between. Since one apical Cd atom is coordinated by pyridine, only two SPh groups per cluster must be bridging to render all apical Cd atoms tetrahedrally coordinated (the forth corner Cd atom is coordinated by a terminal SPh group) and to render the whole network neutral. In this way, an uncharged 1D polymeric chain of connected clusters is formed. To the best knowledge, this is the first 1D chain of CdS clusters connected through SR bridges.
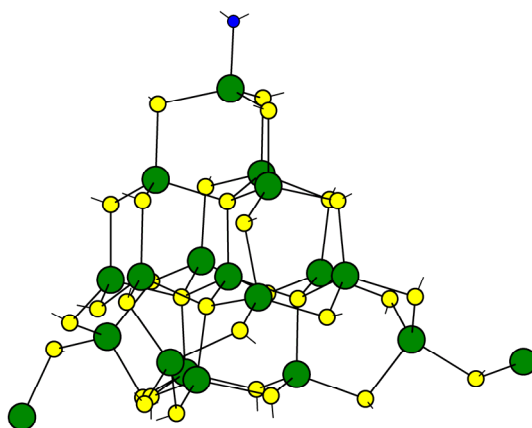
*Figure 4.28. Molecular structure of [Cd$_{17}$S$_4$(SPh)$_{26}$Py]$_\infty$ (**Cd17-Py**). The phenyl groups and pyridine rings (on top) were omitted for clarity.*

The clusters **Cd54-Py**, **Cd54-L**, and **Cd54-DMF** have the same tetrahedral Cd$_{54}$S$_{28}$(SPh)$_{52}$L$_x$ structure (Figure 4.29) with probably 7.5 pyridine ligands (**Cd54-Py**) (see below), x pyridine/DMF ligands (**Cd54-L**) and 4 DMF ligands (**Cd54-DMF**) in the apical positions. Their core structure is the same as that of anionic Cd54 clusters such as [Cd$_{54}$S$_{32}$(SPh)$_{48}$(H$_2$O)$_4$]$^{4-}$[59] which can be described as a hybrid between a cubic zinc blende-type core (16 adamantane CdS cages) and hexagonal wurtzite-type corners (4 barrelene CdS cages at each of the corners). To get a neutral cluster with the same core structure, four μ_3-bridging sulfide ions in the structure of [Cd$_{54}$S$_{32}$(SPh)$_{48}$L$_4$]$^{4-}$ must be replaced by μ_3-SPh groups, probably one on each face of the super-tetrahedral cluster core. As a matter of fact, residual electron density was found in all three structures which was assigned to phenyl rings attached to the μ_3-S atoms located at the faces of the Cd54 super-tetrahedron. However, the phenyl groups were disordered in a sense that each of the three μ_3-S atoms at each face of the tetrahedron can be substituted by a thiophenolate group. Each (μ_3-)phenyl group position was thus refined with 33 % occupancy and reasonable thermal parameters were obtained. μ_3-Coordination of thiolate ligands in CdS clusters or Cd complexes is unusual and was found in the CSD database only in six complexes. Examples are [Cd$_{10}$(SCH$_2$CH$_2$OH)$_{16}$]$^{4+}$[55] or Cd$_{10}$(SCH$_2$CH$_2$OH)$_{16}$Cl$_4$[137] with four μ_3-coordinating ligands.
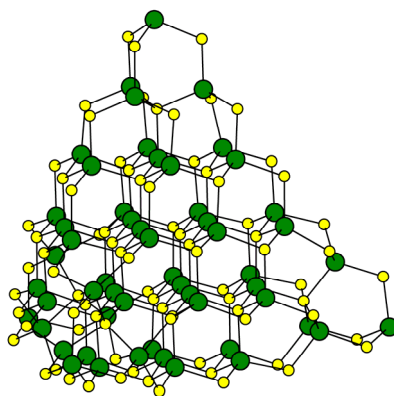
*Figure 4.29. Molecular structure of Cd$_{54}$S$_{28}$(SPh)$_{52}$L$_x$ (**Cd54-Py**: L = pyridine, **Cd54-L**: L = pyridine or DMF, **Cd54-DMF**: L = DMF). The phenyl groups and ligands L were omitted for clarity.*

The assignment of the ligands L in the structures was problematic. In **Cd54-L** and **Cd54-DMF**, the ligands could not be assigned unequivocally from the residual electron density. The situation was complicated by a 3-fold axis passing through the vertices and high cluster mobility resulting in relatively big thermal ellipsoids of the apical Cd atoms. Thus, only an oxygen atom was placed in tetrahedral position to each vertex Cd atom of the Cd54 tetrahedron, which could be refined satisfactorily.

In **Cd54-Py**, three pyridine positions were found at each vertex Cd atom (Figure 4.30). This renders these Cd atoms octahedrally coordinated. However, the occupancy of these pyridine sites could not be determined with sufficient accuracy. One of the pyridine positions at three of the four vertices overlapped with a pyridine position of neighboring Cd54 cluster. Therefore, the three non-overlapping pyridine rings were refined with 100% occupancy, all the others with 50% occupancy. This makes total of 7.5 pyridine ligands for one cluster. However, this number of pyridine ligands is only approximate and is probably overestimated. The average Cd–N distance in **Cd54-Py** is 263(3) pm. For comparison, the Cd–N distances in CdS clusters with pyridine ligands in tetrahedral Cd coordination are in the range 225–233 pm (**Cd17-Py**, Ref. 60, 65), which supports the octahedral coordination of the vertex Cd atoms in **Cd54-Py**.
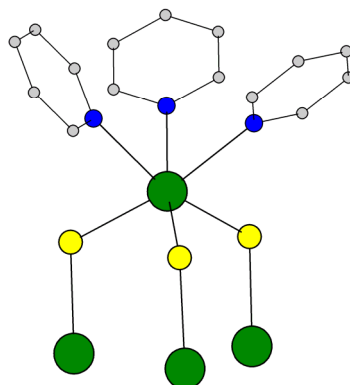
*Figure 4.30. Arrangement of three pyridine ligands on one vertex of the Cd54 tetrahedron in crystal structure of **Cd54-Py**.*

4.2.4 Conclusions

The structure of compound **Cd10b** formed by thermolysis of $[Cd_{10}S_4(SPh)_{16}]^{4-}$ (**Cd10a**), which should have composition of $Cd_{10}S_4(SPh)_{12}$ and was planned to be used for cluster functionalization, was investigated in solid state and various solvents. Analysis in solid state revealed that part of the cluster grew unspecifically during the heat treatment. Bigger CdS clusters and/or NPs were formed, as indicated by the solid state ^{113}Cd NMR spectra, UV/Vis and SAXS investigation and UV/Vis and DLS measurements in weakly coordinating solvents (MeCN, THF). On the other hand it was shown that part of **Cd10a** retained its Cd10 core structure since crystals of $(NHEt_3)_4[Cd_{10}S_4(SPh)_{16}]$ could be crystallized after addition of four equivalents of PhSH/NEt₃ to a suspension of **Cd10b** in MeCN. These conclusions are in disagreement with the investigation of Farneth *et al.*[54] claiming that **Cd10b** is a neutral $Cd_{10}S_4(SPh)_{12}$ cluster that tends to aggregate to different degrees in the solid state and in solution. This difference should not be caused by modification of the thermal treatment of **Cd10a**, instead, different data interpretation might be the reason.

Additional information was obtained in strongly coordinating solvents (pyridine, DMF, DMSO). From pyridine solutions of **Cd10b**, clusters with Cd17 (**Cd17-Py**) and Cd54 (**Cd54-Py**, **Cd54-L**) cores crystallized by addition of other solvents. DMF and DMSO solutions showed appreciable changes in the UV/Vis and NMR spectra when heated to 80 °C. Neutral Cd54 clusters (**Cd54-DMF**, **Cd54-DMSO**) crystallized from these solutions. These structural changes of **Cd10b** can be attributed to rearrangement processes in strongly coordinating solvents, as already observed for the **Cd10a** cluster in DMSO and DMF (Chapter 4.1).

The obtained Cd54 clusters (**Cd54-Py**, **Cd54-L**, **Cd54-DMF**) are unusual because they are not charged owing to μ_3-PhS groups. Such a μ_3-coordination could be a way how bigger clusters could be stabilized by decreasing their overall charge (Table 2.1). Syntheses of **Cd54-DMF** and **Cd54-DMSO** are relatively easy and no other solid by-product was obtained. This renders them suitable for applications which require use of neutral CdS clusters.

However, it should be clear now that the compound **Cd10b** does not have the desired structure of a tetrahedral cluster with 4 free Cd coordination sites and thus cannot be used for preparation of functional CdS clusters.

5 Part II: Functional CdS Clusters

In the second part of the thesis, functional CdS clusters were investigated in a similar way as non-functional clusters in the first part. Functional CdS clusters represent surface modified clusters capable of a further reaction or, in a special case, of a polymerization reaction. Thus, clusters containing dangling –OH, –NH$_2$, –COOH groups or unsaturated bonds on the surface are suitable candidates. Different known clusters containing such groups were summarized in Chapter 2.2. Clusters with –OH and –NH$_2$ groups should be able of further reactions, which will be examined in following chapters. Carboxy groups are not suitable for this purpose, since they coordinate to Cd which would lead to cluster agglomeration/aggregation.[113] Additionally, preliminary results on radical polymerization in the presence of a model CdS cluster are summarized in this part of the thesis.

For the synthesis of functional clusters, two methods were used: in-situ functionalization and post-synthesis modification by exchange reactions (see Chapter 2.2, Scheme 2.3).

5.1 CdS Clusters Functionalized by Hydroxy Groups

Different clusters stabilized by thiolates containing –OH groups are known and structurally characterized. They have been summarized in Chapter 2.2.2 (see also Table 2.2). The most important are [Cd$_{10}$(SCH$_2$CH$_2$OH)$_{16}$]$^{4+}$ (**Cd10c**),[55,56,57] [Cd$_{17}$S$_4$(SCH$_2$CH$_2$OH)$_{26}$]$_\infty$ (**Cd17b**),[63] and Cd$_{32}$S$_{14}$(SCH$_2$CH(OH)CH$_3$)$_{36}$(H$_2$O)$_4$[66] clusters. All of them are synthesized by in-situ functionalization, *i.e.* by cluster synthesis directly in the presence of the functional stabilizing ligand. **Cd10c** was used as the model cluster (Figure 5.1), because it can be readily synthesized with high yields and with a variety of counter-anions (see later). In contrast, syntheses of **Cd17b** and the Cd32 cluster are not that straightforward.[63,66] Strictly speaking, **Cd10c** is not a CdS cluster, since it does not contain sulfidic bridges, only coordinated ligand. Thus, it should be denoted rather as a polynuclear Cd complex.[80] In spite of that it will be called CdS cluster in the following.
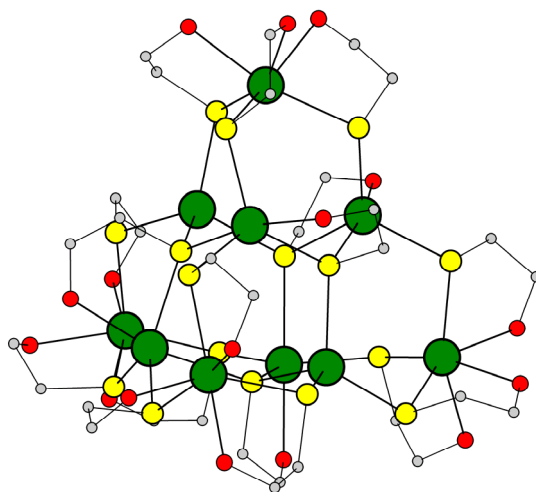
*Figure 5.1. Molecular structure of the cationic cluster [Cd$_{10}$(SCH$_2$CH$_2$OH)$_{16}$]$^{4+}$ (**Cd10c**), according to the crystal structure of **Cd10c-BF$_4$·6H$_2$O** (see later).*

Cd10c clusters have previously been synthesized and crystallographically characterized with different counter-anions: SO_4^{2-}, ClO_4^-.[55,57] The perchlorate has been investigated also by means of solution[68] and solid-state[114,57] NMR, UV/Vis absorption[68] and Raman spectroscopy.[68] Water and DMF solutions were used.

5.1.1   Syntheses and Crystal Structures

Cd10c clusters with nitrate, perchlorate, and tetrafluoroborate counter-anions were synthesized by a modification of the method of Schwarzenbach *et al.*[56] $HSCH_2CH_2OH$ (or its aqueous solution) was added to an aqueous solution of $Cd(acetate)_2$, followed by addition of an aqueous solution of a salt containing the corresponding counter-anion. Heating to 60 °C and/or addition of more water was sometimes applied in order to dissolve the formed white precipitate. Then, after standing at room temperature or 4 °C, colorless crystals of the product crystallized. They were usually recrystallized from hot water solution in order to remove residual acetate. In this way, crystal structures of NO_3^- and BF_4^- salts were obtained (preparative details can be found in the Experimental Part):

$[Cd_{10}(SCH_2CH_2OH)_{16}](NO_3)_4 \cdot 2H_2O$ (**Cd10c-NO$_3$·2H$_2$O**),

$[Cd_{10}(SCH_2CH_2OH)_{16}](BF_4)_4 \cdot H_2O$ (**Cd10c-BF$_4$·H$_2$O**),

$[Cd_{10}(SCH_2CH_2OH)_{16}](BF_4)_4 \cdot 6H_2O$ (**Cd10c-BF$_4$·6H$_2$O**).
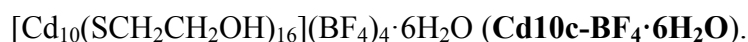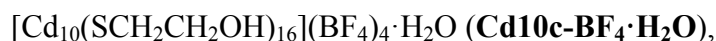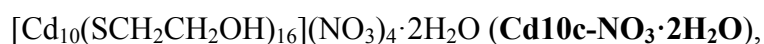
All of them crystallized in the monoclinic space group *C*2/*c*. Corresponding crystallographic details can be found in Chapter 6.4 and Table 6.6. The structure of the cationic complex $[Cd_{10}(SCH_2CH_2OH)_{16}]^{4+}$ was principally identical with the one described in Ref. 57 (ClO_4^- as anion), with a C_2 axis passing through two Cd atoms situated on opposite edges of the cluster tetrahedron. The cluster is comprised of three chemically inequivalent Cd sites, 4 x CdS_3O_3, 4 x CdS_4O, and 2 x CdS_4 (through which the C_2 axis passes), and three chemically inequivalent $-SCH_2CH_2OH$ ligands, 8 x $\mu_2-SCH_2CH_2OH$ (bridging the CdS_4O and CdS_3O_3 sites), 4 x $\mu_2-SCH_2CH_2OH$ (bridging the CdS_4 and CdS_3O_3 sites), and 4 x $\mu_3-SCH_2CH_2OH$ (bridging the CdS_4 and two CdS_4O sites).

All three structures show a relatively high proportion of disordered ligands, which could be conveniently handled by low-temperature measurement in the case of **Cd10c-BF$_4$·6H$_2$O**. Beside this, positions of almost all OH- and H_2O-hydrogen atoms were easily found in residual electron density map and refined in **Cd10c-BF$_4$·6H$_2$O**. Thus, a very nice novel picture of hydrogen bond network around a **Cd10c** cluster was obtained, with distances d_{O-O} = 2.753(4)–2.914(5) Å, d_{O-F} = 2.681(4)–3.003(4) Å, each proton having a suitable acceptor (Figure 5.2, left).

Another crystal modification of **Cd10c-BF$_4$**, $[Cd_{10}(SCH_2CH_2OH)_{16}](BF_4)_4 \cdot 2DMSO$ (**Cd10c-BF$_4$·2DMSO**), was obtained after dissolution of **Cd10c-BF$_4$** in DMSO and recrystallization by addition of excess *n*BuOH. The structure of the cationic complex is again principally identical. Interesting is here the hydrogen bond network created from ligand –OH groups (all protons were found in the residual electron density map) to BF_4^- and DMSO. Besides one proton at an apical –OH group, with a relatively long hydrogen bond to BF_4^-

(3.310(3) Å), all protons have a suitable acceptor (d_{O-O} = 2.62(2)–2.88(3) Å, d_{O-F} = 2.718(3)–2.902(3) Å) (Figure 5.2, right).
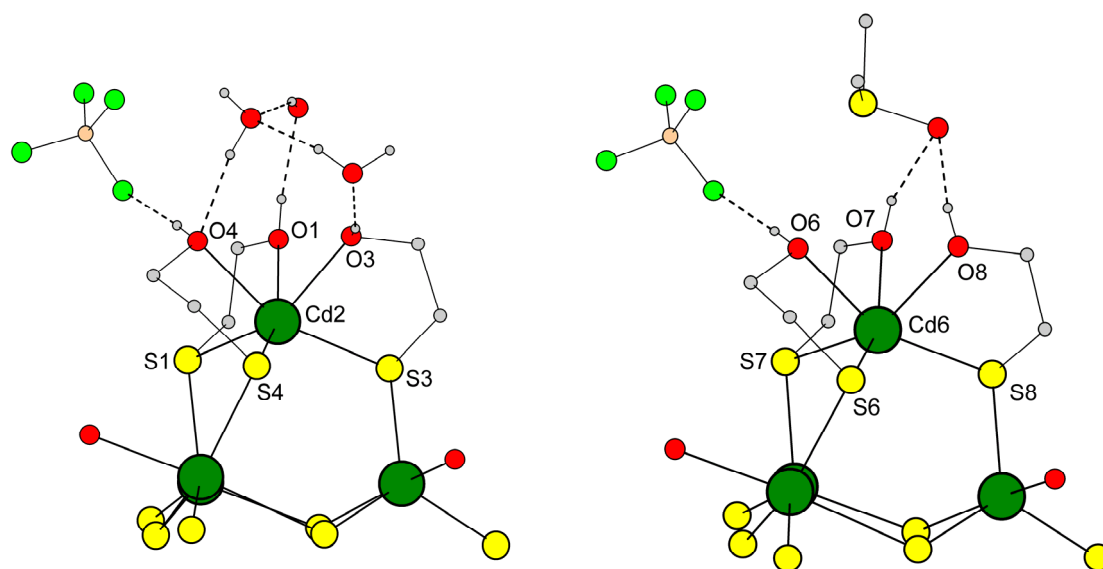
*Figure 5.2. Hydrogen bond network formed around the apical CdS_3O_3 sites in **Cd10c**. Left: **Cd10c-BF$_4$·6H$_2$O**, right: **Cd10c-BF$_4$·2DMSO**.*

All crystal structures have channels, parallel to the *b*-axis, which are filled with nitrate, water, or DMSO molecules but not with tetrafluoroborate. Another point which should be pointed out is that the anion species do not coordinate to Cd directly, but through a hydrogen bond network. This is also the case for **Cd10c-ClO$_4$·8H$_2$O**.[57]

Crystals of **Cd10c-NO$_3$·2H$_2$O** were dried for different time periods in vacuum and were characterized also by powder XRD which was in good agreement with the powder pattern calculated from the single-crystal data (see Experimental Part, Figure 6.6). However, the solid-state [113]Cd NMR spectrum of **Cd10c-NO$_3$·2H$_2$O** (Figure 5.3) did not reveal a pattern similar to previous solid-state NMR investigation, which correlated well with single-crystal structures for different **Cd10c** clusters:[114,57] As already mentioned, the cationic core of **Cd10c** clusters consists of four distorted octahedral CdS_3O_3 sites (apical positions), four distorted trigonal-bipyramidal CdS_4O sites, and two distorted tetrahedral CdS_4 sites (Figure 5.1). However, crystallographically, two different Cd positions are present for each site. Thus, six crystallographically different Cd sites have to be expected in solid samples. Indeed, solid-state [113]Cd NMR spectra for **Cd10c-ClO$_4$·8H$_2$O** and **Cd10c-SO$_4$·4H$_2$O** showed six signals each (Table 5.1).[57] After dehydrating of the samples, the "doubled" resonances coalesced and only three signals were observed for **Cd10c-ClO$_4$**. This was not the case for **Cd10c-SO$_4$**. The reason for the coalescence could be the almost S_4 symmetry of the **Cd10c** cation for the perchlorate but not for the sulfate salt after removal of water molecules, which resulted in both Cd sites of each kind to become equivalent for **Cd10c-ClO$_4$**.[57] For **Cd10c-NO$_3$·2H$_2$O**, no sharp resonances were observed in the [113]Cd NMR spectrum (Figure 5.3). Nevertheless, the [113]Cd chemical shift ranges fit relatively well with the shifts observed for different Cd sites in **Cd10c** clusters (signals at around 290 and 525 ppm are spinning

satelites). The origin of this discrepancy is not known, since the powder XRD diffractograms were in good agreement with the crystal structure.
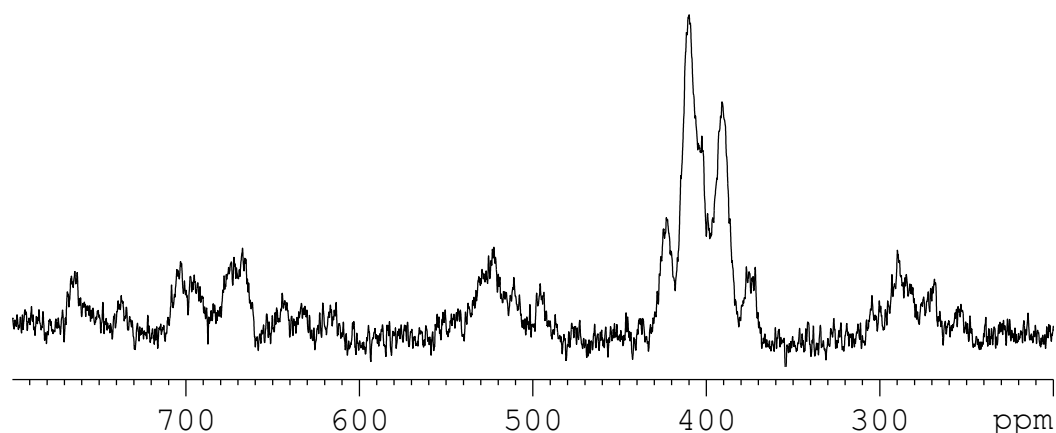
*Figure 5.3. Solid-state ^{113}Cd NMR spectrum (CP-MAS at 8 kHz) of **Cd10c-NO$_3$·2H$_2$O**.*

*Table 5.1. Solid-state ^{113}Cd NMR shift data of diverse **Cd10c** clusters, from Ref. 57.*

Compound	resonance		
	CdS$_3$O$_3$	CdS$_4$O	CdS$_4$
Cd10c-ClO$_4$·8H$_2$O	420	513	667
	426	520	684
Cd10c-ClO$_4$ [a]	417	509	690
Cd10c-SO$_4$·4H$_2$O	408	498	640
	418	524	722
Cd10c-SO$_4$ [a]			642
	409	505	674
		521	703

[a] Dried at 80 °C.

5.1.2   The [Cd$_{10}$(SCH$_2$CH$_2$OH)$_{16}$]$^{4+}$ Cluster in Solution

The molecular structure of **Cd10c** clusters in solution, which should adopt the S_4 symmetry in solution compared with the C_2 symmetry in solid state, was investigated previously in H$_2$O and DMF solutions.[68] It has been shown that the molecular structure in solution is in good agreement with the crystal structure, and that some temperature dependent exchange processes take place:[68]

– ^{113}Cd NMR spectra are reversible below 70 °C in D$_2$O and d$_7$-DMF.

– In both D$_2$O and d$_7$-DMF, two ^{113}Cd signals with intensity ratio 3:2 are obtained (at −20 to +20 °C in DMF and at 0–20 °C in water). The signal at ca. 535 ppm belongs to the mixed CdS$_4$O/CdS$_4$ site, the one at ca. 400 ppm to CdS$_3$O$_3$.

– Temperature dependent ^{113}Cd NMR measurements in d$_7$-DMF revealed that CdS$_4$O and CdS$_4$ sites exchange with each other which leads to splitting of the resonance at

ca. 535 ppm below ca. −10 °C. The resonance at ca. 400 ppm shifted downfield with increasing temperature. Since coordination of oxo-ligands to Cd causes upfield shift of [113]Cd resonances, both changes support an equilibrium process related to the decoordination of ligand −OH groups which is shifted to the right side with increasing temperature:

$$(RS)_3Cd\overset{S}{\underset{\underset{H}{O}}{\diagdown}} \quad \rightleftharpoons \quad (RS)_3Cd\overset{S}{\diagdown}\diagdown_{OH} \tag{5.1}$$
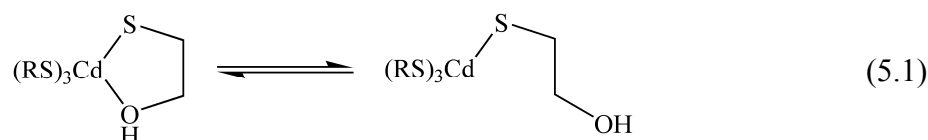
– Consistent with these exchange processes are temperature dependent ^{1}H NMR spectra of the hydroxyl protons in d$_7$-DMF: from −27 to +39 °C two signals with ratio 3:1 are observed (the 8 and 4 different μ_2–SCH$_2$CH$_2$OH are equivalent in solution due to averaging of CdS$_4$O and CdS$_4$ sites, thus 12 μ_2–SCH$_2$CH$_2$OH and 4 μ_3–SCH$_2$CH$_2$OH ligands are present). The more intense signal shifts from 5.98 to 5.57 ppm, the less intense from 6.82 to 6.44 ppm, which is toward the more shielded values of the free ligand itself.

Salts of the **Cd10c** cluster were characterized by different NMR techniques in D$_2$O, d$_6$-DMSO, and d$_7$-DMF at room temperature. The results are summarized in Table 5.2 and Figure 5.4. It was supposed that nitrate would coordinate to Cd more strongly than perchlorate (see Experimental Part, Chapter 6.2.1), which could influence the solution behavior. Thus, also **Cd10c** with a non-coordinating anion (tetrafluoroborate) was prepared. However, no substantial differences were observed between the NMR spectra of different **Cd10c** salts. Beside this, solubility of **Cd10c-NO$_3$** was low in water, DMSO, and DMF, which advantaged both **Cd10c-ClO$_4$** and **Cd10c-BF$_4$** and allowed preparation of solutions concentrated enough for obtaining [113]Cd NMR spectra. **Cd10c** clusters were not soluble in MeCN.

Measurements in D$_2$O and d$_7$-DMF were in good agreement with the results of Haberkorn *et al.*[68] In D$_2$O, two sets of broad ligand signals were observed at concentrations 3.1×10^{-3} and 3.4×10^{-2} M with intensity 1:3 (μ_3– and μ_2–SCH$_2$CH$_2$OH, Figure 5.4), whereas the OH proton resonances coincided with solvent residual peak. At higher concentration, the –CH$_2$– resonances were downfield shifted by ca. 0.1 ppm which might correlate with the deshielding effect of Cd and rate of decoordination (Equation 5.1).[68] [113]Cd NMR at higher concentration showed two resonances at 546 and 417 ppm with an intensity ratio of 3:1.2 (Figure 5.5 left, projection), which are somewhat downfield shifted compared with Ref. 68 and do not fit with theoretical 3:2 for CdS$_4$O+CdS$_4$:CdS$_3$O$_3$ sites. A nice pattern in ^{1}H-[113]Cd HMBC correlation was also obtained (Figure 5.5 left); however, correlation signals are missing for the resonance at 417 ppm (compare with the corresponding spectrum in d$_7$-DMF, Figure 5.5 right). This can correlate with higher extent of OH group decoordination (Equation 5.1) in H$_2$O than in DMF, which is supported by the downfield shift of the resonance at 417 ppm compared with 403 ppm in d$_7$-DMF (see later).[68]

In d$_7$-DMF, the NMR behavior corresponded very well with that described in Ref. 68: two sets of ligand ^{1}H resonances (both –CH$_2$–CH$_2$– chains and –OH groups, intensity ratio 1:3

[^{1}H: 7.43 (br, 1 H), 3.96 (br, 2 H), 3.23 (br, 2 H) ppm, ^{13}C: 61.4, 32.8 ppm] and [^{1}H: 6.60 (br, 1 H), 3.80 (br, 2 H), 2.96 (br, 2 H) ppm, ^{13}C: 62.4, 29.8 ppm]) and two ^{113}Cd resonances (at 545 and 403 ppm corresponding to CdS$_4$O+CdS$_4$ and CdS$_3$O$_3$ sites respectively, intensity ratio 3:2) (Table 5.2, Figure 5.4). However, the ^{1}H resonances of the –OH groups were substantially downfield shifted compared with Ref. 68, *i.e.* 6.60 and 7.43 ppm for the more and less intense ligand, respectively. This difference could be due to different solution concentration (0.067 vs. 0.2 M) and thus different coordination strength of the –OH groups to Cd. Additionally, a ^{1}H-^{113}Cd HMBC correlation spectrum was obtained, which corresponds very well with the crystal structure and with the proposed coordination-decoordination behavior of the ligand –OH groups (Equation 5.1[68]). Thus, from the more intense ligand, correlation is observed between CH$_2$S and ^{113}Cd resonance at 403 and 545 ppm (both over 3 bonds) and between CH$_2$O and 545 ppm (over 4 bonds), whereas correlation to 403 ppm (over 3 or 4 bonds) is missing. From the less intense ligand, only correlations over 3 and/or 4 bonds to the CdS$_4$O+CdS$_4$ site at 545 ppm are present, which is in good agreement with the crystal structure. The –OH group of the less intense ligand does coordinate and decoordinate fast from the CdS$_4$O site to the CdS$_4$ site, which leads to the presence of only one signal for a mixed CdS$_4$O/CdS$_4$ site. This is supported by comparison of the ^{113}Cd NMR shift of this site with the solid-state ^{113}Cd NMR spectra or with equivalent CdS$_4$ sites in the **Cd10a** cluster at ca. 600 ppm (Chapter 4.1), since oxygen coordination leads to upfield shift of ^{113}Cd resonances.[68] Beside this, the ^{1}H-^{1}H EXSY spectrum revealed that the two different ligands (μ_3– and μ_2–SCH$_2$CH$_2$OH) exchange between each other on the NMR time scale. Such an exchange would not be that easy to explain as an intramolecular exchange in the **Cd10a** cluster (Scheme 2.2), because it would require disruption of much more bonds. This means that the cluster is relatively labile in solution but in average retains its molecular structure.

*Table 5.2. Summary of NMR measurements of **Cd10c** in different solvents.*

Solvent	Conc. / M	Nr. of –CH$_2$–CH$_2$– chains	Nr. of -OH	^{113}Cd shift / ppm	^{1}H-^{113}Cd correlation
D$_2$O	3.1×10^{-3}	2 (1:3)	1	not measured	not measured
	3.4×10^{-2}	2 (1:3)	1	546, 417 (3:1.2)	to 546 ppm
d$_7$-DMF	6.7×10^{-2}	2 (1:3)	2 (1:3)	545, 403 (3:2.0)	to 545, 403 ppm
d$_6$-DMSO	2.4×10^{-3}	1	1	not found	not found
	6.3×10^{-2}	2 (1:6.5)	3 (1:3.5:4.5)	not found	not found
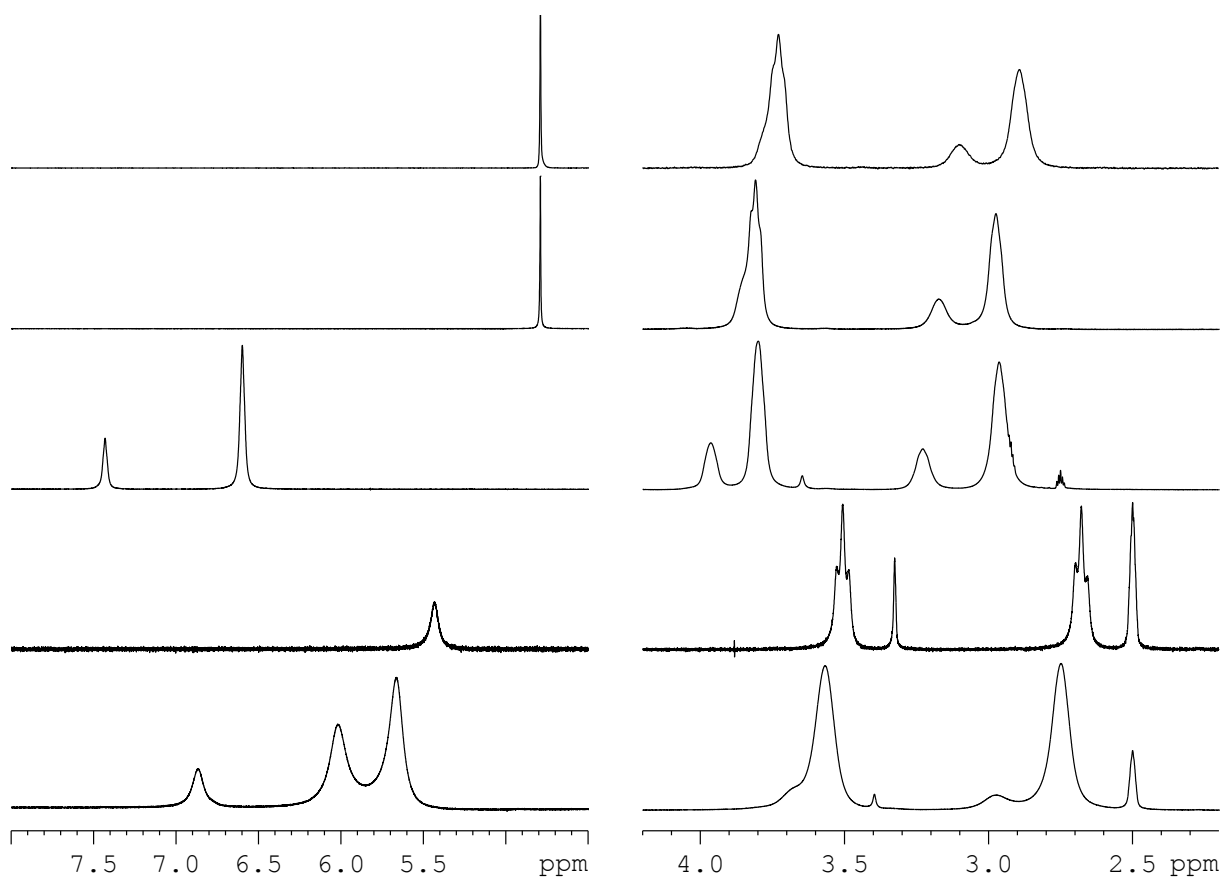
Figure 5.4. ^{1}*H NMR spectra of* **Cd10c** *in different solvents. Down from top: 3.1×10^{-3} and 3.4×10^{-2} M in D_2O, 6.7×10^{-2} M in d_7-DMF, 2.4×10^{-3} and 6.3×10^{-2} M in d_6-DMSO.*
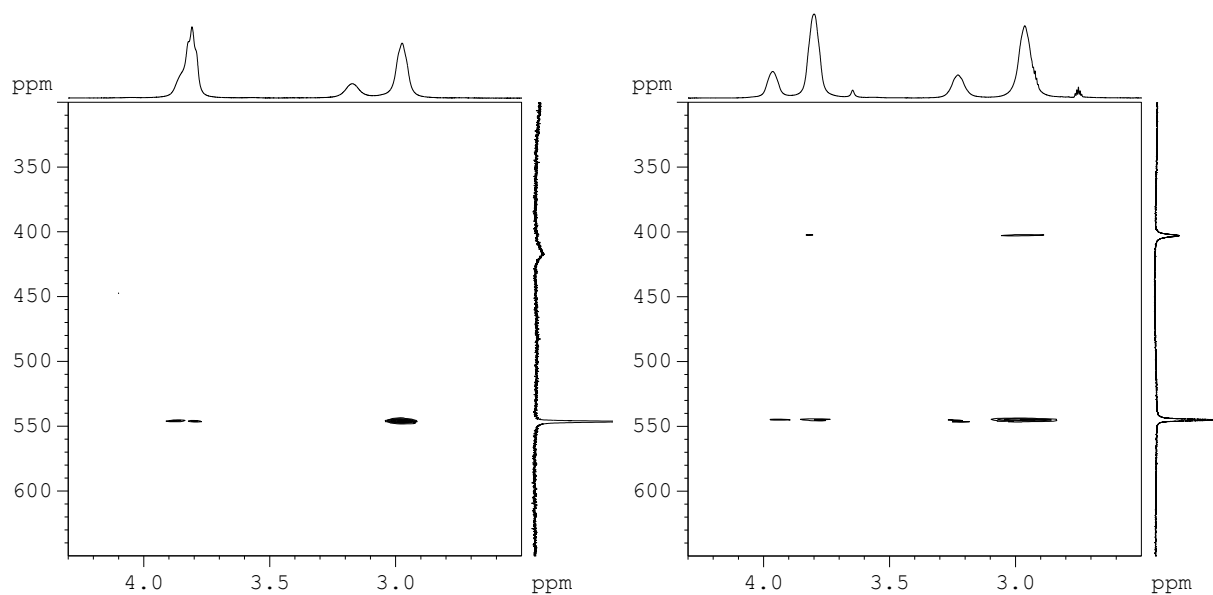
Figure 5.5. ^{1}*H-*^{113}*Cd HMBC spectra of* **Cd10c** *in D_2O (left) and d_7-DMF (right). Corresponding ^{1}H and ^{113}Cd NMR spectra are shown in projections.*

It was supposed that solution behavior of **Cd10c** in DMSO should not differ much to those in water and DMF. However, this was not the case. At low concentration (Table 5.2,

Figure 5.4), only one set of ligand signals was present instead of two [^{1}H: 5.43 (br, 1 H), 3.51 (t, 2 H), 2.68 (t, 2 H) ppm, ^{13}C: 63.2, 29.2 ppm]. No signals in the ^{1}H-^{113}Cd HMBC correlation spectrum were obtained, probably due to low solution concentration. At higher concentration, at least three different sets of ligands signals were present in the ^{1}H NMR spectrum, which were in ratios ca. 1:3.5:4.5 and 1:6.5 according to the –OH and –CH$_2$–S– groups, respectively (^{1}H shifts for OH: 6.87, 6.02, 5.67 ppm, for CH$_2$O: 3.67, 3.56 ppm, for CH$_2$S: 2.94, 2.74 ppm). However, the HSQC spectrum revealed four different sets of ligand signals (^{13}C shifts for CH$_2$O: 60.6, 62.0, 62.8 ppm, for CH$_2$S: 29.4, 32.0 ppm). EXSY spectrum showed that all three –OH groups exchange with each other on the NMR time scale. Despite of relatively high sample concentration, no signals in ^{1}H-^{113}Cd HMBC correlation spectrum were obtained. This might be due to higher exchange rates of different parts of the cluster in solution compared with the DMF solution. In any case, it can be concluded from these NMR measurements that **Cd10c** is not stable in DMSO, that its molecular structure does not fit with the crystal structure and that some other cluster species are present in the solution.

The difference in the solution behavior of **Cd10c** in DMF and DMSO could be explained by similar solvent coordination effect, as observed in the case of **Cd10a** (Chapter 4.1). Therefore, long-time measurements at room temperature were performed in both solvents. However, no changes were observed in the ^{1}H NMR spectra of **Cd10c** in d$_7$-DMF and d$_6$-DMSO (2 months and 3 weeks, respectively), which rather excludes the solvent coordination effect.

What is then the origin of these differences? It is believed that the reason lies in the relationship between the two solvents and their ability to accept hydrogen bonds. DMSO is known to be a stronger hydrogen bond acceptor (HBA) than DMF (both of them have almost highest HBA basicities among organic solvents: 0.710 or 0.69 for DMF and 0.752 or 0.76 for DMSO, Ref. 138 and 139, respectively). Thus DMSO breaks hydrogen bonds in solution more effectively than DMF. Since the cluster is stabilized by hydrogen bonds mainly at the apical Cd positions (see Figure 5.2, left), it is supposed that the cluster is disintegrated in DMSO due to breakage of the hydrogen bond network around the cluster. It seems that the following two facts could stand contradict this theory:

– It was possible to crystallize **Cd10c-BF$_4$·2DMSO** from a 6.7×10^{-2} M DMSO solution of **Cd10c** by adding an excess of *n*BuOH. The crystal structure of the cluster cation is the same as for other **Cd10c** clusters. Beside this, a rich hydrogen bond network from ligand –OH groups to BF$_4^-$ and DMSO was formed (see Figure 5.2, right). However, the crystals were crystallized not from pure DMSO but a mixture with *n*BuOH. *n*BuOH is a good HBA but also a good proton donor (HBA basicity of ca. 0.88 and hydrogen bond donor acidity of 0.79)[139] and thus "blocks" the HBA property of DMSO and itself. Thus the molecular structure of **Cd10c** in DMSO/*n*BuOH solution can differ to that in pure DMSO.

– Dance *et al.*[137] crystallized Cd$_{10}$(SCH$_2$CH$_2$OH)$_{16}$Cl$_4$ by reaction of **Cd10c-ClO$_4$** with Cl$^-$ in DMF. In the crystal structure, the cluster stabilizing hydrogen bond network around the apical Cd sites is broken by Cl coordination, and the non-coordinating –OH groups bind by hydrogen bonds to the neighboring clusters. This could mean that the hydrogen bond network around the apical Cd sites is not necessary for cluster stability. However, it was

not shown that the $Cd_{10}(SCH_2CH_2OH)_{16}Cl_4$ cluster possesses the same molecular structure in solution.[137] Thus, it might be stabilized via hydrogen bond network between neighboring clusters in solid state, but not necessarily in solution.

These facts render the theory about cluster instability in DMSO due to hydrogen bond breakage probable. The difference in HBA basicities of DMF and DMSO is in fact relatively small, but probably high enough to cause the observed differences in the solution behavior of **Cd10c**.

It can be summarized that the molecular structure of **Cd10c** clusters in water and DMF corresponds well with the crystal structure. However, the clusters behave dynamically in solution: the ligand –OH groups coordinate to and decoordinate from both Cd sites (CdS_4O+CdS_4 and CdS_3O_3, Equation 5.1) with a certain rate depending on temperature;[68] the two different ligands (μ_3– and μ_2–SCH_2CH_2OH) exchange with each other at room temperature. In contrary, the molecular structure in DMSO is not identical with the crystal structure. This conclusion was based on higher number of chemically different ligands observed by NMR, which exchanged with each other, as expected from crystal structure. Thus, different species must be present in DMSO solution than **Cd10c**. The differences in the behavior of the cluster in DMF and DMSO were attributed to different ability of the solvents to act as hydrogen bond acceptors (HBA) which leads to easier disruption of cluster stabilizing hydrogen bond network in the case of DMSO. Thus, DMSO is not a suitable solvent for **Cd10c** clusters.

5.1.3 Reactions of the $[Cd_{10}(SCH_2CH_2OH)_{16}]^{4+}$ Cluster

As further step of the investigation, the –OH groups on the surface of **Cd10c** clusters should be reacted, in order to show that the **Cd10c** clusters can eventually be functionalized further (step 3 in Scheme 2.3). To this end, it is necessary that the molecular structure of **Cd10c** in solution is known and that the –OH groups can be decoordinated in solution. The molecular structure in different solvents was investigated in the previous part. It was shown that it corresponds well with the structure obtained by SC-XRD in DMF and water solutions, but not in DMSO. This difference was caused by different ability of the solvents to act as hydrogen bond acceptors (HBA). The release of the coordinated surface –OH groups is related to the coordination-decoordination mechanism (Equation 5.1[68]) which is temperature-dependent. On the other hand it was shown that the –OH groups are important for cluster stabilization in solution. Thus, it might happen that the cluster will be unstable in solution after a reaction.

First, the reaction of **Cd10c** with *acetic anhydride* (Ac$_2$O) was investigated. It was expected that following reaction will take place:

$$ROH + Ac_2O \rightarrow RO{-}Ac + AcOH \tag{5.2}$$

As a model system, a ca. 6.5×10^{-2} M DMSO solution of **Cd10c** (perchlorate and tetrafluoroborate salts) was treated with an 1:2 or 1:16 excess of Ac_2O (cluster:Ac_2O ratio) at room temperature. This was not the best choice due to the cluster instability in DMSO, but enabled thorough characterization of different products which formed during this reaction. ^{1}H NMR spectra are shown in Figure 5.6. The ^{1}H and ^{13}C chemical shifts of different products, which were formed during this reaction, are summarized in Table 5.3. The chemical composition of the products and the chemical shift assignment was based on diverse COSY, HMBC, HSQC spectra and integrals of the peaks which were all in good agreement. The products I ($-SCH_2CH_2OAc$) and V ($-SCH_2CH_2OH$) reveal relatively broad peaks which is an indication of their coordination to Cd and exchange. On the other hand, II ($-SCH_2CH_2OAc$), III ($AcSCH_2CH_2OH$), and IV ($AcSCH_2CH_2OAc$) are characterized by sharp resonances which refers to non-coordinated compounds. This assumption is confirmed for III and IV by the fact that evaporation of reaction solutions in vacuum led to decrease in intensity of III and IV resonances, but not of II. Thus, II is also somehow coordinated to Cd in the solution which is in good agreement with its chemical composition. The reaction with cluster:Ac_2O ratio of 1:2 led to formation of the products I, III, and IV (Figure 5.6), with relative occurrence I>III>IV. III and IV are both S-acetylated. Beside this, the ^{1}H NMR pattern characteristic for the **Cd10c** cluster changed after the reaction in both CH_2 and OH ppm ranges. All attempts to obtain ^{1}H-^{113}Cd HMBC correlation spectra were unsuccessful.
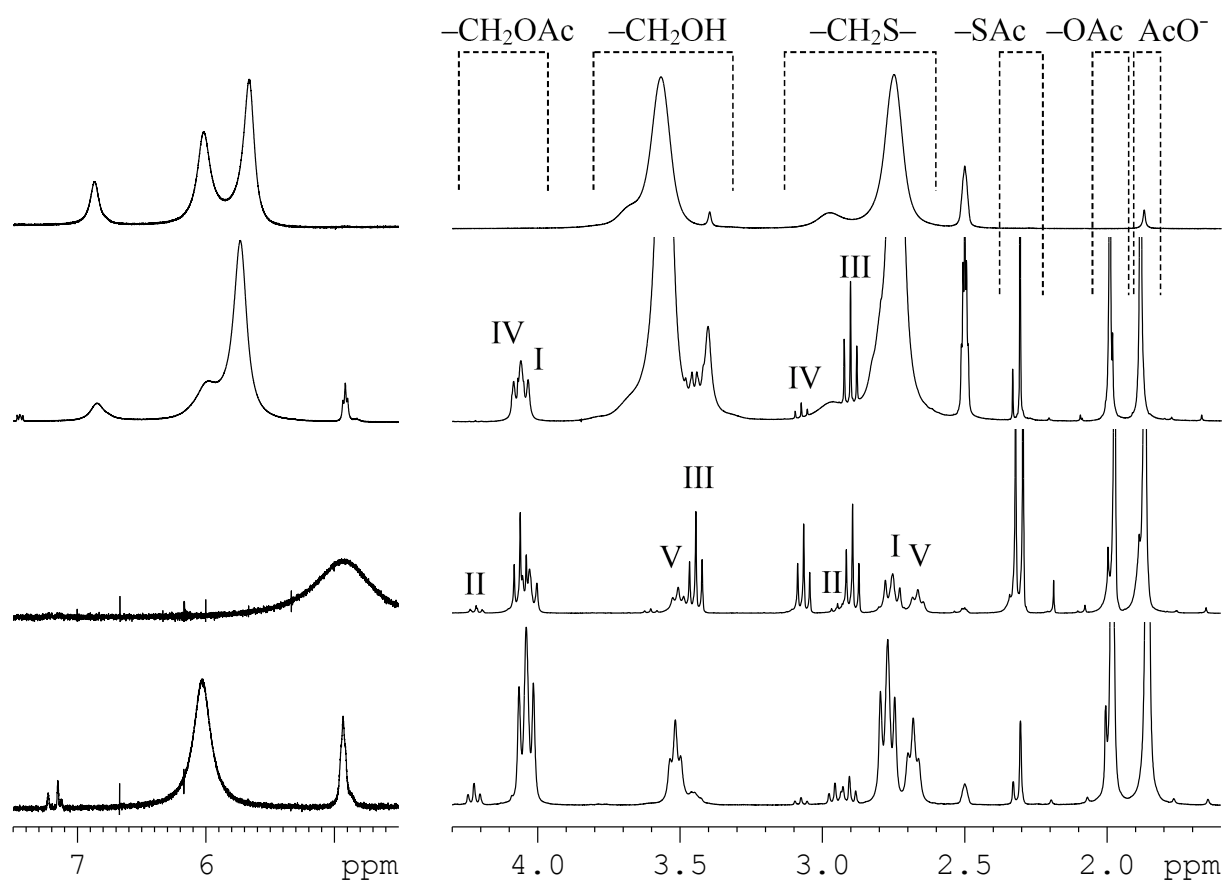
*Figure 5.6. ^{1}H NMR of reaction of **Cd10c** with Ac_2O in d_6-DMSO. Down from top: **Cd10c**:Ac_2O ratio of 1:0, 1:2, and 1:16 (after reaction and after evaporation in vacuum followed by addition of d_6-DMSO). The different products formed are emphasized.*

*Table 5.3. Summary of ^{1}H and ^{13}C NMR chemical shift of different products of reaction of **Cd10c** with Ac$_2$O in d$_6$-DMSO.*

Nr.	Compound	^{1}H and ^{13}C NMR shifts / ppm				
		–CH$_2$–O–	–CH$_2$–S–	–SCOCH$_3$	–OCOCH$_3$	–OH
I	–SCH$_2$CH$_2$OAc	4.04	2.76	–	1.98	–
		66.3	24.9		20.6, 170.5	
II	–SCH$_2$CH$_2$OAc	4.22	2.95	–	2.00	–
		61.7	36.3		20.6, 170.5	
III	AcSCH$_2$CH$_2$OH	3.45	2.90	2.30	–	4.93
		59.8	31.4	30.4, 195.2		
IV	AcSCH$_2$CH$_2$OAc	4.07	3.07	2.33	1.98	–
		62.1	27.2	30.4, 194.7	20.6, 170.5	
V	–SCH$_2$CH$_2$OH	3.52	2.67	–	–	6.03
		62.2	28.8			

The performed experiments show clearly that not only –OH groups react with Ac$_2$O according to Equation 5.2, but the S-side of the ligand is also acetylated (products III and IV, which are both formed already at an 1:2 cluster:Ac$_2$O ratio). S-acetylation could lead to cluster disintegration also if the cluster would be stable in DMSO solution. Therefore, the same reaction with a cluster:Ac$_2$O ratio of 1:2 was carried out in d$_7$-DMF (6.7×10^{-2} M) where the molecular structure of **Cd10c** is equivalent with the crystal structure. The corresponding ^{1}H NMR spectra are shown in Figure 5.7. The reaction needed more time at room temperature than in d$_6$-DMSO. It is obvious that part of the cluster had reacted, which led to different products, and another part stayed unchanged since the characteristic **Cd10c** ^{1}H NMR pattern is present after the reaction. The formed products and their ^{1}H and ^{13}C NMR chemical shifts are summarized in Table 5.4. The chemical composition of the products and the chemical shift assignment was based on COSY and HSQC spectra, similarly to d$_6$-DMSO reaction. The formed products were the same as for the reaction in d$_6$-DMSO (1:2): I, III, and IV (Figure 5.6), with relative occurrence I>III~IV. III and IV are again both S-acetylated. This means, that although the cluster reveals a molecular structure in DMF equivalent to the crystal structure, it will not be stable after the reaction with Ac$_2$O, due to the reaction of the S-side of the ligands.

*Table 5.4. Summary of ^{1}H and ^{13}C NMR chemical shift of different products of reaction of **Cd10c** with Ac$_2$O in d$_7$-DMF.*

| Nr.	Compound	^{1}H and ^{13}C NMR shifts / ppm				
		–CH$_2$–O–	–CH$_2$–S–	–SCOCH$_3$	–OCOCH$_3$	–OH
I	–SCH$_2$CH$_2$OAc	4.19	ca. 3.05	–	2.03	–
		66.7	26.0		20.3	
III	AcSCH$_2$CH$_2$OH	3.59	3.00	2.35	–	5.00
		60.7	33.0	30.1		
IV	AcSCH$_2$CH$_2$OAc	4.14	3.15	2.38	2.01	–
		62.5	27.6	30.1	20.3	
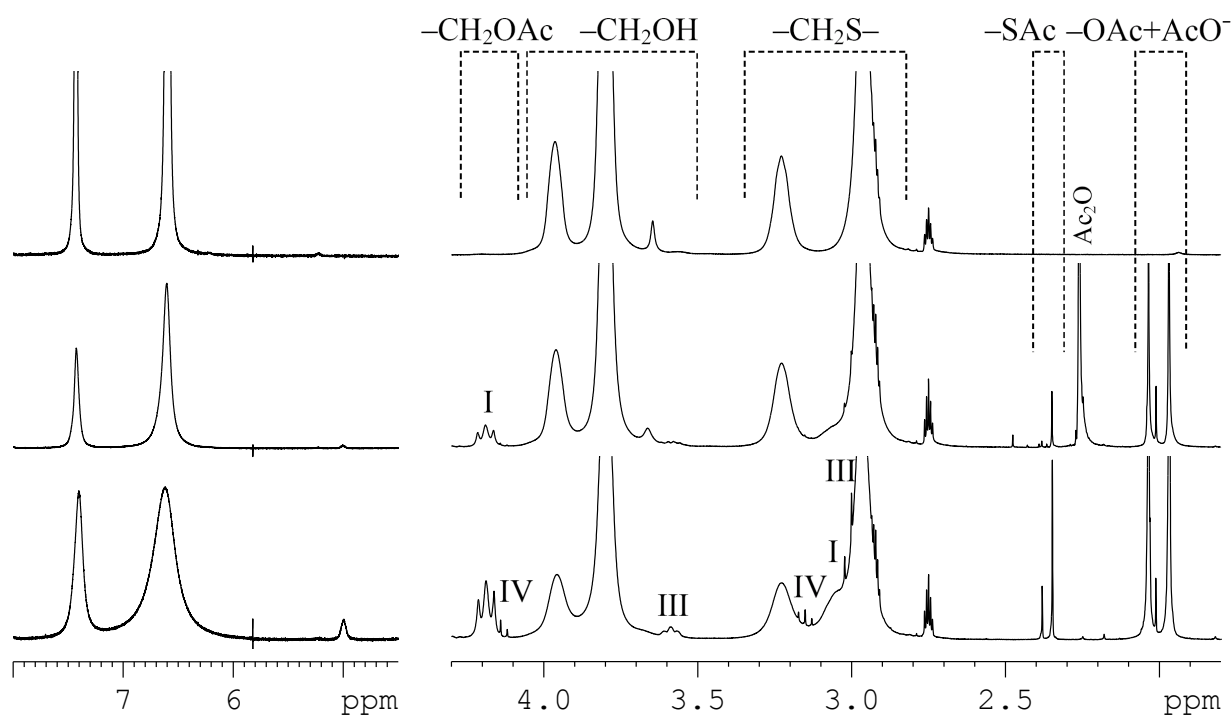
Figure 5.7. ^{1}*H NMR of reaction of **Cd10c** with Ac$_2$O in d$_7$-DMF. Down from top: **Cd10c**:Ac$_2$O ratio of 1:0 and 1:2 (after Ac$_2$O addition and after 4 d at room temperature). The different products formed are emphasized.*

Thus, the reaction of **Cd10c** with Ac$_2$O is not suitable for cluster functionalization due to the reaction of the S-side of the ligand. One reason for this might be the highly dynamic behavior of **Cd10c** in DMF. This could be partially suppressed by lowering the reaction temperature, or by using less dynamic clusters. For example, real CdS clusters like [Cd$_{17}$S$_4$(SCH$_2$CH$_2$OH)$_{26}$]$_\infty$ (**Cd17b**)[63] or Cd$_{32}$S$_{14}$(SCH$_2$CH(OH)CH$_3$)$_{36}$(H$_2$O)$_4$[66] might be suitable candidates (**Cd10c** is not a CdS cluster but a molecular complex). However, the dynamics would not be completely suppressed; therefore the reaction of the S-side of the ligand would still take place but would require longer time. Additionally, the solvent coordination effect could cause cluster growth in both DMF and DMSO, as in the case of **Cd10a** cluster (see Chapter 4.1).

Another point is the formation of acetic acid and acetate during the reaction, which can both coordinate to Cd and lead also to cluster disintegration. The presence of acetic acid was observed only sometimes (presence of an acidic proton at ca. 12 ppm in the ^{1}H NMR spectrum), but acetate was present in every sample. This is another reason why the reaction with Ac$_2$O is not suitable for **Cd10c** functionalization. To avoid this, reaction with acyl chloride (AcCl) could be used instead, in the presence of a base to catch the produced HCl (*e. g.* pyridine). However, it would not protect the S-side of the ligand from reaction.

A selective modification of the –OH groups and not of the S-side of the ligand, should be a silylation reaction with *trimethylchlorosilane* (ClSiMe$_3$):

$$ROH + ClSiMe_3 \rightarrow RO–SiMe_3 + HCl \tag{5.3}$$
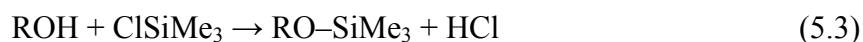
The reaction was performed similarly to the reaction with Ac_2O: to the solution of **Cd10c** in d_6-DMSO and d_7-DMF (7×10^{-2} M), pyridine was added first in order to catch HCl, followed by addition of $ClSiMe_3$. The cluster:$ClSiMe_3$ ratio was 1:4 and 1:2 in DMSO and DMF, respectively. The used cluster:pyridine ratio was somewhat lower than the cluster:$ClSiMe_3$ ratio to ensure a small excess of pyridine. As already mentioned, the molecular structure of **Cd10c** is equal to the crystal structure only in DMF, not in DMSO. Thus, only reaction in DMF should give usable results. However, due to interesting differences, reaction in both solvents will be discussed.

In d_6-DMSO, the **Cd10c**:$ClSiMe_3$ ratio of 1:4 was used. The corresponding ^1H NMR spectra (Figure 5.8) changed with time slightly. In the range around 0.0 ppm, where resonances of different $-SiMe_3$ groups are situated, four different signals were found. They are listed in Table 5.5, together with corresponding ^{13}C and ^{29}Si shifts. The ^1H intensity of the resonance at 0.06 ppm decreased with time, all the others increased. The ^1H pattern for CH_2 and OH groups changed substantially. The cluster pattern was not present any more. Instead, 4 sets of "products" were present, which are summarized in Table 5.6 with corresponding ^{13}C and ^{29}Si shifts. The main product (I) did not show any correlation to Si in the ^1H-^{29}Si HMBC spectrum (Figure 5.9, left), therefore it is considered as some $-SCH_2CH_2OH$ which is different to the ligands originally present on the cluster (highfield shift and sharper resonances of the CH_2 groups, much broader signal of the OH group). The other three products (II–IV) showed ^1H-^{29}Si correlation of the $-CH_2O-$ groups to three ^{29}Si resonances at 16.3 ppm (Figure 5.9, left). Consequently, their structure was assigned as $-SCH_2CH_2OSiMe_3$. Interestingly, the ^{29}Si resonance at 16.3 ppm correlates also with the ^1H resonance at 0.06 ppm, which decreased in intensity with time. This is in contrast with increasing intensity of the CH_2 groups of the products II–IV. The other resonances observed for $-Me$ groups could belong to some $-O-Si-O-$ (^1H: 0.19 and 0.17 ppm) species and to $Me_3Si-O-SiMe_3$ (0.03 ppm).[140] No resonances were obtained in the ^{113}Cd spectrum,. This was expected since for the pure, unmodified cluster also no resonances were observed.

In summary, it appears that the molecular structure of the cluster in DMSO solution was broken after the reaction and only smaller species were present. The ligands were partially O-silylated and not S-silylated (^1H-^{29}Si HMBC), as expected. Beside this, $-Me$ groups were formed which could belong to some $-O-Si-O-$ species, whose origin could not be explained.

*Table 5.5. Summary of ^1H, ^{13}C, and ^{29}Si NMR shifts of different $-SiMe_3$ groups after reaction of **Cd10c** with $ClSiMe_3$ in d_6-DMSO.*

^1H	^{13}C	^{29}Si	Assignment
0.19	0.0	−19.5	−O–Si–O– (?)
0.17	−0.2	−14.8	
0.06	−0.4	16.3	$-CH_2-O-SiMe_3$ products II–IV
0.03	1.8	6.7	$Me_3Si-O-SiMe_3$ (?)
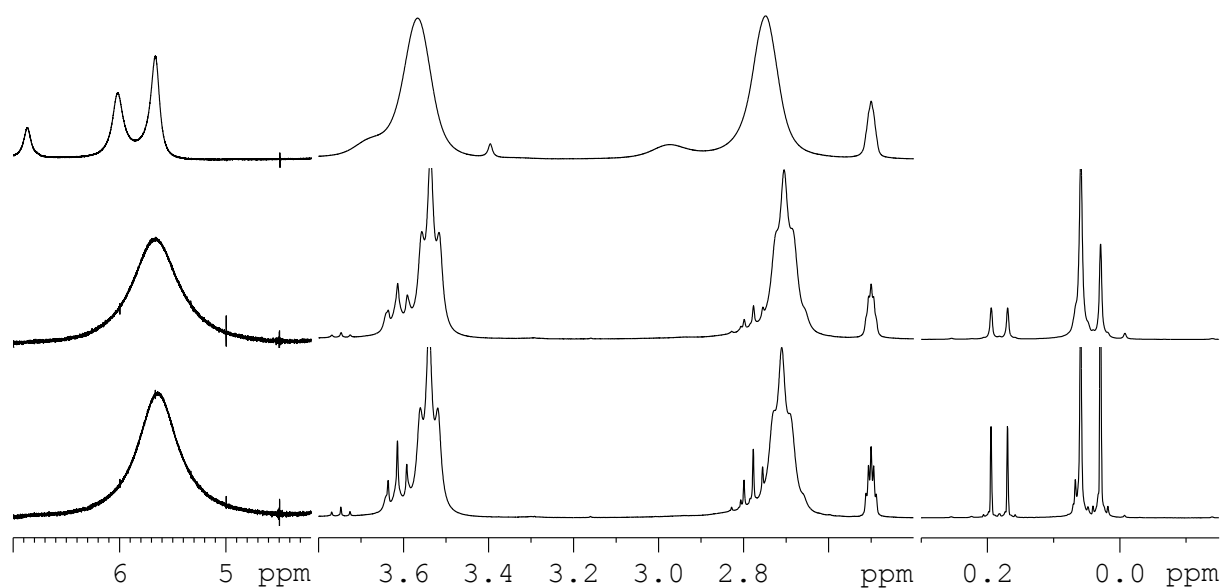
*Figure 5.8. ${}^1H$ NMR of reaction of **Cd10c** with ClSiMe$_3$ in d$_6$-DMSO. Down from top: **Cd10c**:ClSiMe$_3$ ratio of 1:0 and 1:2 (after ClSiMe$_3$ addition and after 2 d at room temperature).*

*Table 5.6. Summary of ${}^1H$ and ${}^{13}C$ NMR chemical shift of different products of reaction of **Cd10c** with ClSiMe$_3$ in d$_6$-DMSO.*

| Nr. | Compound | ${}^1H$ and ${}^{13}C$ (${}^{29}Si$) NMR shifts / ppm | | | |
		–CH$_2$–O–	–CH$_2$–S–	–OSi(CH$_3$)$_3$	–OH
I	–SCH$_2$CH$_2$OH	3.54	2.70	–	5.7
		62.9	29.1		
II	–SCH$_2$CH$_2$OSiMe$_3$	3.75	2.81	0.06	–
		60.4	40.6	−0.4 (17.0)	
III	–SCH$_2$CH$_2$OSiMe$_3$	3.62	2.78	0.06	–
		65.2	41.0	−0.4 (16.2)	
IV	–SCH$_2$CH$_2$OSiMe$_3$	3.61	2.66	0.06	–
		59.5	28.2	−0.4 (16.4)	

More interesting should be the reaction of **Cd10c** with ClSiMe$_3$ (1:2) in d$_7$-DMF, since the molecular structure in DMF is equivalent to the crystal structure. ${}^1H$ NMR spectra (Figure 5.10) show changes with time, similarly to the reaction in DMSO. Four resonances for some –SiMe$_3$ groups were formed initially (Table 5.7). However, the resonance at 0.12 ppm (${}^1H$) was not present in the spectra after 1 d at room temperature. The intensity of the resonance at 0.07 ppm (${}^1H$) decreased with time compared with the remaining two. The ${}^1H$-${}^{29}Si$ HMBC spectrum (Figure 5.9, right) did not reveal any correlation between –CH$_2$– groups and Si, as it was the case in DMSO. The ${}^1H$ NMR pattern of the cluster changed also. Two different ligands were still present, but their intensity ratio changed from 1:3 to ca. 1:4.5 after 6 d at room temperature. The CH$_2$ resonances were slightly highfield shifted ([7.13 (br, 1 H), 3.91 (br, 2 H), 3.20 (br, 2 H) ppm] and [6.57 (br, 1 H), 3.77 (br, 2 H), 2.93 (br, 2 H) ppm]), and the shape of OH resonances changed substantially. No reaction products with sharp resonances were observed. The –SiMe$_3$ group at 0.07 ppm (${}^1H$) can be due to the

71

presence of Me₃Si–O–SiMe₃. The origin of the other two groups, which correlate to 30.3 and 35.0 ppm (^{29}Si), could not be elucidated; however, they do not originate from some –S–SiMe₃ species since they would reveal a chemical shift of ca. 16 ppm (as Me₃SiSMe does[140]).
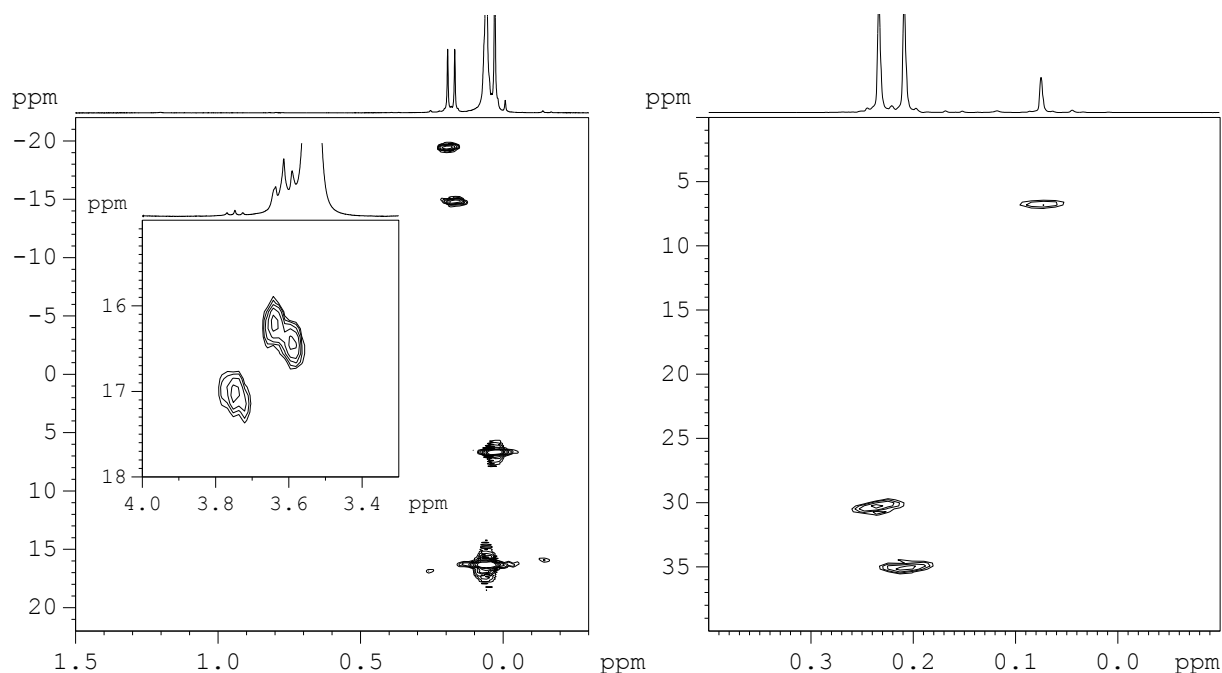
*Figure 5.9. ^{1}H-^{29}Si HMBC spectra after reaction of **Cd10c** with ClSiMe₃. Left: 1:4 **Cd10c**:ClSiMe₃ in d₆-DMSO, right: 1:2 **Cd10c**:ClSiMe₃ in d₇-DMF.*

Although the previously described changes are not so dramatic, and thus no conclusion can be made whether ClSiMe₃ reacted with the cluster and how, the ^{113}Cd NMR spectrum (Figure 5.11) shows clearly that the cluster underwent substantial changes during the reaction. The resonances at 545 and 403 ppm with an intensity ratio of 3:2, which were due to CdS₄O+CdS₄ and CdS₃O₃ sites, were not present anymore. Instead, three most intense resonances were observed at 532, 514, and 446 ppm. Although the shifts of these signals are different, they are located in the expected ppm range. No signals were present in the ^{1}H-^{113}Cd HMBC spectrum. Thus, no conclusion can be made about the cluster stability after the reaction. However, it is clear that not a single cluster was obtained.

*Table 5.7. Summary of ^{1}H, ^{13}C, and ^{29}Si NMR shifts of different –SiMe₃ signals after reaction of **Cd10c** with ClSiMe₃ in d₇-DMF.*

| ^{1}H	^{13}C	^{29}Si	Assignment
0.23	−0.8	30.3	?
0.21	−0.9	35.0	?
(0.12)	−0.9	16.7	?
0.07	1.3	6.8	Me₃Si–O–SiMe₃ (?)
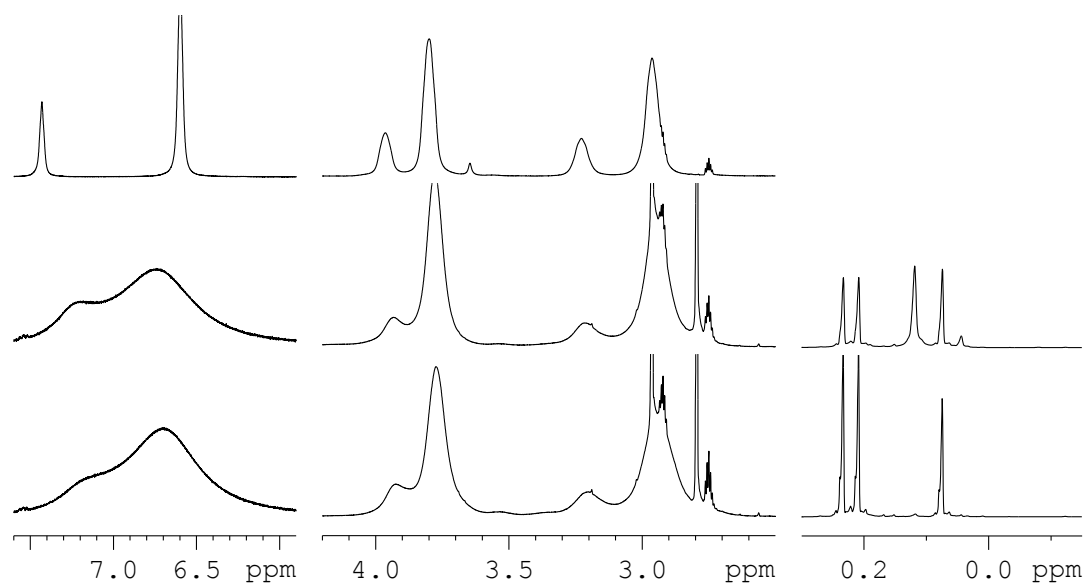
Figure 5.10. ^{1}H NMR of reaction of **Cd10c** with ClSiMe$_3$ in d$_7$-DMF. Down from top: **Cd10c**:ClSiMe$_3$ ratio of 1:0 and 1:2 (after ClSiMe$_3$ addition and after 1 d at room temperature). The resonances at 2.96 and 2.79 ppm are due to DMF used for drying (see Experimental Part).
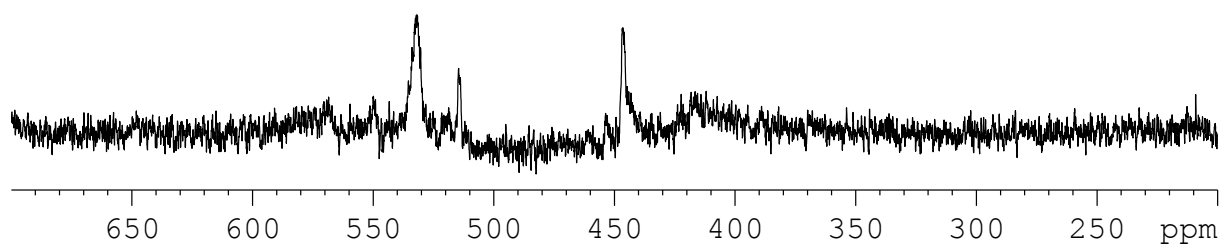
Figure 5.11. ^{113}Cd NMR of reaction of **Cd10c** with 1:2 ClSiMe$_3$ in d$_7$-DMF after 1 d at room temperature.

5.1.4   Conclusions

In this chapter, different aspects of behavior of [Cd$_{10}$(SCH$_2$CH$_2$OH)$_{16}$]$^{4+}$ (**Cd10c**) clusters were summarized. Their molecular structure in solid state was compared with that in solution. The possibility of further reactions of their surface –OH groups and the cluster stability were investigated, based on reactions with acetic anhydride (Ac$_2$O) and trimethylchlorosilane (ClSiMe$_3$).

Cd10c clusters with nitrate, perchlorate, and tetrafluoroborate counter-anions were synthesized by the method of Schwarzenbach *et al.*[56] It was shown by SC-XRD that a rich hydrogen bond network is formed around the apical Cd positions.

The molecular structure of **Cd10c** in solution was investigated by means of diverse NMR measurements. Used **Cd10c** salts did not reveal any differences between each other in solution which excludes coordination of the counter-anions to Cd. The molecular structure in water and DMF solutions was in good agreement with the crystal structure. On the other hand, the spectra in DMSO revealed higher number of ligands than expected which means

that other species than **Cd10c** must be present in the solution. In all investigated solvents, the cluster behaves highly dynamically: the ligand –OH groups coordinate to and decoordinate from both Cd sites (CdS$_4$O+CdS$_4$ and CdS$_3$O$_3$),[68] and the different ligands exchange with each other. The differences in the behavior of **Cd10c** in DMF/water and DMSO were attributed to different ability of the solvents to act as hydrogen bond acceptors (HBA). DMSO, as stronger HBA, leads to easier disruption of cluster-stabilizing hydrogen bond network. This makes it an unsuitable solvent for **Cd10c** clusters.

Further, since it was shown that –OH groups are partially de-coordinated in solution due to the dynamic cluster behavior, reactions of **Cd10c** with Ac$_2$O and ClSiMe$_3$ were investigated. Both DMSO and DMF were used as solvents, although the molecular structure in DMSO differs to the structure in solid state.

Reaction with Ac$_2$O in both DMSO and DMF led to formation of diverse products, some of them being S-acetylated. S-acetylation was observed already in the initial stages of the reaction, when part of the cluster reacted (and, in DMF, a part remained unchanged). One reason for the S-side acetylation can be the fast exchange of the ligands. This proceeds likely through stages with terminal binding mode of the ligands which are then more accessible to reaction with Ac$_2$O. A partial solution for this problem could be use of lower reaction temperature or use of less dynamic clusters. However, if the dynamics would not be completely suppressed, the reaction of the S-side of the ligand would still take place and only would require longer time. Another reason, which renders reaction with Ac$_2$O unsuitable, is the formation of acetic acid and acetate which can coordinate to Cd.

Reaction with ClSiMe$_3$ in DMSO led to O-silylation of part of the ligands. However, the cluster was completely disintegrated in solution. On the other hand, it could not be elucidated exactly how the cluster reacted in DMF. ^{1}H NMR did not show substantial changes and no ligand ^{1}H-^{29}Si HMBC correlation was observed (as in DMSO). S-side silylation, however, could be excluded. The ^{113}Cd NMR spectrum changed and resonances formed, which were in the cluster-corresponding ppm range, but differed to the spectrum of the unmodified cluster. The question, whether the molecular structure of the cluster was maintained during the reaction, could not be answered. Thus the only conclusion which could be made was that the cluster changed and not a single compound was formed by the reaction.

Cd10c was not a suitable cluster for further reactions of its –OH groups because of the following reasons:

– The core of the cluster was not stable enough in solution and required additional stabilization by a hydrogen bond network.

– This cluster stability, which depended on hydrogen bonds, was broken in DMSO, which is a strong HBA, and during reactions of the –OH groups.

Thus, in order to solve this problem, it is necessary to use clusters whose cores are stable enough and which do not require hydrogen bond stabilization. For example, clusters containing sulfidic bridges (*i.e.* real CdS clusters, and not only complexes as **Cd10c** is) should be stable enough. For example, [Cd$_{17}$S$_4$(SCH$_2$CH$_2$OH)$_{26}$]$_∞$ (**Cd17b**)[63] or Cd$_{32}$S$_{14}$(SCH$_2$CH(OH)CH$_3$)$_{36}$(H$_2$O)$_4$[66] could be used (Figure 5.12). An indication that they

do not need hydrogen bond stabilization is the fact that almost all of the ligand –OH groups do not coordinate to Cd in solid state and that the apical Cd sites possess almost tetrahedral coordination with additional Cd–OH interaction weaker than that in **Cd10c** (Figure 5.12). Therefore, such clusters could be stable also after some reaction of the –OH groups. **Cd17b** forms a 3D network of Cd17 clusters connected by bridging thiolate in solid state.[63] It dissolves readily in strongly coordinating solvents (DMF and DMSO) and it seems that its core structure remains intact after dissolution (^{113}Cd NMR, UV/Vis spectra).[63] The Cd32 cluster[66] contains –OH groups on the surface and dissolves in DMF.[66] Its UV/Vis spectrum after dissolution is in good agreement with the Cd32 size, indicating intact dissolution in DMF.[66] So it seems that coordinating solvents cannot be avoided, as it was the case for **Cd10a** (Chapter 4.1). This might lead to undesired cluster rearrangement after longer times and mainly at higher temperatures, which are necessary for the aimed polycondensation reactions.
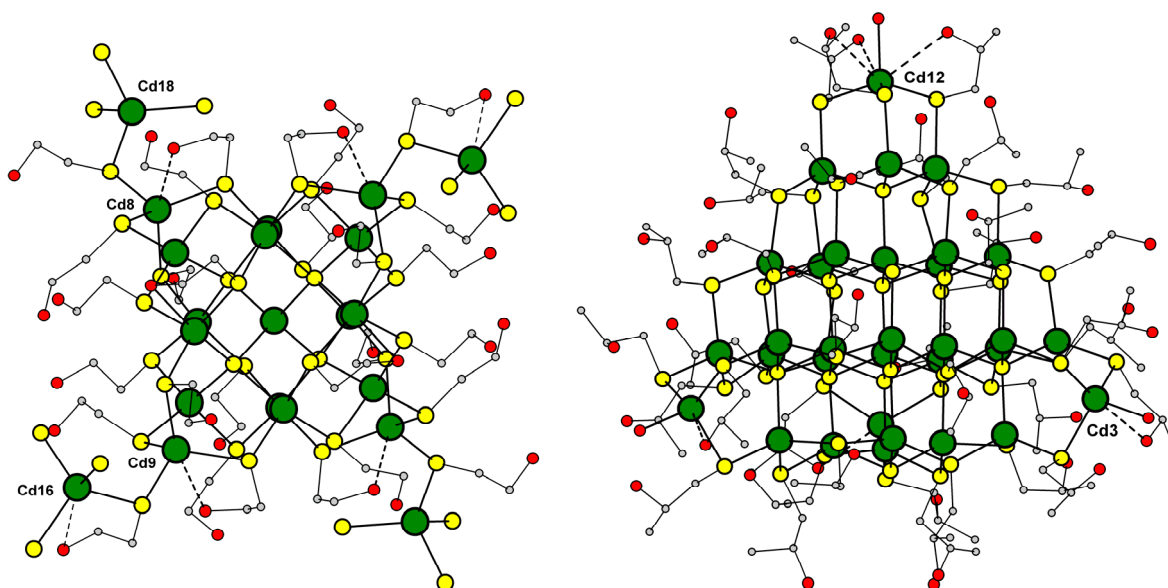
Figure 5.12. Molecular structures of $[Cd_{17}S_4(SCH_2CH_2OH)_{26}]_\infty$ (Cd17b)[63] (left) and $Cd_{32}S_{14}(SCH_2CH(OH)CH_3)_{36}(H_2O)_4$[66] (right), showing Cd–O interactions (dashed lines). Distances: **Cd17b** d_{Cd-O} = *ca. 2.8 and 3.4 Å;* Cd32 d_{Cd-O} = *ca. 2.9 Å (***Cd10c** d_{Cd-O} = *ca. 2.4 Å).*

Besides the reaction of –OH groups with Ac$_2$O and ClSiMe$_3$, a mild reaction with N-acylimidazoles was used for successful functionalization of CdS NPs with –OH groups on the surface:[110]

$$\text{Im} \xrightarrow{\text{RCOCl}} + \text{ImH}^+\text{Cl}^- \xrightarrow{\text{NPs–OH}} \text{NPs–OCOR} + \text{Im} \quad (5.4)$$
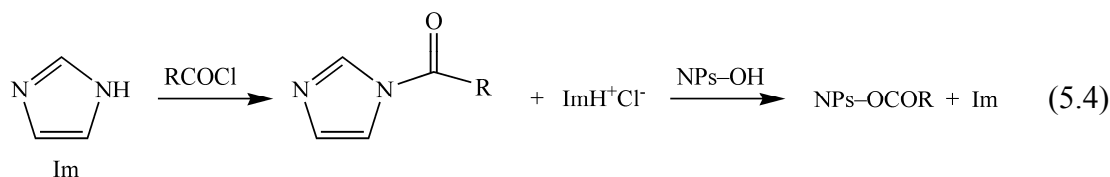
N-acylimidazoles reacted almost selectively with the O-side of the surface ligands and did not cause any structural changes of the used NPs.[110] In this way, incorporation of a double bond functionality onto the cluster surface should be possible, leading to a cluster capable of radical polymerization.

5.2 CdS Clusters Functionalized by Amino Groups

Another possibility of covalent incorporation of CdS clusters into a polymeric matrix is their functionalization with ligands bearing an amino group. However, such clusters were not found in literature. Only a few examples of CdS NP functionalization with ligands like L-cysteine[108] and 4-aminothiophenol (HSPh-pNH$_2$)[111,112] are known. Possible reactions of the –NH$_2$ group were also investigated.[111]

In this chapter, the attempts to synthesize CdS clusters functionalized with –NH$_2$ group are summarized. They are based on two approaches: exchange reactions of (NMe$_4$)$_4$[Cd$_{10}$S$_4$(SPh)$_{16}$] (**Cd10a**) with HSPh-pNH$_2$ and cluster synthesis in the presence of HSPh-pNH$_2$, equivalent to the synthesis of **Cd10a**.

5.2.1 Exchange Reactions of CdS Clusters

Exchange reactions on clusters are possible thanks to cluster dynamics in solutions. Thus, when another thiol is added to a cluster solution, an equilibrium reaction takes place:

$$\diamondsuit\!\!\!\!\diamondsuit\!-\text{SR}^1 \; + \; \text{HSR}^2 \;\rightleftharpoons\; \diamondsuit\!\!\!\!\diamondsuit\!-\text{SR}^2 \; + \; \text{HSR}^1 \qquad (5.5)$$
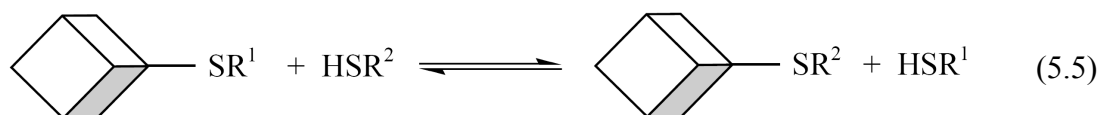
The equilibrium is influenced by many factors:[113] different affinity of the ligands to Cd, excess of one ligand, acidity of the thiols (if HSR^2 has lower acidity compared with HSR^1, the exchange is disfavored). A thorough investigation of exchange reactions of (Me$_4$N)$_2$[Cd$_{17}$S$_4$(SPh)$_{28}$] (**Cd17a**) with various thiols was performed by Lovingood *et al.*[113] by means of electrospray mass spectrometry. Non-functional (alkane and arene thiols) and functional thiols (thiol and thio acids, thiol alcohols and others) were added to an MeCN solution of **Cd17a** at room temperature. The equilibrium was reached within 5 min. Beside different behavior of diverse ligands, an important conclusion about the cluster stability was made: when an excess of ligand is added to the **Cd17a** solution, the cluster loses its [Cd(SR)$_3$]$^-$ caps and is converted to an exchanged **Cd10a** cluster.[113]

In this part, only some additional information to the work of Lovingood *et al.*[113] was obtained. The cluster **Cd10a** was used since its behavior in different solvents was investigated in detail (see Chapter 4.1). **Cd10a** is soluble in MeCN, DMF, and DMSO, however, only MeCN is a suitable solvent. DMF and DMSO are known to cause cluster rearrangement and cluster growth already at room temperature (Chapter 4.1). Beside this, DMSO oxidizes thiols to disulfides.[141] For comparison, few experiments were performed with non-functional thiols (cyclohexyl- and benzylmercaptane) with PhS:RSH = 1:X, X = 10–40, which is a relatively high excess of the exchanging ligand. After mixing at room temperature for one day, the resulting colorless solutions were dried in vacuum to remove solvent and excess thiols. The solid residue was dissolved in d$_3$-MeCN and characterized by ^{1}H NMR. All samples

contained both signals from –SPh and –SR. However, they were not sharp and distinct as in the case of pure **Cd10a**, which is an indication of partial exchange of –SPh by RSH and formation of a cluster with mixed –SPh/SR surface. The total amount of thiols/thiolates in the samples was ca. 10–20 % higher than expected (compared with the Me_4N^+ resonance), probably due to insufficient evacuation and/or due to strong adsorption of PhSH/RSH to the cluster surface. The extent of exchange was improved by higher X and higher boiling point of RSH ($T_{b,PhSH}$ = 169 °C, $T_{b,C6H11SH}$ = 159 °C, $T_{b,PhCH2SH}$ = 194 °C). For cyclohexylmercaptane, with a boiling point lower than PhSH by 10 °C, less than 50 % of –SPh were exchanged. In the case of $PhCH_2SH$ (boiling point 25 °C higher), almost 90 % of –SPh were exchanged by the used method.

Exchange with HSPh-pNH$_2$ was performed in a similar way. However, lower X (0.8–10) and cluster concentration (4–10 mg/ml) were used and the exchanging ligand was added as an MeCN solution. Mixing at room temperature for 1 d resulted in the formation of a white precipitate in a yellow solution (HSPh-pNH$_2$ in MeCN is yellow). The precipitate was soluble in DMF and DMSO, whereas a pale yellow solution formed.

The formation of a precipitate in the case of HSPh-pNH$_2$ was surprising since higher solubility of exchanged cluster was expected due to higher surface polarity. Thus, it must be attributed to successful exchange reaction collateral with coordination of the ligand –NH$_2$ groups to Cd of neighboring clusters in the reaction mixtures and formation of agglomerates/aggregates. As a driving force for such a behavior, decrease of the cluster charge due to replacement of some thiolate ligands (probably terminal) by amino ligands might be expected. If all terminal thiolates in **Cd10a** would be replaced, the cluster charge would decrease from −4 to 0, leading to a neutral 3D cluster network.

Actually, such a behavior is not that surprising. When CdS NPs were functionalized by HSPh-pNH$_2$,[111,112] either the NPs were dissolved in MeCN for TEM measurement and their eventual agglomeration was not mentioned,[112] or they were resuspended in DMF and TEM measurement revealed that they tend to agglomerate.[111] Additionally, it is known that bidentate and quadridentate pyridyl ligands can be used to bridge CdS clusters with Cd17 and Cd32 cores[60,62,65] and 1D to 3D structures can be obtained. These facts are in good agreement with proposed coordination of amino groups to Cd of neighboring clusters.

Additionally, it was shown that this coordination can be broken by strongly coordinating solvents like DMF and DMSO. However, their use has to be avoided (see earlier).

Therefore, exchange reaction of **Cd10a** by HSPh-pNH$_2$ is not a good way of preparation of clusters functionalized by amino groups. It leads to cluster aggregation, which prevents its utilization for further reactions, and the aggregates can be broken only by strongly coordinating solvents, which cause cluster rearrangement.

5.2.2 A Cd17 Cluster with NH$_2$ Groups on the Surface

Attempts to synthesize a **Cd10a** cluster with HSPh-pNH$_2$ instead of PhSH were also performed. The diverse experiments, which were based on the synthesis of **Cd10a** by Dance

et al.[47] (see Equation 2.3 and 2.4), are summarized in Table 5.8. In general, the colorless solution of $Cd(NO_3)_2$ was added to the yellow solution of HSPh-pNH$_2$ + Et$_3$N, which led to an overall concentration of Cd^{2+} of 0.02–0.06 M. Eventually, the Me$_4$NCl solution was added. Then, sulfur or Na$_2$S was added. The mixture was stirred at room temperature until complete dissolution of sulfur. Aliquots of the reaction solutions were treated with different solvents which, in some cases, led to formation of precipitates or crystals.

Crystals of two kinds were synthesized by these procedures. The first one was not a cluster with a Cd10 core, but with a Cd17 core, $\{[Cd_{17}S_4(SPh\text{-}p\text{NH}_2)_{24}(DMF)_2]X_2\}_\infty$ (**Cd17-NH$_2$**), whose anion (X) could not be identified by SC-XRD. For its synthesis, mainly DMF or a DMF/MeOH mixture was used as solvent. The S:Cd ratio varied between (0.6–2.0):5, followed by addition of MeOH which led to the formation of square, plate-like, pale yellow crystals after few days (samples E, H, I, L). Their identity was confirmed by SC-XRD. The same crystals can be obtained by slow diffusion of MeOH into the DMF/MeOH reaction solution. When no MeOH was used during the same synthesis, another type of crystals (cryst. X in Table 5.8), square-shaped, were obtained for S:Cd ratios of 0.9:5 and 1.3:5 (samples I). However, they could not be characterized by SC-XRD because they disintegrated in perfluoropolyether oil used for SC-XRD measurement. Addition of Me$_4$NCl solution did not lead to formation of any crystals. Preparative details can be found in the Experimental Part.

Table 5.8. Summary of diverse experiments aiming to preparation of clusters with HSPh-pNH$_2$ as capping ligand.

| Nr. | Aim | Solvent for | | | S source (S:Cd = 2:5, theoretical) | Another solvent | Product |
		HS-Ph-pNH$_2$ + Et$_3$N	Cd^{2+}	Me$_4$N$^+$			
A	Cd4	MeCN	MeCN	–	–	–	prec.
B	Cd4	MeOH	MeOH	MeOH	–	–	prec.
C, D	Cd10	DMF	MeOH	MeOH	S (1.5:5)	toluene	prec.
E, H	Cd10	DMF	MeOH	–	S (1.6:5)	MeOH toluene, THF, H$_2$O, CH$_2$Cl$_2$, EtOH,	**Cd17-NH$_2$** prec.
					S (2.0:5)	MeOH	**Cd17-NH$_2$**
I	Cd10	DMF	DMF	–	S (0.6:5)	MeOH	**Cd17-NH$_2$**
					S (0.9:5)	– MeOH	cryst. X **Cd17-NH$_2$**
					S (1.3:5)	– MeOH	cryst. X **Cd17-NH$_2$**
					S (2.0:5)	MeOH	**Cd17-NH$_2$**
L	Cd10	DMF	DMF	–	S (1.3:5)	MeOH	**Cd17-NH$_2$**
F, G	Cd10	DMF	MeOH	MeOH	S (2.1:5)	–	prec.
					S (1.4:5)	MeOH, MeCN, EtOH, THF, acetone, H$_2$O	prec.
J, K	dif.	DMF	DMF	–	**Na$_2$S** in MeOH/H$_2$O, dif. ratios	MeOH	only sol. and prec.

$\{[Cd_{17}S_4(SPh\text{-}p\text{NH}_2)_{24}(DMF)_2]X_2\}_\infty$ (**Cd17-NH$_2$**) crystallized in the tetragonal space group $P4_12_12$ or $P4_32_12$ (a = 27.2759(12) Å, c = 61.735(5) Å), and were refined in $P4_32_12$ as racemic twin with final Flack parameter of 0.54(5). There are two different halves of Cd17 clusters in the asymmetric unit which are related with each other by a 2-fold axis. This gives each cluster C_2 symmetry. The axes pass through the central Cd atom of each cluster (Cd05 and Cd24) and are perpendicular to each other. The asymmetric unit might look centrosymmetric (Figure 5.13) but is not. The cluster cores are principally identical with the known **Cd17a** cluster ($[Cd_{17}S_4(SPh)_{28}]^{2-}$).[58] Each is formed from four adamantane cages in the centre and four barrelene cages at each cluster corner. In **Cd17a**, there are 24 bridging and 4 terminal thiolates, whereas in **Cd17-NH$_2$** the terminal thiolates are missing. Two terminal positions (apical Cd atoms) of each cluster are occupied by amino groups of a thiolate from a neighboring cluster. In this way, a connection is formed between neighboring clusters which consists of two ligands with almost parallel phenyl rings (Figure 5.13, Figure 5.14). Thus, 1D chains of Cd17 clusters are present in the crystal structure in the direction of the c-axis, which are helically twisted due to the presence of a 4_3 axis. The clusters are arranged in layers, which are covalently connected to neighboring layers (Figure 5.14). Clusters within each layer display weak interactions between amino groups and nearby phenyl rings (Figure 5.15). The layers contain plenty of void space. The remaining two apical Cd sites of each cluster are coordinated probably by solvent DMF molecules, however, only the bounded oxygen atom was found. According to this assignment, each Cd17 cluster has an overall charge of +2, which is very unusual (Table 2.2).
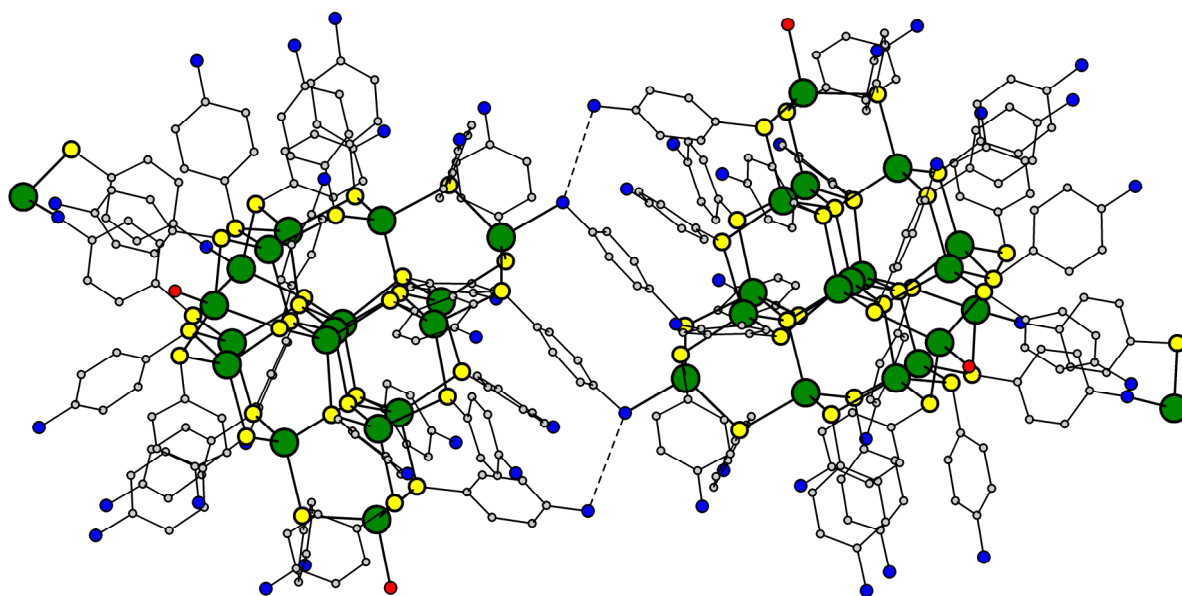
*Figure 5.13. Crystal structure of **Cd17-NH$_2$**, the two clusters belonging to the same asymmetric unit are shown.*
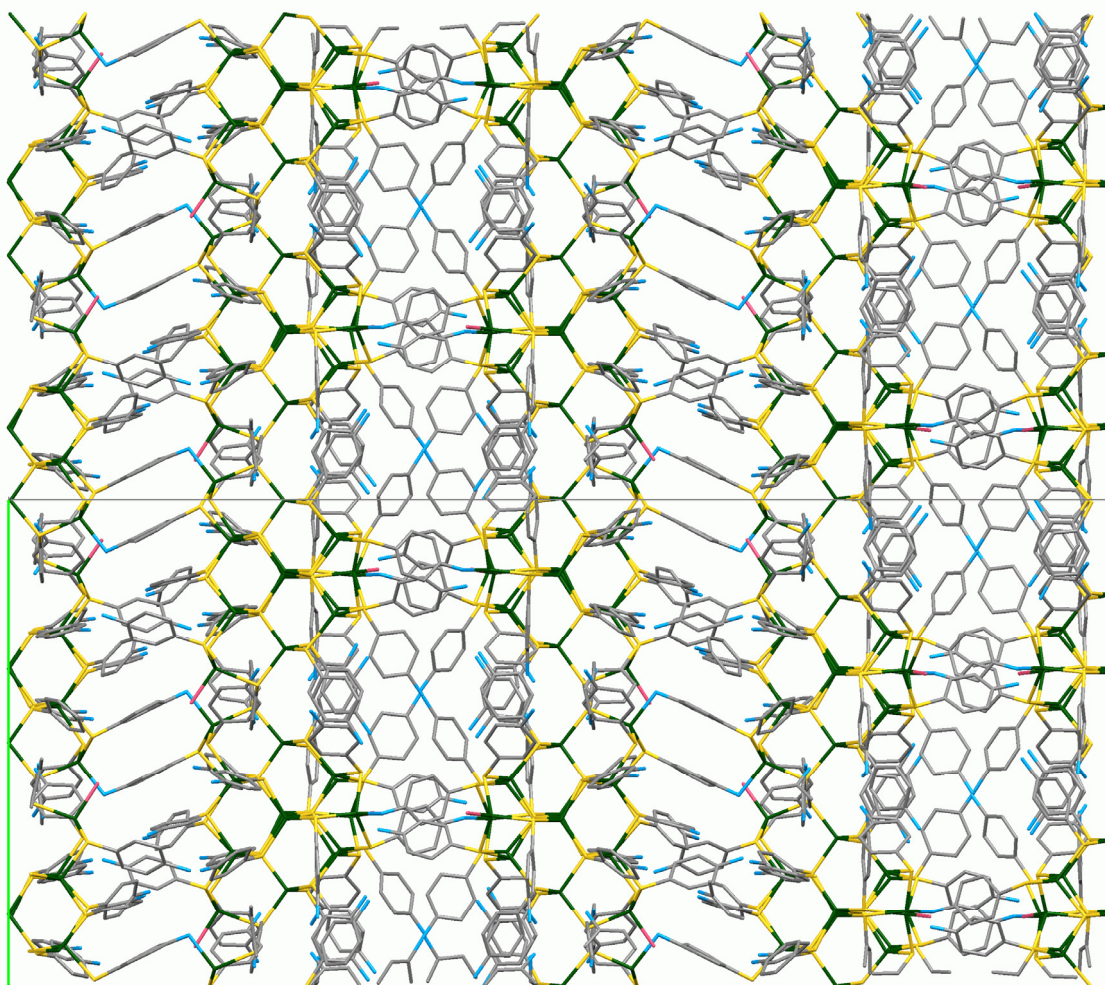
*Figure 5.14. Layers of clusters in **Cd17-NH₂** which are connected via the thiolate bridges. Viewing direction: along* a-*axis.*

There are several possibilities how this charge issue could be explained: (i) There are very large solvent accessible voids in the crystal structure: two with ca. 7648 $\mathring{A}^3$ and 3385 e^- each, which is 33.3 vol.%. Here, beside solvent molecules (DMF, MeOH), the disulfide formed during the synthesis, free thiol, and also anions (nitrate, thiolate) can be placed. The molecules and/or ions in the voids are disordered, and therefore their atomic positions could not be refined by the SC-XRD data. (ii) The distance between DMF oxygen atoms of neighboring clusters is 6.94 Å and between nitrogen and sulfur of bound thiolate is ca. 6.0 Å. Therefore, it could be speculated that the clusters could be connected via another thiolate. However, this possibility can be completely eliminated by the SC-XRD data. Therefore, the missing anions, most probably disordered nitrate, must be located in the void spaces.
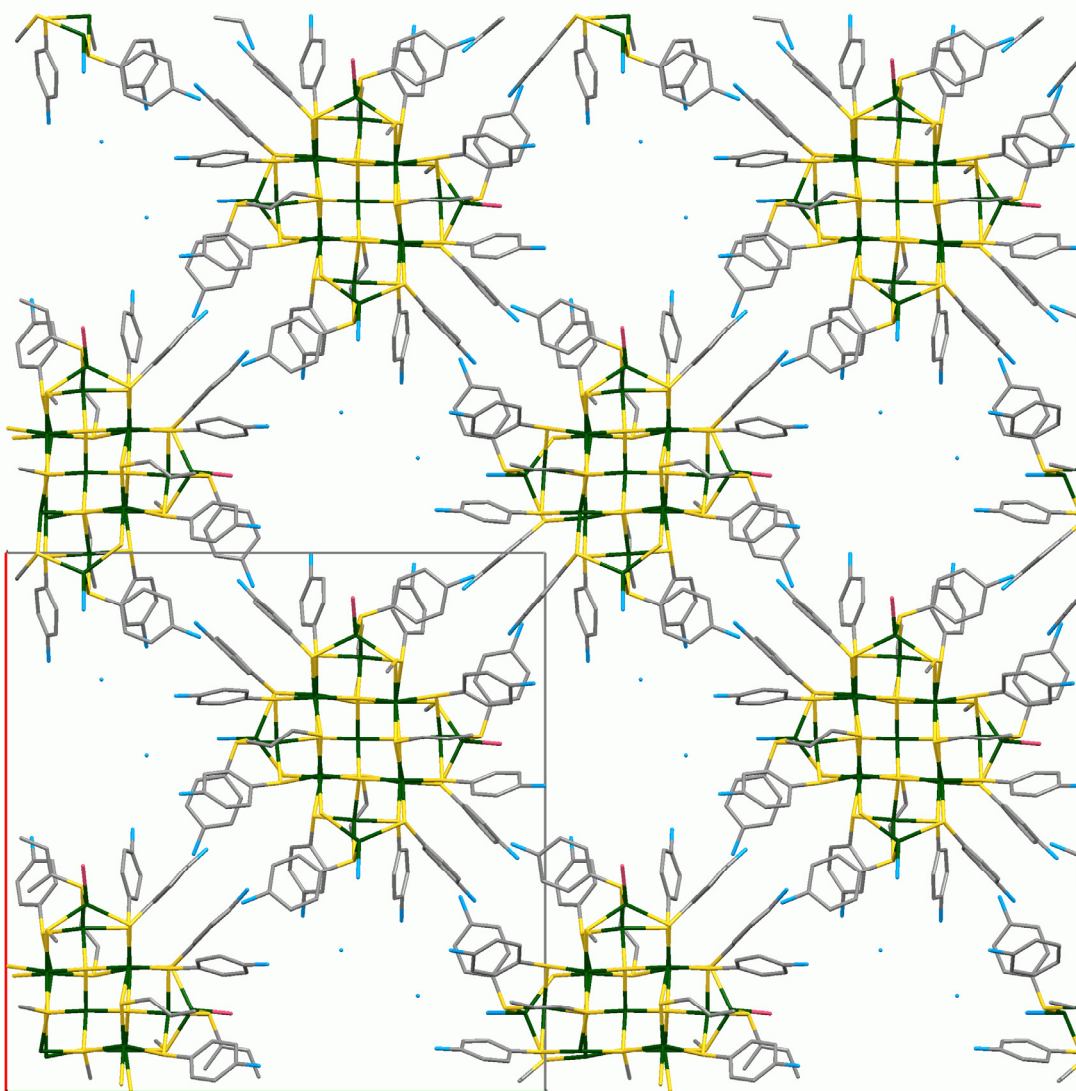
*Figure 5.15. (001) layer of clusters in **Cd17-NH₂**, seen in the direction of c-axis. There is no covalent connection between clusters within the layers, but plenty of void space.*

The crystal structure data indicate that there are strong bonds between clusters within the 1D chains and weaker interactions between neighboring chains. This should influence the behavior of **Cd17-NH₂** in different solvents in that sense that it should be soluble only in solvents which are able to break the Cd–N coordinative bonds. Indeed, the crystals were not soluble in MeCN, but readily soluble in DMF and DMSO (at least 15 mg/ml in both). Surprisingly, the crystals were insoluble in pyridine (proven by DLS measurement of filtered 1.5 mg/ml suspension). This means that pyridine is not able to break the Cd–N bonds and that the Cd–N bonds are stronger in the case of amino group compared with pyridine.

Cd17-NH₂ was characterized also by means of UV/Vis absorption and DLS measurements. In the UV/Vis spectrum, an absorption maximum at ca. 290 nm would be expected according to the size of the cluster (Table 2.2). In DMSO, a shoulder at ca. 305 nm

was observed, whereas in DMF the absorption maximum was poorly resolved. However, the position of the absorption edge (minimum in the 1st derivative curves) was identical for both solvents (Figure 5.16). The absorption features of **Cd17-NH$_2$** originate probably not only from the quantum size effect, but also from ligand transitions (see Figure 5.16, insert). Therefore, no explicit conclusion about the size of the clusters in solution can be drawn from UV/Vis absorption.
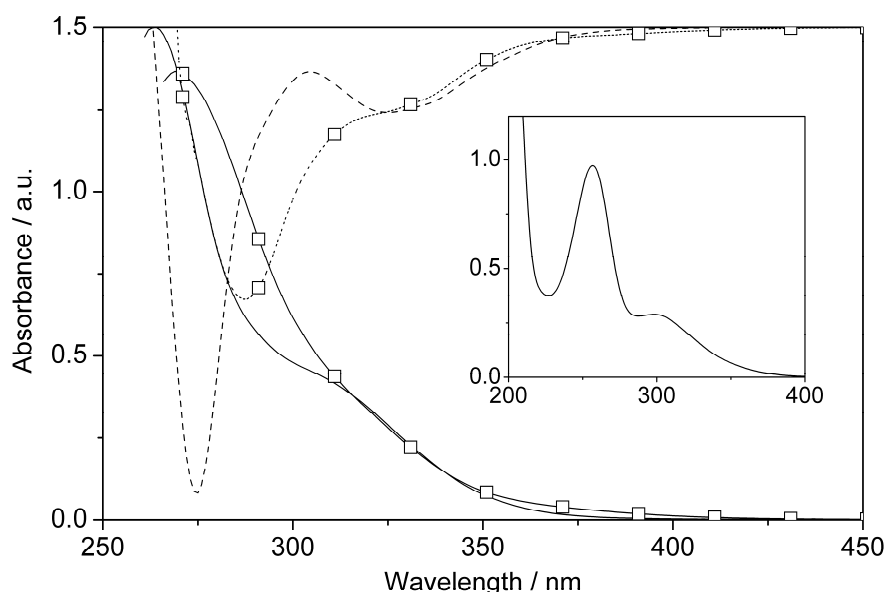
*Figure 5.16. UV/Vis absorption spectra of **Cd17-NH$_2$** in DMSO (–) and DMF (□), concentration for both ca. 0.02 mg/ml. The dashed lines represent 1st derivative curves. Insert: UV/Vis spectrum of HSPh-pNH$_2$ in MeCN.*

DLS measurements (Figure 5.17) confirmed that **Cd17-NH$_2$** crystals are dissolved in in DMSO and DMF and single clusters are present in the solutions (a diameter of ca. 2.3 nm is expected from SC-XRD analysis). However, a low proportion of aggregates with radius 2.5–6.5 nm was present at higher concentration in DMF (insert in Figure 5.17). Interestingly, the mean peak position was substantially higher for DMSO compared with DMF (1.17 vs. 0.73 and 0.79 nm, in DMF, the values are higher than real due to the 0.5 nm evaluation limit), whereas the DMSO value is in better agreement with the supposed cluster size and the size in DMF is too small. However, such discrepancy was observed also for **Cd10a** in solvents where its molecular structure should be identical with the crystal structure (MeCN) and a bigger size was obtained in strongly coordinating DMSO due to particle growth (Chapter 4.1). Thus, it cannot be excluded, that the **Cd17-NH$_2$** cluster grows in DMSO.
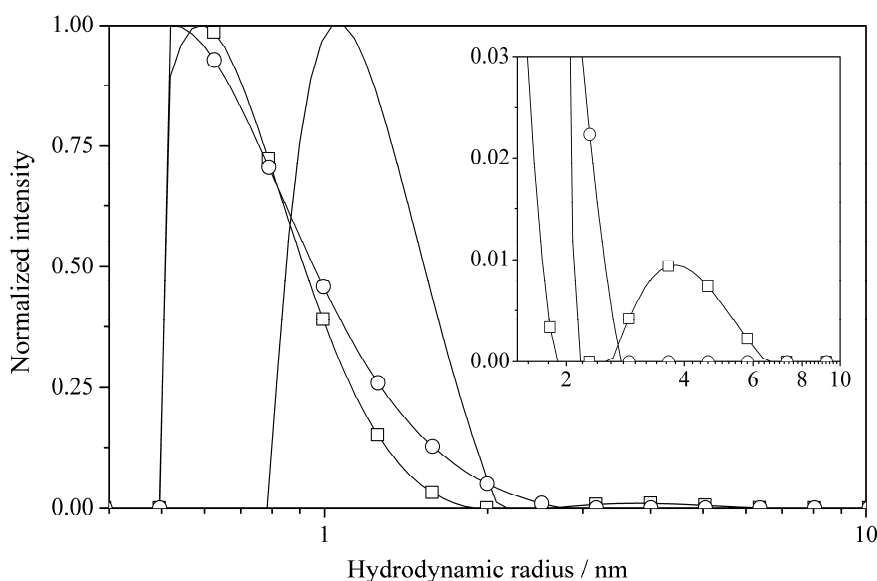
*Figure 5.17. DLS size distribution curves of **Cd17-NH₂** in DMSO (5.5 mg/ml, –) and DMF (17 mg/ml, □, and 8.5 mg/ml, ○).*

NMR characterization of **Cd17-NH₂** was performed in d_6-DMSO (15 mg/ml). First, a 5.5 mg/ml solution in DMSO was prepared which was dried in vacuum after 1 h of mixing, in order to ensure breakage of the 1D chains of clusters and to replace coordinated DMF by DMSO. Then, d_6-DMSO was added. Therefore, a strong DMSO signal ([1]H: 2.54 ppm, [13]C: 40.1 ppm) was present in the spectra, beside the solvent residual peak. ^{1}H NMR and COSY spectra (Figure 5.18 and Figure 5.19) revealed that at least five different –SPh-pNH₂ ligands were present in the solution. The most intense are numbered in the COSY spectrum (Figure 5.19). The ligands 2–5 have broader signals then ligand 1, therefore it can be supposed that ligand 1 is not bound to any cluster species. And indeed, the EXSY spectrum (Figure 5.19), which shows both the dipol-dipol interactions and exchange signals between different ^{1}H nuclei, contains two correlations: 2+5 and 3+4, but none involving ligand 1. This means that ligands within these pairs exchange or are located close to each other. The HSQC spectrum did not resolve the different ligands. All of the aromatic protons in the *ortho* position to S showed HSQC correlation to resonances at 132.7–133.5 ppm ([1]H: 6.54–7.09 ppm), protons in the *ortho* position to N to resonances at 113.8–114.0 ppm ([1]H: 6.04–6.53 ppm). The number of ligands is not in agreement with the molecular structure in solution if a cluster with composition $[Cd_{17}S_4(SPh\text{-}p\text{NH}_2)_{24}(DMSO)_4]^{2+}$ is expected. Two different ligands would be expected in this case with a ratio 1:1 (12 bridging ligands bound to the apical Cd atoms and 12 bridging ligands located on the faces of the cluster tetrahedron). For example, ligands 3 and 4 could belong to the supposed Cd17 cluster (since their intensity is almost equal and they show correlation through space). The origin of the other ligands cannot be explained so far, but a cluster rearrangement due to strongly coordinating solvent (Chapter 4.1) is very probable.
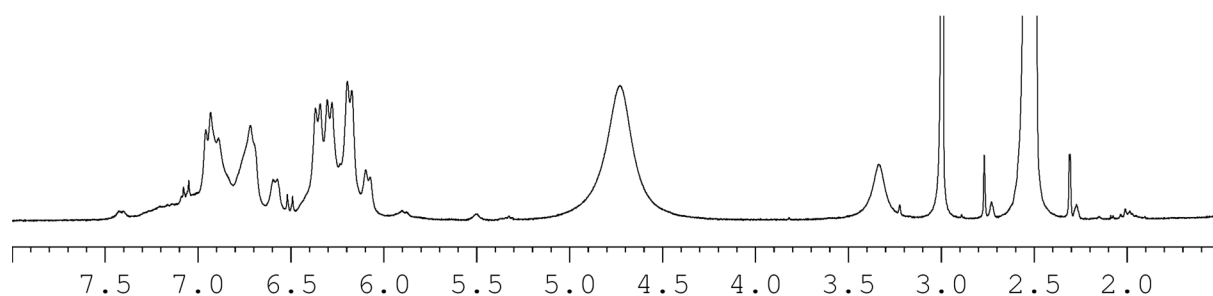
*Figure 5.18. ^{1}H NMR spectrum of **Cd17-NH$_2$** in d_6-DMSO (15 mg/ml).*
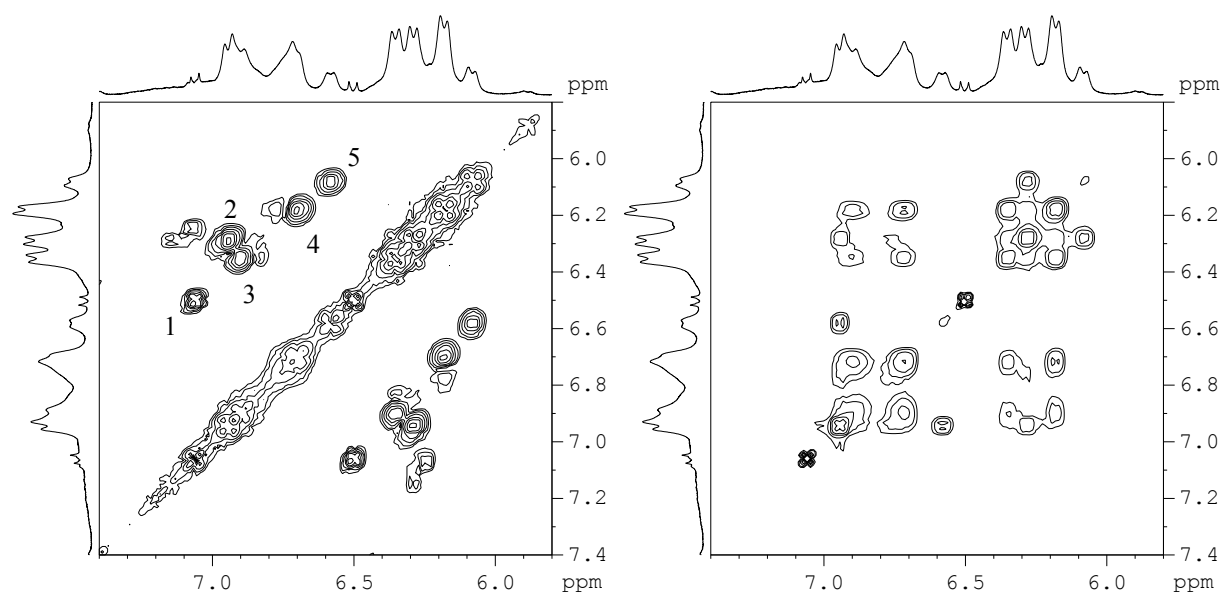
*Figure 5.19. COSY (left) and EXSY (right) NMR spectra of **Cd17-NH$_2$** in d_6-DMSO (15 mg/ml). The correlation peaks in COSY are numbered in the same way as different kinds of ligands in the text.*

Beside this, only one broad resonance for amino groups was observed in the ^{1}H NMR spectrum (4.73 ppm). Its integrated intensity corresponds well with the intensity of aromatic protons (2.0:4.1). A strong resonance at 2.99 ppm (^{13}C: 41.7 ppm) was also observed. This was assigned to coordinated DMSO, since it showed a correlation in the EXSY spectrum to the free DMSO and solvent residual peak. Its integrated intensity revealed a ligand:DMSO ratio of 24:6.1, thus coordinated DMSO is in slight excess compared with the ideal structure. However, not only the ideal cluster structure is present in solution. The coordinated DMSO is thus lowfield shifted by 0.45 ppm compared with free DMSO, which is in good agreement with the deshielding effect of Cd: ^{1}H lowfield shift of –OH groups directly coordinated to Cd of ca. 2 ppm[68] and ca. 0.2 ppm lowfield shift of DMSO coordinated to Ru.[142]

The ^{113}Cd NMR spectrum showed the presence of at least 6 different signals: at 623, 617, 578, 577, 495, 493 ppm with integrals 1.00:0.46:0.79(1:1):0.85(3:2) (the ratios in parentheses belong to the coincided resonances at 578, 577 and 495, 493 ppm, respectively, see Figure 5.20). The supposed [Cd$_{17}$S$_4$(SPh-pNH$_2$)$_{24}$(DMSO)$_4$]$^{2+}$ cluster in solution should have three different Cd sites with coordination Cd(SPh-pNH$_2$)$_3$(DMSO)$_1$, CdS$_1$(SPh-pNH$_2$)$_3$, and CdS$_4$ with ratio 4:12:1. The first two would be expected at ca. 580 and 620 ppm, the last one

at ca. 740 ppm (see Chapter 4.2.2). The CdS_4 site does not have to be observed necessarily due to its long relaxation time. It is clear that the number of observed signals is higher then expected. However, some of the resonances can be assigned to the supposed Cd17 cluster: at 623 and 578 or 577 ppm, and a ratio of 10:4 would be achieved. The other signals belong probably to other species; signals at 495 and 493 ppm would belong to Cd which is coordinated by DMSO to a higher extent.
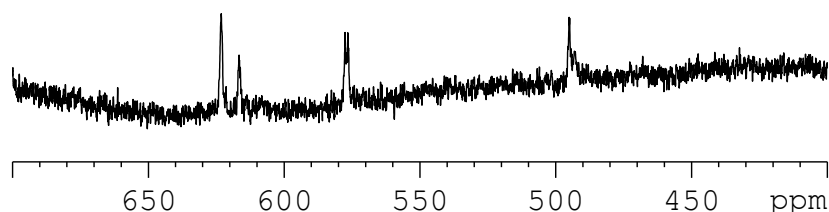
*Figure 5.20. ^{113}Cd NMR spectrum of **Cd17-NH$_2$** in d$_6$-DMSO (15 mg/ml).*

The NMR characterization of **Cd17-NH$_2$** in d$_6$-DMSO revealed that a cluster with supposed molecular structure $[Cd_{17}S_4(SPh\text{-}pNH_2)_{24}(DMSO)_4]^{2+}$ is present in solution. With high probability, however, other species are also present. Their origin could not be elucidated. It is supposed that DMSO causes a similar rearrangement reaction of **Cd17-NH$_2$** as in the case of **Cd10a** (Chapter 4.1) and that additional signals observed in ^{1}H and ^{113}Cd NMR spectra belong to the formed products. Thus, the **Cd17-NH$_2$** cluster is not stable in solutions of strongly coordinating solvents (DMSO and DMF) and not soluble in weakly coordinating ones (MeCN). Therefore, it cannot be utilized for further reactions and should not be considered a useful functionalized cluster.

5.2.3 Conclusions

In this chapter, the ways of preparing clusters functionalized by amino groups were investigated. Two methods were chosen: exchange reactions with HSPh-pNH$_2$ on **Cd10a** cluster and direct synthesis of a CdS cluster in the presence of HSPh-pNH$_2$.

The exchange reactions could be performed only in MeCN as relatively weakly coordinating solvent, because in other solvents (DMSO, DMF) the cluster structure would be changed (see Chapter 4.1). The exchange was performed on 4–10 mg/ml solutions and with slight excess of HSPh-pNH$_2$ at room temperature. A white precipitate was formed, which was soluble in DMSO and DMF. This was attributed to a successful exchange reaction concomitant with coordination of amino groups to neighboring clusters, which can be broken by strongly coordinating solvents. Therefore, the direct exchange of stabilizing ligands of **Cd10a** with HSPh-pNH$_2$ is not a good way of obtaining clusters functionalized with amino groups.

The direct synthesis of a CdS cluster in the presence of HSPh-pNH$_2$ was aiming to obtain a Cd10 cluster. However, syntheses similar to the Dance *et al.*[47] for **Cd10a**, which were performed in DMF/MeOH mixtures, led to formation of a Cd17 cluster: {[Cd$_{17}$S$_4$(SPh-

*p*NH$_2$)$_{24}$(DMF)$_2$]X$_2$}$_\infty$ (**Cd17-NH$_2$**). It was characterized by SC-XRD which revealed the presence of 1D chains of Cd17 clusters connected by two amino groups of neighboring ligands. However, the overall charge of each cluster was +2 and the corresponding anions (X) could not be identified. A lot of void space in the structure (ca. 33 %) presumes that the missing anions could be located there (*e.g.* nitrate which was used during the synthesis). Crystals of **Cd17-NH$_2$** were soluble in strongly coordinating solvents: DMSO, DMF, but not in pyridine. Their DMSO and DMF solutions were characterized by means of UV/Vis and DLS measurements. DLS revealed that single clusters were present in both solutions. However, the size in DMSO was substantially higher which could indicate that the cluster already underwent rearrangement due to the solvent coordination effect. The same conclusion was made from different NMR measurements, since part of the observed signals could be satisfactorily assigned to the supposed molecular structure of **Cd17-NH$_2$** in DMSO solution, but the remaining signals could not be identified. Thus, **Cd17-NH$_2$** is not a suitable compound for further functionalization because it requires dissolution in strongly coordinating solvents, upon which its molecular structure is changed.

Thus, both ways of preparation of clusters with amino groups on the surface failed on the natural ability of amino groups to coordinate to Cd. This ability could be partially weakened by using amides instead of amines, *e.g.* HSPh-*p*NHCOCH$_3$ instead of HSPh-*p*NH$_2$. Surprisingly, HSPh-*p*NHCOCH$_3$ was not soluble in MeCN and therefore, not suitable for reactions in the first approach. However, if the reaction conditions are tuned properly, both exchange reactions and direct cluster synthesis could lead to desired clusters. Then, the same or similar approach could be used for synthesis of clusters capped by –SPh-*p*NHCOC=CH$_2$(CH$_3$) which could be suitable for radical polymerization.

5.3   Possibility of Radical Polymerization in the Presence of CdS Clusters

As already mentioned in Chapter 2.2.1, it is necessary to investigate the possibility of radical reactions in the presence of CdS clusters, since the data presented in literature are not explicit. CdS clusters could be degraded in the presence of radicals or could quench the radicals, which are both undesirable effects for successful covalent incorporation of clusters into a polymeric matrix by means of radical polymerization.

In this chapter, the results on the possible radical polymerization in the presence of CdS clusters will be summarized. These are preliminary investigations and further research would be necessary.

$(NMe_4)_4[Cd_{10}S_4(SPh)_{16}]$ (**Cd10a**) was chosen as a model CdS cluster, since its behavior in solution was well understood (see Chapter 4.1). The following reaction conditions were used:

- water- and oxygen-free atmosphere, protection from sunlight: in order to exclude oxidation and photodegradation effects,
- MeCN as solvent: as relatively weakly coordinating solvent it allows cluster dissolution,
- cluster concentration 8–10 mg/ml in MeCN: cluster solubility limit,
- methyl methacrylate (MMA) as monomer: monomer and polymer are soluble in MeCN, they should not strongly coordinate to the cluster,
- azobisisobutyronitrile (AIBN) as initiator: soluble in MeCN, thermal initiator with relatively low decomposition temperature ($T10 = 65\ °C$),[143]
- reaction time, temperature = 16 h, 60 °C: this should be relatively mild reaction conditions for **Cd10a** in MeCN, AIBN conversion was calculated as 42 % (see Appendix 9.2),
- cluster:monomer:radical = 1:99:1 (**Cd10a**:MMA:AIBN = 24.6:73.9:1.5 wt%): this is relatively high cluster proportion (wt%) for an inorganic-organic hybrid material, but if the cluster has an influence on the radical polymerization, it should become easily evident with such a high amount.

These reaction conditions are comparable with those used for preparation of inorganic-organic hybrid materials by radical polymerizations of Zr oxo clusters with MMA, only the cluster wt% is much higher (ca. 10 wt% in Ref. 116). However, the rate of radical formation is relatively low at this temperature taking into account that radical polymerizations are usually performed around temperatures of 1 h half life which is 81 °C for AIBN.[144] Thus, higher polydispersities are to be expected for the chosen reaction conditions. On the other hand, this experiment is aiming at preparation of polymers cross-linked by clusters, where problems with gelation times arise due to high radical concentration and presence of cross-linking units.[116] Hence, low initiator decomposition rate could be of advantage later.

Prior to the intrinsic radical polymerization in the presence of the **Cd10a** cluster, it had to be verified how particular reactants of the system interact with each other. Thus, experiments RP1–7, summarized in Table 5.9, were performed.

*Table 5.9. Summary of experiments leading to radical polymerization in the presence of the **Cd10a** cluster (RP8). Reaction conditions: 60 °C, 16 h, c_{Cd10a} = 8–10 mg/ml, c_{MMA} = ca. 26 mg/ml, rad. = radicals produced from AIBN with calculated conversion 42 %.*

Sample	Components	Mol. ratio	Characterization	Result
RP1	**Cd10a**	–	^{1}H NMR, UV/Vis	partial rearrangement, formation of Cd54
RP2		1:0.2(0.25)	^{1}H NMR, UV/Vis	partial rearrangement, formation of bigger clusters
RP3	**Cd10a**, rad. (AIBN)	1:1(1.2)	^{1}H NMR, UV/Vis	partial rearrangement, formation of bigger clusters
RP4		1:16(19)	dif. NMR, UV/Vis	complete rearrangement, formation of bigger clusters
RP5	MMA	–	^{1}H NMR	no change
RP6	**Cd10a**, MMA	1:99	^{1}H NMR	cluster similar to RP1 and RP2, MMA did not change
RP7	MMA, rad. (AIBN)	99:1(1.2)	^{1}H NMR, GPC	polymerization
RP8	**Cd10a**, MMA, rad. (AIBN)	1:99:1(1.2)	^{1}H NMR, GPC, UV/Vis	polymerization as in RP7, cluster as in RP2

5.3.1 Preliminary Experiments

The experiments performed prior to polymerization with the cluster can be divided into three groups (Table 5.9):

i.   **Cd10a** alone (RP1),

ii. **Cd10a** + radicals (RP2–4),

iii. **Cd10a** + MMA (RP5, RP6).

The first deals with the rearrangement reaction of **Cd10a** in MeCN at the chosen reaction conditions, as discussed in Chapter 4.1. In the second group, the influence of radicals on the stability of **Cd10a** was investigated. In the third group, the stability of **Cd10a**, especially of its PhS$^-$ ligands, in the presence of an unsaturated organic compound (like MMA) was examined at room temperature and at the used reaction conditions.

The UV/Vis and ^{1}H NMR spectra of the rearrangement of **Cd10a** alone at 60 °C/16 h are depicted in Figure 5.21 and Figure 5.22. Using these data, its conversion was calculated to 13 and 12 %, respectively (Table 5.10, see Appendix 9.1 for more details of the calculation from UV/Vis absorption). Similarly to the rearrangement at 75 °C/21 h (Figure 4.8), an absorption maximum at 350 nm in the UV/Vis spectrum indicated that a low proportion of a Cd54 cluster was present after the heating, which was calculated to ca. 6 wt% from the overall amount of **Cd10a**. The spectrum changed also in the range of **Cd10a** absorption. Whereas a sharp maximum and shoulder were observed at 256 and 290 nm before heating, samples after heating (75 °C/21 h and 60 °C/16 h) show the two features "merged" together (Figure 4.8).

This is associated with the formation of a $[Cd(SPh)_x(MeCN)_y]^{(2-x)}$ byproduct (see Chapter 4.1 and Appendix 9.1).

The rearrangement extent, and amount of formed Cd54 cluster, are substantially lower than at 75 °C/21 h (26–27 % and 12–13 %). Thus the chosen reaction conditions are relatively mild for the cluster and can be used for radical polymerization. However, the cluster rearrangement has to be taken into account.

*Table 5.10. Comparison of **Cd10a** conversion calculated from UV/Vis and ^{1}H NMR spectra for diverse experiments, UV/Vis values in the presence of radicals being overestimated.*

Reaction conditions	Sample	**Cd10a**:radical(AIBN) (mol. ratio)	UV/Vis conversion / %	^{1}H NMR conversion / %
75 °C / 21 h	–	1:0	26	27
60 °C / 16 h	RP1	1:0	13	12
	RP6	1:0	–	10
	RP2	1:0.2(0.25)	26	14
	RP3	1:1(1.2)	47	40
	RP4	1:16(19)	100	100
	RP8	1:1(1.2)	35	17
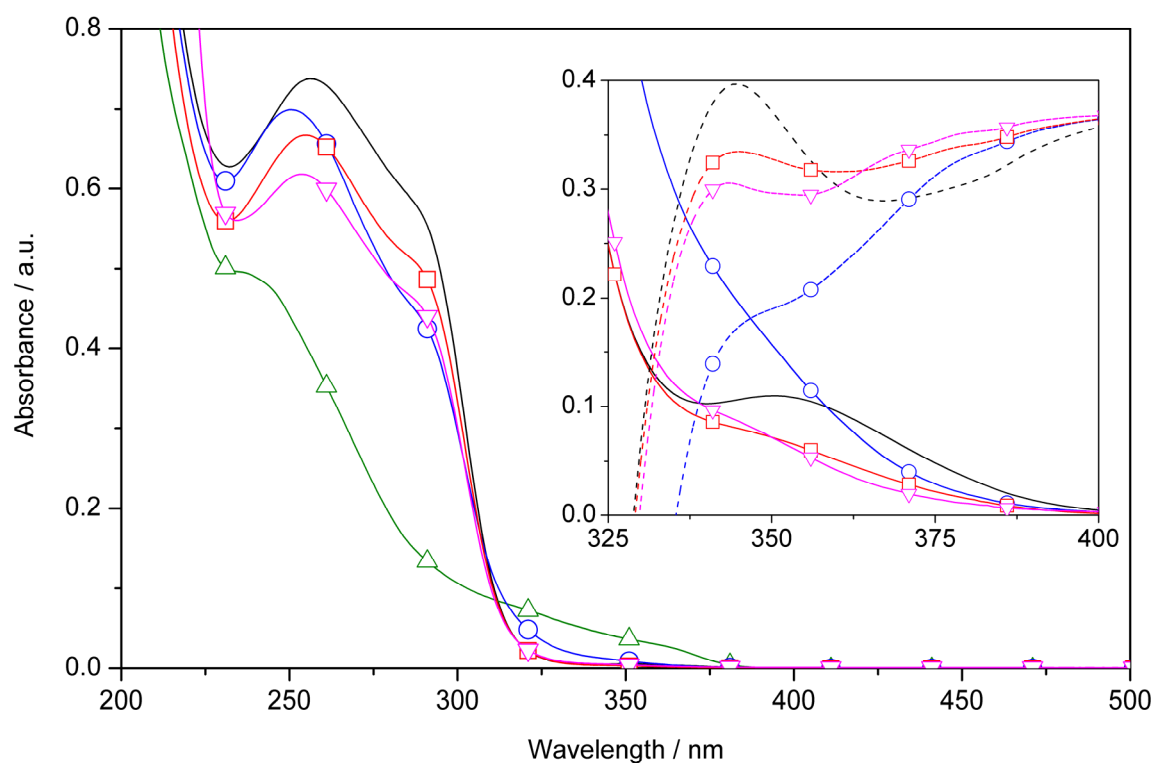
*Figure 5.21. UV/Vis absorption spectra of samples RP1 (–), RP2 (□), RP3 (○), RP4 (△), RP8 (▽). A concentration 0.010 mg/ml (insert 0.20 mg/ml) of **Cd10a** was used. Dashed curves represent first derivatives of the absorption curves.*
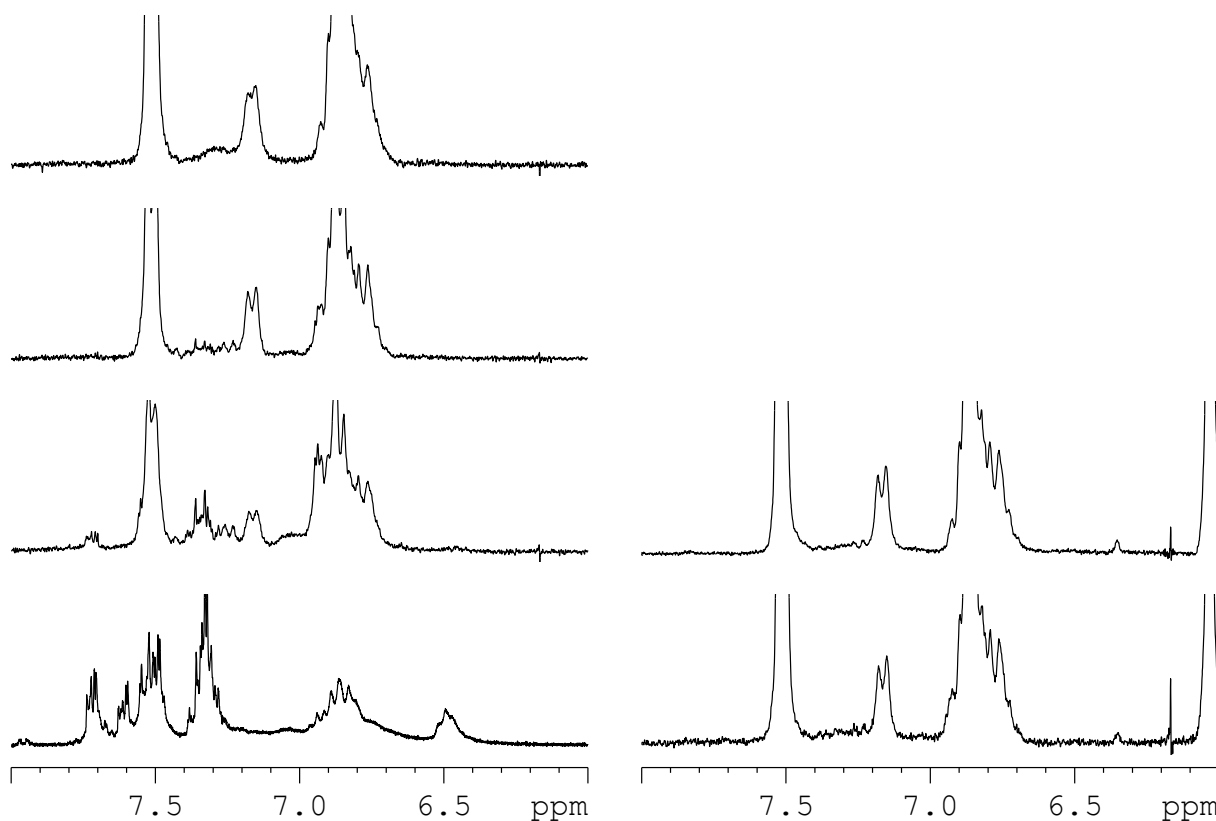
*Figure 5.22. ^{1}H NMR spectra of samples heat-treated with increasing concentration of AIBN: RP1, RP2, RP3, and RP4 (left, down from top), in the presence of MMA (RP6) (right up), and after the radical polymerization (RP8). Area of **Cd10a** PhS signals is depicted.*

In the second group, the **Cd10a** cluster was heat-treated in the presence of AIBN (RP2–4). The UV/Vis (Figure 5.21) and NMR (Figure 5.22) spectra differed to the spectra of **Cd10a** in the absence of radicals (RP1). In the UV/Vis spectra, formation of small amount of bigger clusters was obvious, which increased with increasing initiator concentration. The absorption features were not as distinguished as for pure **Cd10a** and only indistinctive shoulders at around 350 nm were visible. Differences were observed also in the range of **Cd10a** absorption. Whereas for pure **Cd10a** the sharp maximum and shoulder at 256 and 290 nm are "merged" after heating due to the presence of $[Cd(SPh)_x(MeCN)_y]^{(2-x)}$ (Figure 4.8), this is not the case when radicals are present. Other features were observed instead: (a) the absorption at 256 nm increased compared to the absorption at 290 nm from the ratio of 1.28 for pure **Cd10a**, through 1.35 and 1.59 for samples RP2 and RP3, to the ratio of 2.86 for sample RP4 and (b) the maximum at 256 nm shifted to lower wavelengths (255, 250, and 235 for RP2–4). This could be caused by formation of other byproducts than $[Cd(SPh)_x(MeCN)_y]^{(2-x)}$. This conclusion is supported also by calculation of the **Cd10a** conversion from UV/Vis data which led to negative concentration of $[Cd(SPh)_x(MeCN)_y]^{(2-x)}$ for all radical samples (see Appendix 9.1).

Additionally, when the UV/Vis spectrum of the sample with high initiator concentration (RP4), with complete conversion of **Cd10a**, is compared with spectra of the Cd54 cluster and of a mixture of clusters and NPs (sample B2, Chapter 4.1) (Figure 5.23), the similarity is

obvious. The absorption edge of the sample RP4 and Cd54 match almost exactly (370 and 372 nm), meaning that the biggest clusters in sample RP4 are Cd54 clusters. However, smaller clusters are also present. In contrast, sample B2 contains also bigger NPs with an absorption edge at 392 nm. The shoulder/maximum at 235, 240, and 251 nm in RP4, Cd54, and B2 originates from a higher order excitonic transition which is also size dependent,[10] being in good agreement with particle sizes deduced from the first order band gap transition. Thus, the spectrum of sample RP4 contains with high probability only features from CdS clusters and not from other species. This explains also the subsequent shift of the maximum from 255 to 235 nm and the increase of absorption at 256 nm compared with 290 nm with increasing initiator concentration. Thus, calculation of the **Cd10a** conversion was performed only with **Cd10a** and Cd54 (summarized in Table 5.10, see also Appendix 9.1). The data show that the cluster rearranges to a higher extent at higher radical concentration, similar to the values obtained from ^{1}H NMR data (Table 5.10). However, the conversions were higher than those from ^{1}H NMR, which might be due to use of pure Cd54 absorption spectrum although also smaller clusters were present in the samples, or due to calculation with only two wavelengths separated only by 20 nm. Thus, more accurate calculation would be necessary.

Figure 5.23. UV/Vis absorption spectrum of sample RP4 (–) compared with spectrum of a Cd54 cluster in THF (□) and NPs from sample B2 (Chapter 4.1) in MeCN (○). Concentration ca. 0.01 mg/ml, insert ca. 0.05 mg/ml was used. Dashed curves represent first derivatives of the absorption curves.
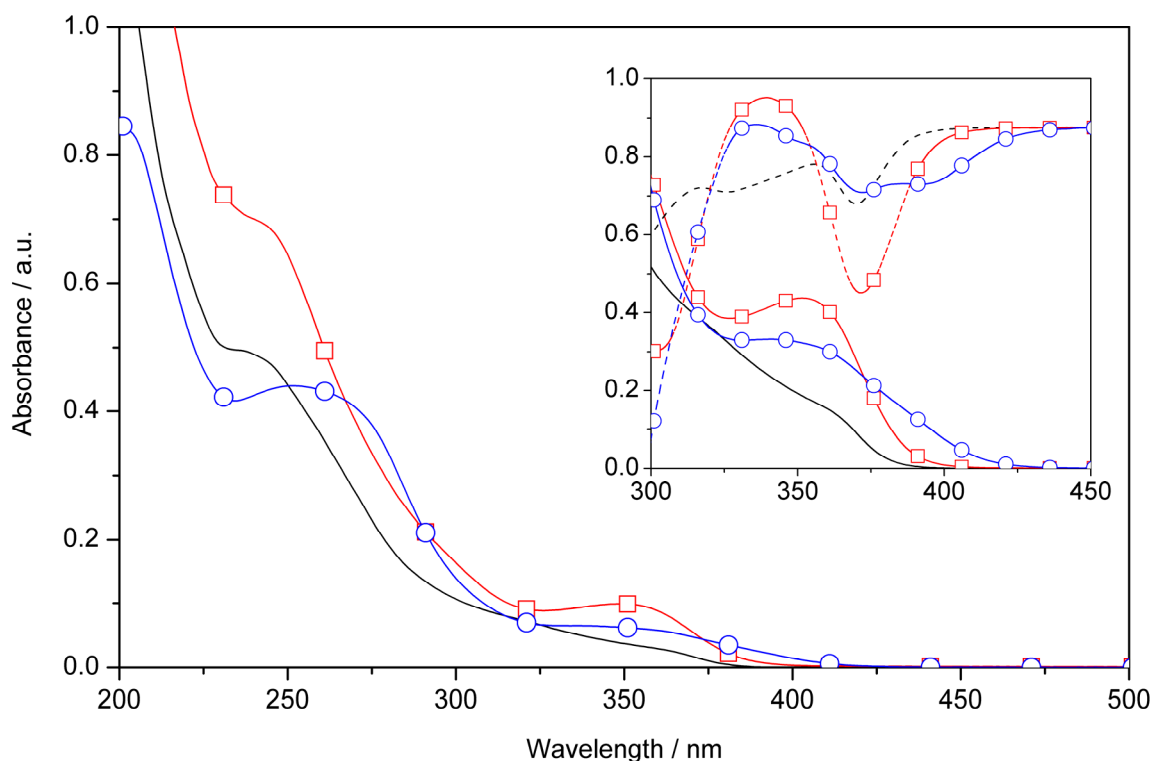
More details could be obtained from the ^{1}H NMR spectra of samples RP2–4 (Figure 5.22). With increasing initiator concentration, more intense signals of some byproducts were present in the spectra. The cluster conversion was calculated from the integrals of the *ortho*-protons of the terminal and bridging PhS groups by comparison with the integral of the whole aromatic part. The results are summarized in Table 5.10 and show clearly that the proportion of rearranged **Cd10a** increases with increasing initiator ratio. Additionally, a downfield shift of the NMe$_4^+$ protons with increasing initiator concentration was observed, from 2.95 through 2.97 to 3.04 ppm.

The sample RP4 was investigated also by COSY, HSQC, and HMBC correlations. The signals in the aromatic part of the ^{1}H NMR spectrum might be divided into sharp and broader signals. The sharp would belong to some byproducts which are not bound in complexes or clusters (> 7.2 ppm), whereas the broader would be coordinated on the cluster surface (< 7.1 ppm and at ca. 7.55 ppm). From the byproducts with sharp signals, only the presence of PhSSPh could be deduced with high probability [7.54 (d, 2 H), 7.36 (t, 2 H), 7.31 (t, 1 H) ppm] from ^{1}H, COSY, and HSQC spectra. Additionally, two other aromatic byproducts were present which could not be identified by means of NMR. In the samples with lower radical ratio (RP2 and RP3), the presence of PhSSPh is also very probable, but some of the other byproducts were not observed.

The presence of PhSSPh was expected. Formation of disulfides was previously observed in deaerated solutions of CdS NPs as a result of photodegradation processes.[21,24] Simultaneously, bigger NPs were formed due to destruction of the ligand shell.[21,24] This is in very good agreement with the present conclusion. However, thiophenolate-capped CdS clusters (Cd1, Cd4, and Cd10) form other decomposition products upon illumination: thianthrene, dibenzothiophene, and thiophenol (Scheme 2.1).[67] These, or some of them, might be expected also in the reaction of **Cd10a** with radicals. NMR is no suitable technique for their identification, but investigation by means of mass spectroscopy would be helpful.

Another interesting part of the ^{1}H NMR spectra of samples containing AIBN is around 2 ppm (Figure 5.24), where decomposition products of AIBN resonate. Sample RP4 was investigated also by COSY, HSQC, and HMBC, thus hints on the character of the AIBN decomposition products were obtained. All samples showed the following signals in this ppm range after heating: solvent residual peak (1.94 ppm), AIBN (1.68 ppm), water (2.14–2.16 ppm, confirmed by absence of HSQC correlation signal), an unknown peak A (2.09 ppm), and an unknown peak B (1.47 ppm). In the sample RP4, A, B, and AIBN signals had shoulders and additional small signals were present at 1.82, 1.80, 1.59, 1.55, 1.53, 1.28, and 1.25 ppm. ^{1}H-^{13}C correlations of AIBN, A, and B signals are summarized in Table 5.11. Correlations of AIBN and signal B are easy to follow and are similar to each other. Only shifts of the tertiary carbon are different, namely downfield shifted in AIBN due to the deshielding effect of the azo group. On the other hand, peak A shows HMBC correlation to a ^{13}C signal at 207.6 ppm which might belong to an aldehyde, ketone, or allene, all of them being quite improbable. However, well known cage reactions of an initiator radical pair formed from AIBN lead to ketenimine formation, which is the major byproduct (Scheme 9.1 in Appendix).[145] Such a ketenimine would have ^{13}C NMR shifts corresponding

to the observed 207.6 ppm, but should also show another shift at 50–70 ppm,[146] which was not present in the HMBC correlation spectrum. Thus, the most probable structure elements responsible for signals A and B are shown in Table 5.11. The probability of cage reactions depends on the rate of radical diffusion from each other and influences the initiator efficiency. In addition, the intensity of the water signal increased during heating in all samples containing radicals. This might be an indication that the samples contained traces of O_2 which could react with radicals and form some –OH species.
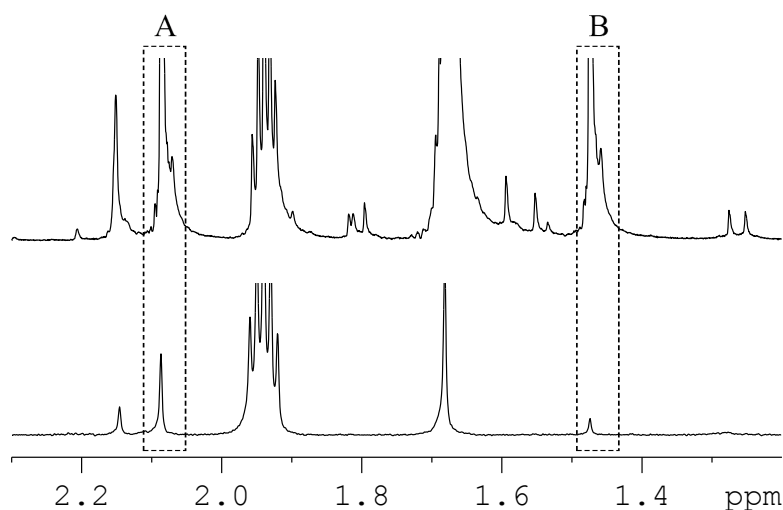
*Figure 5.24. ^1H NMR spectra of samples with **Cd10a**:radical ratios of 1:16 and 1:1 (RP4 and RP3) in the range of AIBN products. The byproducts A and B are emphasized.*

Table 5.11. ^1H-^{13}C NMR correlations in the sample RP4, NMR shifts in ppm.

^1H NMR compound	shift	HSQC shift	assignment	HMBC shift	assignment	Structure element
AIBN	1.68	25.3	–CH$_3$	69.2 120.6	*tert.* C –CN	
A	2.09	30.9	–CH$_3$	207.6	aldehyde, ketone, or allene	
B	1.48	23.0	–CH$_3$	40.5 123.4	*tert.* C –CN	

In sample RP4, many small crystals, which were colorless, plate-like, hexagonally-shaped and bright in polarized light, were formed during the heat treatment. Unfortunately, only their cell parameters could be obtained by SC-XRD: hexagonal P, 8.58, 21.83 Å or orthorhombic C, 8.58, 14.85, 21.83 Å and the structure could not be solved.

In conclusion, the presence of radicals influences rearrangement processes of the **Cd10a** cluster substantially. Other mechanism and higher conversions were observed with increasing initiator concentration. The ratio cluster:AIBN = 1:19 led to complete disappearance of **Cd10a** and formation of Cd54 and smaller clusters and of oxidation byproducts like PhSSPh and others. It has to be concluded that the presence of high radical concentration is dangerous for the **Cd10a** cluster, which is not unexpected. However, smaller concentrations appear to be relatively harmless. Thus, radical polymerization should be performed with lower initiator concentration.

In the third group, possible changes of MMA in the presence or absence of **Cd10a** at room temperature and during the heat treatment were investigated by ^{1}H NMR (RP5 and RP6). Pure MMA did not change in the course of 2 days at room temperature and after heat treatment. Only a solvent residual peak (1.94 ppm) and MMA peaks [6.03 (br, 1 H), 5.60 (p, 1 H), 3.70 (s, 3 H), 1.91 (br, 3 H)] were present. Surprisingly, MMA with **Cd10a** did not show any changes at the same reaction conditions. No signs of the thiol-ene reaction (see Chapter 2.2.1) were observed, only, as expected, ca. 10 % cluster rearrangement (Figure 5.25, Figure 5.22, and Table 5.10). However, the ^{1}H NMR pattern of the aromatic part was more similar to the sample containing radicals (RP2) than to pure **Cd10a** (RP1). Only solvent residual peak, MMA, and **Cd10a** peaks (6.6–7.6 ppm for aromatic and 2.95 ppm for NMe$_4^+$ protons) were present in the ^{1}H NMR spectrum. This is an essential experiment since it confirms the relative stability of thiolates containing double bonds and also clusters capped by them, *i.e.* they do not undergo thiol-ene reaction as corresponding thiols do. Eventually, a similar experiment with higher **Cd10a**:MMA ratio (lower amount of MMA) could be useful.
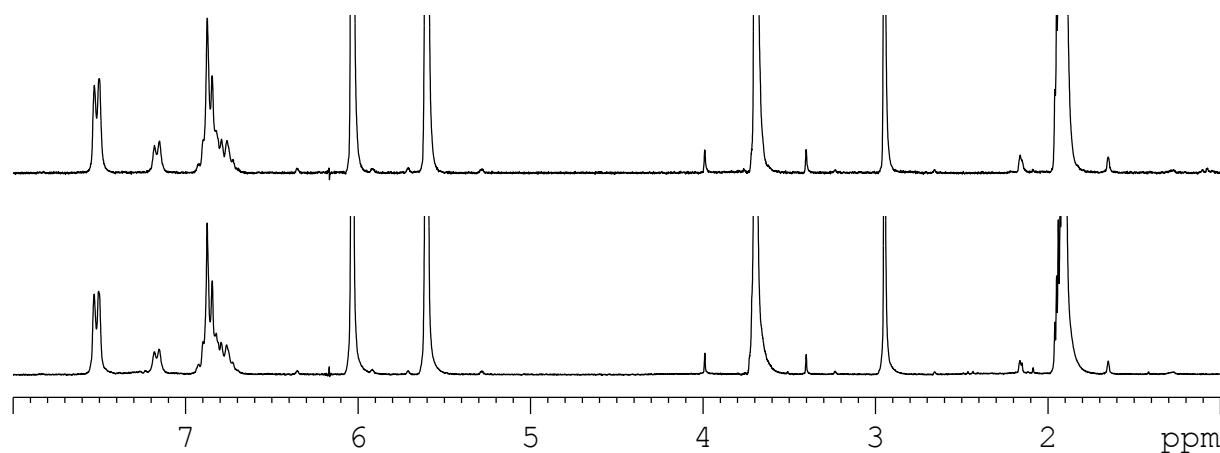
*Figure 5.25. ^{1}H NMR spectra of the sample containing **Cd10a** and MMA (RP6) before (up) and after (down) heating.*

5.3.2 Radical Polymerization with and without Cluster

The preliminary experiments leading to the radical polymerization with the **Cd10a** cluster led to the following conclusions which have to be considered:

- **Cd10a** rearrangement in MeCN of ca. 15 % leads to formation of Cd54 cluster and $[Cd(SPh)_3]^-$-like species.

- The stability of **Cd10a** decreases with increasing initiator concentration. Formation of Cd54 and smaller clusters proceeds by another mechanism than without radicals, namely by destruction of the ligand shell and formation of PhSSPh and other oxidation products.

- The **Cd10a**:AIBN ratio 1:0.25 results in low **Cd10a** degradation of ca. 14 %.

- **Cd10a** is relatively stable in the presence of MMA, confirmed by the absence of any signs of a thiol-ene reaction.

Finally, radical polymerization in the presence of **Cd10a** was performed (RP8). The reaction conditions were equivalent to those of the preliminary experiments and are summarized in Table 5.9. The sample RP8 was a pale yellow solution in which **Cd10a**, its degradation products, and the polymer were dissolved. Questions of interest were whether the cluster quenches radicals, thus whether polymerization is possible and whether the chain length and monomer conversion are influenced by the presence of the cluster, and how the cluster changes during the reaction. In order to answer the first question, a comparison with a polymerization in the absence of cluster (RP7) was necessary. A relatively high proportion of cluster was employed (1 mol%, 24.6 wt%) in order to allow the cluster effect to become evident. High initiator concentration was used (**Cd10a**:AIBN = 1:1.2) although it was shown in the previous part that this leads to relatively high cluster degradation (ca. 40 %). However, another radical "acceptor", present during the polymerization (MMA), could decrease the radical destruction effect on the cluster.

The cluster conversion in sample RP8 was calculated from UV/Vis and ^{1}H NMR spectra (Figure 5.21 and Figure 5.22), similar as in the previous part, to 35 and 17 %, respectively, the UV/Vis value being overestimated. The conversion, band gap absorption features, and ^{1}H NMR spectrum in the aromatic range are very similar to those in sample RP2 with a cluster:AIBN ratio of 1:0.25. This means that the radical destruction effect was indeed decreased in the presence of MMA. Such a cluster degradation could be acceptable.

To elucidate the cluster influence on radical quenching and on the course of the polymerization, the ^{1}H NMR spectra of samples with and without the cluster after polymerization were compared first (Figure 5.26). The spectra are almost identical in the range 0–6.5 ppm. Shifts for solvent, MMA, AIBN and its decomposition products A and B (see Table 5.11) are identical with those described in the previous part. The chemical shift for NMe_4^+ also did not change much (2.95 ppm). However, new signals arose which originate from PMMA. They are all broad and have identical chemical shifts and intensities for both samples RP7 and RP8 (intense: 3.59, 1.83, 1.01, 0.81 ppm, and less intense: ca. 1.99, 1.50, 1.35, 1.22 ppm). The MMA conversion was calculated using the decay of =CH_2 integrals (at

6.03 and 5.60 ppm) compared with the constant integrals of the –OMe groups (at 3.70 and 3.59 ppm). Values of 47 and 46 % for samples RP7 and RP8 were obtained.
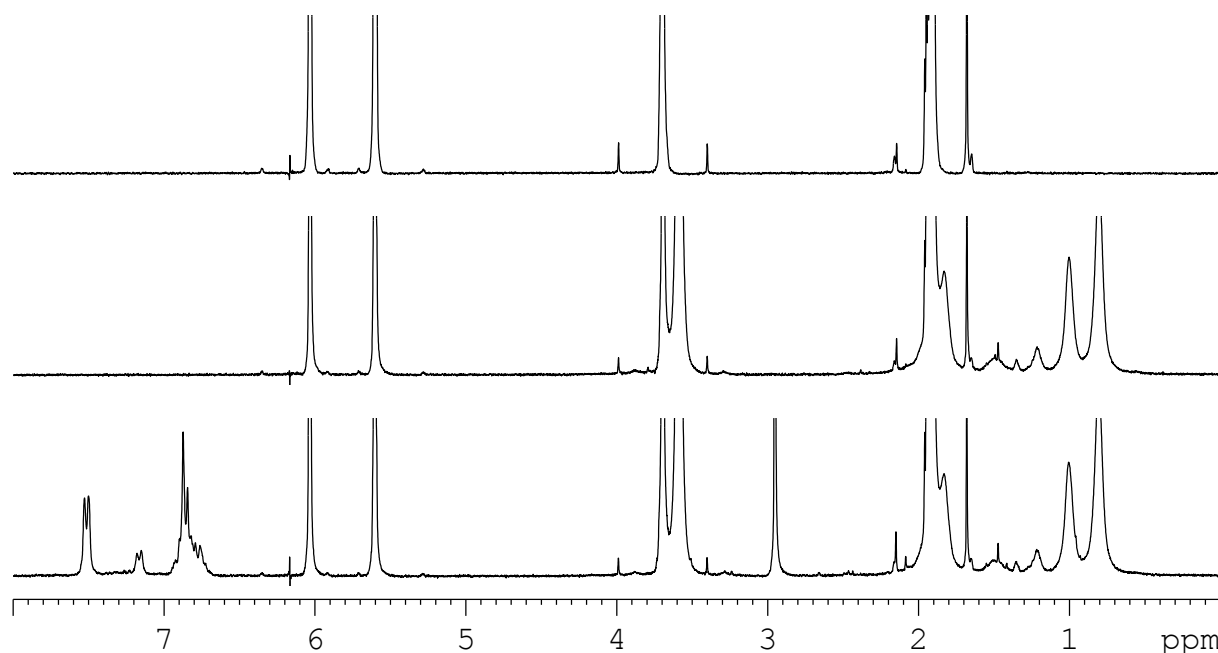
*Figure 5.26. ^{1}H NMR spectra of samples before radical polymerization without **Cd10a** (top, RP7) and after radical polymerization without (center, RP7) and with (bottom, RP8) **Cd10a**).*

It thus appears very promising that the presence of the **Cd10a** cluster during a radical polymerization does not have a great influence on the course of polymerization. To obtain more information, the chain length of PMMA in samples RP7 and RP8 was measured by gel permeation chromatography (GPC). To this end, the solvent was evaporated from the solutions RP7 and RP8, the residue was dissolved in THF (**Cd10a** is not soluble and was removed by filtration), and the resulting polymer solutions were measured. The molecular mass distributions are depicted in Figure 5.27. The distribution curves are almost identical for both samples (Figure 5.27), but the sample without cluster (RP7) has a shoulder at highest molecular weights. This difference leads probably to higher number, weight, and Z average molecular weights (M_n, M_w, M_z) and a higher polydispersity index (PDI) for sample RP7 (Table 5.12). What the exact origin of this difference is cannot be stated currently, and more detailed investigation would be necessary. Both samples have a relatively high PDI which could be caused by almost linear time-dependence of radical formation during the polymerization (see Appendix 9.2). However, optimization of the polymerization conditions, which have not been done at this stage, would improve the polydispersity.
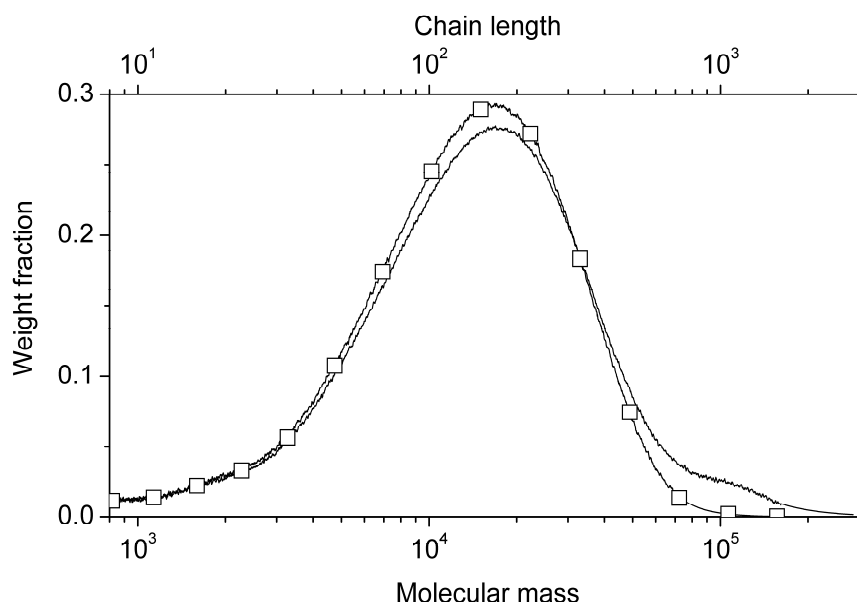
*Figure 5.27. Molecular mass distribution of PMMA prepared by radical polymerization without (RP7, –) and with (RP8, □) the **Cd10a** cluster, determined by GPC.*

*Table 5.12. Comparison of number, weight, and Z average molecular masses and PDI for polymerization without (RP7) and with (RP8) the **Cd10a** cluster.*

Sample	M_n	M_w	M_z	PDI
RP7	9.1	21.5	47.7	2.4
RP8	8.4	17.3	27.5	2.1

At the chosen reaction conditions and reactant ratios, no substantial differences were observed by ^{1}H NMR and GPC between polymerization with and without the cluster, meaning that the cluster does not have a large influence. If the cluster would quench radicals, lower monomer conversion would be expected compared with the sample without cluster, since lower amount of radicals would be available for polymerization. This might be indeed the case since monomer conversion of 46 % was observed for sample with the cluster, whereas 47 % of monomer reacted in the sample without the cluster. In any case, some of the radicals are surely depleted for oxidation of the cluster ligand shell, and therefore such a decrease of available radical concentration is very probable. On the other hand, molecular mass distribution would not be influenced by radical quenching in the low conversion polymerization range. However, a shoulder at high molecular masses in molecular mass distribution curve is missing in the presence of cluster (Figure 5.27). This might indicate that the cluster has an influence on the mechanism of polymerization termination, similarly to polymerizations photoinitiated by CdS NPs.[100] Thus, it seems that if there is any influence of **Cd10a** on radical polymerization, it is very small and does not exclude the possibility of radical polymerization in the presence of **Cd10a**. However, it has to be kept in mind that the components in the system (cluster, radicals) influence each other. Therefore, small effects on

polymerization, as well as on the molecular structure of the cluster are to be expected and are probably unavoidable.

5.3.3 Conclusions

In this part, the possibility of radical polymerization in the presence of CdS clusters was investigated on a model system composed of **Cd10a** as cluster, MMA as monomer, AIBN as initiator, and MeCN as solvent, at 60 °C/16 h. This investigation was necessary since literature dealing with radical polymerizations on or with CdS clusters/NPs is not consistent. Questions which should have been answered were:

− how and to which extent the cluster changes its molecular structure at given reaction conditions and in the presence of radicals,

− whether the cluster is stable in the presence of molecules containing double bonds,

− whether radical polymerization can be conducted in the presence of the cluster and whether it is influenced somehow by the cluster.

The investigation was carried out in several steps in order to find out how particular components of the system interact with each other: (i) pure **Cd10a**, (ii) **Cd10a** with radicals, (iii) **Cd10a** with monomer, (iv) radical polymerization with and without cluster.

(i) Pure **Cd10a** rearranged in MeCN at 60 °C/16 h as expected, however to a relatively small extent (ca. 12 %). This rearrangement proceeds very probably by same mechanism as in DMSO (Chapter 4.1), *i.e.* under formation of byproducts like $[Cd(SPh)_x(MeCN)_y]^{(2-x)}$ and bigger clusters (Cd54).

(ii) **Cd10a** rearranged by a different mechanism in the presence of radicals, by which the ligand shell was oxidized. Disulfide, PhSSPh, was identified by NMR, but other oxidation products were probably also formed. Then, since the cluster was not stabilized sufficiently, it aggregated with other cluster molecules and formed bigger clusters, Cd54 being the biggest one. The rearrangement degree increased with increasing initiator concentration. At a cluster:AIBN ratio = 1:0.25, ca. 14 % of **Cd10a** rearranged. This radical effect on the cluster is not unexpected and cannot be avoided during a radical polymerization, but a degradation degree of 14 % could be acceptable.

(iii) **Cd10a** with MMA monomer showed no signs of a thiol-ene reaction, meaning that thiolates capping a CdS cluster are stable in the presence of a double bond. Thus, clusters capped by thiolates containing double bond should be relatively stable. However, partial rearrangement (ca. 10 %) of the cluster was observed, probably due to the solvent coordination effect.

(iv) No substantial differences were observed by ^{1}H NMR and GPC between radical polymerization with and without the cluster. However, small effects cannot be excluded. Some of the radicals are consumed for oxidation of the cluster ligand shell and thus are not involved in the polymerization. This leads to small lowering of monomer conversion in the presence of cluster (46 vs. 47 %). This, on the other hand, influences the molecular structure of the cluster and leads to its destabilization and formation of bigger clusters, with

a conversion of ca. 17 %. These effects were expected and cannot be avoided. Only a small part of cluster and radicals is involved in these "side" reactions. Therefore, a radical polymerization in the presence of cluster is principally possible.

This means that a weak solvent coordination effect does not play an important role during radical polymerization, but radicals cause destabilization and growth of the cluster. However, the radical effect is not that pronounced that it would cause complete cluster conversion. In the model experiment, only 17 % of the cluster changed its structure. Thus, by careful adjustment of the reaction conditions (reactant ratio, temperature, time) this value could be substantially reduced. On the other hand, a much lower radical concentration might lead to a much less pronounced cluster degradation due to the radical effect and might again favor the solvent coordination effect. This could be possibly avoided using lower temperatures together with low temperature thermal initiators, *e.g.* other dialkyldiazenes (Ph$_3$C-N=N-Ph, PhMe$_2$C-N=N-CMe$_2$Ph), dialkyl hyponitriles (PhMe$_2$C-O-N=N-O-CMe$_2$Ph, tBu-O-N=N=O-tBu), or peroxides (tBuOO-CO-CO-OO-tBu) with T10 = 35, 45, 29, 42, and 26 °C, respectively.[145] All of these parameters might be adjusted in order to decrease cluster rearrangement and obtain higher monomer conversions.

Another conclusion is that clusters stabilized by thiolates can be functionalized by double bonds. This can be achieved either by preparation of the cluster in the presence of the functional ligand (thiolate instead of thiol, "in-situ functionalization") or by functionalizing of existing ligands ("ligand functionalization"). Exchange reactions would not be suitable because of problematic separation of exchanged thiophenolate and functionalized cluster (see Chapter 5.2.1). In-situ functionalization could be performed by modification of the synthesis of the **Cd10a** cluster by using sodium 4-vinylbenzylthiolate (Na-VBT) instead of thiophenol. Na-VBT should be relatively stable and not so difficult to synthesize from 4-chloromethyl styrene via thiourea method.[88,91,147] The synthesis of a Cd10-VBT cluster should be similar to the synthesis of **Cd10a**. Differences might arise from different basicity and nucleophilicity of R–Ph–CH$_2$–S$^-$ compared with PhS$^-$.

Ligand functionalization could be used for clusters containing –OH groups on the surface, like the **Cd17b** cluster if its molecular structure is not much changed in solution (see Chapter 5.1.4). Then the –OH group could be reacted with silanes[83,107] or N-acylimidazoles[110] containing double bonds and used further for radical polymerization. However, the coupling reaction will probably not lead to quantitatively reacted ligands, which would make cluster crystallization and characterization difficult. On the other hand, the number of reactive sites on the cluster could be tuned in this way.

A last opportunity should be mentioned: radical polymerization photoinitiated by a cluster (see Chapter 2.2.1). This might work, but could easily lead to undesired cluster photodecomposition. However, if the e^- acceptor and donor systems are designed carefully (Scheme 2.5), photodecomposition might be avoided. Then no thermal initiation would be necessary, which would eliminate solvent coordination effects and, hopefully, also radical effects on cluster.

6   Experimental Part

6.1   General Techniques and Used Materials

Standard Schlenk techniques were employed for all operations using a double-manifold vacuum line with high-purity dry argon. Oxygen was removed from all solvents using Schlenk and cannula techniques by sparging of argon. Additionally, MeCN, DMSO, DMF, pyridine, CH_2Cl_2, toluene, and THF were dried and purified by standard methods[148] prior to deoxygenation. Most of the chemicals were used as received (Table 6.1). Ac_2O was distilled, dried, deoxygenated and stored at $-20\ °C$. MMA was distilled to remove the stabilizer, dried, deoxygenated and stored at $-20\ °C$ in the dark.

Table 6.1. Summary of chemicals used.

Name	Abbreviation	Supplier	Purity
cadmium nitrate tetrahydrate	$Cd(NO_3)_2 \cdot 4H_2O$	Aldrich	98 %
		Fluka	$\geq$ 99 %
cadmium acetate dihydrate	$Cd(acetate)_2 \cdot 2H_2O$	Aldrich	98 %
cadmium chloride	$CdCl_2$	Acros Organics	for anal.
thiophenol	PhSH	Aldrich	97 %
cyclohexylmercaptane	$C_6H_{11}SH$	Aldrich	97 %
benzylmercaptane	$PhCH_2SH$	Alfa Aesar	99 %
2-mercaptoethanol	$HSCH_2CH_2OH$	Aldrich	$\geq$ 99 %
4-aminothiophenol	HSPh-pNH$_2$	Aldrich	97 %
sulfur	S	Aldrich	reag. grade, subl.
sodium sulfide nonahydrate	$Na_2S \cdot 9H_2O$	Aldrich	$\geq$ 98 %
triethylamine	NEt_3	Fluka	$\geq$ 99.5 %
tetramethylammonium chloride	NMe_4Cl	Aldrich	97 %
sodium perchlorate monohydrate	$NaClO_4 \cdot H_2O$	Aldrich	98 %
sodium nitrate	$NaNO_3$	Aldrich	99 %
sodium tetrafluoroborate	$NaBF_4$	Aldrich	$\geq$ 98 %
acetic anhydride	Ac_2O	Aldrich	$\geq$ 98 %
trimethylchlorosilane	$ClSiMe_3$	Aldrich	$\geq$ 98 %
methyl methacrylate	MMA	Aldrich	$\geq$ 99 %
azobisisobutyronitrile	AIBN	Acros Organics	98 %

6.2 Analytical Techniques

6.2.1 Single Crystal X-Ray Diffraction

Crystals suitable for single-crystal X-ray diffraction (SC-XRD) were taken directly from the reaction solutions, selected in perfluoropolyether oil, mounted on a Bruker AXS SMART diffractometer with an APEX CCD area detector or on a Bruker AXS KAPPA APEX II diffractometer with an APEX II CCD area detector and measured usually in a nitrogen stream at 100 K. Graphite-monochromated Mo-K_α radiation ($\lambda = 71.073$ pm) was used for all measurements. The data collection covered at least a hemisphere of the reciprocal space using $0.3°$ ω-scan frames. The crystal-to-detector distance was 5–6 cm. The data were corrected for polarization and Lorentz effects, and an empirical absorption correction (SADABS) was applied.[149] The cell dimensions were refined with all unique reflections. The structures were solved with direct or Patterson methods (SHELXS97) and refinement to convergence was carried out with the full-matrix least squares method based on F^2 (SHELXL97).[150,151]

The details of structure refinement and data on different crystal structures are summarized in Chapter 6.4. Assignment of labels can be found in Appendix 9.3 (Table 9.3).

6.2.2 Powder X-Ray Diffraction

Powder X-ray diffraction (powder XRD) measurements were performed on a Philips X'Pert Pro diffractometer system [Cu-K_α radiation ($\lambda = 1.542$ Å) equipped with an X'Celerator multi-channel detector, Bragg-Brentano geometry]. The samples were placed on a single-crystal Si wafer sample holder and measured with a rate of $3°$/min.

6.2.3 Small-Angle X-Ray Scattering

Small-angle X-ray scattering (SAXS) measurements and interpretation were performed by Silvia Pabisch and Prof. Peterlik, University of Vienna, with Cu-K_α radiation from a rotating anode generator (Nanostar, BRUKER AXS) equipped with a pinhole camera and an area detector (VANTEC 2000). The SAXS intensity patterns were corrected for background scattering and then radially averaged to obtain the function $I(q)$, where $q = (4\pi/\lambda) \sin\theta$ is the scattering vector, 2θ the angle between incident and diffracted beam, and $\lambda = 0.1542$ nm the X-ray wavelength. The scattering intensities $I(q)$ were fitted with asymmetric Gaussian and Lorentzian functions for the samples with concentration of 10 mg/l (B1 and B3) and 40 mg/l (B2 and B4), respectively (Chapter 4.1.1, Figure 6.1). The maximum and the half-width from the fits in reciprocal space were then converted into NP distances and distribution widths in real space. The evaluation of **Cd10b** scattering curve was based on the Beaucage approach of form and structure factors.[152]
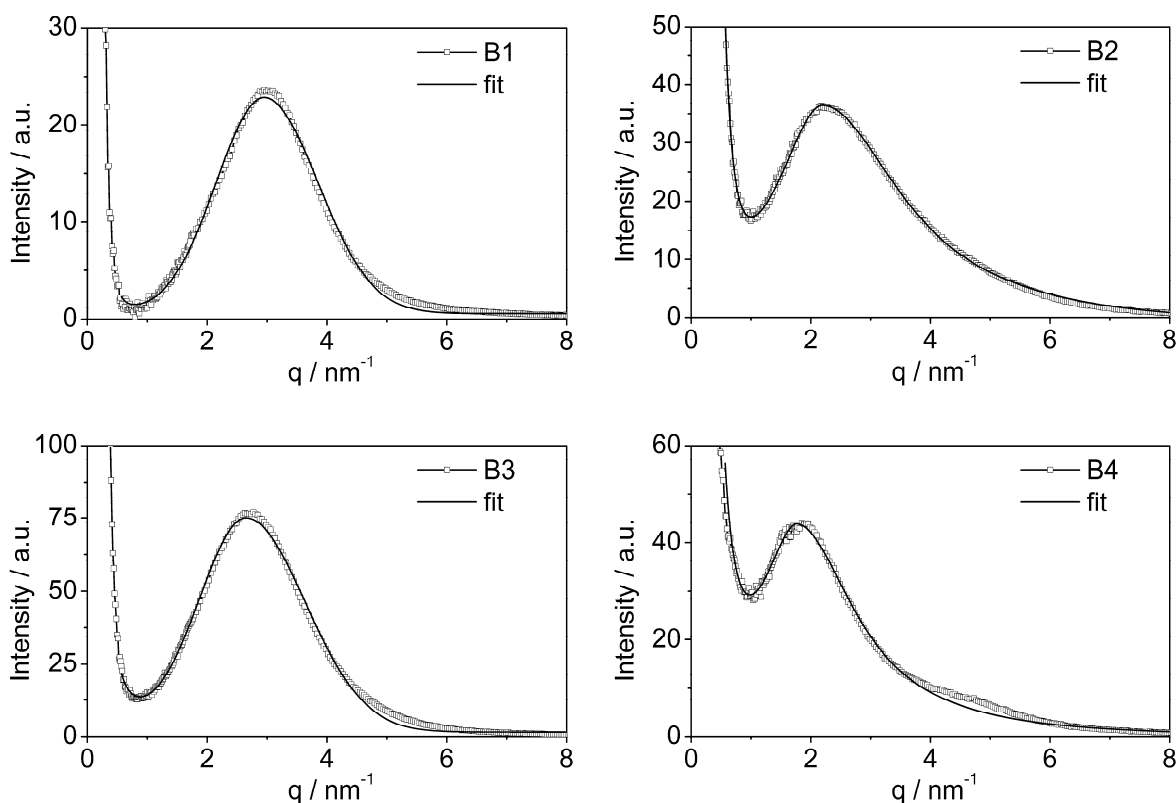
Figure 6.1. Asymmetric Gaussian (left) and Lorentzian (right) fits of SAXS scattering curves for CdS NPs isolated from samples B1, B3 and B2, B4 by addition of toluene (see Chapter 4.1.1).

6.2.4 Nuclear Magnetic Resonance Spectroscopy

Solution NMR spectra were recorded on a Bruker DPX 300 (^{1}H: 300.13 MHz, ^{13}C: 75.47 MHz, ^{113}Cd: 66.61 MHz) and a Bruker AVANCE 250 (^{1}H: 250.13 MHz, ^{13}C: 62.86 MHz) equipped with a 5 mm inverse-broadband probe head with a z-gradient unit. 2D experiments were measured with Bruker standard pulse sequences (COSY (Correlated Spectroscopy), EXSY (Exchange Spectroscopy), HSQC (Heteronuclear Single Quantum Correlation), HMBC (Heteronuclear Multiple-Bond Correlation), ^{1}H-^{113}Cd HMBC). Complex **Cd4b** in d_6-DMSO was measured at concentration 100 mg/ml. **Cd10b** in d_5-pyridine solution was measured at concentration 100 mg/ml, resonance at 443 ppm had FWHM = 2.1 ppm. **Cd10b** in d_6-DMSO was measured at concentration 50 mg/ml before and after heating to 80 °C for 4 h. NMR solvents were purchased from euriso-top in high purity grade and were stored over molecular sieve at argon atmosphere.

Solid state NMR spectra were recorded on a Bruker AVANCE 300 (^{13}C: 75.47 MHz, ^{113}Cd: 66.61 MHz) equipped with a 4 mm broadband MAS probe head. ^{13}C NMR spectra were recorded with ramped CP/MAS (Cross Polarization and Magic Angle Spinning) and ^{113}Cd NMR spectra with HPDEC (High-power Decoupling). The rotor spinning speed was 6–15 kHz.

Shifts for both solution and solid state ^{113}Cd NMR were referenced against 1 M Cd(NO$_3$)$_2$ (aq) (δ = 0). For comparison, literature data were re-calculated to 1 M Cd(NO$_3$)$_2$ (aq) as

102

reference. 0.1 M $Cd(NO_3)_2$ (aq) resonates at 17 ppm, while the chemical shift difference is 65 ppm for $Cd(NO_3)_2$ (aq) from 4 M to infinite dilution.[153] Comprehensive summary of [113]Cd NMR standards can be found in Table 6.2.

Table 6.2. Summary of [113]Cd NMR standards and relationships between them. Chemical shift (δ) in ppm. All solutions are aqueous solutions, unless indicated otherwise (HF = high field resonance, LF = low field resonance).

Substance	δ relative to			Reference standard	Difference of ref. standard relative to 0.1 M $Cd(NO_3)_2$
	0.1 M $Cd(NO_3)_2$	1 M $Cd(NO_3)_2$	reference standard		
$Cd(NO_3)_2 \cdot 4H_2O$ (s)	−116	−99	0[154,155]	$Cd(NO_3)_2 \cdot 4H_2O$ (s)	−116[154,155]
$CdSO_4$ (s)	−74	−57	42.4[154]	$Cd(NO_3)_2 \cdot 4H_2O$ (s)	−116[154,155]
HF $3CdSO_4 \cdot 8H_2O$ (s)	−73.5	−56.5	−73.5[53,156]	0.1 M $Cd(NO_3)_2$	0
4 M $Cd(NO_3)_2$	−61.3	−44.3	0[157]	4 M $Cd(NO_3)_2$	−61.3[157,158]
LF $3CdSO_4 \cdot 8H_2O$ (s)	−60.9	−43.9	−60.9[53,156]	0.1 M $Cd(NO_3)_2$	0
1 M $Cd(ClO_4)_2$ (DMF)	−41.8	−24.8	−45.5[68]	0.1 M $Cd(ClO_4)_2$	3.7[53,156]
1 M $Cd(ClO_4)_2$ (MeOH)	−25.7	−8.7	−29.4[68]	0.1 M $Cd(ClO_4)_2$	3.7[53,156]
0.5 M $Cd(ClO_4)_2$ (DMSO)	−22.3	−5.3	−26.0[68]	0.1 M $Cd(ClO_4)_2$	3.7[53,156]
1 M $Cd(NO_3)_2$	−17	0	0[this work]	1 M $Cd(NO_3)_2$	−17[this work]
2 M $Cd(ClO_4)_2$	−2.1	14.9	−5.8[68]	0.1 M $Cd(ClO_4)_2$	3.7[53,156]
0.1 M $Cd(NO_3)_2$	0	17	0[53,156]	0.1 M $Cd(NO_3)_2$	0
1 M $CdSO_4$	0.9	17.9	−2.8[158]	0.1 M $Cd(ClO_4)_2$	3.7[53,156]
1 M $Cd(ClO_4)_2$	1.5	18.5	−2.2[68]	0.1 M $Cd(ClO_4)_2$	3.7[53,156]
	2.6	19.6	−1.1[158]	0.1 M $Cd(ClO_4)_2$	3.7[53,156]
0.1 M $Cd(ClO_4)_2$	3.7	20.7	3.7[53,156]	0.1 M $Cd(NO_3)_2$	0
inf. dil. $Cd(ClO_4)_2$	5	22	5[53,156]	0.1 M $Cd(NO_3)_2$	0
2 M, 1 M, 0.5 M $Cd(ClO_4)_2$	5(5)	22(5)	121(5)[114]	$Cd(NO_3)_2 \cdot 4H_2O$ (s)	−116[154,155]
0.2 M $Cd(ClO_4)_2$ (Py)	83.9	100.9	80.2[68]	0.1 M $Cd(ClO_4)_2$	3.7[53,156]
CdO (s)	399(10)	416(10)	515[114,154]	$Cd(NO_3)_2 \cdot 4H_2O$ (s)	−116[154,155]
$CdMe_2$ (l)	647	664	643[158]	0.1 M $Cd(ClO_4)_2$	3.7[53,156]
CdS (s, wurtzite)	689	706	42.3[16]	$CdMe_2$ (l)	647[53,156,158]
CdS (s, wurtzite)	692(5)	709(5)	808[114,154]	$Cd(NO_3)_2 \cdot 4H_2O$ (s)	−116[154,155]

6.2.5   UV/Vis Absorption

Solution UV/Vis absorption spectra were recorded on a Perkin-Elmer Lambda 35 UV/Vis spectrophotometer in 1 cm quartz cuvettes against air. Spectra of the pure solvents were subtracted. Solid-state spectra of the micron-sized powders were measured as mineral oil dispersions between quartz plates with a Labsphere integrating sphere.

In this thesis, an absorption edge is defined as an inflection point of the absorption curve, *i.e.* a minimum of the first derivative curve.[121]

6.2.6 Dynamic Light Scattering

Dynamic light scattering (DLS) experiments were performed with an ALV/CGS-3 Compact Goniometer system equipped with an ALV/LSE-5003 Multiple τ Digital Correlator (ALV-GmbH, Germany) at a scattering angle of 90° and a 632.8 nm JDSU laser 1145P. All measurements were carried out at 25 ± 0.1°C in glass containers. Measured intensity correlation functions were regularized fitted by $g_2(t)$ function with radius distribution limits 0.5 and 2500 nm. Mass weight linear distribution functions are presented. The distribution curves of **Cd10b** in different solvents are summarized in Figure 6.2.
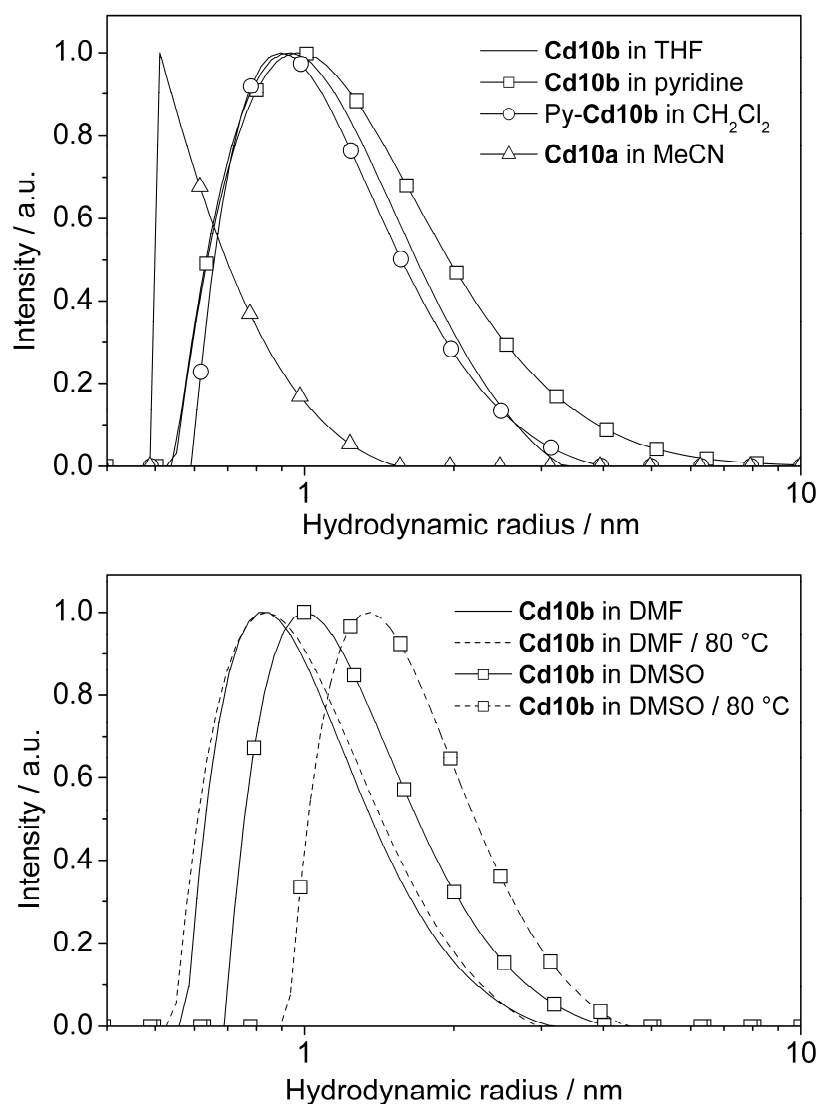
Figure 6.2. DLS distribution curves of (up) **Cd10b** *in THF and pyridine (1.2, 100 mg/ml), Py-adduct of* **Cd10b** *in CH₂Cl₂ (10 mg/ml),* **Cd10a** *in MeCN (12 mg/ml) and (down) of* **Cd10b** *in DMF (<6 mg/ml) and DMSO (6 mg/ml) before and after heating at 80 °C for 14 h.*

6.2.7   Gel Permeation Chromatography

Gel permeation chromatography (GPC) measurements were performed on THF solutions filtered through a 0.2 μm Nylon syringe filter to remove undissolved solid substances. Waters system including a 515 HPLC pump, a 717 autosampler, a 2410 differential refractive index detector and Styragel columns (HR 0.5, 3, and 4) was used at 40 °C at a rate of 1 ml/min. The system was calibrated using linear polystyrene standards. Molecular weight analysis was carried out using Viscotek Omnisec 4.5.6.

6.2.8   Thermogravimetric Analysis

Thermogravimetric analysis (TGA) of **Cd10a** was carried out on a Netzsch TG209C instrument, with a heating program equivalent to the synthesis of **Cd10b** (a heating phase with a rate of 4 K/min to 180 °C followed with a constant phase at 180 °C for 6 h) in N_2 atmosphere at a flow rate of 25 ml/min. Temperature calibration was performed using standard Netzsch calibration sets.

6.2.9   Elemental Analysis

Elemental analysis was performed at the Microanalytical Laboratory at the Institute of Physical Chemistry, University of Vienna, on Eurovector EA3000 CHNS-O elemental analyzer.

6.3   Syntheses

6.3.1   Rearrangement of $[Cd_{10}S_4(SPh)_{16}]^{4-}$ in Coordinating Solvents

$(NMe_4)_4[Cd_{10}S_4(SPh)_{16}]$ (**Cd10a**) was synthesized as described in Ref. 47 and recrystallized from boiling MeCN. The structure of the prepared compound was verified by means of powder XRD, which was in good agreement with theoretical diffractogram calculated from **Cd10a-2**. A new polymorph of **Cd10a** (**Cd10a-3)** was obtained by addition of three or seven equivalents of toluene to a 40 or 10 mg/ml solution of **Cd10a** in DMSO after 1 d at room temperature. The crystals were characterized by SC-XRD.

Samples B1–B4 were prepared by dissolution of **Cd10a** in DMSO at room temperature followed by a 30 min warming-up phase and a 16 or 72 h heating phase at 80 °C. Details are summarized in Table 4.2.

$(NMe_4)_2[Cd(SPh)_4]$ (**Cd1**) was prepared as described in Ref. 47. The crystals of a new polymorph of **Cd1** (**Cd1-2**) were obtained by cooling the reaction solution to −20 °C instead of recrystallization from iPrOH.[159] When the crystals of **Cd1-2** were separated from the reaction mixture, and MeOH was added to the solution, monoclinic crystals of the known

polymorph of **Cd1**[159] were obtained after cooling to −20 °C. The molecular structure of **Cd1-2** is very similar to the known polymorph.

[$Cd_4(SPh)_8$]$_\infty$ (**Cd4b**)[49] was obtained by two methods from reaction solution B1: (a) addition of 10 volume equivalents of MeOH to B1 (10 mg/ml of **Cd10a** in DMSO heated at 80 °C for 16 h), followed by addition of 5 equivalents of H_2O. Centrifugation after two weeks resulted in the separation of a pale yellow precipitate and a clear colorless solution. The solution was left undisturbed at room temperature for one week. This resulted in the formation of small crystals of **Cd4b**. (b) Addition of 17 equivalents of methanol to B1, followed by centrifugation after 2 weeks resulted in separation of a pale yellow precipitate and a clear colorless solution. Then 3 equivalents of water were added to the solution. This resulted in the formation of small crystals of **Cd4b** after one week. Powder XRD confirmed the presence of **Cd4b** as the only crystalline phase in both cases (Figure 6.3).

(NMe$_4$)$_2$[$Cd_8S(SPh)_{16}$] (**Cd8**) was obtained from reaction solution B1 (10 mg/ml of **Cd10a** in DMSO heated at 80 °C for 16 h) by addition of 8 volume equivalents of MeOH and 6 equivalents of H_2O, centrifugation after few days and addition of 3 equivalents of *i*PrOH. Crystals were formed after 7 d of standing at room temperature. Yield 18 % based on **Cd10a**.
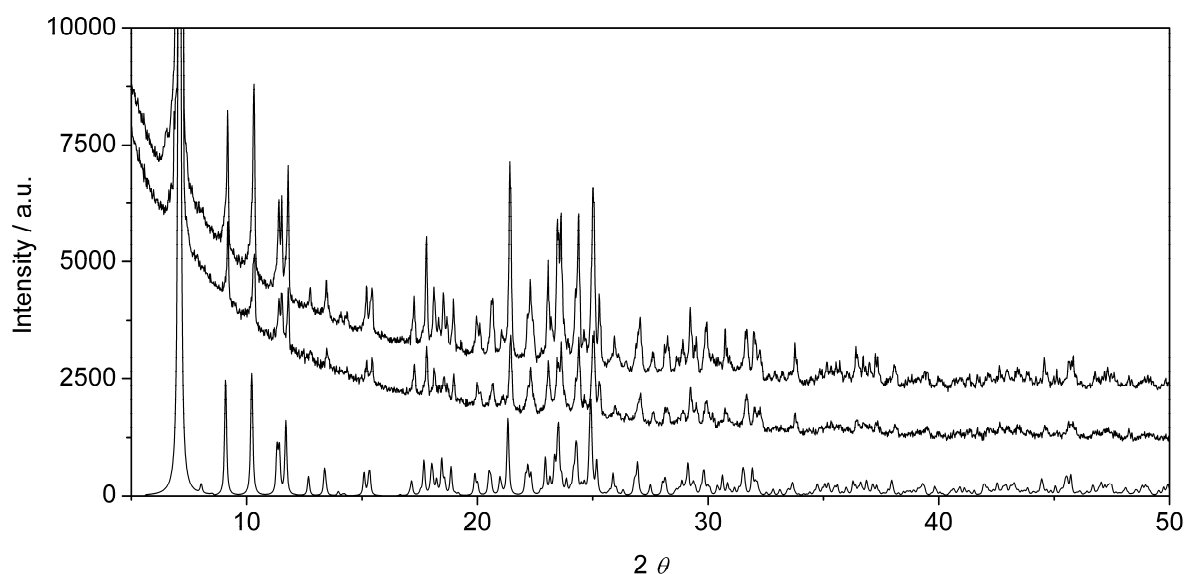
*Figure 6.3. X-ray powder diffractogram of samples prepared from crystals **Cd4b** (sample B1 (a) and (b)) and calculated pattern from **Cd4b**[49] (down from top).*

6.3.2   Characterization of "Cd$_{10}$S$_4$(SPh)$_{12}$" in Solid State and Solution

(NMe$_4$)$_4$[$Cd_{10}S_4(SPh)_{16}$] (**Cd10a**) was synthesized as described in Chapter 6.3.1.

"Cd$_{10}$S$_4$(SPh)$_{12}$" (**Cd10b**) was synthesized by slight modification of the published procedure:[54,118] Cluster **Cd10a** was heated under vacuum at 180 °C for 6 h and a yellow solid was obtained. TGA (Figure 6.4) and elemental analysis showed that composition of

106

Cd10b is almost equivalent to that of the ideal formula and to that presented in Ref. 54. The TGA revealed weight decrease of 21.67 % which corresponds well with the theoretical one of 22.25 %. However, it was obtained in a N_2 stream and not in vacuum which could lead to adsorption of a part of the gaseous products onto the formed powder and, thus, to an artificially low weight decrease. Elemental analysis of **Cd10b** was also in good agreement with the expected formula: $Cd_{10}S_4(SPh)_{12}$ = $C_{72}H_{60}S_{16}Cd_{10}$ (2562.4): calcd. C 33.75, H 2.36, N 0.00, S 20.02; found C 34.3, H 2.3, N 0.07, S 20.8. This corresponds to a formula of $C_{75.5}H_{60.4}N_{0.13}S_{17.2}Cd_{10}$, which, however, could not be assigned to a single $Cd_{10}S_x(SPh)_y(NMe_4)_z$ compound. The reason for this might be the presence of adsorbed NMe_3 and/or MeSPh species (see Equation 4.2). But, as the measured wt.% of N is less than the measurement accuracy of ±0.1 %, it can be supposed that all NMe_4^+ was released from **Cd10a** during the heat treatment (**Cd10a** contains 1.70 wt.% of N).
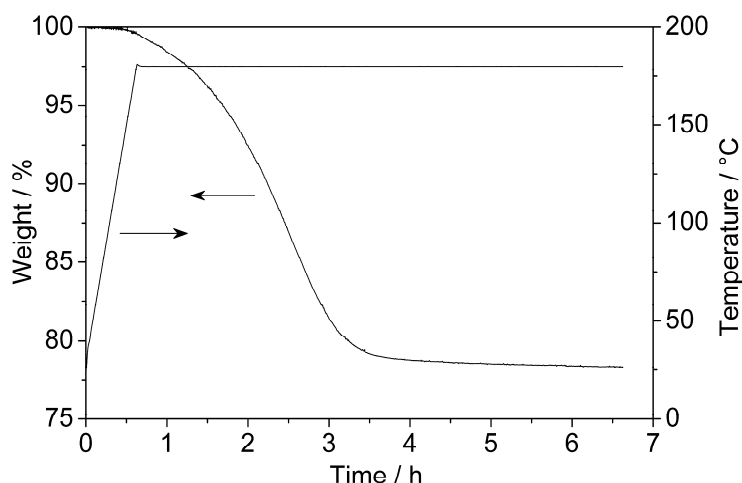
*Figure 6.4. TGA curve of **Cd10a** heated with comparable temperature program as used for the synthesis of **Cd10b**. However, TGA was measured under N_2 stream, whereas **Cd10b** was synthesized in vacuum.*

[Cd_{17}S_4(SPh)_{26}Py]_∞ (**Cd17-Py**): An amount of 139 mg (0.054 mmol) of **Cd10b** was dissolved in 1.5 ml of pyridine. After evaporation of all volatile compounds at room temperature at p <2 mbar, the residue was dissolved in 6 ml of CH_2Cl_2. After 4 days at room temperature, many small crystals were present in the sample which were bright in polarized light. After another 3 weeks, other cubic crystals formed, which were dark in polarized light. None of them had sufficient diffraction quality to be measured by single-crystal XRD. After one additional month, few big block pale-yellow crystals of **Cd17-Py** crystallized which were bright in polarized light. The total solid yield was 98 mg, from which around 10 % were crystals of **Cd17-Py**. Powder XRD of the whole solid product (Figure 6.5) showed presence of CdS clusters/NPs similarly to powder XRD of **Cd10b** (Figure 4.18, the broad reflection centered at ca. 4.5° is due to short range cluster ordering as in SAXS), but also reflections which are in good agreement with the crystal structure of **Cd17-Py**. The reflections at 10.02°, 11.44°, and 18.18° belong probably to the other crystalline compounds.
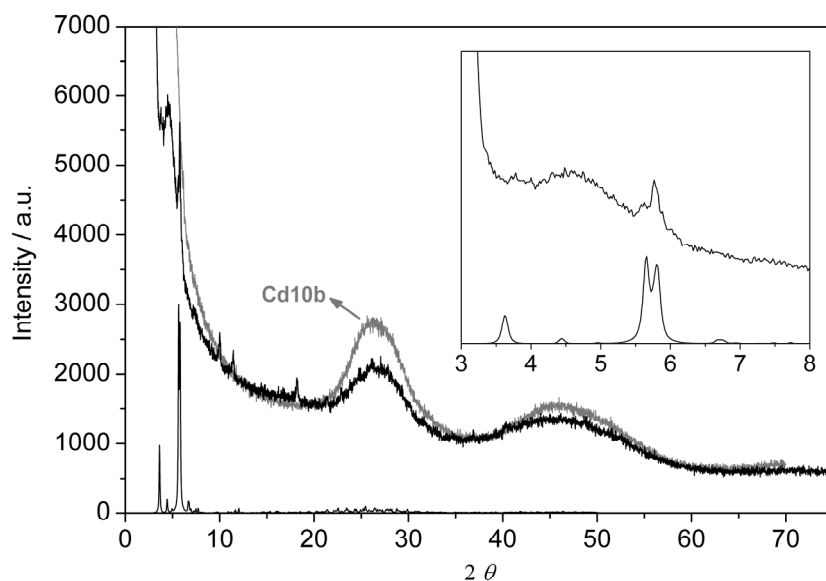
*Figure 6.5. X-ray powder diffractogram of the product mixture at the end of the synthesis of **Cd17-Py** (black curve) and of **Cd10b**. The pattern calculated from SC-XRD data of **Cd17-Py** is shown in the bottom.*

$Cd_{54}S_{28}(SPh)_{52}(Py)_{7.5}$ (**Cd54-Py**): An amount of 116 mg (0.045 mmol) of **Cd10b** was dissolved in 1.1 ml of pyridine, and 2.3 ml of toluene was added. From the formed suspension, few big cubic, pale-yellow crystals of **Cd54-Py** (dark in polarized light) crystallized after one month at room temperature. The yield of solid compounds was 10 mg from which around 70 % was crystalline **Cd54-Py**.

$Cd_{54}S_{28}(SPh)_{52}(L)_{x}$ (L = DMF or Py, **Cd54-L**): An amount of 51 mg (0.020 mmol) of **Cd10b** was dissolved in 0.5 ml of pyridine and 0.37 ml of DMF was added. A turbid suspension was allowed to stand undisturbed at room temperature. After one month, yellow cubic crystals of **Cd54-L** were present together with some precipitate. The yield of solid was 26 mg, from which around 50 % were crystals of **Cd54-L**.

$Cd_{54}S_{28}(SPh)_{52}(DMF)_{4}$ (**Cd54-DMF**): An amount of 60 mg (0.023 mmol) of **Cd10b** was heated in 10 ml of DMF at 80 °C for 14 h. The suspension was then filtered using a Nylon 0.2 μm syringe filter, and 7.5 ml of acetone was added to the solution. The solution was left undisturbed at room temperature, and clear cubic crystals of **Cd54-DMF** (dark in polarized light) crystallized within few days. No other solid species was formed even after few weeks. Yield 6 mg of **Cd54-DMF**.

$Cd_{54}S_{28}(SPh)_{52}(DMSO)_{4}$ (**Cd54-DMSO**): An amount of 6 mg (0.0023 mmol) of **Cd10b** was heated in 1 ml of DMSO at 80 °C for 14 h. Then 3 ml of toluene was added. The resulting solution was allowed to stand undisturbed at room temperature. After one month, small yellow cubic crystals were present as the only solid phase. They were too small for single-crystal XRD characterization. They were characterized by UV/Vis absorption as a cluster with a Cd54 core. Yield 0.5 mg of **Cd54-DMSO**.

6.3.3 CdS Clusters Functionalized by Hydroxy Groups

Syntheses of **Cd10c** clusters with various anions (NO_3^-, ClO_4^-, and BF_4^-) were performed according to the method of Schwarzenbach et al.[56] NO_3^- and BF_4^- salts have not been characterized with SC-XRD before.

$[Cd_{10}(SCH_2CH_2OH)_{16}](NO_3)_4$ (**Cd10c-NO₃**) was synthesized by subsequent addition of solutions of 1.11 g of $NaNO_3$ (13.1 mmol) in 5.0 ml of H_2O and 0.29 ml of $HSCH_2CH_2OH$ (4.1 mmol) in 10 ml of H_2O to the solution of 0.691 g of $Cd(acetate)_2 \cdot 2H_2O$ (2.59 mmol) in 20 ml of H_2O. The formed solution was left undisturbed at room temperature, which led to crystallization after few hours. The crystals were characterized by SC-XRD and composition of $[Cd_{10}(SCH_2CH_2OH)_{16}](NO_3)_4 \cdot 2H_2O$ (**Cd10c-NO₃·2H₂O**) was confirmed. After washing and drying in vacuum, powder XRD was measured, which was in good agreement with the crystal structure (Figure 6.6). Yield: 0.328 g (= 48.6 %, theoretical yield 0.675 g). The crude crystalline product was recrystallized from hot water solution, in order to remove residual adsorbed acetate.
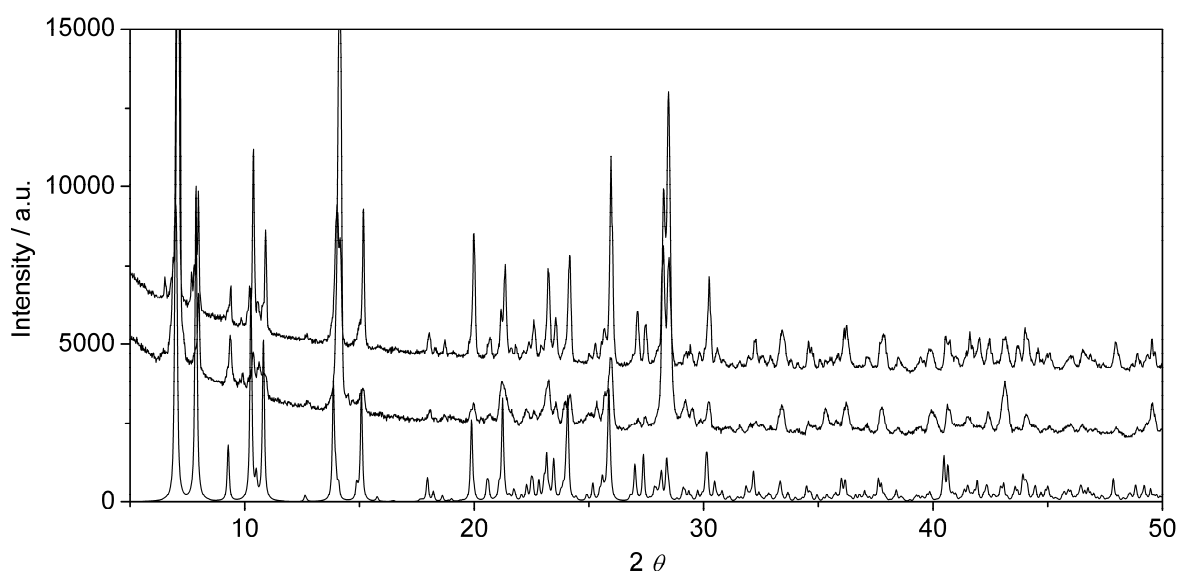
*Figure 6.6. Powder XRD pattern of **Cd10c-NO₃** prepared by drying of **Cd10c-NO₃·2H₂O** for 10 min and 3 h in vacuum and calculated from the crystal structure (down from top).*

$[Cd_{10}(SCH_2CH_2OH)_{16}](ClO_4)_4$ (**Cd10c-ClO₄**) was synthesized by slow direct addition of 0.74 ml of $HSCH_2CH_2OH$ (10.6 mmol) to the solution of 1.761 g of $Cd(acetate)_2 \cdot 2H_2O$ (6.61 mmol) in 14 ml of H_2O. To the resulting solution, 3.945 g of $NaClO_4$ (32.2 mmol) in 5.5 ml of H_2O was added and a white precipitate was formed at the end of the addition. Heating to 60 °C and addition of 15.6 ml of H_2O resulted in dissolution of the precipitate. The solution was left undisturbed and crystals crystallized within one day at 4 °C. The structure was confirmed by cell parameter measurements which were in agreement with Ref. 57. The formed crystals were washed with H_2O and dried under vacuum. Yield: 1.137 g (= 62.4 %, theoretical yield 1.822 g).

$[Cd_{10}(SCH_2CH_2OH)_{16}](BF_4)_4$ (**Cd10c-BF$_4$**) was synthesized by slow direct addition of 2.16 ml of $HSCH_2CH_2OH$ (30.7 mmol) to the solution of 5.121 g of $Cd(acetate)_2 \cdot 2H_2O$ (19.2 mmol) in 30 ml of H_2O. To the resulting solution, 15.057 g of $NaBF_4$ (137 mmol) in 25 ml of H_2O was added, and a white precipitate was formed after 5 min of stirring the reaction solution at room temperature. Heating to 60 °C resulted in dissolution of the precipitate. The solution was left undisturbed and crystals formed within one day at 4 °C. The crystal structure was determined by SC-XRD, with composition $[Cd_{10}(SCH_2CH_2OH)_{16}](BF_4)_4 \cdot H_2O$ (**Cd10c-BF$_4 \cdot$H$_2$O**). The formed crystals were washed with H_2O and dried under vacuum. Yield: 2.519 g (= 48.5 %, theoretical yield 5.194 g). Recrystallization of the crude crystals from saturated water solution at 60 °C resulted in crystals with slightly different structure, $[Cd_{10}(SCH_2CH_2OH)_{16}](BF_4)_4 \cdot 6H_2O$ (**Cd10c-BF$_4 \cdot$6H$_2$O**), which contained more solvent water in the structure. **Cd10c-BF$_4$** was recrystallized also from a DMSO solution (200 mg/ml = 6.7×10^{-2} M) by a 42-fold excess of *n*BuOH. After 2 weeks at 4 °C, crystals were formed, which were characterized by SC-XRD ($[Cd_{10}(SCH_2CH_2OH)_{16}](BF_4)_4 \cdot 2DMSO$ (**Cd10c-BF$_4 \cdot$2DMSO**)). Addition of other solvents (THF, $CHCl_3$, MeCN, MeOH, EtOH) to the DMSO solution did not lead to formation of any crystalline products.

The yield of these syntheses can be much improved, if a lower crystallization temperature or more saturated reaction solutions at higher temperatures were used. However, such procedures led to microcrystalline products instead of a single-crystals. Beside this, fast direct addition of $HSCH_2CH_2OH$ to the Cd^{2+} solution resulted in the formation of a white polymeric material with a composition of $Cd(SCH_2CH_2OH)_2$[56,160] which did not dissolve after addition of water, the anion solution, and/or after heating.

The solutions of **Cd10c** clusters in d$_6$-DMSO or d$_7$-DMF for NMR reaction with pyridine and ClSiMe$_3$ were previously dried over 4 Å molecular sieve or by evacuating of the corresponding solution in order to remove traces of water.

6.3.4   CdS Clusters Functionalized by Amino Groups

Exchange reactions were performed in deoxygenated MeCN. To the solution of **Cd10a** in MeCN (ca. 10 mg/ml), either pure exchanging thiol (cyclohexyl- or benzylmercaptane) or its solution in MeCN (HSPh-*p*NH$_2$) was added with ratio PhS:RSH = 1:*X*. In the case of cyclohexyl- and benzylmercaptane (*X* = 10–40) the resulting colorless solution was mixed at room temperature for 1 d and no change was observed. The solutions were evaporated in vacuum for 18 h in order to remove the solvent and excess exchanged and unexchanged thiols (both PhSH and RSH). The solid residue was washed with MeOH, dried, dissolved in d$_3$-MeCN, and characterized by ^{1}H NMR. Exchange with HSPh-*p*NH$_2$ was performed in a similar way, but lower *X* was used (*X* = 0.8–10). After mixing the cluster and yellow HSPh-*p*NH$_2$ solution in MeCN, the resulting yellow solution was deoxygenated followed by stirring at room temperature for 1 d. This led to formation of a white precipitate in a yellow solution, even at low *X* and low **Cd10a** concentration (4–10 mg/ml). The precipitate was separated by

decantation, washed with MeOH and dried in vacuum. After dissolution in DMF and DMSO (10 mg/ml), a pale yellow solution was obtained.

Crystals of $\{[Cd_{17}S_4(SPh–pNH_2)_{24}(DMF)_2]X_2\}_\infty$ (probably with nitrate as anion X, **Cd17-NH₂**) can be synthesized in different ways (Table 5.8). For SC-XRD characterization (sample E), they were prepared as follows: the colorless solution of 0.194 g of $Cd(NO_3)_2·4H_2O$ (0.629 mmol) in 2.0 ml of MeOH was added to the yellow solution of 0.202 g of HSPh-pNH₂ (1.61 mmol) and 0.23 ml of Et₃N (1.7 mmol) in 10 ml of DMF. To the resulting yellow solution, 6.5 mg of S (0.20 mmol) was added and 10 ml of DMF was used to wash the S powder from the Schlenk tube walls. Sulfur dissolved after ca. 30 min of stirring at room temperature. Aliquot of 5.0 ml of the reaction solution was treated with 5.0 ml of MeOH. Small square-shaped plate-like yellow crystals were formed within 3 d at room temperature, which were characterized by SC-XRD.

Preparation of sample L (Table 5.8), which was used for solution characterization, was as follows: solution of 0.168 g of $Cd(NO_3)_2·4H_2O$ (0.546 mmol) in 1.7 ml of DMF was added to the solution of 0.177 g of HSPh-pNH₂ (1.37 mmol) and 0.20 ml of Et₃N (1.5 mmol) in 4.0 ml of DMF. To the resulting yellow solution, 4.5 mg of S (0.14 mmol) was added and 2.4 ml of DMF was used to wash the S powder from the Schlenk tube walls. After the sulfur powder was dissolved, 7.6 ml of MeOH was added. A microcrystalline precipitate was formed within few hours. After one week of crystallization, the solution above the crystals (2nd fraction, ca. 15 ml) was placed into another Schlenk tube, 10 ml of MeOH were added and was left to crystallize for 3 weeks at room temperature. The structure of few crystals from the 1st fraction was estimated by cell parameter measurement using SC-XRD, which was identical with **Cd17-NH₂**. Both crystalline fractions were washed with 5 ml of MeCN twice and dried in vacuum. The powder XRD pattern did not show sharp reflections (Figure 6.7). The intense reflections at 2θ = 4.5–6 ° were shifted to higher 2θ compared with the pattern calculated from SC-XRD data, which corresponds to smaller distances and means that the structure shrank during drying. However, explicit identification by means of powder XRD was not possible. Yield: 110 mg (81 + 29), which corresponds to ca. 66 % based on Cd and M_r(**Cd17-NH₂**) = 5165.
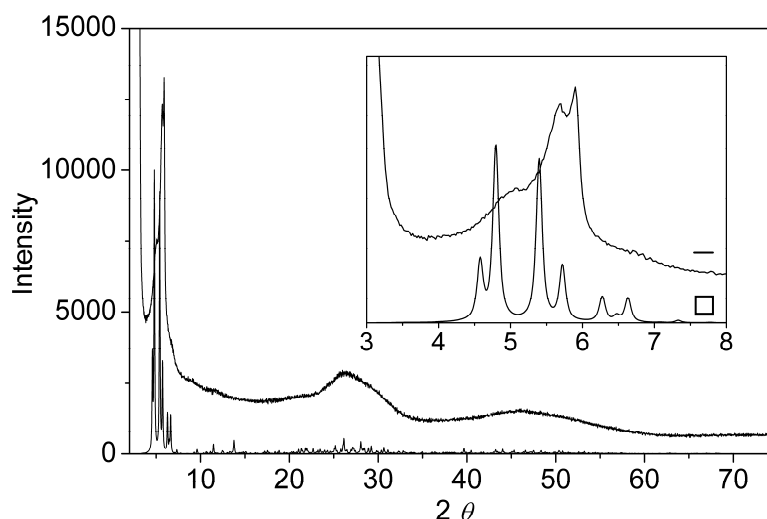
*Figure 6.7. Powder XRD pattern of **Cd17-NH₂** after drying in vacuum for 4 h (–) and calculated from SC-XRD data (□).*

6.3.5 Possibility of Radical Polymerization in the Presence of CdS Clusters

The composition and visible changes of samples prepared in this section are summarized in Table 6.3. All samples were colorless solutions before heating. The experiments were performed as NMR experiments with d_3-MeCN as solvent in Young tubes in the absence of O_2 and protected from sunlight. This allowed direct observation using NMR and preservation of inert atmosphere. However, mixing of the reaction solutions was not possible in Young tubes. Compositions calculated from NMR were in good agreement with initial compositions. The Young tubes with samples were immersed into a 60 °C oil bath equipped with temperature regulator and heated for 16 h. UV/Vis spectra of the samples were measured diluted with MeCN.

*Table 6.3. Summary of experiments leading to radical polymerization in the presence of the **Cd10a** cluster (RP8). Reaction conditions: 60 °C, 16 h, c_{MMA} = ca. 26 mg/ml, rad. = radicals produced from AIBN with calculated conversion 42 %.*

Sample	Components	Cd10a concentration (mg/ml)	Preparation composition, molar ratio	Visible changes after reaction
RP1	**Cd10a**	10.0	–	colorless solution
RP2	**Cd10a**, rad. (AIBN)	10.0	1:0.21(0.25)	very pale yellow solution
RP3		10.0	1:1.03(1.23)	very pale yellow solution
RP4		10.0	1:15.9(18.9)	pale yellow solution + crystals
RP5	MMA	–	–	colorless solution
RP6	**Cd10a**, MMA	8.6	1:99.6	colorless solution
RP7	MMA, rad. (AIBN)	–	99:1.01(1.20)	colorless solution
RP8	**Cd10a**, MMA, rad. (AIBN)	8.6	1:99.2:1.02(1.21)	very pale yellow solution

The crystals present in sample RP4 were plate-like, hexagonally shaped, bright in polarized light, and had relatively big sizes (0.3×0.3 mm, but very thin). Only their cell parameters could be obtained by SC-XRD measurement of a non-merohedrally twinned crystal: hexagonal P, 8.58, 21.83 Å or orthorhombic C, 8.58, 14.85, 21.83 Å.

Samples RP7 and RP8 were prepared for GPC measurement as follows. First, the solvent was evaporated at 40 mbar and the residues (glass-like, colorless material in RP7 and powdered, white material in RP8) were dried at 2 mbar for 2 h, which should remove solvent traces and unreacted MMA. Then THF was added, in order to obtain 10 mg/ml of PMMA in THF if 100 % of MMA would polymerize (this corresponds to addition of 1.5 ml THF to evaporated 0.6 ml reaction solution). A colorless solution and a white suspension (since the **Cd10a** cluster is not soluble in THF) were obtained from samples RP7 and RP8, respectively, which were both filtered through a 0.2 μm Nylon syringe filter. Thus, THF solutions containing only PMMA from samples RP7 and RP8 were obtained, which were directly used for GPC measurements.

6.4 Crystallographic Data

6.4.1 Rearrangement of $[Cd_{10}S_4(SPh)_{16}]^{4-}$ in Coordinating Solvents

In all structures, all non-hydrogen atoms were refined with anisotropic displacement parameters. Hydrogen atoms were placed on calculated positions. Some of the phenyl rings were disordered over two positions. In this case, their carbon atoms were constrained to form a regular hexagon. Important parameters for all structures are summarized in Table 6.4.

CCDC-762159 (for **Cd10a-3**), 762160 (for **Cd1-2**) and 762161 (for **Cd8**) contain the supplementary crystallographic data. These data can be obtained free of charge from The Cambridge Crystallographic Data Center via www.ccdc.cam.ac.uk/data_request/cif.

*Table 6.4. Crystallographic data for $(NMe_4)_4[Cd_{10}S_4(SPh)_{16}]$ (**Cd10a-3**), $(NMe_4)_2[Cd(SPh)_4]$ (**Cd1-2**) and $(NMe_4)_2[Cd_8S(SPh)_{16}]$ (**Cd8**).*

	Cd10a-3	Cd1-2	Cd8
Formula	$C_{112}H_{128}Cd_{10}N_4S_{21.5}$	$C_{32}H_{44}Cd_1N_2S_4$	$C_{104}H_{110}Cd_8N_2O_3S_{17}$
Formula weight	3343.47	697.33	2880.16
Crystal size, mm	0.28×0.20×0.15	0.05×0.05×0.03	0.25×0.03×0.03
Meas. temp., K	100	298	100
Crystal system	orthorhombic	tetragonal	monoclinic
Space group	*Aba*2	*P*4$_3$2$_1$2	*P*2$_1$/*n*
a, pm	2799.8(6)	1032.46(6)	1837.2(5)
b, pm	2931.7(6)		2529.7(7)
c, pm	1693.3(3)	3273.1(4)	2517.4(7)
β, deg			102.861(4)
V [pm^3] ·10^6	13899(5)	3489.0(5)	11406(5)

	Cd10a-3	Cd1-2	Cd8
Z	4	4	4
ρ_{calc}, g cm^{-3}	1.598	1.328	1.677
μ, mm^{-1} (Mo, K$_\alpha$)	1.862	0.888	1.820
θ_{max}, deg	28.33	25.00	25.00
rflns measd	64719	19452	40725
unique rflns	17078	3078	19602
rflns $I > 2\sigma(I)$	13201	1865	10818
parameters	708	303	1293
R_1 $(I > 2\sigma(I))$	0.048	0.046	0.052
wR_2 $(I > 2\sigma(I))$	0.117	0.059	0.105
GOF for I^2	1.147	1.005	0.961
min./max., e Å^{-3}	1.25/−1.25	0.28/−0.31	1.60/−1.12

6.4.2 Characterization of "Cd$_{10}$S$_4$(SPh)$_{12}$" in Solid State and Solution

The data for all structures were of poor quality because of high degree of cluster and ligand disorder, which resulted in a resolution of about 1 Å. Also the CdS overstructure influenced the appearance of diffraction patterns and quality of the data. Residual electron density was high in all structures and could not be exactly assigned to disordered solvent molecules in substantially big void spaces, so it was removed by the program package PLATON (Squeeze).[161] Calculated densities and absorption coefficients are consequently lower than the real values. Important parameters for all structures are summarized in Table 6.5. Site occupancies of the μ_3-PhS groups in **Cd54-Py**, **Cd54-L**, and **Cd54-DMF** were set to 0.33. Their anisotropic parameters are reasonable, but they have slightly higher standard deviations than μ_2-PhS groups. Phenyl rings in the vicinity of the μ_3-PhS groups were disordered.

[Cd$_{17}$S$_4$(SPh)$_{26}$Py]$_\infty$ (**Cd17-Py**): All Cd and S atoms were refined with anisotropic displacement parameters. All C and N atoms were treated isotropically to get a sufficient data-to-parameter ratio. Hydrogen atoms were inserted only to phenyl groups with relatively small U_{iso}. The highest peaks in residual electron density map are located ca. 1 Å from Cd atoms.

Cd$_{54}$S$_{28}$(SPh)$_{52}$(Py)$_{7.5}$ (**Cd54-Py**): All Cd, S, C, and N atoms were refined with anisotropic displacement parameters. All phenyl and pyridine rings were treated as rigid hexagons. The occupancy factor for pyridine ligands was not refined but set to 1.0 at one corner and 0.5 at the remaining three corners of the tetrahedron, resulting in overall 7.5 pyridine ligands per cluster. Hydrogen atoms were not inserted. The highest peaks in residual electron density map are located ca. 1 Å from Cd atoms.

Cd$_{54}$S$_{28}$(SPh)$_{52}$(L)$_x$ (L = DMF or Py, **Cd54-L**): All Cd, S, C, and O atoms were refined with anisotropic displacement parameters. Hydrogen atoms were added to the phenyl rings in calculated positions. The apex DMF or pyridine ligands could not be distinguished in the

114

residual electron density, except the Cd-bonded oxygen atom. The structure is very similar to **Cd54-DMF**, but the data are much worse (compare in Table 6.5).

$Cd_{54}S_{28}(SPh)_{52}(DMF)_4$ (**Cd54-DMF**): All Cd, S, C, and O atoms were refined with anisotropic displacement parameters, but hydrogen atoms were not added to the phenyl rings. The apex DMF ligands could not be distinguished in the residual electron density, except the Cd-bonded oxygen atom.

CCDC-767707 (for **Cd17-Py**), 767708 (for **Cd54-Py**) and 767709 (for **Cd54-DMF**) contain the supplementary crystallographic data. These data can be obtained free of charge from The Cambridge Crystallographic Data Center via www.ccdc.cam.ac.uk/data_request/cif.

*Table 6.5. Summary of crystallographic parameters for $[Cd_{17}S_4(SPh)_{26}Py]_\infty$ (**Cd17-Py**), $Cd_{54}S_{28}(SPh)_{52}(Py)_{7.5}$ (**Cd54-Py**), $Cd_{54}S_{28}(SPh)_{52}(L)_x$ (L = DMF or Py, **Cd54-L**), $Cd_{54}S_{28}(SPh)_{52}(DMF)_4$ (**Cd54-DMF**).*

	Cd17-Py	Cd54-Py	Cd54-L	Cd54-DMF
Formula	$C_{161}H_{135}Cd_{17}N_1S_{30}$	$C_{349.5}H_{297.5}Cd_{54}N_{7.5}S_{80}$	$C_{312}H_{260}Cd_{54}O_4S_{80}$	$C_{324}H_{288}Cd_{54}N_4O_4S_{80}$
Formula weight	4956.3	13236.9	12707.6	12936.0
Crystal size, mm	0.20×0.15×0.15	0.25×0.20×0.12	0.33×0.26×0.25	0.32×0.24×0.15
Meas. temp., K	100	100	100	100
Crystal system	monoclinic	cubic	cubic	cubic
Space group	$P2_1$/c	$P-43n$	$F-43c$	$F-43c$
a, pm	2439.1(3)	4731.6(1)	4753.0(2)	4768.0(4)
b, pm	2617.3(3)			
c, pm	3069.8(4)			
β, deg	92.539(2)			
$V \cdot 10^6$, pm^3	19578(4)	105928(4)	107374(9)	108395(14)
Z	4	8	8	8
ρ_{calc}, g cm^{-3}	1.681	1.660	1.572	1.585
μ, mm^{-1} (Mo, K$_\alpha$)	2.165	2.467	2.430	2.409
θ_{max}, deg	25.00	22.50	24.80	24.99
Rflns measd	103074	849271	156356	101570
Unique rflns	34425	23086	7708	7969
Rflns $I > 2\sigma(I)$	11732	15999	3710	2932
Parameters	1069	1411	357	471
Restraints	689	2444	955	969
R_1 ($I > 2\sigma(I)$)	0.0972	0.1161	0.1805	0.1120
wR_2 ($I > 2\sigma(I)$)	0.2287	0.2789	0.5089	0.3251
GOF for I^2	0.866	1.092	1.043	1.060
Min./max., e Å^{-3}	2.525/−1.304	1.612/−1.075	2.526/−3.003	1.363/−0.846
$V_{solvent\ accessible\ voids}$, Å^3 / unit cell	3197.3	26457.1	32024.4	35806.1
e^- in solvent accessible voids / unit cell	218.0	1629.1	1584.3	1318.4

115

6.4.3 CdS Clusters Functionalized by Hydroxy Groups

All non-hydrogen atoms were refined with anisotropic thermal parameters. Important crystallographic parameters are summarized in Table 6.6 for all following structures.

$[Cd_{10}(SCH_2CH_2OH)_{16}](NO_3)_4 \cdot 2H_2O$ (**Cd10c-NO$_3$·2H$_2$O**): some of the ligand chains are disordered over two positions. Only few H atoms on OH groups were found in the residual electron density map, which were then placed and refined with a fixed distance from the parent atom. Relatively high residual electron density (1.88) is caused by partial cluster disorder.

$[Cd_{10}(SCH_2CH_2OH)_{16}](BF_4)_4 \cdot H_2O$ (**Cd10c-BF$_4$·H$_2$O**): some of the ligand chains are disordered over two positions. No H atom on OH groups was found in the residual electron density map. Thermal parameters of the BF_4^- anions are high, which is caused by their high mobility at room temperature. The residual electron density peak is located 1.069 Å from Cd4.

$[Cd_{10}(SCH_2CH_2OH)_{16}](BF_4)_4 \cdot 6H_2O$ (**Cd10c-BF$_4$·6H$_2$O**): some of the ligand chains are disordered over two positions. All H atoms on OH groups and almost all on H$_2$O were found in the residual electron density map. The relatively high residual electron density peak (2.25) is located 1.055 Å from F4A and is caused by disorder of a BF$_4$ group.

$[Cd_{10}(SCH_2CH_2OH)_{16}](BF_4)_4 \cdot 2DMSO$ (**Cd10c-BF$_4$·2DMSO**): some of the ligand chains are disordered over two positions. All H atoms on OH groups were found in the residual electron density map. The solvent DMSO molecule is disordered over two positions. The oxygen position in DMSO was distinguished according to distances to the central S atom (d_{S-O} = 1.55(1) Å, d_{S-C} = 1.77(1)–1.79(1) Å) and to the possible H-bond network formation. No nBuOH was found in the crystal structure despite of its large excess during the recrystallization. The highest residual electron density peak (1.21) is located 0.757 Å from Cd5.

Table 6.6. Crystallographic data for $[Cd_{10}(SCH_2CH_2OH)_{16}](NO_3)_4 \cdot 2H_2O$ (Cd10c-NO$_3$·2H$_2$O), $[Cd_{10}(SCH_2CH_2OH)_{16}](BF_4)_4 \cdot H_2O$ (Cd10c-BF$_4$·H$_2$O), $[Cd_{10}(SCH_2CH_2OH)_{16}](BF_4)_4 \cdot 6H_2O$ (Cd10c-BF$_4$·6H$_2$O), and $[Cd_{10}(SCH_2CH_2OH)_{16}](BF_4)_4 \cdot 2DMSO$ (Cd10c-BF$_4$·2DMSO).

	Cd10c-NO$_3$·2H$_2$O	Cd10c-BF$_4$·H$_2$O	Cd10c-BF$_4$·6H$_2$O	Cd10c-BF$_4$·2DMSO
Formula	$C_{32}H_{84}Cd_{10}$-$N_4O_{30}S_{16}$	$C_{32}H_{82}B_4Cd_{10}$-$F_{16}O_{17}S_{16}$	$C_{32}H_{92}B_4Cd_{10}$-$F_{16}O_{22}S_{16}$	$C_{36}H_{92}B_4Cd_{10}$-$F_{16}O_{18}S_{18}$
Formula weight	2641.99	2723.18	2813.26	2861.42
Crystal size, mm	0.15×0.07×0.05	0.20×0.15×0.15	0.13×0.13×0.04	0.17×0.08×0.05
Meas. temp., K	298	298	100	100
Crystal system	monoclinic	monoclinic	monoclinic	monoclinic
Space group	*C2/c*	*C2/c*	*C2/c*	*C2/c*
a, pm	3367.7(3)	3403.9(18)	3170.6(4)	3237.01(14)
b, pm	1252.80(10)	1321.0(6)	1328.19(17)	1314.43(6)
c, pm	2531.5(2)	2531.5(14)	2461.9(3)	2527.42(18)
β, deg	131.190(1)	130.895(17)	125.606(2)	126.881(1)

	Cd10c-NO$_3$·2H$_2$O	Cd10c-BF$_4$·H$_2$O	Cd10c-BF$_4$·6H$_2$O	Cd10c-BF$_4$·2DMSO
V [pm^3] ·10^6	8037.3(11)	8605(8)	8429.3(18)	8601.7(8)
Z	4	4	4	4
ρ_{calc}, g cm^{-3}	2.183	2.102	2.217	2.210
μ, mm^{-1} (Mo, K$_\alpha$)	3.075	2.888	2.956	2.943
θ_{max}, deg	28.00	25.00	28.00	28.00
Rflns measd	37820	37172	30156	41270
Unique rflns	9692	7293	10159	10368
Rflns $I > 2\sigma(I)$	6656	5111	8838	8886
Parameters	463	492	530	542
Restraints	251	718	270	314
R_1 ($I > 2\sigma(I)$)	0.063	0.065	0.028	0.022
wR_2 ($I > 2\sigma(I)$)	0.152	0.197	0.063	0.049
GOF for I^2	1.067	1.061	1.028	1.055
Min./max., e Å^{-3}	1.88/−0.87	1.30/−0.71	2.25/−1.25	1.21/−0.68

6.4.4   CdS Clusters Functionalized by Amino Groups

The crystal structure of $\{[Cd_{17}S_4(SPh–pNH_2)_{24}(DMF)_2]X_2\}_\infty$ (probably with nitrate as anion X, **Cd17-NH$_2$**) was solved by direct methods in orthorhombic space group $C222_1$ (a = 38.605(3) Å, b = 38.606(3) Å, c = 61.791(5) Å) and then transformed into the tetragonal space group $P4_32_12$ (a = 27.2759(12) Å, c = 61.735(5) Å) after suggestion of the program PLATON.[161] It was refined as a racemic twin with Flack parameter of 0.54(5). Since PLATON[161] did not suggest that center of symmetry needs to be added, the crystal was most likely 50:50 inversion twin with no absolute configuration determination possible.[162] Thus, the structure could be as well refined in space group $P4_12_12$. The charge imbalance was discussed in Chapter 5.2.2. Residual electron density in solvent accessible voids of ca. 33 vol.% was high and could not be exactly assigned to disordered solvent molecules, so it was removed by the program package PLATON (Squeeze).[161] Calculated densities and absorption coefficients are consequently lower than real values. All C and N atoms were refined with isotropic displacement parameters. Geometrical restraints were applied to all C and N atoms of the ligands. Atoms of the coordinated DMF molecules were not found in residual electron density. H atoms bound to C atoms were refined in calculated positions with fixed distance. H atoms bound to amino groups were not found. Important crystallographic parameters for this structure are summarized in Table 6.7.

*Table 6.7. Crystallographic data for $\{[Cd_{17}S_4(SPh–pNH_2)_{24}(DMF)_2]^{2+}\}_\infty$ (**Cd17-NH$_2$**).*

	Cd17-NH$_2$		Cd17-NH$_2$
Formula	$C_{150}H_{158}Cd_{17}N_{26}O_2S_{28}$	Rflns measd	434912
Formula weight	5165.5	Unique rflns	39294
Crystal size, mm	0.33×0.16×0.1	Rflns $I > 2\sigma(I)$	22506
Meas. temp., K	100	Parameters	1102
Crystal system	tetragonal	Restraints	4601
Space group	$P4_32_12$	R_1 ($I > 2\sigma(I)$)	0.1058
a, pm	2727.59(12)	wR_2 ($I > 2\sigma(I)$)	0.2893
c, pm	6173.5(5)	GOF for I^2	1.097
V [pm^3] $\cdot 10^6$	45929(5)	Min./max., e Å^{-3}	1.77/−3.20
Z	8	$V_{\text{solv accessible voids}}$, Å^3 / unit cell	15296
ρ_{calc}, g cm^{-3}	1.494		
μ, mm^{-1} (Mo, K$_\alpha$)	1.835	e^- in solvent accessible voids / unit cell	6769
θ_{max}, deg	24.78		

7   Summary and Outlook

The aim of this work was to prepare hybrid materials with photoluminescent properties by covalent incorporation of functional CdS clusters into a polymeric matrix. This required to proceed in two steps: (i) synthesis and characterization of functional CdS clusters, (ii) synthesis and characterization of hybrid materials prepared from them by polymerization in the presence of an organic monomer.

However, a pre-step turned out to be necessary in order to ensure that the molecular structure of used clusters does not change, or changes in a precisely defined way during functionalization and incorporation into the polymeric matrix. This is also the topic of the first part of the thesis which deals with characterization of non-functional CdS clusters in solution at conditions similar to polymerization conditions.

First, the non-functional CdS cluster $(NMe_4)_4[Cd_{10}S_4(SPh)_{16}]$ (**Cd10a**) was used for the basic investigation. It was chosen because it is easy to synthesize, well investigated in solid state and in solution and its structural changes can be easily monitored by ^{113}Cd NMR and UV/Vis spectroscopy. Actually, it was expected to be relatively stable in solution and thus suitable for somewhat harsher conditions of polymerizations. However, it turned out that the cluster is unstable in coordinating solvents (DMSO, DMF, and MeCN) in which it is soluble. This was expressed by formation of bigger CdS clusters and NPs in these solutions which was proven by various characterization methods (UV/Vis, DLS, powder XRD, and SAXS). The growth was fast at room temperature in DMSO and DMF. Longer time periods and higher temperature were necessary in MeCN. **Cd10a** transformed completely within 90 min in DMSO at 80 °C, 21 h at 75 °C were necessary to achieve ca. 25 % rearrangement in MeCN. Thus, the used solvents can be ordered according to increasing rearrangement rate: MeCN < DMF < DMSO. The kind of CdS clusters and NPs formed during the transformation differed depending on the solvent, time, and temperature. Usually, clusters with Cd32 and Cd54 cores were obtained (typical UV/Vis absorption), but also bigger NPs were present in DMSO solutions. All attempts to crystallize some of the clusters from the reaction solutions were unsuccessful.

The mechanism of this rearrangement was investigated in DMSO in detail. If a bigger cluster/NP is formed from **Cd10a**, change of chemical composition is required and some byproduct(s) has to be formed. It was shown that this is indeed the case. The notion of a possible growth mechanism was obtained from the mechanism proposed by Cumberland et al.[123] for the growth of $Li_4[Cd_{10}Se_4(SPh)_{16}]$ heated in hexadecylamine (HDA), which started with the fragmentation of the Cd10 cluster and loss of apical $[Cd(SPh)_3]^-$ species upon which the residual smaller Cd_xSe_y species aggregated and formed bigger clusters or NPs. Such a mechanism is probable also for **Cd10a** in DMSO, would explain the compositional differences and also formation of a new thiophenolate group in all samples (NMR). It was proven in this work, that the cluster rearrangement indeed involves release of apical $[Cd(SPh)_3]^-$ species from the cluster. The proof was based on the characterization of the byproduct formed during the transformation, $[Cd(SPh)_x(DMSO)_y]^{(2-x)}$ (x = ca. 3), according to diverse NMR, UV/Vis, and crystallization experiments. It is very probable that the

119

rearrangement in DMF proceeds by the same mechanism, which cannot be stated for MeCN solutions. However, the rearrangement rate can be very probably correlated with the coordination strength of the solvents which then increases in the order MeCN < DMF < DMSO.

The second cluster, which was investigated, was "$Cd_{10}S_4(SPh)_{12}$" (**Cd10b**), formed by thermolysis of **Cd10a**. Its composition was claimed to be $Cd_{10}S_4(SPh)_{12}$,[54] thus having four free Cd coordination sites suitable for further functionalization. First, it was shown, that the thermolysis product **Cd10b** does not have the stated composition. Analysis in solid state revealed that part of the cluster grew unspecifically during the heat treatment. Bigger CdS clusters and/or NPs were formed, as indicated by the solid state ^{113}Cd NMR spectra, UV/Vis, and SAXS investigation and also UV/Vis and DLS in weakly coordinating solvents (MeCN, THF). On the other hand, part of **Cd10a** retained its Cd10 core structure since crystals of $(NHEt_3)_4[Cd_{10}S_4(SPh)_{16}]$ could be crystallized after addition of four equivalents of $PhSH/NEt_3$ to a suspension of **Cd10b** in MeCN. These conclusions are in disagreement with the original work of Farneth *et al.*[54] claiming that **Cd10b** is a neutral $Cd_{10}S_4(SPh)_{12}$ cluster that tends to aggregate to different degrees in the solid state and in solution. **Cd10b** is thus not suitable for further functionalization since it does not have a precisely defined compositions and molecular structure.

Additional information was obtained for **Cd10b** solutions of strongly coordinating solvents (pyridine, DMF, DMSO). Cluster rearrangement due to solvent coordination took place again. Thus, changes in the NMR, UV/Vis, and DLS were observed, when DMF and DMSO solutions were heated, which were attributed to formation of bigger CdS clusters/NPs. Beside this, diverse Cd17 and Cd54 clusters were crystallized from the solutions. The obtained Cd54 clusters were unusual because they were uncharged owing to the presence of rare μ_3-PhS groups.

Thus, it was shown on the two examples of **Cd10a** and **Cd10b** clusters that their molecular structure changes upon dissolution and/or heating in strongly coordinating solvents like DMSO, DMF, and pyridine. Weakly coordinating solvents (MeCN) cause also cluster rearrangement, but to a much lower extent. Therefore, substantial attention has to be paid for the solvent and reaction conditions choice. Coordinating solvents should be rather avoided because the structural integrity of the clusters cannot be ensured. On the other hand, the clusters are usually soluble only in coordinating solvents. A possibility, how to adjust the cluster solubility, could be preparation of clusters stabilized by phosphines at the terminal ligand positions, like in the case of few CdSe and CdTe clusters which are soluble in CH_2Cl_2 and/or $CHCl_3$,[38,130,131] or use of more bulky counter-cations, *e.g.* $NnBu_4^+$ for $(NnBu_4)_4[Cd_{10}S_4(SPh)_{16}]$.

A driving force for the rearrangement could possibly be the decrease of the overall cluster charge, when negatively charged species are released from the apical cluster positions. Therefore, clusters with low negative charge density or neutral clusters, such as $[Cd_{17}S_4(SPh)_{28}]^{2-}$ [58] or $Cd_{32}S_{14}(SPh)_{36}L_4$[64], might be more stable against the solvent coordination effect.

In the second part of the thesis, the knowledge about solvent coordination effects was used for the synthesis of functional CdS clusters and their further reactions. However, it was not always possible to avoid use of coordinating solvents.

As a cluster with *hydroxy* groups on the surface, known $[Cd_{10}(SCH_2CH_2OH)_{16}]^{4+}$ (**Cd10c**)[56] was chosen because of its easy and straightforward synthesis. The identity of its molecular structure in solid state and in water, DMF, and DMSO solutions was investigated. In water and DMF, good agreement was obtained with the crystal structure. On the other hand, the NMR spectra in DMSO revealed a higher number of ligand signals than expected. This means that other species than **Cd10c** must also be present in the solution. In all investigated solvents, the cluster behaved highly dynamically: the ligand –OH groups coordinate to and decoordinate from both Cd sites (CdS_4O+CdS_4 and CdS_3O_3),[68] and the different kinds of ligands exchange with each other. The differences between the behavior in DMF/water and DMSO were not attributed to solvent coordination effect as in the previous part, but to different ability of the solvents to act as hydrogen bond acceptors (HBA). DMSO, as stronger HBA, leads to easier disruption of the cluster-stabilizing hydrogen bond network, which renders it an unsuitable solvent for **Cd10c** cluster.

On the other hand, as the –OH groups are that important for cluster stability, it might be expected that the cluster will be disintegrated also after a reaction where –OH groups would be employed. The reaction of **Cd10c** with acetic anhydride (Ac_2O) led to acetylation of both sides of the ligand chain: the expected O-side, but also of the S-side. This caused complete cluster degradation in both DMSO and DMF even at low Ac_2O ratios. This renders reaction of clusters substituted by hydroxy-functionalized thiolates with Ac_2O unsuitable.

Ttrimethylchlorosilane ($ClSiMe_3$) reacted only with the O-side of **Cd10c** ligand chains. This led to complete disintegration of the cluster species in DMSO solution. In DMF, the exact reaction progress could not be elucidated; however, the ^{113}Cd NMR spectrum changed substantially after the reaction which is a sign of a change of cluster core.

Thus, **Cd10c** is not a suitable cluster for further reactions of its –OH groups because it requires stabilization by hydrogen bond network which is broken in some solvents and during reaction of the –OH groups. A possible solution for this problem could be use of real CdS clusters (**Cd10c** is only a polynuclear Cd complex) which could be more stable due to presence of sulfidic bridges. However, such clusters might be more sensitive to the solvent coordination effect.

Clusters functionalized by *amino* groups were also investigated. In the first approach, thiolate groups on **Cd10a** were exchanged by HSPh-pNH$_2$ in MeCN. However, this led to formation of a precipitate since the –NH$_2$ groups coordinated to neighboring clusters and formed aggregates in this way. The second approach was similar to the synthesis of **Cd10a** only HSPh-pNH$_2$ was used instead of PhSH. This resulted in the formation of a new Cd17 cluster with –NH$_2$ groups on the surface: $\{[Cd_{17}S_4(SPh\text{-}p NH_2)_{24}(DMF)_2]X_2\}_\infty$ (**Cd17-NH₂**). It was characterized by single-crystal XRD in solid state. The missing anions (X) could not be found, but nitrate situated in the large void spaces is probable. The structure is formed by 1D chains of Cd17 clusters connected by two SPh-pNH$_2$ ligands each (the –NH$_2$ groups coordinate to the apical Cd positions of neighboring clusters). In solution, the Cd–N

coordinative bonds have to be broken by the solvent in order to obtain single clusters of a composition $[Cd_{17}S_4(SPh\text{-}p\text{NH}_2)_{24}(\text{solvent})_4]^{2+}$. Thus, **Cd17-NH₂** was soluble in strongly coordinating solvents DMSO and DMF, but not in pyridine. It appears (DLS and NMR characterization) that **Cd17-NH₂** underwent rearrangement in DMSO due to the solvent coordination effect, but further investigation is necessary. Thus, according to the present knowledge, **Cd17-NH₂** is not a suitable cluster for further functionalization because it requires dissolution in strongly coordinating solvents.

The final part of the work deals with *radical polymerization* in the presence of the non-functional cluster **Cd10a**. Surprising results were obtained, since it was expected that **Cd10a** will be completely destroyed by radicals, that it is not stable in the presence of unsaturated ligands (due to thiol-ene reaction), and that polymerization will be influenced by its presence. Reaction conditions (MeCN, 60 °C/16 h), which were chosen to be relatively mild for the cluster, resulted in rearrangement of ca. 12 %. In the presence of radicals (formed from AIBN) another growth mechanism was observed, that is oxidation of the cluster ligand shell by radicals to PhSSPh followed by aggregation of unprotected cluster cores. The rearrangement degree increased with increasing initiator concentration. A **Cd10a**:AIBN ratio of 1:0.25 led to ca. 14 % cluster rearrangement which could be acceptable. When **Cd10a** was exposed to MMA at the given reaction conditions, no signs of the thiol-ene reaction were observed by NMR, only partial cluster rearrangement. This means that clusters capped by thiolates containing double bonds should be stable. For radical polymerization with and without **Cd10a** (**Cd10a**, MMA, AIBN, MeCN, 60 °C/16 h), ¹H NMR and GPC showed that there were no substantial differences. At the chosen reaction conditions (concentration of different reagents), **Cd10a** was rearranged to ca. 17 % due to the presence of radicals, which was expected and cannot be avoided. If the reaction conditions are tuned more carefully, a lower rearrangement degree could be achieved. In any case, it means that radical polymerization in the presence of CdS clusters is principally possible.

This part led to two important conclusions: clusters stabilized by thiolates containing double bonds are stable, and radical polymerization in the presence of CdS clusters is possible, although the cluster structure is changed partially. Therefore, as next step of the investigation, clusters stabilized by 4-vinylbenzylthiolate could be prepared and incorporated into a polymeric matrix by radical polymerization. However, 100 % preservation of the cluster cannot be achieved in the presence of radicals.

Incorporation of clusters into a polymeric matrix and maintaining their precisely defined structure is not an easy task, if ever possible. It requires cluster dissolution, for which coordinating solvents are necessary, which, on the other hand, cause cluster rearrangement. This influences also the solution behavior of clusters bearing functional groups. Radical polymerization turned out to be possible and relatively successful in the presence of clusters; however, part of the cluster grows due to oxidation of the ligand shell by radicals.

8 References

[1]   A. L. Rogach, D. V. Talapin, H. Weller, Semiconductor nanoparticles. *Colloids and Colloid Assembles.* WILEY-VCH: Weinheim, **2004**, 603 pp. ISBN: 3-527-30660-9.

[2]   J. F. Corrigan, M. W. DeGroot, Large semiconductor molecules. *The Chemistry of Nanomaterials.* WILEY-VCH: Weinheim, **2004**, 741 pp. ISBN: 3-527-30686-2.

[3]   Y. Wang, N. Herron, Quantum size effects on the exciton energy of CdS clusters. *Phys. Rev. B* **1990**, *42*, 7253–7255.

[4]   Y. Wang, N. Herron, Nanometer-sized semiconductor clusters: materials synthesis, quantum size effects, and photophysical properties. *J. Phys. Chem.* **1991**, *95*, 525–532.

[5]   G. Schmid, M. Bäumle, M. Geerkens, I. Heim, Ch. Osemann, T. Sawitowski, Current and future applications of nanoclusters. *Chem. Soc. Rev.* **1999**, *28*, 179–185.

[6]   A. P. Alivisatos, Semiconductor clusters, nanocrystals, and quantum dots. *Science* **1996**, *271*, 933–937.

[7]   H. Weller, Quantized semiconductor particles: a novel state of matter for materials science. *Adv. Mater.* **1993**, *5*, 88–95.

[8]   A. P. Alivisatos, Perspectives on the physical chemistry of semiconductor nanocrystals. *J. Phys. Chem.* **1996**, *100*, 13226–13239.

[9]   R. Rossetti, S. Nakahara, L. E. Brus, Quantum size effects in the redox potentials, resonance Raman spectra, and electronic spectra of CdS crystallites in aqueous solution. *J. Chem. Phys.* **1983**, *79*, 1086–1088.

[10]   L. E. Brus, Electron–electron and electron–hole interactions in small semiconductor crystallites: the size dependence of the lowest excited electronic state. *J. Chem. Phys.* **1984**, *80*, 4403–4409.

[11]   D. J. Norris, Electronic structure in semiconductor nanocrystals. *Semiconductor and Metal Nanocrystals.* M. Dekker: New York, NY, **2004**, 484 pp. ISBN: 0-8247-4716-X.

[12]   P. E. Lippens, M. Lannoo, Calculation of the band gap for small CdS and ZnS crystallites. *Phys. Rev. B* **1989**, *39*, 10935–10942.

[13]   D. Brust, J. C. Phillips, F. Bassani, Critical points and ultraviolet reflectivity of semiconductors. *Phys. Rev. Let.* **1962**, *9*, 94–97.

[14]   M. V. Rama Krishna, R. A Friesner, Exciton spectra of semiconductor clusters. *Phys. Rev. Let.* **1991**, *67*, 629–632.

[15]   S. Sapra, D. D. Sarma, Electronic structure and spectroscopy of semiconductor nanocrystals. *The Chemistry of Nanomaterials.* WILEY-VCH: Weinheim, **2004**, 741 pp. ISBN: 3-527-30686-2.

[16]   N. Herron, Y. Wang, H. Eckert, Synthesis and characterization of surface-capped, size-quantized CdS clusters. Chemical control of cluster size. *J. Am. Chem. Soc.* **1990**, *112*, 1322–1326.

[17]   W. W. Yu, X. Peng, Formation of high-quality CdS and other II–VI semiconductor nanocrystals in noncoordinating solvents: tunable reactivity of monomers. *Angew. Chem. Int. Ed.* **2002**, *41*, 2368–2371.

[18]   A. L. Stroyuk, A. I. Kryukov, S. Ya. Kuchmii, V. D. Pokhodenko, Quantum size effects in the photonics of semiconductor nanoparticles. *Theor. Exp. Chem.* **2005**, *41*, 67–91.

[19]   E. F. Hilinski, P. A. Lucas, Y. Wang, A picoseconds bleaching study of quantum-confined cadmium sulfide microcrystallites in a polymer film. *J. Chem. Phys.* **1988**, *89*, 3435–3441.

[20]   Y. Wang, A. Suna, J. McHugh, E. F. Hilinski, P. A. Lucas, R. D. Johnson, Optical transient bleaching of quantum-confined CdS clusters: the effects of surface-trapped electron–hole pairs. *J. Chem. Phys.* **1990**, *92*, 6927–6939.

[21]   C.-H. Fischer, A. Henglein, Photochemistry of colloidal semiconductors. 31. Preparation and photocatalysis of CdS sols in organic solvents. *J. Phys. Chem.* **1989**, *93*, 5578–5581.

[22]   J. Aldana, Y. A. Wang, X. Peng, Photochemical instability of CdSe nanocrystals coated by hydrophilic thiols. *J. Am. Chem. Soc.* **2001**, *123*, 8844–8850.

[23]   A. Henglein, Photodegradation and fluorescence of colloidal cadmium sulfide in aqueous solution. *Ber. Bunsen-Ges.* **1982**, *86*, 301–305.

[24]   J. G. C. Veinot, J. Galloro, L. Pugliese, R. Pestrin, W. J. Pietro, Surface functionalization of cadmium sulfide quantum-confined nanoclusters. 5. Evidence of facile surface-core electronic communication in the photodecomposition mechanism of functionalized quantum dots. *Chem. Mater.* **1999**, *11*, 642–648.

[25]   S. Baral, A. Fojtik, H. Weller, A. Henglein, Photochemistry and radiation chemistry of colloidal semiconductors. 12. Intermediates of the oxidation of extremely small particles of CdS, ZnS, and Cd_3P_2 and size quantization effects (a pulse radiolysis study). *J. Am. Chem. Soc.* **1986**, *108*, 375–378.

[26]   G. Kalyuzhny, R. W. Murray, Ligand effects on optical properties of CdSe nanocrystals. *J. Phys. Chem. B* **2005**, *109*, 7012–7021.

[27] L. Spanhel, M. Haase, H. Weller, A. Henglein, Photochemistry of colloidal semiconductors. 20. Surface modification and stability of strong luminescing CdS particles. *J. Am. Chem. Soc.* **1987**, *109*, 5649–5655.

[28] A. R. Kortan, R. Hull, R. L. Opila, M. G. Bawendi, M. L. Steigerwald, P. J. Caroll, L. E. Brus, Nucleation and growth of CdSe on ZnS quantum crystallite seeds, and vice versa, in inverse micelle media. *J. Am. Chem. Soc.* **1990**, *112*, 1327–1332.

[29] M. A. Hines, P. Guyot-Sionnest, Synthesis and characterization of strongly luminescing ZnS–capped CdSe nanocrystals. *J. Phys. Chem.* **1996**, *100*, 468–471.

[30] M. Danek, K. F. Jensen, C. B. Murray, M. G. Bawendi, Synthesis of luminescent thin-film CdSe/ZnSe quantum dot composites using CdSe quantum dots passivated with an overlayer of ZnSe. *Chem. Mater.* **1996**, *8*, 173–180.

[31] X. Peng, M. C. Schlamp, A. V. Kadavanich, A. P. Alivisatos, Epitaxial growth of highly luminescent CdSe/CdS core/shell nanocrystals with photostability and electronic accessibility. *J. Am. Chem. Soc.* **1997**, *119*, 7019–7029.

[32] H. Peng, L. Zhang, C. Soeller, J. Travas-Sejdic, Preparation of water-soluble CdTe/CdS core/shell quantum dots with enhanced photostability. *J. Lumin.* **2007**, *127*, 721–726.

[33] Y. He, H.-T. Lu, L.-M. Sai, Y.-Y. Su, M. Hu, C.-H. Fan, W. Huang, L.-H. Wang, Microwave synthesis of water-dispersed CdTe/CdS/ZnS core-shell-shell quantum dots with excellent photostability and biocompatibility. *Adv. Mater.* **2008**, *20*, 3416–3421.

[34] J. Bang, J. Park, J. H. Lee, N. Won, J. Nam, J. Lim, B. Y. Chang, H. J. Lee, B. Chon, J. Shin, J. B. Park, J. H Choi, K. Cho, S. M. Park, T. Joo, S. Kim, ZnTe/ZnSe (core/shell) type-II quantum dots: their optical and photovoltaic properties. *Chem. Mater.* **2010**, *22*, 233–240.

[35] J. Zeng, W. Lu, X. Wang, B. Wang, G. Wang, J. G. Hou, Fine tuning photoluminescence properties of CdSe nanoparticles by surface states modulation. *J. Colloid Interface Sci.* **2006**, *298*, 685–688.

[36] C. Barglik-Chory, C. Remenyi, C. Dem, M. Schmitt, W. Kiefer, C. Gould, C. Ruester, G. Schmidt, D. M. Hofmann, D. Pfisterer, G. Mueller, Synthesis and characterization of manganese doped CdS nanoparticles. *Phys. Chem. Chem. Phys.* **2003**, *5*, 1639–1643.

[37] V. Ladizhansky, S. Vega, Doping of CdS nanoparticles by Co^{2+} ions studied by NMR. *J. Phys. Chem. B* **2000**, *104*, 5237–5241.

[38] M. W. DeGroot, N. J. Taylor, J. F. Corrigan, Controlled Synthesis of Ternary II-II'-VI Nanoclusters and the Effects of Metal Ion Distribution on Their Spectral Properties. *Inorg. Chem.* **2005**, *44*, 5447–5458.

[39] R. Gill, M. Zayats, I. Willner, Semiconductor quantum dots for bioanalysis. *Angew. Chem. Int. Ed.* **2008**, *47*, 7602–7625.

[40] S. Günes, N. S. Sariciftci, Hybrid solar cells. *Inorg. Chim. Acta* **2008**, *361*, 581–588.

[41] A. Makhal, H. Yan, P. Lemmens, S. K. Pal, Light harvesting semiconductor core–shell nanocrystals: ultrafast charge transport dynamics of CdSe–ZnS quantum dots. *J. Phys. Chem. C* **2010**, *114*, 627–632.

[42] F. Wang, S. Hu, Electrochemical sensors based on metal and semiconductor nanoparticles. *Microchim. Acta* **2009**, *165*, 1–22.

[43] A. L. Stroyuk, A. I. Kryukov, S. Ya. Kuchmii, V. D. Pokhodenko, Quantum size effects in semiconductor photocatalysis. *Theor. Exp. Chem.* **2005**, *41*, 207–228.

[44] W. Li, S. Ismat Shah, Semiconductor nanoparticles for photocatalysis. *Encyclopedia of Nanoscience and Nanotechnology* Vol. 9. American Scientific Publishers: Valencia, California, **2004**, 961 pp. ISBN: 1-58883-001-2.

[45] P. Feng, X. Bu, N. Zheng, The interface chemistry between chalcogenide clusters and open framework chalcogenides. *Acc. Chem. Res.* **2005**, *38*, 293–303.

[46] K. S. Hagen, R. H. Holm, Stereochemistry of $[Cd_4(SC_6H_5)_{10}]^{2-}$, a cage complex related to the cadmium–cysteinate aggregates in metallothioneins. *Inorg. Chem.* **1983**, *22*, 3171–3174.

[47] I. G. Dance, A. Choy, M. L. Scudder, Syntheses, properties, and molecular and crystal structures of $(Me_4N)_4[E_4M_{10}(SPh)_{16}]$ (E = S, Se; M = Zn, Cd): molecular supertetrahedral fragments of the cubic metal chalcogenide lattice. *J. Am. Chem. Soc.* **1984**, *106*, 6285–6295.

[48] K. S. Hagen, D. W. Stephan, R. H. Holm, Metal ion exchange reactions in cage molecules: the systems $[M_{4-n}M'_n(SC_6H_5)_{10}]^{2-}$ (M, M' = Fe(II), Co(II), Zn(II), Cd(II)) with adamantane-like stereochemistry and the structure of $[Fe_4(SC_6H_5)_{10}]^{2-}$. *Inorg. Chem.* **1982**, *21*, 3928–3936.

[49] D. Craig, I. Dance, R. Garbutt, Die dreidimensionale, nichtmolekulare, polyadamantanartige Struktur von $Cd(SPh)_2$. *Angew. Chem.* **1986**, *98*, 178–179.

[50] I. G. Dance, R. G. Garbutt, T. D. Bailey, Aggregated structures of the compounds $Cd(SC_6H_5X-4)_2$ in DMF solution. *Inorg. Chem.* **1990**, *29*, 603–608.

[51] Q. Zhang, T. Wu, X. Bu, T. Tran, P. Feng, Ion pair charge-transfer salts based on metal chalcogenide clusters and methyl viologen cations. *Chem. Mater.* **2008**, *20*, 4170–4172.

[52] G. S. H. Lee, K. J. Fisher, D. C. Craig, M. L. Scudder, I. G. Dance, [ECd$_8$(E'Ph)$_{16}$]$^{2-}$ cluster chemistry (E, E' = S, Se, Te). *J. Am. Chem. Soc.* **1990**, *112*, 6435–6437.

[53] G. S. H. Lee, K. J. Fisher, A. M. Vassallo, J. V. Hanna, I. G. Dance, Solid-state ^{113}Cd NMR of three structural isomers of [S$_4$Cd$_{10}$(SPh)$_{16}$]$^{4-}$. *Inorg. Chem.* **1993**, *32*, 66–72.

[54] W. E. Farneth, N. Herron, Y. Wang, Bulk semiconductors from molecular solids: a mechanistic investigation. *Chem. Mater.* **1992**, *4*, 916–922.

[55] P. Strickler, Structure of a novel polynuclear complex related to the sphalerite lattice. *J. Chem. Soc. Chem. Comm.* **1969**, *12*, 655–656.

[56] G. Schwarzenbach, K. Gautschi, J. Peter, K. Tunaboylu, Polynuclear cadmium-thioglycolate complexes. *Kungliga Tekniska Hoegskolans Handlingar* **1972**, *271*, 293–304.

[57] S. Lacelle, W. C. Stevens, D. M. Kurtz, Jr., J. W. Richardson, Jr., R. A. Jacobson, Crystal and molecular structure of [Cd$_{10}$(SCH$_2$CH$_2$OH)$_{16}$](ClO$_4$)$_4$·8H$_2$O. Correlations with ^{113}Cd NMR spectra of the solid and implications for cadmium–thiolate ligation in proteins. *Inorg. Chem.* **1984**, *23*, 930–935.

[58] G. S. H. Lee, D. C. Craig, I. Ma, M. L. Scudder, T. D. Bailey, I. G. Dance, [S$_4$Cd$_{17}$(SPh)$_{28}$]$^{2-}$, the first member of a third series of tetrahedral [S$_w$M$_x$(SR)$_y$]$^{z-}$ clusters. *J. Am. Chem. Soc.* **1988**, *110*, 4863–4864.

[59] N. Zheng, X. Bu, H. Lu, Q. Zhang, P. Feng, Crystalline superlattices from single-sized quantum dots. *J. Am. Chem. Soc.* **2005**, *127*, 11963–11965.

[60] N. Zheng, X. Bu, H. Lu, L. Chen, P. Feng, One-dimensional assembly of chalcogenide nanoclusters with bifunctional covalent linkers. *J. Am. Chem. Soc.* **2005**, *127*, 14990–14991.

[61] Q. Zhang, X. Bu, J. Zhang, T. Wu, P. Feng, Chiral semiconductor frameworks from cadmium sulfide clusters. *J. Am. Chem. Soc.* **2007**, *129*, 8412–8413.

[62] Q. Zhang, X. Bu, Z. Lin, T. Wu, P. Feng, Organization of tetrahedral chalcogenide clusters using a tetrahedral quadridentate linker. *Inorg. Chem.* **2008**, *47*, 9724–9726.

[63] T. Vossmeyer, G. Reck, L. Katsikas, E. T. K. Haupt, B. Schulz, H. Weller, A "double-diamond superlattice" built up of Cd$_{17}$S$_4$(SCH$_2$CH$_2$OH)$_{26}$ clusters. *Science* **1995**, *267*, 1476–1479.

[64] N. Herron, J. C. Calabrese, W. E. Farneth, Y. Wang, Crystal structure and optical properties of Cd$_{32}$S$_{14}$(SC$_6$H$_5$)$_{36}$·DMF$_4$, a cluster with a 15 Angstrom CdS core. *Science* **1993**, *259*, 1426–1428.

[65] N. Zheng, X. Bu, J. Lauda, P. Feng, Zero- and two-dimensional organization of tetrahedral cadmium chalcogenide clusters with bifunctional covalent linkers. *Chem. Mater.* **2006**, *18*, 4307–4311.

[66] T. Vossmeyer, G. Reck, B. Schulz, L. Katsikas, H. Weller, Double-layer superlattice structure built up of Cd$_{32}$S$_{14}$(SCH$_2$CH(OH)CH$_3$)$_{36}$·4H$_2$O clusters. *J. Am. Chem. Soc.* **1995**, *117*, 12881–12882.

[67] T. Türk, U. Resch, M. A. Fox, A. Vogler, Cadmium benzenethiolate clusters of various size: molecular models for metal chalcogenide semiconductors. *J. Phys. Chem.* **1992**, *96*, 3818–3822.

[68] R. A. Haberkorn, L. Que, Jr., W. O. Gillum, R. H. Holm, C. S. Liu, R. C. Lord, Cadmium-113 Fourier transform nuclear magnetic resonance and Raman spectroscopic studies of cadmium(II)–sulfur complexes, including [Cd$_{10}$(SCH$_2$CH$_2$OH)$_{16}$]$^{4+}$. *Inorg. Chem.* **1976**, *15*, 2408–2414.

[69] H. Döllefeld, H. Weller, A. Eychmüller, Particle–particle interactions in semiconductor nanocrystal assemblies. *Nano Letters* **2001**, *1*, 267–269.

[70] I. Dance, K. Fisher, Metal chalcogenide cluster chemistry. *Prog. Inorg. Chem.* **1994**, *41*, 637–803.

[71] I. Dance, G. Lee, The chemistry of cadmium chalcogenide clusters [ECd$_8$(E'R)$_{16}$]$^{2-}$, [E$_4$Cd$_{10}$(E'R)$_{16}$]$^{4-}$, and [E$_4$Cd$_{17}$(E'R)$_{28}$]$^{2-}$. *Spec. Publ. – R. Soc. Chem.* **1993**, *131*, 87–94.

[72] P. O'Brien, N. Picket, Strategies for the scalable synthesis of quantum dots and related nanodimensional materials. *The Chemistry of Nanomaterials*. WILEY-VCH: Weinheim, **2004**, 741 pp. ISBN: 3-527-30686-2.

[73] A. Eychmüller, Synthesis and characterization of II–VI nanoparticles. *Nanoparticles from Theory to Applications*. WILEY-VCH: Weinheim, **2004**, 434 pp. ISBN 3-527-30507-6.

[74] Z. A. Peng, X. Peng, Nearly monodisperse and shape-controlled CdSe nanocrystals via alternative routes: nucleation and growth. *J. Am. Chem. Soc.* **2002**, *124*, 3343–3353.

[75] S. Kudera, M. Zanella, C. Giannini, A. Rizzo, Y. Li, G. Gigli, R. Cingolani, G. Ciccarella, W. Spahl, W. J. Parak, L. Manna, Sequential growth of magic-sized CdSe nanocrystals. *Adv. Mater.* **2007**, *19*, 548–552.

[76] V. N. Soloviev, A. Eichhöfer, D. Fenske, U. Banin, Molecular limit of a bulk semiconductor: size dependence of the "bang gap" in CdSe cluster molecules. *J. Am. Chem. Soc.* **2000**, *122*, 2673–2674.

[77] H.-J. Liu, J. T. Hupp, M. A. Ratner, Electronic structure and spectroscopy of cadmium thiolate clusters. *J. Phys. Chem.* **1996**, *100*, 12204–12213.

[78] T. Vossmeyer, L. Katsikas, M. Giersig, I. G. Popovic, K. Diesner, A. Chemseddine, A. Eychmueller, H. Weller, CdS nanoclusters: synthesis, characterization, size dependent oscillator strength, temperature shift of the excitonic transition energy, and reversible absorbance shift. *J. Phys. Chem.* **1994**, *98*, 7665–7673.

[79] I. G. Dance, J. K. Saunders, Cd–Cd coupling in the ^{113}Cd NMR spectra (including 2-dimensional COSY) of molecular polycadmium thiolate aggregates. *Inorg. Chim. Acta* **1985**, *96*, L71–L73.

[80] I. G. Dance, Applications of Cd N.M.R. to polycadmium complexes. III Effects of Zn/Cd and Se/S substitution in the tetra-adamantanoid cage $[S_4Cd_{10}(SPh)_{16}]^{4-}$ in relation to heterometal metallothioneins. *Aust. J. Chem.* **1985**, *38*, 1745–1755.

[81] T. Løver, G. A. Bowmaker, W. Henderson, R. P. Cooney, Electrospray mass spectrometry of some cadmium thiophenolate complexes and of a thiophenolate capped CdS cluster. *Chem. Commun.* **1996**, *5*, 683–685.

[82] T. Løver, W. Henderson, G. A. Bowmaker, J. M. Seakins, R. P. Cooney, Electrospray mass spectrometry of thiophenolate-capped clusters of CdS, CdSe, and ZnS and of cadmium and zinc thiophenolate complexes: observation of fragmentation and metal, chalcogenide, and ligand exchange processes. *Inorg. Chem.* **1997**, *36*, 3711–3723.

[83] G. Kickelbick, U. Schubert, Organic functionalization of metal oxide nanoparticles. *Synthesis, Functionalization and Surface Treatment of Nanoparticles*. American Scientific Publishers, **2003**, 350 pp. ISBN 1-58883-009-8.

[84] U. Schubert, Inorganic-organic hybrid polymers based on surface-modified metal oxide clusters. *Macromol. Symp.* **2008**, *267*, 1–8.

[85] J. F. Corrigan, O. Fuhr, D. Fenske, Metal chalcogenide clusters on the border between molecules and materials. *Adv. Mater.* **2009**, *21*, 1867–1871.

[86] T. Posner, Beiträge zur Kenntniss der ungesättigten Verbindungen. II. Über die Addition von Mercaptanen an ungesättigte Kohlenwasserstoffe. *Berichte der Deutschen Chemischen Gesellschaft* **1905**, *38*, 646–657.

[87] F. R. Mayo, C. Walling, The peroxide effect in the addition of reagents to unsaturated compounds and in rearrangement reactions. *Chem. Rev.* **1940**, *27*, 351–412.

[88] C. Lü, Z. Cui, Y. Wang, Z. Li, C. Guan, B. Yang, J. Shen, Preparation and characterization of ZnS–polymer nanocomposite films with high refractive index. *J. Mater. Chem.* **2003**, *13*, 2189–2195.

[89] J. F. Ford, T. J. Vickers, C. K. Mann, J. B. Schlenoff, Polymerization of a thiol-bound styrene monolayer. *Langmuir* **1996**, *12*, 1944–1946.

[90] A. A. Farah, R. A. Alvarez-Puebla, H. Fenniri, Chemically stable silver nanoparticle-crosslinked polymer microspheres. *J. Colloid Interface Sci.* **2008**, *319*, 572–576.

[91] J. Liu, Y. Wang, Q. Fu, X. Zhu, W. Shi, Branched polymer via free radical polymerization of chain transfer monomer: A theoretical and experimental investigation. *J. Polym. Sci. A Polymer Chem.* **2008**, *46*, 1449–1459.

[92] A. Kumar, E. Janata, A. Henglein, Photochemistry of colloidal semiconductors. 25. Quenching of CdS fluorescence by excess positive holes. *J. Phys. Chem.* **1988**, *92*, 2587–2591.

[93] S. L. Guo, E. Ding, S. M. Liu, Y. Q. Yin, Synthesis, characterization, and radical scavenging effects of polynuclear thiolate complexes. *J. Inorg. Biochem.* **1998**, *70*, 7–10.

[94] M. Laferrière, R. E. Galian, V. Maurel, J. C. Scaiano, Non-linear effects in the quenching of fluorescent quantum dots by nitroxyl free radicals. *Chem. Commun.* **2006**, 257–259.

[95] J. C. Scaiano, M. Laferrière, R. E. Galian, V. Maurel, P. Billone, Non-linear effects in the quenching of fluorescent semiconductor nanoparticles by paramagnetic species. *Phys. Stat. Sol. A* **2006**, *203*, 1337–1343.

[96] V. Maurel, M. Laferrière, P. Billone, R. Godin, J. C. Scaiano, Free radical sensor based on CdSe quantum dots with added 4-amino-2,2,6,6-tetramethylpiperidine oxide functionality. *J. Phys. Chem. B* **2006**, *110*, 16353–16358.

[97] E. Heafey, M. Laferrière, J. C. Scaiano, Comparative study of the quenching of core and core-shell CdSe quantum dots by binding and non-binding nitroxides. *Photochem. Photobiol. Sci.* **2007**, *6*, 580–584.

[98] H. Matsumoto, T. Sakata, H. Mori, H. Yoneyama, Preparation of monodisperse CdS nanocrystals by size selective photocorrosion. *J. Phys. Chem.* **1996**, *100*, 13781–13785.

[99] A. J. Hoffman, G. Mills, H. Yee, M. R. Hoffmann, Q-sized CdS: Synthesis, characterization, and efficiency of photoinitiation of polymerization of several vinylic monomers. *J. Phys. Chem.* **1992**, *96*, 5546–5552.

[100] I. G. Popovic, L. Katsikas, U. Mueller, J. S. Velickovic, H. Weller, The homogeneous photopolymerization of methyl methacrylate by colloidal cadmium sulfide. *Macromol. Chem. Phys.* **1994**, *195*, 889–904.

[101] A. L. Stroyuk, V. M. Granchak, S. Ya. Kuchmii, Polymerization of butylmethacrylate in isopropanol, photoinduced by quantum-sized CdS particles. *Theor. Exp. Chem.* **2001**, *37*, 174–179.

[102] A. L. Stroyuk, I. V. Sobran, A. V. Korzhak, A. E. Raevskaya, S. Ya. Kuchmiy, Photopolymerization of water-soluble acrylic monomers induced by colloidal CdS and $Cd_xZn_{1-x}S$ nanoparticles. *Colloid Polym. Sci.* **2008**, *286*, 489–498.

[103] N. C. Strandwitz, A. Khan, S. W. Boettcher, A. A. Mikhailovsky, C. J. Hawker, T.-Q. Nguyen, G. D. Stucky, One- and two-photon induced polymerization of methylmethacrylate using colloidal CdS semiconductor quantum dots. *J. Am. Chem. Soc.* **2008**, *130*, 8280–8288.

[104] K. Sill, T. Emrick, Nitroxide-mediated radical polymerization from CdSe nanoparticles. *Chem. Mater.* **2004**, *16*, 1240–1243.

[105] A. C. C. Estevez, A. Barros-Timmons, T. Monteiro, T. Trindade, Polymer encapsulation of CdE (E = S, Se) quantum dot ensembles via in-situ radical polymerization in miniemulsion. *J. Nanosci. Nanotechnol.* **2005**, *5*, 766–771.

[106] H. Zhang, Z. Cui, Y. Wang, K. Zhang, X. Ji, C. Lü, B. Yang, M. Gao, From water-soluble CdTe nanocrystals to fluorescent nanocrystal–polymer transparent composites using polymerizable surfactants. *Adv. Mater.* **2003**, *15*, 777–780.

[107] L. Chen, J. Zhu, Q. Li, S. Chen, Y. Wang, Controllable synthesis of functionalized CdS nanocrystals and CdS/PMMA nanocomposite hybrids. *Eur. Polym. J.* **2007**, *43*, 4593–4601.

[108] Y. Nosaka, N. Ohta, T. Fukuyama, N. Fujii, Size control of ultrasmall CdS particles in aqueous solution by using various thiols. *J. Colloid Interface Sci.* **1993**, *155*, 23–29.

[109] A. L. Rogach, A. Kornowski, M. Gao, A. Eychmüller, H. Weller, Synthesis and characterization of a size series of extremely small thiol-stabilized CdSe nanocrystals. *J. Phys. Chem. B* **1999**, *103*, 3065–3069.

[110] J. G. C. Veinot, M. Ginzburg, W. J. Pietro, Surface functionalization of cadmium sulfide quantum-confined nanoclusters. 3. Formation and derivatives of a surface phenolic quantum dot. *Chem. Mater.* **1997**, *9*, 2117–2122.

[111] J. G. C. Veinot, J. Galloro, L. Pugliese, V. Bell, R. Pestrin, W. J. Pietro, Surface functionalization of cadmium sulfide quantum-confined nanoclusters. 4. Formation and reactivity of an aniline surface quantum dot. *Can. J. Chem.* **1998**, *76*, 1530–1539.

[112] L. K. Yeung, K. Sooklal, R. Mahtab, B. Zhang, R. D. Adams, C. J. Murphy, A comparison of the photophysical properties of thiolate-capped CdS quantum dots with thiolate-capped CdS molecular clusters. *Mat. Res. Soc. Symp. Proc.* **2000**, *571*, 247–252.

[113] T. Løver, W. Henderson, G. A. Bowmaker, J. M. Seakins, R. P. Cooney, Functionalization and capping of a CdS nanocluster: A study of ligand exchange by electrospray mass spectrometry. *Chem. Mater.* **1997**, *9*, 1878–1886.

[114] P. DuBois Murphy, W. C. Stevens, T. T. P. Cheung, S. Lacelle, B. C. Gerstein, D. M. Kurtz, Jr., High-resolution ^{113}Cd NMR of solids. Correlation of spectra with the molecular structure of a decanuclear cadmium(II) complex. *J. Am. Chem. Soc.* **1981**, *103*, 4400–4405.

[115] M. A. Olshavsky, H. R. Allcock, Synthesis of CdS nanoparticles in solution and in a polyphosphazene matrix. *Chem. Mater.* **1997**, *9*, 1367–1376.

[116] F. R. Kogler, *Synthesis and Characterization of Transition Metal Oxo Clusters and their Use as Co-Monomers in the Preparation of Hybrid Polymers*. Ph.D. thesis **2005**, Vienna University of Technology.

[117] T. Løver, G. A. Bowmaker, J. M. Seakins, R. P. Cooney, Vibrational spectroscopic study of thiophenolate-capped nanoclusters of CdS and of cadmium thiophenolate complexes. *Chem. Mater.* **1997**, *9*, 967–975.

[118] T. Hiratani, K. Konishi, Surface-cap-mediated host–guest chemistry of semiconductor CdS: Intercalative cation accumulation around a phenyl-capped CdS cluster and its notable effects on the cluster photoluminescence. *Angew. Chem. Int. Ed.* **2004**, *43*, 5943–5946.

[119] K. Konishi, T. Hiratani, Turn-on and selective luminescence sensing of copper ions by a water-soluble $Cd_{10}S_{16}$ molecular cluster. *Angew. Chem. Int. Ed.* **2006**, *45*, 5191–5194.

[120] T. Tsuboi, Y. Takaguchi, S. Tsuboi, Preparation and photosensitizing property of novel $Cd_{10}S_{16}$ molecular cluster dendrimer. *Chem. Commun.* **2008**, 76–78.

[121] O. Alvarez-Fregoso, J. G. Mendoza-Alvarez, O. Zelaya-Angel, Quantum confinement in nanostructured CdNiTe composite thin films. *J. Appl. Phys.* **1997**, *82*, 708–711.

[122] W. W. Yu, X. Peng, Formation of high-quality CdS and other II–VI semiconductor nanocrystals in noncoordinating solvents: tunable reactivity of monomers. *Angew. Chem. Int. Ed.* **2002**, *41*, 2368–2371.

[123] S. L. Cumberland, K. M. Hanif, A. Javier, G. A. Khitrov, G. F. Strouse, S. M. Woessner, C. S. Yun, Inorganic clusters as single-source precursors for preparation of CdSe, ZnSe, and CdSe/ZnS nanomaterials. *Chem. Mater.* **2002**, *14*, 1576–1584.

[124] M. G. Berrettini, G. Braun, J. G. Hu, G. F. Strouse, NMR analysis of surfaces and interfaces in 2-nm CdSe. *J. Am. Chem. Soc.* **2004**, *126*, 7063–7070.

[125] M. W. DeGroot, H. Rösner, J. F. Corrigan, Control of metal-ion composition in the synthesis of ternary II-II'-VI nanoparticles by using a mixed-metal cluster precursor approach. *Chem. Eur. J.* **2006**, *12*, 1547–1554.

[126] D. D. Lovingood, R. E. Oyler, G. F. Strouse, Composition control and localization of S^{2-} in CdSSe quantum dots grown from $Li_4[Cd_{10}Se_4(SPh)_{16}]$. *J. Am. Chem. Soc.* **2008**, *130*, 17004–17011.

[127] Z. Li, W. Cai, J. Sui, Large-scale preparation of CdS quantum dots by direct thermolysis of a single-source precursor. *Nanotechnology* **2008**, *19*, 1–7.

[128] C. Tuinenga, J. Jasinski, T. Iwamoto, V. Chikan, *In situ* observation of heterogeneous growth of CdSe quantum dots: Effect of indium doping on the growth kinetics. *ACS Nano* **2008**, *2*, 1411–1421.

[129] K.-L. Tang, X.-L. Jin, S.-J. Jia, Y.-Q. Tang, Synthesis of high nuclearity cadmium-sulfur clusters. (II). Formations and crystal structures of two octanuclear cadmium-sulfur clusters. *Jiegou Huaxue* **1995**, *14*, 399–404.

[130] S. Behrens, M. Bettenhausen, A. C. Deveson, A. Eichhöfer, D. Fenske, A. Lohde, U. Woggon, Synthesis and structure of the nanoclusters $[Hg_{32}Se_{14}(SePh)_{36}]$, $[Cd_{32}Se_{14}(SePh)_{36}(PPh_3)_4]$, $[P(Et)_2(Ph)C_4H_8OSiMe_3]_5[Cd_{18}I_{17}(PSiMe_3)_{12}]$, and $[N(Et)_3C_4H_8OSiMe_3]_5[Cd_{18}I_{17}(PSiMe_3)_{12}]$. *Angew. Chem. Int. Ed.* **1996**, *35*, 2215–2218.

[131] A. Eichhöfer, A. Aharoni, U. Banin, Synthesis, structure, and optical properties of new cadmium chalcogenide clusters of the type $[Cd_{10}E_4(E'Ph)_{12}(PR_3)_4]$, (E, E' = Te, Se, S). *Z. Anorg. Allg. Chem.* **2002**, *628*, 2415–2421.

[132] K. Konishi, T. Hiratani, Cation–π-driven fluorescence signalling of ammonium cations by naphthyl-substituted $Zn_{10}S_{16}$ and $Cd_{10}S_{16}$ clusters. *Chem. Letters* **2006**, *35*, 184–185.

[133] A. Eichhöfer, Thermal properties of $[M_{10}Se_4(SePh)_{12}(PR_3)_4]$ (M = Zn, Cd, Hg) cluster molecules – synthesis and structure of $[Cd_{32}Se_{14}(SePh)_{36}(L)_4]$; L = OPPh$_3$, OC$_4H_8$. *Eur. J. Inorg. Chem.* **2005**, 1245–1253.

[134] A. Eichhöfer, O. Hampe, Investigating the thermolysis products of $[Cd_{10}Se_4(SePh)_{12}(PnPr_3)_4]$ – the new cluster ion $[Cd_{17}Se_4(SePh)_{28}]^{2-}$. *J. Cluster Sci.* **2007**, *18*, 494–504.

[135] N. Herron, A. Suna, Y. Wang, Synthesis of ≈10 Å thiophenolate-capped CdS clusters. Observation of a sharp absorption peak. *J. Chem. Soc. Dalton Trans.* **1992**, 2329–2335.

[136] N. Zheng, H. Lu, X. Bu, P. Feng, Metal-chelate dye-controlled organization of $Cd_{32}S_{14}(SPh)_{40}^{4-}$ nanoclusters into three-dimensional molecular and covalent open architecture. *J. Am. Chem. Soc.* **2006**, *128*, 4528–4529.

[137] I. G. Dance, R. G. Garbutt, D. C. Craig, Applications of cadmium NMR to polycadmium complexes. IV. Reactions of $[Cd_{10}(SCH_2CH_2OH)_{16}]^{4+}$ with chloride ion, and the crystal and molecular structure of hexadeca(2-hydroxyethanethiolato)tetrachlorodecacadmium $[Cd_{10}(SCH_2CH_2OH)_{16}Cl_4]$. *Aust. J. Chem.* **1986**, *39*, 1449–1463.

[138] M. J. Kamlet, R. W. Taft, The solvatochromic comparison method. I. The *β*-scale of solvent hydrogen-bond acceptor (HBA) basicities. *J. Am. Chem. Soc.* **1976**, *98*, 377–383.

[139] M. J. Kamlet, J.-L. M. Abboud, M. H. Abraham, R. W. Taft, Linear solvation energy relationships. 23. A comprehensive collection of the solvatochromic parameters, *π**, *α*, and *β*, and some methods for simplifying the generalized solvatochromic equation. *J. Org. Chem.* **1983**, *48*, 2877–2887.

[140] H. Marsmann, ^{29}Si-NMR spectroscopic results. *NMR 17, Basic Principles and Progress*. Springer Verlag: Berlin, Heidelberg, **1981**. 235 pp. ISBN: 978-0387104140.

[141] C. N. Yiannios, J. V. Karabinos, Oxidation of Thiols by Dimethyl Sulfoxide, *J. Org. Chem.* 1963, 28, 3246–3248.

[142] Q. A. Paula, A. A. Batista, E. E. Castellano, J. Ellena, On the lability of dimethysulfoxide (DMSO) coordinated to the $\{Ru^{II}-NO^+\}$ species: X-ray structures of *mer*-$[RuCl_3(DMSO)_2(NO)]$ and *mer*-$[RuCl_3(CD_3CN)(DMSO)(NO)]$. *J. Inorg. Biochem.* **2002**, *90*, 144–148.

[143] Sigma-Aldrich, "Thermal Initiators: Decomposition Rate and Half-Life", available at http://www.sigmaaldrich.com/etc/medialib/docs/Aldrich/General_Information/thermal_initiators.Par.0001.File.tmp/thermal_initiators.pdf (accessed on 2010-03-02).

[144] K. Matyjaszewski, T. P. Davis, *Handbook of Radical Polymerization*. WILEY-INTERSCIENCE: Hoboken, **2002**, 920 pp. ISBN: 0-471-39274-X.

[145] G. Moad, D. H. Solomon, *The Chemistry of Radical Polymerization*. ELSEVIER Ltd: Oxford, **2006**, 639 pp. ISBN: 0-08-044288-9.

[146] H. J. Reich, "C-13 Chemical Shifts", available at http://www.chem.wisc.edu/areas/reich/handouts/nmr-c13/cdata.htm (accessed on 2010-04-04).

[147] J. B. Schlenoff, J. R. Dharia, H. Xu, L. Wen, M. Li, Adsorption of thiol-containing copolymers onto gold. *Macromolecules*. **1995**, *28*, 4290–4295.

[148] W. L. F. Armarego, D. D. Perrin, *Purification of Laboratory Chemicals*. Butterworth-Heinemann: Oxford, **1996**, pp. 529, ISBN: 0-7506-3761-7.

[149] G. M. Sheldrick, SADABS, Program for Empirical Absorption Correction of Area Detector Data, University of Göttingen, Göttingen (Germany) **2008**.

[150] G. M. Sheldrick, SHELXS/L-97, Programs for Crystal Structure Determination, University of Göttingen, Göttingen (Germany) **1997**.

[151] G. M. Sheldrick, A short history of *SHELX*. *Acta Cryst.* **2008**, *A64*, 112–22.

[152] G. Beaucage, Approximations leading to a unified exponential/power-law approach to small-angle scattering. *J. Appl. Cryst.* **1995**, *28*, 717–728.

[153] R. J. Kostelnik, A. A. Bothner-By, Cadmium-113 nuclear magnetic resonance studies of cadmium(II)ligand binding in aqueous solutions. I. The effect of diverse ligands on the cadmium-113 chemical shift. *J. Mag. Res.* **1974**, *14*, 141–151.

[154] P. DuBois Murphy, B. C. Gerstein, Principal components of the cadmium-113 shielding tensors in cadmium sulfate hydrates: Nuclear magnetic resonance study of cadmium coordinated with oxygen. *J. Am. Chem. Soc.* **1981**, *103*, 3282–3286.

[155] T. T. P. Cheung, L. E. Worthington, P. DuBois Murphy, B. C. Gerstein, Solid-state NMR studies of cadmium: cadmium-113-proton cross polarization and magic-angle spinning. *J. Mag. Res.* **1980**, *41*, 158–168.

[156] G. E. Maciel, M. Borzo, High resolution ^{113}Cd nuclear magnetic resonance by pulse Fourier transform. *J. Chem. Soc., Chem. Commun.* **1973**, 394a–394a.

[157] G. K. Carson, P. A. W. Dean, M. J. Stillman, A multinuclear (^{1}H, ^{13}C, ^{113}Cd) nuclear magnetic resonance and magnetic circular dichroism spectroscopic study of thiolate complexes of cadmium. *Inorg. Chim. Acta* **1981**, *56*, 59–71.

[158] A. D. Cardin, P. D. Ellis, J. D. Odom, J. W. Howard, Jr., Cadmium-113 fourier transform nuclear magnetic resonance spectroscopy. *J. Am. Chem. Soc.* **1975**, *97*, 1672–1679.

[159] N. Ueyama, T. Sugawara, K. Sasaki, A. Nakamura, S. Yamashita, Y. Wakatsuki, H. Yamazaki, N. Yasuoka, X-ray structures and far-infrared and Raman spectra of tetrahedral thiophenolato and selenophenolato complexes of zinc(II) and cadmium(II). *Inorg. Chem.* **1988**, *27*, 741–747.

[160] H.-B. Bürgi, 57. Stereochemistry of polynuclear cadmium(II) thioglycolates: Crystal structure of cadmium(II) bisthioglycolate. *Helvetica Chimica Acta* **1974**, *57*, 513–519.

[161] A. L. Spek, Single-crystal structure validation with the program *PLATON*, *J. Appl. Cryst.* **2003**, *36*, 7–13.

[162] H. D. Flack, G. Bernardinelli, The use of X-ray crystallography to determine absolute configuration. *Chirality* **2008**, *20*, 681–690.

9 Appendix

9.1 Calculation of $[Cd_{10}S_4(SPh)_{16}]^{4-}$ Conversion in MeCN from UV/Vis Spectra

The mechanism, which was derived in Chapter 4.1 for **Cd10a** rearrangement in DMSO, was used for calculation of **Cd10a** conversion in MeCN in the absence or presence of AIBN (see Chapters 4.1.1 and 5.3). Data obtained by UV/Vis absorption were employed (see Figure 4.8 and Figure 5.21). The UV/Vis spectra of samples heated in the absence of radicals showed a distinct maximum at ca. 350 nm which corresponds to formation of Cd54 clusters. The spectra of other samples were similar but the band-gap transition of the formed clusters was not so pronounced. Thus, the following reaction was employed for the conversion calculation:

$$x\ [Cd_{10}S_4(SPh)_{16}]^{4-} \rightarrow y\ [Cd(SPh)_3]^- + z\ [Cd_{54}S_{32}(SPh)_{48}]^{4-} \qquad (9.1)$$
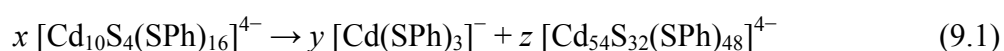
where $x \cong 25$, $y \cong 88$, $z \cong 3$. Probably also other reaction byproducts (mononuclear Cd complexes with lower amount of PhS$^-$) should be used for calculation, but were omitted for simplification. Approximate values of extinction coefficients were estimated at three different wavelengths (255, 275, and 350 nm) which correspond to absorption maxima of the three components (Table 9.1).

*Table 9.1. Extinction coefficients (ε_λ) and molecular masses (M_r) of components used in the calculation of **Cd10a** conversion in MeCN.*

	λ / nm	**Cd10a**	$[Cd(SPh)_3]^-$	Cd54
	255	2.6×10^5	2.3×10^4	7.6×10^5
ε_λ / l mol^{-1} cm^{-1}	275	2.3×10^5	3.4×10^4	4.4×10^5
	350	~0	~0	1.1×10^5
estimated		in MeCN	as ¾ of absorption of $(NMe_4)_2[Cd(SPh)_4]$ in MeCN	diverse Cd54 in THF, DMF, DMSO
M_r		3295.6	514.074	12633.15

The calculation led to reasonable values for rearrangement in the absence of radicals which were comparable with data obtained by ^{1}H NMR (Table 5.10). However, the ratio of reaction products (y/z) was 5 and 14, which differs from theoretical value 29.

In the presence of radicals (experiments RP2–4, and RP8 in Table 5.9), a negative concentration of $[Cd(SPh)_3]^-$ was obtained for all samples. This means that another mechanism than formation of $[Cd(SPh)_3]^-$ species must be responsible for the cluster growth. A few possibilities are described in Chapter 5.3.1. Therefore calculation without $[Cd(SPh)_3]^-$ and using absorptions at 255 and 275 nm was performed. This confirmed the trend of increasing conversion with increasing initiator concentration obtained from ^{1}H NMR data, however, the values were overestimated (Table 5.10).

9.2   Calculation of AIBN Conversion

Conversion of AIBN into radicals at 60 °C/16 h was calculated from data on thermal initiators (Table 9.2)[143] using Arrhenius equation. Thus, $k_{d,60\,°C} = 9.42 \times 10^{-6}$ s^{-1} was obtained, which is in good agreement with the literature value $k_{d,60\,°C} = 9.6 \times 10^{-6}$ s^{-1},[145] which correspond to 41.9 and 42.5 %[145] (= 42 %) conversion after 16 h at 60 °C. Since one AIBN molecule is decomposed to two radicals, 1 mol AIBN should lead to production of 0.84 mol radicals in the course of 16 h at 60 °C. Thus the molar ratio **Cd10a**:radical = 1:1.00 is equivalent to the molar ratio **Cd10a**:AIBN = 1:1.19 for 42 % AIBN conversion. However, real conversions (calculated from NMR data of samples RP2–4, Table 5.9) were somewhat lower and only ca. 35 % of AIBN was decomposed. This is unexpected since k_d should increase with dielectric constant of the medium,[145] and MeCN has a relatively high dielectric constant. Therefore, the real concentration of radicals is lower than given in Table 5.9. Additionally, it is reduced by cage reactions of the primary radicals (see Scheme 9.1). It should be also noted that radicals were formed with almost linear time-dependence (Figure 9.1) in the course of 16 h.

Table 9.2. Decomposition rates (k_d) of AIBN depending on temperature, taken from Ref. 143 and 144.

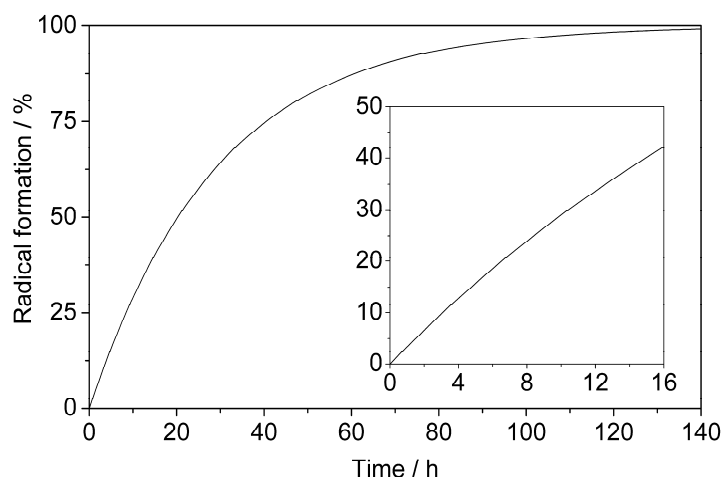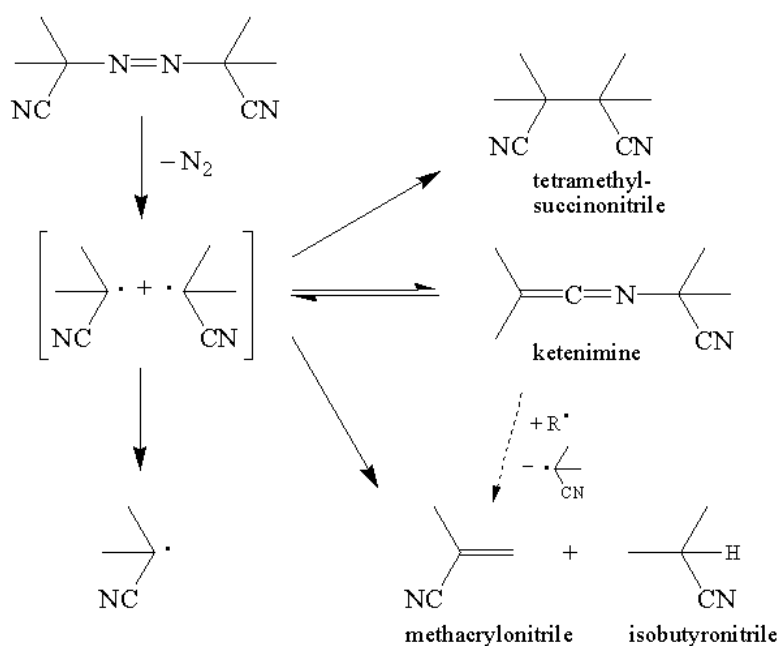| T / °C	k_d / s^{-1}
50	2.20×10^{-6}
65	1.93×10^{-5}
70	3.20×10^{-5}
81	1.93×10^{-4}
100	1.50×10^{-3}

Figure 9.1. Dependence of radical formation from AIBN on time at 60 °C, calculated for a first order reaction.

Scheme 9.1. Cage reactions of radical pairs produced from AIBN, according to Ref. 145.

9.3 List of Crystal Structures

Table 9.3. List of crystal structures with formula, abbreviation, and measurement label.

Formula	Abbreviation	Measurement label
$(NMe_4)_4[Cd_{10}S_4(SPh)_{16}]$	**Cd10a-3**	mb132
$(NMe_4)_2[Cd(SPh)_4]$	**Cd1-2**	mb133
$(NMe_4)_2[Cd_8S(SPh)_{16}]$	**Cd8**	mb137
$[Cd_{17}S_4(SPh)_{26}Py]_\infty$	**Cd17-Py**	mb072
$Cd_{54}S_{28}(SPh)_{52}(Py)_{7.5}$	**Cd54-Py**	mb089
$Cd_{54}S_{28}(SPh)_{52}(L)_x$ (L = DMF or Py)	**Cd54-L**	mb125
$Cd_{54}S_{28}(SPh)_{52}(DMF)_4$	**Cd54-DMF**	mb092
$[Cd_{10}(SCH_2CH_2OH)_{16}](NO_3)_4 \cdot 2H_2O$	**Cd10c-NO$_3$·2H$_2$O**	mb085
$[Cd_{10}(SCH_2CH_2OH)_{16}](BF_4)_4 \cdot H_2O$	**Cd10c-BF$_4$·H$_2$O**	mb091
$[Cd_{10}(SCH_2CH_2OH)_{16}](BF_4)_4 \cdot 6H_2O$	**Cd10c-BF$_4$·6H$_2$O**	mb095
$[Cd_{10}(SCH_2CH_2OH)_{16}](BF_4)_4 \cdot 2DMSO$	**Cd10c-BF$_4$·2DMSO**	mb096
$\{[Cd_{17}S_4(SPh\text{-}pNH_2)_{24}(DMF)_2]^{2+}\}_\infty$	**Cd17-NH$_2$**	mb100

Curriculum Vitae

Name	Mária Bendová
Address	Nitrianske Sučany 481, 972 21, Slovakia
Nationality	Slovak
Date and Place of Birth	May 21st, 1983, Bojnice, Slovakia

Education

10/2006–06/2010	PhD studies at Vienna University of Technology, Institute of Materials Chemistry, Austria; Supervisor Prof. Ulrich Schubert; Topic "Investigation of CdS Clusters in Solution for their Use as Building Blocks in Hybrid Materials"
03/2009	6th European Winter School on Neutron and Synchrotron Radiation (NESY), Planneralm, Austria
09/2001–09/2006	Master studies at Brno University of Technology, Institute of Materials Chemistry, Czech Republic
01–07/2006	Diploma thesis at SCHOTT AG, Research & Development, Germany; Supervisor Dr. Falk Gabel; Topic "High-temperature Phase Transformations in Commercial Glass-ceramics of the LAS-system"
08–12/2004	Erasmus/Socrates scholarship at Lund University, Chemistry Department, Sweden
09/1993–06/2001	High school education at Gymnázium V. B. N., Prievidza, Slovakia, high school with extended education of German language

Professional Experience

since 07/2010	PostDoc position at Leibniz Institute for Solid State and Materials Research Dresden, Institute for Integrative Nanosciences, Germany
10/2006–06/2010	Project assistant at Vienna University of Technology, Institute of Materials Chemistry, Austria
07–09/2005	Internship at SCHOTT AG, Research & Development, Germany; Supervisor Dr. Christian Roos, Topic "Determination of Temperature Homogeneity in Laboratory Ovens"
08/2002	Internship at Development Institute of Petrochemistry, Prievidza, Slovakia